DISS. ETH NO. 29947

Impacts and uncertainty of climate change on mountain hydrology and its extremes: An approach using high-resolution stochastic climate simulations

A thesis submitted to attain the degree of

DOCTOR OF SCIENCES
(Dr. sc. ETH Zurich)

presented by

JORGE SEBASTIÁN MORAGA NAVARRETE

MSc. in Civil Engineering, Universidad de Concepción

born on 03.06.1989

accepted on the recommendation of
Prof. Dr. Paolo Burlando, supervisor
Prof. Dr. Nadav Peleg, co-examiner
Prof. Dr. Hayley Fowler, co-examiner
Prof. Dr. Harald Kunstmann, co-examiner
Prof. Dr. Peter Molnar, co-examiner

2024

dedicado a Yeyo

Impacts and uncertainty of climate change on mountain hydrology and its extremes: An approach using high-resolution stochastic climate simulations

ABSTRACT

This thesis delves into the hydrological responses of mountainous catchments in the Swiss Alps to climate change, with a particular emphasis on understanding and underscoring the importance of spatial variability, uncertainties in projections, and the impact of intensified extreme rainfall. Initially, the study explores the significant spatial variability in hydrological responses at the sub-catchment level, driven by changes in precipitation patterns, snowmelt, and evapotranspiration across different elevations. The analysis employs a high-resolution two-dimensional weather generator model alongside a distributed hydrological model, detecting notable shifts in streamflow patterns, particularly a winter increase and summer decrease projected towards the end of the 21st century under the RCP8.5 emission scenario.

To address the inherent uncertainties in climate and hydrological projections, this thesis introduces a novel framework designed to quantify and partition the sources of uncertainty across different scales. The framework combines the use climate of model outputs, a high-resolution weather generator, and a distributed hydrological model to produce large ensembles of future climate and hydrological variables at high resolution. Applying this approach to two representative mountainous catchments, the analysis underscores the dominant role of precipitation's natural variability in engendering uncertainty, alongside the identification of robust change signals in specific hydrological components like snowmelt and liquid precipitation, especially during warm seasons and at higher elevations.

Further, to enhance the realism in simulating the intensification of extreme rainfall, an improved version of the weather generator model is introduced. This revised model successfully mimics the Clausius-Clapeyron relation, reflecting the observed scaling of heavy rainfall with temperature. By employing this enhanced model to assess future rainfall impacts on hydrological responses, a more accurate depiction of the potential intensification of short-duration heavy rainfall in future climates is achieved, providing a more realistic assessment of future hydrological impacts even for short durations.

Overall, this work provides an improved understanding of the complex interplay between climate change and hydrological processes in mountainous terrains, enhancing the predictive capacity regarding the hydrological behaviour of such regions in a warming climate. Through a detailed spatial analysis, rigorous uncertainty quantification, and an enhanced representation of extreme rainfall, this thesis contributes to deciphering the complex hydrological implications of climate change in mountainous environments.

Auswirkungen und Unsicherheiten des Klimawandels auf die Gebirgshydrologie und ihre Extreme: Ein Ansatz mit hochauflösenden stochastischen Klimasimulationen

ZUSAMMENFASSUNG

Diese Dissertation befasst sich mit den hydrologischen Reaktionen von Gebirgseinzugsgebieten in den Schweizer Alpen auf den Klimawandel. Besonderes Augenmerk liegt dabei auf dem Verständnis und der Betonung der Bedeutung der räumlichen Variabilität, den Unsicherheiten in den Prognosen und den Auswirkungen verstärkter extremer Niederschläge. Zunächst wird in der Studie die erhebliche räumliche Variabilität der hydrologischen Reaktionen auf der Ebene der Teileinzugsgebiete untersucht, die durch Veränderungen der Niederschlagsmuster, der Schneeschmelze und der Evapotranspiration in verschiedenen Höhenlagen bedingt sind. Bei der Analyse wird ein hochauflösendes zweidimensionales Wettergeneratormodell zusammen mit einem räumlich gegliederten hydrologischen Modell verwendet. Dabei werden bemerkenswerte Verschiebungen in den Abflussmustern der Flüsse festgestellt, insbesondere eine Zunahme im Winter und eine Abnahme im Sommer, die gegen Ende des 21. Jahrhunderts unter dem Emissionsszenario RCP8.5 prognostiziert werden.

Um die inhärenten Unsicherheiten in den klimatischen und hydrologischen Prognosen anzugehen, wird in dieser Arbeit ein neuartiges System zur Quantifizierung und Aufteilung der Unsicherheitsquellen auf verschiedenen Ebenen eingeführt. Das System kombiniert die Verwendung der Klimamodellausgaben, des hochauflösenden Wettergenerators und des räumlich gegliederten hydrologischen Modells, um grosse Ensembles zukünftiger klimatischer und hydrologischer Variablen in hoher Auflösung zu erstellen. Durch die Anwendung dieses Ansatzes auf zwei repräsentative Gebirgseinzugsgebiete unterstreicht die Analyse die dominante Rolle der natürlichen Variabilität des Niederschlags bei der Entstehung von Unsicherheiten. Gleichzeitig werden robuste Veränderungssignale in spezifischen hydrologischen Komponenten wie Schneeschmelze und Flüssigniederschlag identifiziert, insbesondere während warmer Jahreszeiten und in höheren Lagen.

Um die Intensivierung extremer Niederschläge realistischer zu simulieren, wird eine verbesserte Version des Wettergeneratormodells eingeführt. Dieses überarbeitete Modell ahmt erfolgreich die Clausius-Clapeyron-Beziehung nach und spiegelt die beobachtete Skalierung von Starkniederschlägen mit der Temperatur wider. Durch den Einsatz dieses verbesserten Modells wird eine genauere Darstellung der potenziellen Intensivierung kurzzeitiger Starkniederschläge in zukünftigen Klimaverhältnissen erreicht, was eine realistischere Bewertung künftiger hydrologischer Auswirkungen selbst für kurze Ereignisse ermöglicht.

Insgesamt eröffnet diese Arbeit ein besseres Verständnis des komplexen Zusammenspiels zwischen Klimawandel und hydrologischen Prozessen in Gebirgsregionen und verbessert die

Vorhersagefähigkeit hinsichtlich des hydrologischen Verhaltens solcher Regionen in einem sich erwärmenden Klima. Durch eine detaillierte räumliche Analyse, eine rigorose Quantifizierung der Unsicherheiten und eine verbesserte Darstellung extremer Niederschläge trägt diese Dissertation dazu bei, die komplexen hydrologischen Auswirkungen des Klimawandels in Gebirgsregionen zu entschlüsseln.

ACKNOWLEDGMENTS

It has been said many times before, but it bears repeating: I could not be where I am without my family. I therefore begin this acknowledgement by thanking Carmen and Jorge, my parents whom I love dearly, as well as Irvin, Luis, Sergio and Evie, Eduardo and Patricia, Patricia and Aida, and many others who have given me so much without ever asking for anything in return. The truth is I have been very lucky to have been loved by many throughout what now feels like very long years. Being away from them has been the hardest part of this adventure.

This thesis is the result of the contributions of many. The ideas of co-authors, supervisors, examiners and colleagues are reflected in one way or another in this manuscript, for which I am profoundly grateful. I owe a special debt of gratitude to Nadav Peleg, whose boundless patience and optimism repeatedly helped me find my way when I felt lost. His knowledge, passion, and generosity have been invaluable to me, and for this, I am immensely thankful.

The best part of my journey in Zurich has been the extraordinary people I met along the way. I am fortunate to count a long list of friends and colleagues who have made my time there unforgettable. I am especially proud to call Zuzana and Silvan, Martina and Marco, Felipe, and Jacob and Moira my friends, for they have stood by me through thick and thin and become like a family away from home. I truly believe that I could not have made it without them. Nor could I have done it without Camila, who, despite the distance, has been by my side every step of the way. This was not the first battle we fought together, and there are many more to come.

CONTENTS

1 INTRODUCTION

1.1 MOTIVATION

1.1.1 The importance of mountain hydrology

Mountains and the rivers originating from them are fundamental to life as we know it. As a matter of fact, while mountainous areas represent around 20% of the global land surface (12–24%, depending on the definition; Huddleston et al., 2003; Kapos et al., 2000; Körner et al., 2011) and are inhabited by roughly 12% of the global population, these so-called water towers of the world (Immerzeel et al., 2020) provide an estimated 60–80% of the global available freshwater supply, used in 68% of the world's irrigated land surface (Intergovernmental Panel on Climate Change (IPCC), 2023). For instance, the European Alps contribute 1.9 times more water to Europe's catchments than suggested by their surface area (Viviroli & Weingartner, 2004; Weingartner et al., 2007). Furthermore, up to 60% of the sediments that flow into the oceans come from high-elevation mountains (Syvitski et al., 2005), and more than 50% of soil erosion occurs on slopes that are steeper than 10% (Larsen et al., 2014). Many economic sectors, including tourism, mining, agriculture, and energy, are highly dependent on the balance of mountain hydrological systems. For example, hydropower generation, which is primarily based in mountains, accounts for a sixth of the world's energy production and 70% of all renewable energy (World Energy Council, 2016). Additionally, mountainous catchments provide invaluable ecosystems that sustain up to a third of all known land-based biodiversity (Körner, 2004). In summary, the significance of comprehending mountainous hydrological systems cannot be overstated.

Mountainous areas—including the European Alps—are especially vulnerable to the effects of climate change (Gobiet et al., 2014; Immerzeel et al., 2020). In recent decades, changes attributed to global warming have been observed in diminishing snow and glacier cover (Beniston et al., 2018; Huss et al., 2017; Jenicek et al., 2018), prolonged low-flow periods (Floriancic et al., 2020), intensification of extremes rainfalls (Ban et al., 2015; Bao et al., 2017; Barbero et al., 2017; Fischer & Knutti, 2016; Lenderink et al., 2017; Peleg et al., 2018; Westra et al., 2014), increasing, decreasing and shifting the timing of floods (Blöschl et al., 2017, 2019), more frequent landslides and debris flows (Gariano & Guzzetti, 2016; Hirschberg et al., 2020; Scheidl et al., 2020), changes in biomass and evapotranspiration (Mastrotheodoros et al., 2020), among others; all the while our dependence on mountain water resources is projected to increase (e.g., Viviroli et al., 2020), leading to potentially disastrous economic consequences (Savelsberg et al., 2018; Weingartner et al., 2013)

Deepening our understanding of hydrological systems and attempting to project the responses of catchments to a changing climate becomes, therefore, indispensable. Yet, while projecting the responses of any natural system can be challenging, mountainous catchments pose a particularly interesting modelling problem. On the one hand, mountains are notorious for their diversity in soil, vegetation, land use, and topography, which demands a detailed characterization of their properties. On the other hand, their mere presence can generate especial atmospheric phenomena associated with intense precipitations over relatively small extents, such as the so-called orographic effect. This combination of highly heterogeneous modelling domains and rapidly-changing external inputs makes modelling of mountainous catchments especially challenging, not the least because it demands high-resolution representations of climate data for which the resolution of widely-available simulations is not sufficient.

1.1.2 Future climate and its extremes

Driven by concerns about climate change, scientists and engineers have dedicated extensive efforts to understand global climate dynamics and their potential future trajectories. Among the main outcomes of this enterprise are complex computational models that seek to describe the energy and mass transfers in the oceans and atmosphere. These models, known as General Circulation Models (GCMs) or Global Climate Models (also Earth System Models), form the foundation of our understanding of global-scale climate changes resulting from human-generated greenhouse gas (GHG) emissions, including temperature and precipitation changes (Tokarska et al., 2020). Consequently, they are essential inputs for researchers and practitioners who aim to predict the Earth's response to changing climate conditions, and thus provide vital information for stakeholders and policy makers (see, e.g., their prominence in the consequential IPCC reports, Intergovernmental Panel on Climate Change (IPCC), 2023).

One of the most significant limitations of GCMs is their computational cost. They use complex mathematical algorithms to simulate the various processes involved in the Earth's climate system, which results in a high demand for memory and processing power. Despite access to some of the world's largest and most advanced computational infrastructure, the execution of long-term simulations can take months. Furthermore, the large amounts of data generated by these simulations require substantial storage capacity. These practical constraints have hindered progress in increasing the resolution of GCMs. As a result, most GCM outputs are limited to daily time steps, and relatively coarse grids (in the order of 0.5° to 2.2°).

To mitigate the limitations presented by low model resolution, researchers frequently downscale GCM outputs before using them as inputs for climate impact studies. Regional Climate Models (RCMs) fill this gap by solving the atmospheric physics at higher spatial and temporal resolutions (e.g., Sørland et al., 2021) in what is commonly referred to as dynamical downscaling. Despite their high computational cost, modellers have vastly extended the coverage and resolution of RCMs in recent decades, now covering nearly the entire global landmass at resolutions of 11-44 km and daily time steps (Giorgi, 2019; Sørland et al., 2021; Tapiador et al., 2020).

Some issues, however, require much finer climate representations. Mountainous regions exemplify this, with climates that can vary dramatically over short distances and timeframes. As a consequence, the coarse resolutions offered by GCMs or RCMs are inadequate to characterize the hydrology of these complex domains. This has ramifications for our comprehension of climate change impacts, particularly in regions like the Swiss Alps where the interplay of elevation, topography, and hydrology is complex (Smiatek & Kunstmann, 2019; Teutschbein & Seibert, 2012). Conversely, a high-resolution representation of climate variables, and of the hydrological response, is essential to improve our understanding of hydrological dynamics of these complex environments (Daly et al., 2017; He et al., 2019; Xu & Di Vittorio, 2021; Zhu et al., 2023), and can signify a step-change in the accuracy and meaningfulness of hydrological projections.

A separate set of challenges is posed by attempting to represent extreme meteorological events—such as intense rainfall, prolonged droughts, or scorching heatwaves—which significantly impact hydrological responses. In statistical sciences, these rare events are usually studied through 'extreme value analysis' where the most extreme occurrences are extracted from long time series data are used to calibrate statistical models for reliable risk assessments (Coles, 2001). When only short time series are available, however, the results are highly uncertain and are therefore unsuitable to inform decisions. Moreover, the requirement for long time series considering climate change conflicts with a key assumption in extreme value analysis: stationarity of the underlying population distribution. In other words,

this means that the entire time series must be representative of a particular climate condition which, in the context of a rapidly changing climate, is untenable. In theory, this paradox could be resolved by simulating a large enough number of time series that represent the same climate conditions, starting from different but plausible initial conditions, which is what Single Model Initial-Condition Large Ensembles (SMILEs) aim to do (Deser et al., 2020; Lehner et al., 2020; Maher et al., 2021; Milinski et al., 2020; Wyser et al., 2021). These large ensembles could be used to extract numerous realizations of 20-30 years-long records, offering a pragmatic solution by assuming quasi-stationarity over these shorter periods and allowing for a robust statistical analysis of extremes. Notwithstanding, we do not yet have the capabilities to downscale these large ensembles (whose horizontal resolution range from ~2.8 to ~1°) to fine resolutions using dynamical climate models due to the large computational demands of RCMs, thus limiting their direct application on impact assessment studies.

1.1.3 The uncertainty of change

"The only constant is change" – Heraclitus

The ancient wisdom of Heraclitus underscores the inherent unpredictability of our world, a sentiment that resonates deeply when discussing the uncertainties of climate change. Understanding the nature of uncertainty is crucial for making informed decisions, especially as we strive for science-informed climate change policies, . For instance, while quantifying the vast uncertainties in climate projections is a recognized challenge (Hoegh-Guldberg et al., 2018), climate impact studies often fail to communicate uncertainty effectively (Kause et al., 2021), or neglect it altogether.

Three main factors drive the uncertainty of climate projections (Deser, 2020; Deser, et al., 2012; Hawkins & Sutton, 2011; Fatichi et al., 2016):

- **Emission scenarios**: We cannot precisely forecast future greenhouse gas emissions due to unpredictable technological and policy changes.
- **Climate model uncertainties**: Climate models are not perfect and cannot perfectly simulate the complex real world, and each model attempts to represent complex physical processes using their own unique set of equations.
- **Stochastic uncertainty**: It refers to the innate randomness, or 'internal climate variability,' within climate systems. Unlike deterministic processes, where outcomes can be precisely predicted, certain aspects of climate can only be understood as stochastic processes, which are inherently probabilistic and unpredictable.

Quantifying the contribution of its sources is crucial to addressing the uncertainty of climate projections. This exercise, known as uncertainty partition (Fatichi et al., 2016; Hawkins & Sutton, 2011; Lehner et al., 2020), can inform researchers about which parts of the modelling chain introduce the most uncertainty into the projections. It can also help determine how much of the uncertainty is due to factors that we can improve, such as quantification of emissions and representativeness of climate models, and how much is due to irreducible stochastic uncertainty. However, uncertainty partitioning can be challenging due to the need for long records. Obtaining such data can be particularly difficult in regions or periods with limited observational records, which can lead to incomplete or biased assessments of climate patterns and future projections. Furthermore, quantifying the uncertainty around statistics for extreme events, which themselves require long and stationary records, is simply not possible without the aid of multiple realizations of robust climate models. And this is, as argued further above, not yet feasible.

1.1.4 Statistical downscaling of climate

While dynamical downscaling models, such as RCMs, are indispensable for understanding regional-scale impacts of climate change, they may not fully address the challenges of enhancing the resolution of climate data and extending climate records and simulations. Statistical downscaling methods emerge as valuable tools in this context, utilizing statistical relationships between coarse atmospheric variables and local observations to interpolate and extrapolate climate data to a finer resolution. Unlike dynamical downscaling, which is grounded in the numerical modelling of physical processes, statistical downscaling is rooted in observed data patterns. Its primary goal is to interpolate and extrapolate climate data from coarse-resolution datasets to a finer resolution, making it especially valuable for heterogeneous terrains like mountains. Thus, statistical downscaling can either complement or serve as an alternative to dynamical downscaling methods, offering a tailored approach to predicting future climate at a high resolution (Maraun et al., 2010). However, statistical downscaling inherently relies on the assumption that historical climate relationships remain valid under future scenarios, a premise that may not hold due to the non-stationary nature of climate change. This limitation underscores the intrinsic challenges of representativeness in observation-based regression methods for future climates, as they may not accurately capture the dynamics of an evolving climate system.

Broadly, statistical downscaling methods can be classified as:

1. **Regression Models**: These models establish linear (or sometimes non-linear) statistical relationships between large-scale atmospheric predictors and local-scale climate variables. The foundation of regression models lies in the premise that local climate is influenced by broader atmospheric conditions, which can be captured through historical observations. By identifying and applying these statistical relationships, regression models can predict local climate conditions based on future projections or scenarios of large-scale atmospheric variables. However, one limitation is their assumption of stationarity in the relationship between large-scale drivers and local climate responses, which may not hold under changing climate conditions, potentially limiting their predictive accuracy in future scenarios.
2. **Weather Type Models**: These models categorize weather into distinct types or patterns based on observed atmospheric conditions, such as pressure configurations or wind patterns. Each weather type is associated with specific local climate characteristics. By analysing historical data, WTMs identify the frequency and climatic conditions associated with each weather type. For future projections, these models estimate changes in the frequency or characteristics of weather types based on changes in large-scale atmospheric conditions predicted by climate models.

1.1.5 Stochastic weather generators

Central to our discussion on climate uncertainty, stochastic weather generators offer an alternative to statistical methods by reproducing not only the signal in climate processes, but also the climate variability in the form a stochastic noise. Unlike the deterministic dynamical and statistical models, stochastic models are capable of simulating multiple realizations of possible weather sequences, allowing us to quantify the magnitude of stochastic uncertainty. This offers a deeper insight into the unpredictable nature of climate events and makes them particularly relevant for understanding rare events.

Additionally, Stochastic Weather Generators (WGs) are powerful tools to counteract the limitations set by scarce observational data and, by adapting their parameters, the assumptions of stationarity in extreme value analysis. Based on statistical methods, WGs can efficiently simulate random sequences of climate variables, most commonly precipitation,

which mimic the statistical properties and correlations of real-world observations. The generated data can then be used to extend the limited observational record, granting researchers the ability to conduct analyses and simulations that would otherwise be constrained by data availability. For instance, by means of proper reparameterization, WGs can generate long simulations that encapsulate the stochastic variability for different specific climate scenarios, allowing for a more comprehensive understanding of climate patterns and the potential impacts of changing climate conditions, and facilitating the statistical analysis of rare weather phenomena in future climates.

Many different weather generators were developed over the years, each with its own unique spatial and temporal scope, modelling philosophy, and intended application (Fowler et al., 2007; Wilks & Wilby, 1999). Given the already-stated importance of spatial resolution in hydrological impact analyses, let us introduce for now the three categories based on their spatial scope:

1. **Single-Site WG**: Focused on individual locations, these models typically derive their data from a single weather station, simulating climate statistics for one or more cross-correlated variables (e.g., Fatichi et al., 2011).
2. **Multi-Site WG**: An extension of the single-site concept, these models emulate the records from a station network, simulating climate statistics across multiple, interrelated points. This approach acknowledges the inter-site correlations of climate variables over expansive regions (e.g., Sparks et al., 2018; Steinschneider et al., 2019; Verdin et al., 2018).
3. **Two-Dimensional WG**: These models generate semi-continuous spatial fields, capturing the intricate spatial features of climate variables. Their design is particularly beneficial for scenarios where spatial variability plays a pivotal role. However, their intricate nature, combined with the need for extensive observational data, computational power, and storage, has led to fewer endeavours in their development. Notable models in this category include the STORM model (Singer et al., 2018) and AWE-GEN-2d (Peleg et al., 2017).

Given the challenges highlighted earlier—namely, the resolution of climate models, the analysis of extreme values, and the quantification of uncertainty—WGs emerge as an appealing solution. Their ability to simulate high-resolution climate time series, especially through two-dimensional models, directly addresses the spatial and temporal resolution issue. Furthermore, by generating extensive synthetic records, WGs allow researchers to delve deeper into uncertainty quantification and provide a robust platform for analysing extreme weather events.

1.1.6 Temperature and extreme precipitation

An additional challenge in the study of climate change is the widely observed dependence between air temperature and extreme precipitation. Rooted in thermodynamics, the Clausius-Clapeyron equation states that as air temperature increases, so does its water-holding capacity at a rate of approximately 7% per degree Celsius (e.g., O'Gorman & Schneider, 2009; Trenberth et al., 2003). This relationship has been widely observed in the increase of extreme precipitation, especially in areas prone to convective precipitation events (Ali et al., 2021a; Ali et al., 2021; Berg et al., 2013; Fischer & Knutti, 2016; Fowler et al., 2021; Molnar et al., 2015; Westra et al., 2014).

GCMs and RCMs rely on adopting simplified parametrizations, which often result in compromised estimates of sub-daily extremes and an unsatisfactory simulation of the observed temperature-scaling seen in empirical records (Ban et al., 2014; Fischer et al., 2015). Moreover, their spatial resolution is insufficient to portray convective processes, which results

in an underestimation of the effects of the Clausius-Clapeyron rate on extreme precipitation (Ban et al., 2018; Pichelli et al., 2021).

Conversely, dynamical convection-permitting models (CPMs) provide a solution to the limitations of traditional climate models by offering finer spatial resolutions (0.25–10 km^2), which allows for more accurate simulations of short-duration, convection-driven rainfall spells (Prein et al., 2020). CPMs demonstrate that such intense rainfall often originate from convective processes and project that temperature-scaling rates are likely to persist in future global warming contexts (Ban et al., 2018; Kendon et al., 2017; Pichelli et al., 2021; Vergara-Temprado et al., 2021), emphasizing the need to account for temperature-scaling in extreme rainfall projections.

However, CPMs are constrained by hefty computational requirements as much as other dynamical models. This typically limits their outputs to short and singular simulations of few climate variables (Gutowski et al., 2020; Schär et al., 2020), thus hindering a comprehensive analysis of extreme events or evaluations of projection uncertainties. Recognizing this limitation, weather generators (WGs) are a valuable alternative to produce extensive climate records without the computational burden of CPMs and, ideally, can be formulated to account for the temperature dependence of precipitation. In such case, WGs would offer the best of both worlds: the ability to generate large, high-resolution ensembles of climate data while also capturing the main features of climate dynamics and how they relate to changes in temperature. However, as it stands, such a tool is yet to be developed.

1.2 THESIS OBJECTIVE AND RESEARCH QUESTIONS

This thesis was conceived within the framework of the Hydro-CH2018 project (National Centre for Climate Services NCCS, n.d.), an effort aimed to update the hydrological scenarios of Switzerland under climate change. This initiative is an attempt to bring together and develop state-of-the-art datasets, numerical models, and analysis techniques. Its goal is to enhance our hydrological understanding to inform effective climate change mitigation and adaptation strategies. In support of Hydro-CH2018's objectives and motivated by the essential role of mountainous regions in global water cycles, I aim **to enhance the estimation of climate change impacts on the hydrological responses of mountainous catchments**.

As underscored by the preceding sections, tackling this issue requires addressing multiple complexities and challenges. Notably, there is a need to improve the tools and methodologies currently in use to investigate climate change impacts, especially at relatively small hydrological scales. Consequently, I set out to address the following research gaps:

I. **High Resolution Climate Scenarios**: High-resolution data is essential, particularly in areas with complex landscapes like mountainous regions. Climate effects vary at different scales and are highly sensitive to catchment elevation, so coarse datasets can miss details crucial for understanding climate impacts.
II. **Uncertainty in Hydrological Projections**: While uncertainty is inherent to any climate projection, its propagation into the hydrological response and partition of its components has not been adequately addressed.
III. **Impacts of Rising Temperatures on Extreme Rainfall**: There is a pressing need for modelling tools that can represent how rising temperatures influence extreme precipitation events based on physical relations, while capable of producing long, high-resolution simulations.

Specifically, this work focuses on an in-depth analysis of two mesoscale catchments located in the Swiss Alps: The Thur and the Kleine Emme, which are elaborated upon in Chapter 2.

These catchments were selected as they exemplify sites with complex topography and wide elevation ranges, making them prime candidates to advance knowledge about the hydrologic response of Alpine and pre-Alpine basins to climate change by means of novel downscaling techniques and high-resolution modelling. Moreover, the river networks in these catchments are mostly untouched. This makes them ideal case studies for undisturbed systems. Through these case studies, I look to answer the following research questions:

RQ1. **What will be the response of small-scale Alpine catchments to climate change?** This question aims to elucidate the interplay between changing precipitation patterns, snowmelt processes, and evapotranspiration across different elevations and their cumulative impact on hydrological responses. To answer it, the thesis sets the following research objectives:

- Develop and validate a framework that leverages the capabilities of an advanced weather generator to simulate large ensembles of high-resolution climate data.
- Characterize the small-scale hydrological response of Alpine catchments to climate change.
- Quantify the impact of climate change on extreme hydrological events in Alpine catchments.

RQ2. **What is the magnitude and the potential to narrow the uncertainty in climate and hydrological projections?** This question seeks to refine our understanding and methods for dealing with the inherent uncertainties in climate modelling, aiming for a clearer distinction between reducible and stochastic uncertainties. In answering it, the following objectives are achieved:

- Quantify the uncertainty in climate projections and their propagation into the hydrological response across mountainous catchments.
- Estimate the contribution of internal climate variability to assess the potential for narrowing the uncertainty in hydrological projections.

RQ3. **How will the increase in temperature affect hydrological extremes in future climates?** Through this question, the research investigates the implications of increased extreme rainfall events due to the Clausius-Clapeyron relation. on hydrological systems, especially considering the potential for more severe and frequent flooding events. The question relates to the following objectives:

- Develop a new version of a stochastic weather generator capable of simulating realistic temperature-conditioned precipitation properties.
- Measure the effect of increasing temperature on the intensification of extreme rainfall in the Alps.
- Compare the hydrological impacts estimated with and without considering temperature-conditioned precipitation properties.

1.3 OUTLINE

To answer these questions, I present a novel methodology and improved numerical models that allow a comprehensive estimation of hydrological projections, thus directly contributing to the aims of Hydro-CH2018. First, I introduce a new modelling framework. It integrates outputs from multiple RCMs to account for the role of climate projection uncertainty on the impact of basin hydrology, a two-dimensional weather generator to account for intrinsic climate variability and its interplay with climate projections variability on basin hydrology impacts, and a physically based hydrological model to enable the separation of climate change impacts on precipitation-runoff transformation components and on their propagation and transformation across the basin. The modelling framework acts as a virtual laboratory that allows simulating large ensembles of high-resolution climate and hydrological data under a broad set of forcing

climate scenarios. This framework is detailed in Chapter 2—based on the published work by Moraga et al. (2021)—which shows how it is used to characterize the impact of climate change on the hydrology of the two study sites, thus answering RQ1. In Chapter 3—which presents the work published by Moraga et al. (2022)—the generated ensembles are used to quantify and partition the uncertainty of climate and hydrological projections in order to answer RQ2. Chapter 4 presents an article currently in review, in which an updated version of the AWE-GEN-2d weather generator is developed and used to improve the characterization of extreme rainfall events. The performance of the new model is then showcased using the example of the Kleine Emme catchment, thereby answering RQ3. The concluding Chapter 5 summarizes the main results and highlights their relevance to the broader scientific field.

1.4 REFERENCES

Ali, H., Fowler, H.J., Lenderink, G., Lewis, E., Pritchard, D., 2021a. Consistent Large-Scale Response of Hourly Extreme Precipitation to Temperature Variation Over Land. Geophysical Research Letters 48, e2020GL090317. https://doi.org/10.1029/2020GL090317

Ali, H., Peleg, N., Fowler, H.J., 2021b. Global Scaling of Rainfall With Dewpoint Temperature Reveals Considerable Ocean-Land Difference. Geophysical Research Letters 48, e2021GL093798. https://doi.org/10.1029/2021GL093798

Ban, N., Rajczak, J., Schmidli, J., Schär, C., 2018. Analysis of Alpine precipitation extremes using generalized extreme value theory in convection-resolving climate simulations. Climate Dynamics 1–15. https://doi.org/10.1007/s00382-018-4339-4

Ban, N., Schmidli, J., Schär, C., 2014. Evaluation of the convection-resolving regional climate modeling approach in decade-long simulations. Journal of Geophysical Research: Atmospheres 119, 7889–7907. https://doi.org/10.1002/2014JD021478

Ban, N., Schmidli, J., Schär, C., 2015. Heavy precipitation in a changing climate: Does short-term summer precipitation increase faster? Geophysical Research Letters 42, 1165–1172. https://doi.org/10.1002/2014GL062588

Bao, J., Sherwood, S.C., Alexander, L.V., Evans, J.P., 2017. Future increases in extreme precipitation exceed observed scaling rates. Nature Climate Change 7, 128–132. https://doi.org/10.1038/nclimate3201

Barbero, R., Fowler, H.J., Lenderink, G., Blenkinsop, S., 2017. Is the intensification of precipitation extremes with global warming better detected at hourly than daily resolutions? Geophysical Research Letters 44, 974–983. https://doi.org/10.1002/2016GL071917

Beniston, M., Farinotti, D., Stoffel, M., Andreassen, L.M., Coppola, E., Eckert, N., Fantini, A., Giacona, F., Hauck, C., Huss, M., Huwald, H., Lehning, M., López-Moreno, J.-I., Magnusson, J., Marty, C., Morán-Tejéda, E., Morin, S., Naaim, M., Provenzale, A., Rabatel, A., Six, D., Stötter, J., Strasser, U., Terzago, S., Vincent, C., 2018. The European mountain cryosphere: a review of its current state, trends, and future challenges. The Cryosphere 12, 759–794. https://doi.org/10.5194/tc-12-759-2018

Berg, P., Moseley, C., Haerter, J.O., 2013. Strong increase in convective precipitation in response to higher temperatures. Nature Geoscience 6, 181–185. https://doi.org/10.1038/ngeo1731

Blöschl, G., Hall, J., Parajka, J., Perdigão, R.A.P., Merz, B., Arheimer, B., Aronica, G.T., Bilibashi, A., Bonacci, O., Borga, M., Čanjevac, I., Castellarin, A., Chirico, G.B., Claps, P., Fiala, K., Frolova, N., Gorbachova, L., Gül, A., Hannaford, J., Harrigan, S., Kireeva, M., Kiss,

A., Kjeldsen, T.R., Kohnová, S., Koskela, J.J., Ledvinka, O., Macdonald, N., Mavrova-Guirguinova, M., Mediero, L., Merz, R., Molnar, P., Montanari, A., Murphy, C., Osuch, M., Ovcharuk, V., Radevski, I., Rogger, M., Salinas, J.L., Sauquet, E., Šraj, M., Szolgay, J., Viglione, A., Volpi, E., Wilson, D., Zaimi, K., Živković, N., 2017. Changing climate shifts timing of European floods. Science 357, 588–590. https://doi.org/10.1126/science.aan2506

Blöschl, G., Hall, J., Viglione, A., Perdigão, R.A.P., Parajka, J., Merz, B., Lun, D., Arheimer, B., Aronica, G.T., Bilibashi, A., Boháč, M., Bonacci, O., Borga, M., Čanjevac, I., Castellarin, A., Chirico, G.B., Claps, P., Frolova, N., Ganora, D., Gorbachova, L., Gül, A., Hannaford, J., Harrigan, S., Kireeva, M., Kiss, A., Kjeldsen, T.R., Kohnová, S., Koskela, J.J., Ledvinka, O., Macdonald, N., Mavrova-Guirguinova, M., Mediero, L., Merz, R., Molnar, P., Montanari, A., Murphy, C., Osuch, M., Ovcharuk, V., Radevski, I., Salinas, J.L., Sauquet, E., Šraj, M., Szolgay, J., Volpi, E., Wilson, D., Zaimi, K., Živković, N., 2019. Changing climate both increases and decreases European river floods. Nature 573, 108–111. https://doi.org/10.1038/s41586-019-1495-6

Coles, S., 2001. An Introduction to Statistical Modeling of Extreme Values, Springer Series in Statistics. Springer London, London. https://doi.org/10.1007/978-1-4471-3675-0

Daly, C., Slater, M.E., Roberti, J.A., Laseter, S.H., Swift Jr, L.W., 2017. High-resolution precipitation mapping in a mountainous watershed: ground truth for evaluating uncertainty in a national precipitation dataset. International Journal of Climatology 37, 124–137. https://doi.org/10.1002/joc.4986

Deser, C., 2020. “Certain uncertainty: The role of internal climate variability in projections of regional climate change and risk management.” Earth’s Future 8. https://doi.org/10.1029/2020ef001854

Deser, C., Lehner, F., Rodgers, K.B., Ault, T.R., Delworth, T.L., DiNezio, P.N., Fiore, A.M., Frankignoul, C., Fyfe, J.C., Horton, D.E., Kay, J.E., Knutti, R., Lovenduski, N.S., Marotzke, J., McKinnon, K.A., Minobe, S., Randerson, J.T., Screen, J.A., Simpson, I.R., Ting, M., 2020. Insights from Earth system model initial-condition large ensembles and future prospects. Nature Climate Change. https://doi.org/10.1038/S41558-020-0731-2

Deser, C., Phillips, A., Bourdette, V., Teng, H., 2012. Uncertainty in climate change projections: The role of internal variability. Climate Dynamics 38, 527–546. https://doi.org/10.1007/s00382-010-0977-x

Fatichi, S., Ivanov, V.Y., Paschalis, A., Peleg, N., Molnar, P., Rimkus, S., Kim, J., Burlando, P., Caporali, E., 2016. Uncertainty partition challenges the predictability of vital details of climate change. Earth’s Future 4, 240–251. https://doi.org/10.1002/2015EF000336

Fischer, A.M., Keller, D.E., Liniger, M.A., Rajczak, J., Schär, C., Appenzeller, C., 2015. Projected changes in precipitation intensity and frequency in Switzerland: a multi-model perspective. International Journal of Climatology 35, 3204–3219. https://doi.org/10.1002/joc.4162

Fischer, E.M., Knutti, R., 2016. Observed heavy precipitation increase confirms theory and early models. Nature Climate Change 6, 986–991. https://doi.org/10.1038/nclimate3110

Floriancic, M.G., Berghuijs, W.R., Jonas, T., Kirchner, J.W., Molnar, P., 2020. Effects of climate anomalies on warm-season low flows in Switzerland. Hydrology and Earth System Sciences 24, 5423–5438. https://doi.org/10.5194/hess-24-5423-2020

Fowler, H.J., Blenkinsop, S., Tebaldi, C., 2007. Linking climate change modelling to impacts studies: recent advances in downscaling techniques for hydrological modelling. International Journal of Climatology 27, 1547–1578. https://doi.org/10.1002/joc.1556

Fowler, H.J., Lenderink, G., Prein, A.F., Westra, S., Allan, R.P., Ban, N., Barbero, R., Berg, P., Blenkinsop, S., Do, H.X., Guerreiro, S., Haerter, J.O., Kendon, E.J., Lewis, E., Schaer, C., Sharma, A., Villarini, G., Wasko, C., Zhang, X., 2021. Anthropogenic intensification of short-duration rainfall extremes 2, 107–122. https://doi.org/10.1038/s43017-020-00128-6

Gariano, S.L., Guzzetti, F., 2016. Landslides in a changing climate. Earth-Science Reviews 162, 227–252. https://doi.org/10.1016/j.earscirev.2016.08.011

Giorgi, F., 2019. Thirty Years of Regional Climate Modeling: Where Are We and Where Are We Going next? Journal of Geophysical Research: Atmospheres 124, 5696–5723. https://doi.org/10.1029/2018JD030094

Gobiet, A., Kotlarski, S., Beniston, M., Heinrich, G., Rajczak, J., Stoffel, M., 2014. 21st century climate change in the European Alps—A review. Science of The Total Environment 493, 1138–1151. https://doi.org/10.1016/j.scitotenv.2013.07.050

Gutowski, W.J., Ullrich, P.A., Hall, A., Leung, L.R., O'Brien, T.A., Patricola, C.M., Arritt, R.W., Bukovsky, M.S., Calvin, K.V., Feng, Z., Jones, A.D., Kooperman, G.J., Monier, E., Pritchard, M.S., Pryor, S.C., Qian, Y., Rhoades, A.M., Roberts, A.F., Sakaguchi, K., Urban, N., Zarzycki, C., 2020. The Ongoing Need for High-Resolution Regional Climate Models: Process Understanding and Stakeholder Information. Bulletin of the American Meteorological Society 101, E664–E683. https://doi.org/10.1175/BAMS-D-19-0113.1

Hawkins, E., Sutton, R., 2011. The potential to narrow uncertainty in projections of regional precipitation change. Climate Dynamics 37, 407–418. https://doi.org/10.1007/s00382-010-0810-6

He, C., Chen, F., Barlage, M., Liu, C., Newman, A., Tang, W., Ikeda, K., Rasmussen, R., 2019. Can Convection-Permitting Modeling Provide Decent Precipitation for Offline High-Resolution Snowpack Simulations Over Mountains? Journal of Geophysical Research: Atmospheres 124, 12631–12654. https://doi.org/10.1029/2019JD030823

Hirschberg, J., Fatichi, S., Bennett, G.L., McArdell, B.W., Peleg, N., Lane, S.N., Schlunegger, F., Molnar, P., 2020. Climate Change Impacts on Sediment Yield and Debris-Flow Activity in an Alpine Catchment. Journal of Geophysical Research: Earth Surface. https://doi.org/10.1029/2020jf005739

Hoegh-Guldberg, O., Jacob, D., Bindi, M., Brown, S., Camilloni, I., Diedhiou, A., Djalante, R., Ebi, K., Engelbrecht, F., Guiot, J., Hijioka, Y., Mehrotra, S., Payne, A., Seneviratne, S.I., Thomas, A., Warren, R., Zhou, G., Halim, S.A., Achlatis, M., Alexander, L.V., Allen, M., Berry, P., Boyer, C., Byers, E., Brilli, L., Buckeridge, M., Cheung, W., Craig, M., Ellis, N., Evans, J., Fischer, H., Fraedrich, K., Fuss, S., Ganase, A., Gattuso, J.P., Greve, P., Bolaños, T.G., Hanasaki, N., Hasegawa, T., Hayes, K., Hirsch, A., Jones, C., Jung, T., Kanninen, M., Krinner, G., Lawrence, D., Lenton, T., Ley, D., Liverman, D., Mahowald, N., McInnes, K., Meissner, K.J., Millar, R., Mintenbeck, K., Mitchell, D., Mix, A.C., Notz, D., Nurse, L., Okem, A., Olsson, L., Oppenheimer, M., Paz, S., Petersen, J., Petzold, J., Preuschmann, S., Rahman, M.F., Rogelj, J., Scheuffele, H., Schleussner, C.-F., Scott, D., Séférian, R., Sillmann, J., Singh, C., Slade, R., Stephenson, K., Stephenson, T., Sylla, M.B., Tebboth, M., Tschakert, P., Vautard, R., Wartenburger, R., Wehner, M., Weyer, N.M., Whyte, F., Yohe, G., Zhang, X., Zougmoré, R.B., 2018. Impacts of 1.5°C Global Warming on Natural and Human Systems.

Huddleston, B., Ataman, E., Bloise, M., Bel, J., Franceschini, G., 2003. Towards a GIS-based analysis of mountain environments and populations 34.

Huss, M., Bookhagen, B., Huggel, C., Jacobsen, D., Bradley, R. s., Clague, J. j., Vuille, M., Buytaert, W., Cayan, D. r., Greenwood, G., Mark, B. g., Milner, A. m., Weingartner, R., Winder, M., 2017. Toward mountains without permanent snow and ice. Earth's Future 5, 418–435. https://doi.org/10.1002/2016EF000514

Immerzeel, W.W., Lutz, A.F., Andrade, M., Bahl, A., Biemans, H., Bolch, T., Hyde, S., Brumby, S., Davies, B.J., Elmore, A.C., Emmer, A., Feng, M., Fernández, A., Haritashya, U., Kargel, J.S., Koppes, M., Kraaijenbrink, P.D.A., Kulkarni, A.V., Mayewski, P.A., Nepal, S., Pacheco, P., Painter, T.H., Pellicciotti, F., Rajaram, H., Rupper, S., Sinisalo, A., Shrestha, A.B., Viviroli, D., Wada, Y., Xiao, C., Yao, T., Baillie, J.E.M., 2020. Importance and vulnerability of the world's water towers. Nature 577, 364–369. https://doi.org/10.1038/s41586-019-1822-y

Intergovernmental Panel on Climate Change (IPCC), 2023. Climate Change 2022 – Impacts, Adaptation and Vulnerability: Working Group II Contribution to the Sixth Assessment Report of the Intergovernmental Panel on Climate Change, 1st ed. Cambridge University Press. https://doi.org/10.1017/9781009325844

Jenicek, M., Seibert, J., Staudinger, M., 2018. Modeling of Future Changes in Seasonal Snowpack and Impacts on Summer Low Flows in Alpine Catchments. Water Resources Research 54, 538–556. https://doi.org/10.1002/2017WR021648

Kapos, V., Rhind, J., Edwards, M., Price, M.F., Ravilious, C., 2000. Developing a map of the world's mountain forests. Forests in sustainable mountain development: a state of knowledge report for 2000. Task Force on Forests in Sustainable Mountain Development., IUFRO Research Series 4–19. https://doi.org/10.1079/9780851994468.0004

Kause, A., Bruin, W.B. de, Domingos, S., Mittal, N., Lowe, J., Fung, F., 2021. Communications about uncertainty in scientific climate-related findings: a qualitative systematic review. Environ. Res. Lett. 16, 053005. https://doi.org/10.1088/1748-9326/abb265

Kendon, E.J., Ban, N., Roberts, N.M., Fowler, H.J., Roberts, M.J., Chan, S.C., Evans, J.P., Fosser, G., Wilkinson, J.M., 2017. Do Convection-Permitting Regional Climate Models Improve Projections of Future Precipitation Change? Bulletin of the American Meteorological Society 98, 79–93. https://doi.org/10.1175/BAMS-D-15-0004.1

Kharin, V.V., Zwiers, F.W., Zhang, X., Wehner, M., 2013. Changes in temperature and precipitation extremes in the CMIP5 ensemble. Climatic Change 119, 345–357. https://doi.org/10.1007/s10584-013-0705-8

Körner, C., 2004. Mountain Biodiversity, Its Causes and Function. ambi 33, 11–17. https://doi.org/10.1007/0044-7447-33.sp13.11

Körner, C., Paulsen, J., Spehn, E.M., 2011. A definition of mountains and their bioclimatic belts for global comparisons of biodiversity data. Alp Botany 121, 73. https://doi.org/10.1007/s00035-011-0094-4

Larsen, I.J., Montgomery, D.R., Greenberg, H.M., 2014. The contribution of mountains to global denudation. Geology 42, 527–530. https://doi.org/10.1130/G35136.1

Lehner, F., Deser, C., Maher, N., Marotzke, J., Fischer, E., Brunner, L., Knutti, R., Hawkins, E., 2020. Partitioning climate projection uncertainty with multiple Large Ensembles and CMIP5/6. Earth System Dynamics Discussions 11, 1–28. https://doi.org/10.5194/esd-2019-93

Lenderink, G., Barbero, R., Loriaux, J.M., Fowler, H.J., 2017. Super-Clausius–Clapeyron Scaling of Extreme Hourly Convective Precipitation and Its Relation to Large-Scale Atmospheric Conditions. Journal of Climate 30, 6037–6052. https://doi.org/10.1175/JCLI-D-16-0808.1

Maher, N., Milinski, S., Ludwig, R., 2021. Large ensemble climate model simulations: introduction, overview, and future prospects for utilising multiple types of large ensemble. Earth System Dynamics 12, 401–418. https://doi.org/10.5194/esd-12-401-2021

Maraun, D., Wetterhall, F., Ireson, A.M., Chandler, R.E., Kendon, E.J., Widmann, M., Brienen, S., Rust, H.W., Sauter, T., Themel, M., Venema, V.K.C., Chun, K.P., Goodess, C.M., Jones, R.G., Onof, C., Vrac, M., Thiele-Eich, I., 2010. Precipitation downscaling under climate change: Recent developments to bridge the gap between dynamical models and the end user. Reviews of Geophysics 48. https://doi.org/10.1029/2009RG000314

Mastrotheodoros, T., Pappas, C., Molnar, P., Burlando, P., Manoli, G., Parajka, J., Rigon, R., Szeles, B., Bottazzi, M., Hadjidoukas, P., Fatichi, S., 2020. More green and less blue water in the Alps during warmer summers. Nature Climate Change 10, 155–161. https://doi.org/10.1038/s41558-019-0676-5

Milinski, S., Maher, N., Olonscheck, D., 2020. How large does a large ensemble need to be. Earth System Dynamics Discussions. https://doi.org/10.5194/ESD-11-885-2020

Molnar, P., Fatichi, S., Gaál, L., Szolgay, J. and Burlando, P., 2015. Storm type effects on super Clausius–Clapeyron scaling of intense rainstorm properties with air temperature. Hydrology and Earth System Sciences, 19(4), pp.1753-1766

Moraga, J.S., Peleg, N., Molnar, P., Fatichi, S., Burlando, P., 2022. Uncertainty in high-resolution hydrological projections: Partitioning the influence of climate models and natural climate variability. Hydrological Processes 36, e14695. https://doi.org/10.1002/hyp.14695

National Centre for Climate Services NCCS (n.d.) Hydro-Ch2018 hydrological scenarios, National Centre for Climate Services NCCS. Available at: https://www.nccs.admin.ch/nccs/en/home/climate-change-and-impacts/hydro-ch2018-hydrological-scenarios.html (Accessed: 09 February 2024).

O'Gorman, P.A., Schneider, T., 2009. The physical basis for increases in precipitation extremes in simulations of 21st-century climate change. Proceedings of the National Academy of Sciences 106, 14773–14777. https://doi.org/10.1073/pnas.0907610106

Peleg, N., Fatichi, S., Paschalis, A., Molnar, P., Burlando, P., 2017. An advanced stochastic weather generator for simulating 2-D high-resolution climate variables. Journal of Advances in Modeling Earth Systems 9, 1595–1627. https://doi.org/10.1002/2016MS000854

Peleg, N., Marra, F., Fatichi, S., Molnar, P., Morin, E., Sharma, A., Burlando, P., 2018. Intensification of convective rain cells at warmer temperatures observed from high-resolution weather radar data. Journal of Hydrometeorology JHM-D-17-0158.1. https://doi.org/10.1175/JHM-D-17-0158.1

Pichelli, E., Coppola, E., Sobolowski, S., Ban, N., Giorgi, F., Stocchi, P., Alias, A., Belušić, D., Berthou, S., Caillaud, C., Cardoso, R.M., Chan, S., Christensen, O.B., Dobler, A., de Vries, H., Goergen, K., Kendon, E.J., Keuler, K., Lenderink, G., Lorenz, T., Mishra, A.N., Panitz, H.-J., Schär, C., Soares, P.M.M., Truhetz, H., Vergara-Temprado, J., 2021. The first multi-model ensemble of regional climate simulations at kilometer-scale resolution part 2: historical and

future simulations of precipitation. Clim Dyn 56, 3581–3602. https://doi.org/10.1007/s00382-021-05657-4

Prein, A.F., Rasmussen, R., Castro, C.L., Dai, A., Minder, J., 2020. Special issue: Advances in convection-permitting climate modeling. Clim Dyn 55, 1–2. https://doi.org/10.1007/s00382-020-05240-3

Savelsberg, J., Schillinger, M., Schlecht, I., Weigt, H., 2018. The Impact of Climate Change on Swiss Hydropower. Sustainability 10, 2541. https://doi.org/10.3390/su10072541

Schär, C., Fuhrer, O., Arteaga, A., Ban, N., Charpilloz, C., Girolamo, S.D., Hentgen, L., Hoefler, T., Lapillonne, X., Leutwyler, D., Osterried, K., Panosetti, D., Rüdisühli, S., Schlemmer, L., Schulthess, T.C., Sprenger, M., Ubbiali, S., Wernli, H., 2020. Kilometer-Scale Climate Models: Prospects and Challenges. Bulletin of the American Meteorological Society 101, E567–E587. https://doi.org/10.1175/BAMS-D-18-0167.1

Scheidl, C., Heiser, M., Kamper, S., Thaler, T., Klebinder, K., Nagl, F., Lechner, V., Markart, G., Rammer, W., Seidl, R., 2020. The influence of climate change and canopy disturbances on landslide susceptibility in headwater catchments. Science of the Total Environment 742, 140588. https://doi.org/10.1016/j.scitotenv.2020.140588

Singer, M.B., Michaelides, K., Hobley, D.E.J., 2018. STORM 1.0: a simple, flexible, and parsimonious stochastic rainfall generator for simulating climate and climate change. Geoscientific Model Development 11, 3713–3726. https://doi.org/10.5194/gmd-11-3713-2018

Smiatek, G., Kunstmann, H., 2019. Simulating future runoff in a complex terrain alpine catchment with EURO-CORDEX data. J. Hydrometeorol. 20, 1925–1940. https://doi.org/10.1175/JHM-D-18-0214.1

Sørland, S.L., Brogli, R., Pothapakula, P.K., Russo, E., Van de Walle, J., Ahrens, B., Anders, I., Bucchignani, E., Davin, E.L., Demory, M.-E., Dosio, A., Feldmann, H., Früh, B., Geyer, B., Keuler, K., Lee, D., Li, D., van Lipzig, N.P.M., Min, S.-K., Panitz, H.-J., Rockel, B., Schär, C., Steger, C., Thiery, W., 2021. COSMO-CLM regional climate simulations in the Coordinated Regional Climate Downscaling Experiment (CORDEX) framework: a review. Geoscientific Model Development 14, 5125–5154. https://doi.org/10.5194/gmd-14-5125-2021

Sparks, N. J., Hardwick, S. R., Schmid, M., Toumi, R., 2018. IMAGE: a multivariate multi-site stochastic weather generator for European weather and climate. Stochastic environmental research and risk assessment, 32, 771-784.

Steinschneider, S., Ray, P., Rahat, S.H. Kucharski, J., 2019. A weather-regime-based stochastic weather generator for climate vulnerability assessments of water systems in the western United States. Water Resources Research, 55(8), pp.6923-6945.

Syvitski, J.P.M., Vörösmarty, C.J., Kettner, A.J., Green, P., 2005. Impact of Humans on the Flux of Terrestrial Sediment to the Global Coastal Ocean. Science 308, 376–380. https://doi.org/10.1126/science.1109454

Tapiador, F.J., Navarro, A., Moreno, R., Sánchez, J.L., García-Ortega, E., 2020. Regional climate models: 30 years of dynamical downscaling. Atmospheric Research 235, 104785. https://doi.org/10.1016/j.atmosres.2019.104785

Tokarska, K.B., Stolpe, M.B., Sippel, S., Fischer, E.M., Smith, C.J., Lehner, F. Knutti, R., 2020. Past warming trend constrains future warming in CMIP6 models. Science advances, 6(12), p.eaaz9549.

Trenberth, K.E., Dai, A., Rasmussen, R.M., Parsons, D.B., 2003. The changing character of precipitation. Bulletin of the American Meteorological Society 84, 1205-1217+1161. https://doi.org/10.1175/BAMS-84-9-1205

Verdin, A., Rajagopalan, B., Kleiber, W., Podestá, G. Bert, F., 2018. A conditional stochastic weather generator for seasonal to multi-decadal simulations. Journal of Hydrology, 556, pp.835-846.Vergara-Temprado, J., Ban, N., Schär, C., 2021. Extreme Sub-Hourly Precipitation Intensities Scale Close to the Clausius-Clapeyron Rate Over Europe. Geophysical Research Letters 48, e2020GL089506. https://doi.org/10.1029/2020GL089506

Viviroli, D., Kummu, M., Meybeck, M., Kallio, M., Wada, Y., 2020. Increasing dependence of lowland populations on mountain water resources. Nat Sustain 3, 917–928. https://doi.org/10.1038/s41893-020-0559-9

Viviroli, D., Weingartner, R., 2004. The hydrological significance of mountains: from regional to global scale. Hydrol. Earth Syst. Sci. 8, 1017–1030. https://doi.org/10.5194/hess-8-1017-2004

Weingartner, R., Schädler, B., Hänggi, P., 2013. Auswirkungen der Klimaänderung auf die schweizerische Wasserkraftnutzung. Geographica Helvetica 68, 239–248. https://doi.org/10.5194/gh-68-239-2013

Weingartner, R., Viviroli, D., Schädler, B., 2007. Water resources in mountain regions: a methodological approach to assess the water balance in a highland-lowland-system. Hydrological Processes 21, 578–585. https://doi.org/10.1002/hyp.6268

Westra, S., Fowler, H.J., Evans, J.P., Alexander, L.V., Berg, P., Johnson, F., Kendon, E.J., Lenderink, G., Roberts, N.M., 2014. Future changes to the intensity and frequency of short-duration extreme rainfall. Reviews of Geophysics 52, 522–555. https://doi.org/10.1002/2014RG000464

Wilks, D.S., Wilby, R.L., 1999. The weather generation game: a review of stochastic weather models. Progress in Physical Geography: Earth and Environment 23, 329–357. https://doi.org/10.1177/030913339902300302

World Energy Council, 2016. World energy resources 2016. World Energy Council, London, UK.

Wyser, K., Koenigk, T., Fladrich, U., Fuentes-Franco, R., Karami, M., Kruschke, T., 2021. The SMHI Large Ensemble (SMHI-LENS) with EC-Earth3.3.1. Geoscientific Model Development. https://doi.org/10.5194/GMD-14-4781-2021

Xu, Z., Di Vittorio, A., 2021. Hydrological analysis in watersheds with a variable-resolution global climate model (VR-CESM). Journal of Hydrology 601, 126646. https://doi.org/10.1016/j.jhydrol.2021.126646

Zhu, B., Xie, X., Wang, Y., Zhao, X., 2023. The Benefits of Continental-Scale High-Resolution Hydrological Modeling in the Detection of Extreme Hydrological Events in China. Remote Sensing 15, 2402. https://doi.org/10.3390/rs15092402

2 REVEALING THE IMPACTS OF CLIMATE CHANGE ON MOUNTAINOUS CATCHMENTS THROUGH HIGH-RESOLUTION MODELLING

Chapter based on the published article Moraga, J. S., Peleg, N., Fatichi, S., Molnar, P., & Burlando, P. (2021). Revealing the impacts of climate change on mountainous catchments through high-resolution modelling. **Journal of Hydrology**, 603, 126806. https://doi.org/10.1016/j.jhydrol.2021.126806

ABSTRACT

Mountainous catchments cover a broad range of elevations and their response to a warming climate is expected to vary significantly in space. Nevertheless, studies on climate change impacts typically examine the changes in flow statistics only at the catchment outlet. In this study, we instead demonstrate the high variability of the hydrological response to climate change at the sub-catchment scale, investigating in detail the contribution of all components of the hydrological cycle in two mountainous catchments (Thur and Kleine Emme) in the Swiss Alps. The analysis was conducted with a two-dimensional weather generator model that simulated gridded climate variables at an hourly and 2-km resolution until the end of the 21st century for the RCP8.5 emission scenario. The climate ensemble was used as input into a distributed hydrological model to estimate the changes in hydrological processes at 100-m and hourly resolutions. Climate models show that precipitation intensifies during winter but weakens during summer in the order of ±5–10% toward the end of the century. Temperature will rise by up to 4°C, leading to a 50% reduction in snowmelt, 10% increase in evapotranspiration, and shift in precipitation type from snowfall to rainfall. As a result, streamflow is projected to increase by 40% in winter but decrease by 20% to 40% during summer, with winter floods becoming more frequent. The changes to streamflow (mean and extreme low and high flows) at the sub-catchments show a strong dependency with elevation. In contrast to the small changes projected at the outlet of the catchments, streamflow shows a reduction at higher elevations (up to -20% change in mean streamflow for sub-catchments at elevations exceeding 1400 m) and an increase at lower elevations (up to +5% for Kleine Emme and +20% for the Thur at elevations below 600 m). These impacts are tied to the changes in precipitation, as well as changes in snowmelt (at high elevation) and evapotranspiration (at low elevation). The results reveal the causes and diversity of hydrological response to climate change, emphasizing the importance of investigating the distributed impacts of climate change in mountainous environments.

2.1 INTRODUCTION

Global warming is affecting hydrological processes in many regions and across various space-time scales. Mountainous catchments are no exception: a diminishing snow cover and glacier retreat (Blanc and Schaedler, 2014; Beniston et al., 2018; Bultot et al., 1994; Etter et al., 2017; Jenicek et al., 2018; Jörg-Hess et al., 2015), and changes in intense meteorological events, such as prolonged droughts and intensification of extreme precipitation (Ban et al., 2015; Bao et al., 2017; Fischer et al., 2015; Lenderink et al., 2017; Peleg et al., 2018; Westra et al., 2014), suggest that their hydrological cycle could undergo significant alterations. Among the expected consequences are increased hazards such as floods, low flows, landslides, or debris flows (Brunner et al., 2019; Floriancic et al., 2020; Gariano and Guzzetti, 2016; Hirschberg et al., 2020; Kos et al., 2016; Scheidl et al., 2020), which in turn can lead to serious impacts on infrastructure, irrigation demand, hydropower production, and tourism, with significant

economic consequences (Abegg et al., 2007; Zubler et al., 2015; Savelsberg et al., 2018; Weingartner et al., 2013). Adapting to these changes and mitigating their effects requires modelling the hydrological response of mountainous catchments at scales appropriate for the involved hydrological processes and suitable to represent the highly heterogeneous mountainous topography. This implies spatial resolutions in the order of kilometers and time steps of hours or less (e.g., Mastrotheodoros et al., 2020). Achieving this level of detail is challenging, as modelling at these fine scales demands substantial computational resources and large amounts of high-resolution observations to calibrate and validate models. Moreover, a changing climate means that relations between hydro-meteorological variables in the past may no longer hold in the future, questioning the validity of data-driven relations in predicting future behavior (Milly et al., 2008). Hence, the appeal of physically based distributed models for estimating the hydrological response to a changing climate.

Physically based (also known as process based) hydrological models are suited to estimate the hydrological response of catchments under changing climatic forcing (Fatichi et al., 2016). With little to no parameter calibration, they capture the dynamics of atmosphere-land interactions and reproduce them, in theory, for any catchment or climatic input. While spatially lumped hydrological models cannot reproduce the diversity of responses within the catchments, distributed models can provide a meaningful cause-and-effect association throughout the catchment (Mascaro et al., 2015). By forcing them with climate variables from climate models, physically based hydrological models can be used to compute the impact of global warming on other hydrological variables besides streamflow, such as soil moisture, snowmelt, and evapotranspiration (ET). This approach has provided valuable insights into, for example, the role of storm structure in runoff generation (Paschalis et al., 2014), the sensitivity of climate change response to the overall soil permeability of the catchment (Camici et al., 2017), the relation between runoff and elevation and its meaning for future hydropower production (Fatichi et al., 2015), and the detailed understanding of the eco-hydrological response to changing climate conditions (Mastrotheodoros et al., 2020).

The effects of global warming on individual climate variables are typically inferred from General Circulation Models (GCM) and Regional Climate Models (RCM), albeit at scales that make them unsuitable to study most hydrological processes, in particular at the scale that controls the response of mountainous catchments (Fatichi et al., 2013; Mateo et al., 2017). Therefore, downscaling of climate variables to suitable space-time scales is required (Smiatek and Kunstmann, 2019). This can be accomplished using stochastic weather generators (WG), as alternatives to other dynamic or statistical methods (see review papers by Fowler et al., 2007; Maraun et al., 2010; Trzaska and Schnarr, 2014). Using historical observations and GCM/RCM outputs, WGs combine physical relationships among climatic variables and a stochastic approach to generate synthetic time series that reproduce the statistics of the observed data, and once suitably re-parameterized, simulate climate variables for future periods (e.g., Fatichi et al., 2011; Fowler et al., 2007; Peleg et al, 2017; Semenov & Barrow, 1997; Wilks & Wilby, 1999; Wheater et al., 2005). Most WGs simulate climate variables at either the point scale (Fatichi et al., 2011; Parket al., 2018) or at multiple sites (Bordoy and Burlando, 2014; Keller et al., 2017, 2015). In recent years, two-dimensional WGs were developed, such as STORM (Singer et al., 2018; Singer and Michaelides, 2017) and AWE-GEN-2d (Peleg et al., 2017), capable of downscaling gridded climate variables. Besides downscaling, the purpose of WGs is to produce climatic ensembles, i.e. multiple realizations characterizing the climate conditions, which allows probabilistic analysis of change and quantification of uncertainty.

The present study aims to quantify the effects of climate change on hydrological processes in mountainous catchments and to assess how the hydrological response varies in space. We

hypothesize that the magnitude, and perhaps even the direction (signal), of change will be related to elevation, because some of the hydrological components that contribute to streamflow (e.g., evapotranspiration or snow accumulation and melt) are elevation-dependent. To that end, we combine a high-resolution gridded WG model (AWE-GEN-2d; Peleg et al., 2017) with a distributed hydrological model (Topkapi-ETH; Fatichi et al., 2015) to quantify the impacts of climate change within two mountainous catchments that are exemplary of typical mesoscale catchments in the European Alps. We estimate the impact of climate change throughout the 21st century on a broad range of hydrological processes, such as streamflow, evapotranspiration, soil moisture, and snow water equivalent, to explore (a) the contribution of catchment-wide hydrological processes to annual and seasonal streamflow change at the outlet; (b) the propagation of changes in extreme rainfall to floods, and whether flood changes follow the climatic signal in extreme rainfall; and (c) the signal of streamflow change in many sub-catchments at different elevations, identifying the main hydrological causal components, and answering the question if the signal at the outlets reflects the spatial variability of changes across the catchments.

2.2 METHODS

2.2.1 Study area and data

The Thur and Kleine Emme catchments, which represent typical mountainous sub-Alpine (non-glacierized) catchments, were chosen for this study (Figure A-1). The river regime of both catchments is close to natural. There are no reservoirs, artificial lakes or dams in either of the catchments, nor major withdrawals for irrigation or hydropower production. In addition, the catchments are glacier free.

The Thur catchment is located in the northeastern part of Switzerland (47.4°N, 9.1°E). It is a tributary of the Rhine, with a total drainage area of 1,730 km^2 and an elevation range between 359 and 2,434 m. The average precipitation over the catchment for the present climate is 1,350 mm y^{-1}, the average annual temperature is 8.4 °C, with average streamflow at the outlet of 46.7 $m^3 s^{-1}$ (851 mm yr^{-1}). The Kleine Emme catchment is located in central Switzerland (46.9°N, 8°E). It has a total drainage area of 477 km^2 and an elevation range between 430 and 2,330 m. The precipitation average over the catchment for the present climate is 1,650 mm y^{-1}, and the average streamflow at the outlet is 12.6 $m^3 s^{-1}$ (833 mm yr^{-1}). Except for small cropland areas and villages, the catchments are covered mostly by natural vegetation and pastures. Both catchments have already been studied in the context of climate change impacts in the Alpine domain (Addor et al., 2014; Brunner et al., 2019, 2018; Hakala et al., 2019; Keller et al., 2019; Middelkoop et al., 2001; Muelchi et al., 2020; Rössler et al., 2019).

Topographic information for both catchments was obtained by resampling a 25 m resolution digital elevation model (SwissTopo, 2002) to a 100 m x 100 m grid. Distributed land use information was obtained from the 100 m resolution Corine dataset (CLC, 2012) and soil information was extracted from the soil map of Switzerland (Bodeneignungskarte, 2012). Following Paschalis et al. (2014), the depths of the two top layers of soil for the hydrological model were set as part of the model parameterization, with the top of the groundwater layer set at a 2 m depth for zones nearby rivers and lakes, and at 5 m depth for the rest of the domain.

Meteorological data used for calibration and validation of the WG and the hydrological model (precipitation, temperature and sunshine hours) were obtained from the MeteoSwiss ground station network (SwissMetNet) at hourly resolution (Table A-1). Information on the rainfall spatial structure was derived from the MeteoSwiss C-band weather radar system (data at 2 km and 5 min, Germann et al., 2006). Hourly cloud cover data and geostrophic wind velocity

at 500 hPa were obtained from the MERRA-2 reanalysis dataset (Rienecker et al., 2011). Gridded datasets for temperature (TabsD) and precipitation (RhiresD) at 2 km and daily resolution were obtained from the MeteoSwiss archive (Wüest et al., 2009; MeteoSwiss 2016). Streamflow observations (Thur at Andelfingen and Kleine Emme at Emmen) were provided by the Swiss Federal Office for the Environment.

Nine climate projections obtained from GCM-RCM model-chains from the EURO-CORDEX archive (Jacob et al., 2014; Kotlarski et al., 2014), pre-processed by MeteoSwiss (CH2018, 2018), were used to compute Factors of Change (FC, see section 2.2.2) on a seasonal basis for 30-year moving windows every 10 years until the end of the century. They all follow the RCP8.5 emission scenario path and are available at a spatial resolution of 12.5 km x 12.5 km (Table A-2).

2.2.2 Weather generator

The AWE-GEN-2d model (Two-dimensional Advanced WEather GENerator; Peleg et al., 2017) was used to generate multiple time series at high space-time resolution (e.g., 2 km and 1 h) of the climate variables that are needed as inputs into the hydrological model. That includes precipitation, cloud cover, and near-surface air temperature at 2-m (referred to as temperature here). Based on ground observations of precipitation, the model reproduces the storm arrival (wet-dry durations) as an alternating-renewal process (Peleg and Morin, 2014). Precipitation and cloud fields are simulated jointly. During wet periods, areal statistics (wet area ratio, mean areal precipitation intensity, and cloud area ratio) are calibrated to replicate the storm structure observed by weather radars, while during dry periods the cloud area ratio is calibrated using satellite observations, which are also used to simulate the advection of clouds and precipitation. Near-surface air temperature is simulated for a reference elevation using estimated radiation that depends on the cloud cover generated in the previous step. This value is interpolated to the whole domain through a stochastic lapse rate calibrated by ground temperature observations. The model parameters, calibration and validation processes, and advantages and limitations of the approach are discussed by Peleg et al. (2017). The AWE-GEN-2d model was successfully applied to catchments of different sizes and for various climate regions (e.g., Nyman et al., 2021; Peleg et al., 2020; Skinner et al., 2020), and its validation for the catchments used in this study is presented in Section 2.3.1.

AWE-GEN-2d can be used to generate ensembles of present climate simulations, when calibrated with observed meteorological data. This enables us to represent the natural climate variability, which is a fundamental component to characterize hydrological uncertainties (Fatichi et al. 2014), especially for the extremes as presented in Molnar et al. (2020) and Ruiz-Villanueva and Molnar (2020). To simulate climate variables for future periods, the model is re-parameterized based on data from RCMs and using the FC approach (e.g., Bordoy and Burlando, 2014; Fatichi et al., 2011). FC consist of the ratio or difference between climate statistics estimated from the future and present climate simulations and can be used to force the change signal in AWE-GEN-2d simulations representative of the future. This method has been previously applied in AWE-GEN-2d by Peleg et al. (2019) to produce high-resolution future climate ensembles in a nearby study area.

2.2.3 Hydrological model

The Topkapi-ETH model (Fatichi et al., 2015) was applied to quantify the hydrological response of the catchments to climate change. It is a fully distributed hydrological model that simulates hydrological processes in a physically explicit manner. Surface topography is represented as a regular square grid of hillslope and channel cells, while the subsurface is discretized in three layers simulating the process of infiltration and lateral flow. The top two layers represent shallow and deep soil horizons, where the lateral flow is modelled by the

kinematic-wave approximation dependent on soil moisture content and soil hydraulic properties in hillslope cells (subsurface flow), and surface roughness and water depth and slope in hillslope and channel cells (overland flow and channel flow). The third layer represents the groundwater system and is modelled as a linear reservoir for flow between cells. The model simulates the lateral surface and subsurface flow between cells while considering vertical fluxes such as infiltration, exfiltration, ET, and snow and ice melt over each grid cell. The grids are connected in the surface and subsurface according to topographic gradients.

Topkapi-ETH was selected because it represents a reasonable compromise between a fully physically-based representation of hydrological processes and computational time for large domains (>1,000 km^2), which allows long-term (several decades) high-resolution (sub-kilometer grid cells, hourly time steps) distributed simulation (e.g., Battista et al., 2020a; Fatichi et al., 2015). It can preserve the effects of high-resolution topography, which is an important element of hydrological simulation in complex terrain that relies on representation of overland and channel flow (e.g., Battista et al., 2020). The model parameters, calibration and validation processes, as well as their advantages and limitations are discussed in detail by Fatichi et al. (2015). The model validation is presented in Section 2.3.2.

2.2.4 Experimental design

The numerical experiment performed in this study consisted of simulating large ensembles of climate data using AWE-GEN-2d, which were in turn used as inputs to Topkapi-ETH to obtain simulated present and future hydrological variables (Figure 2-1). As a first step, both models were calibrated independently to simulate the climate and hydrological variables for the current climate conditions. AWE-GEN-2d was calibrated and validated using climate observations obtained between 1982 and 2015, following the methodologies presented by Peleg et al. (2017). The simulated time series include hourly temperature (at a 100 m resolution), precipitation (at a 2 km resolution), and catchment-averaged cloud cover. The hydrological model was calibrated and validated with streamflow at the outlet of the catchments for the period between 2000 and 2009 using observed climate forcing, following the procedures presented by Pappas et al. (2015).

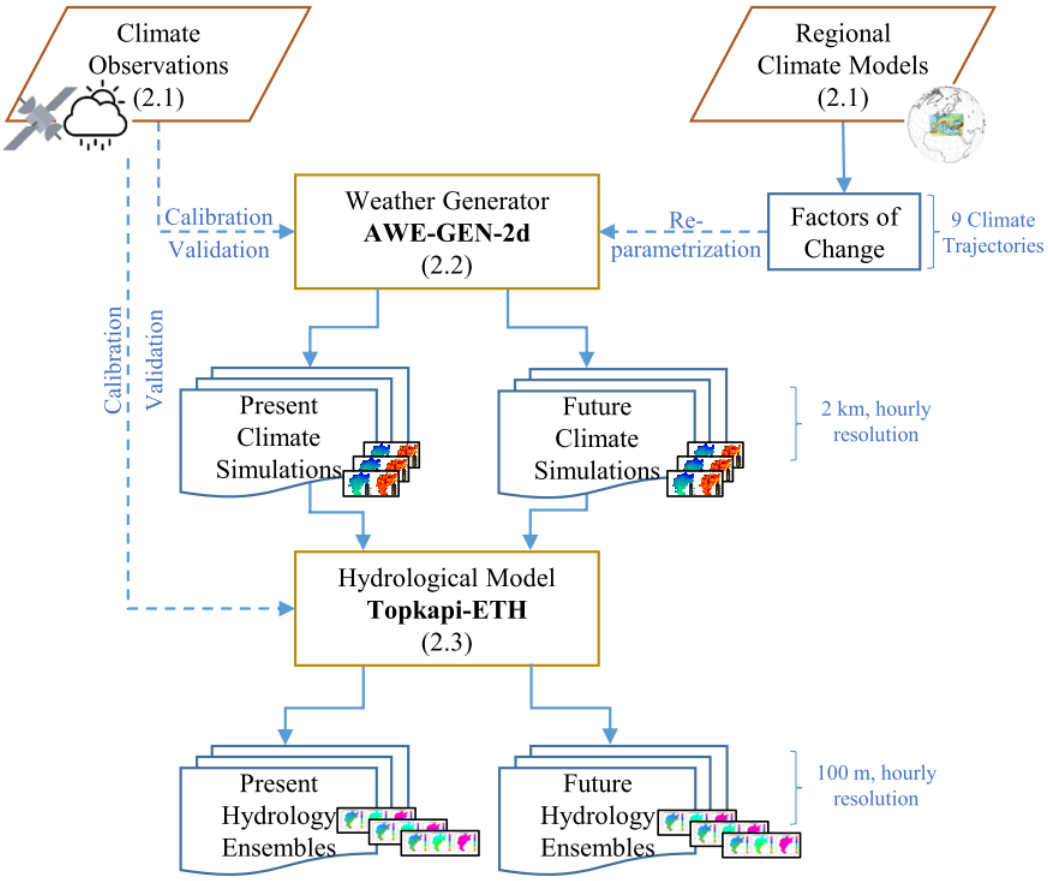

Figure 2-1: A schematic representation of the numerical experiment. Shown in parenthesis are numbers of the relevant sections describing a given component of the methodology.

In a second step, FC were computed for temperature and precipitation using the outputs of the climate models' simulations corresponding to their control (1976–2005) and future periods (2010–2089). Following Peleg et al. (2019), FC were used to re-parametrize AWE-GEN-2d to enable the simulations of continuous time series toward the end of the century. Two climate ensembles were simulated. The ensemble for the present climate consists of 15 realizations (replicates) of 30-years each. The ensemble for the future climate consists of 10 realizations of 80-years each, simulated for each of the nine climate model signals (90 trajectories in total). From this ensemble, the multi-model mean is computed as the average of the nine climate model trajectories and ten realizations. In total, the ensembles consist of 7,650 years of simulations for each catchment (30 x 15 + 80 x 9 x 10).

Third, hydrological ensembles were computed to obtain gridded simulations (at hourly and 100 m resolution) of streamflow, snow height, snowmelt, evapotranspiration (ET), and soil moisture, and point simulations of streamflow at the river network junctions for 97 and 145 sub-catchments in the Kleine Emme and the Thur, respectively (Figure A-2). The selected sub-catchments correspond to river reaches of Strahler order 2 or higher (Strahler, 1957) and can be nested in each other. Last, the impacts of climate change on snow depth, ET, and soil moisture, as well as on the streamflow (mean, minimum and maximum) within the catchments and at the outlet were estimated by comparing the present and future hydrological ensembles.

2.3 VALIDATION OF MODELS

2.3.1 AWE-GEN-2d

The calibration of AWE-GEN-2d requires extensive datasets, thus often leaving few available observations for the validation process. A common assumption and procedure in the validation of WGs is that of using the same dataset necessary for the calibration, but looking at different statistics and scales (Entekhabi et al., 1989; Peleg et al., 2017). For example, comparing the simulated mean annual temperature to the gridded TabsD product on a cell-to-cell basis reveals that most grid cells in Kleine Emme (73%) show a difference between observed and simulated temperatures smaller than 1°C (Figure A-3, all figures related to the WG validation are presented as Supplementary Information). The same applies to the Thur catchment, except for the high-mountain region in the south-east where the underestimation of the temperature can reach up to 3°C (Figure A-3). We also directly compared ground observations with the corresponding simulated grid cell in the domain and found that the WG model captures the observed temperature satisfactorily (Figure A-4): 97% of the simulated months for the Kleine Emme stations are within 1°C of the observed mean, while in Thur the percentage drops to 67%, with the largest mean errors found in Ebnat-Kappel (EBK, 2.5 °C) and the mountain station of Säntis (SAE, 2 °C), which are however still within natural climate variability at those sites. Examining the diurnal cycle of temperature (Figure A-5), we find that the timing of the simulated maximum and minimum daily temperatures agrees well with the observed data at all stations, with the largest mean offsets in hourly temperature of 0.6 °C in Pilatus (PIL, Kleine Emme) and 1.9 °C in Ebnat-Kappel (EBK, Thur).

The spatial distribution of precipitation (Figure A-6) is well captured in Kleine Emme. While there is a slight overestimation of the average precipitation in the WG model over the catchment in comparison to observations, the maximum overestimation is in the order of 4%, thus well within the typical measurement errors and the ~10% expected internal climate variability for annual precipitation in this region (Fatichi et al., 2016a). In the Thur catchment, the model slightly underestimates precipitation in the north (low elevation region) and overestimates precipitation in the southern (mountainous) part, with errors in the order of 3% and well within internal climate variability. On the one hand, the model successfully reproduces the seasonal dynamics in Luzern, Napf and Aadorf-Tänikon stations, while it shows discrepancies during the spring months in Ebnat-Kappel, although observations are still within the variability range of the ensemble simulations (Figure A-7). On the other hand, there are noticeable discrepancies for the stations Pilatus and Säntis where the model does not reproduce the recorded precipitation statistics well, although some discrepancy is expected due to the challenge of measuring precipitation in mountaintop stations. We also evaluated AWE-GEN-2d ability to reproduce extreme precipitation at the hourly scale (Figure A-8). The median extreme hourly precipitation computed from the simulation ensemble indicates that the model generally underestimates the extremes, but we note that (i) the observed line falls within the 5–95th ensemble range (for both Kleine Emme and Thur); and that (ii) there is considerable uncertainty in the estimates of observations as well. We also remark that AWE-GEN-2d was not calibrated to simulate sub-daily precipitation explicitly, but only on daily precipitation amounts.

2.3.2 Topkapi-ETH

Topkapi-ETH was validated at the hourly and monthly scales using streamflow observations at the outlet of the catchments for the 2000–2009 period. The overall agreement of the observed and simulated time series was quantified using the Nash–Sutcliffe Efficiency (NSE) index at the hourly scale, yielding values of 0.64 for Kleine Emme and 0.60 for Thur (Figure A-9). In both catchments, the model tends to slightly underestimate the hourly peak flow values

(Figure A-10). A closer inspection of the simulations shows that the shapes of the hydrographs are reasonably similar, even if in some cases the simulation reaches the peak earlier than the observation. Notwithstanding, the reproduced peak values are within the uncertainty range of the flood series statistical model, especially for return periods lower than 30 years. At the monthly scale (Figure A-11), Topkapi-ETH reaches NSE values of 0.76 and 0.78 for the Kleine Emme and Thur catchments, respectively, even though it underestimates mean flows for October and November in the Thur catchment (up to 13.6 $m^3 s^{-1}$).

While not perfect, we assess that the model characterizes the dynamics of streamflow correctly in terms of seasonality, the timing of the peaks, their magnitude, and hydrograph recessions. Furthermore, the NSE values are within the range obtained using other hydrological models such as HBV, PREVAH and WaSiM for the Thur catchment (0.86, 0.81, 0.70, respectively; Addor et al., 2014), while at the same time achieving good performance at the hourly scale. For sake of consistency and to remove the biases that the weather generated forcing may introduce, the results presented in the following sections are based on the comparison of simulations using the climate ensembles (future vs. present) as input, rather than on a comparison with observed data (i.e. future vs. observed-calibrated model). This is the standard approach anytime WG forcing is used in climate change studies (e.g., Addor et al., 2014; Camici et al., 2017; Fatichi et al., 2015).

2.4 RESULTS

We begin by presenting the results of the changes in climate at the catchment scale and how these changes are affecting the hydrological budget in the catchment and the streamflow at the outlet of the catchment (Section 4.1). Then, the changes to the hydrological budget and streamflow at many sub-catchments, and their relation with elevation, are presented (Section 4.2). All of the future climate statistics represent the multi-model mean, i.e., the combination of simulations using the nine future climate trajectories considered in this study (Table A-2).

2.4.1 Catchment-wide impacts of climate change

The changes in temperature and precipitation are presented in Figure 2-2. Temperature is projected to rise progressively throughout the century until reaching an increase in the order of 4° C in the period 2080-2089 in comparison to the present climate for both catchments. The increase in temperature affects all seasons with slightly higher increases in summer, and is relatively homogenous in space.

In contrast, the changes in precipitation vary in space and time. Precipitation decreases over the mountainous regions (southern areas of the catchments) and increases in the relatively low areas toward the outlets (northwest in the Thur and northeast in the Kleine Emme, Figure 2-2b, 2d). Winters are projected to be wetter, particularly in the Thur catchment, and summers are projected to be drier, especially in the Kleine Emme catchment. Overall, mean precipitation is expected to decrease by 6% in Kleine Emme and increase by 5% in Thur by the end of the century.

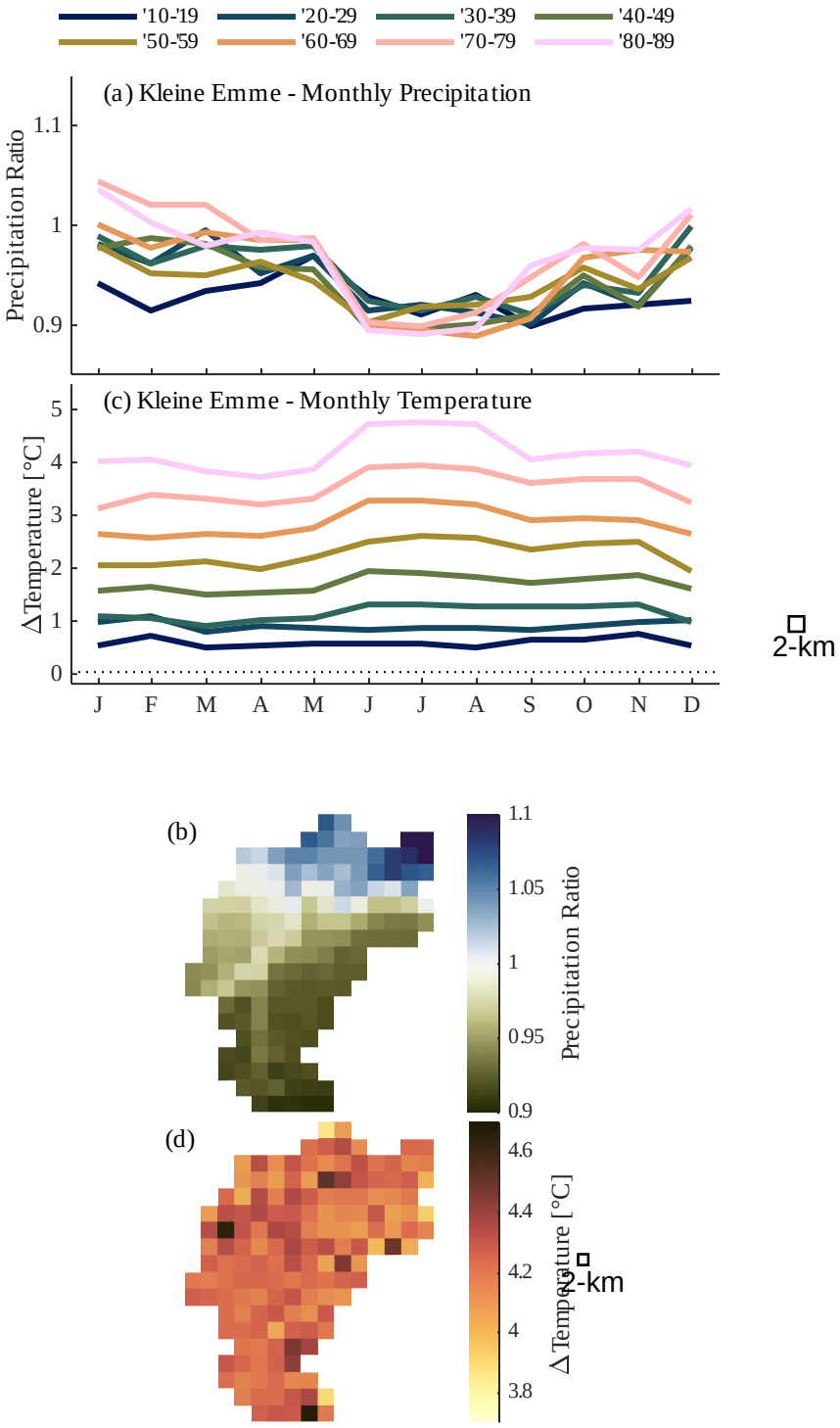
'10-'19
'20-'29
'30-'39
'40-'49
'50-'59
'60-'69
'70-'79
'80-'89
(a) Kleine Emme - Monthly Precipitation
Precipitation Ratio
1.1
1
0.9
(c) Kleine Emme - Monthly Temperature
ΔTemperature [°C]
5
4
3
2
1
0
J F M A M J J A S O N D
2-km
(b)
1.1
1.05
1
0.95
0.9
Precipitation Ratio
(d)
4.6
4.4
4.2
4
3.8
ΔTemperature [°C]
2-km

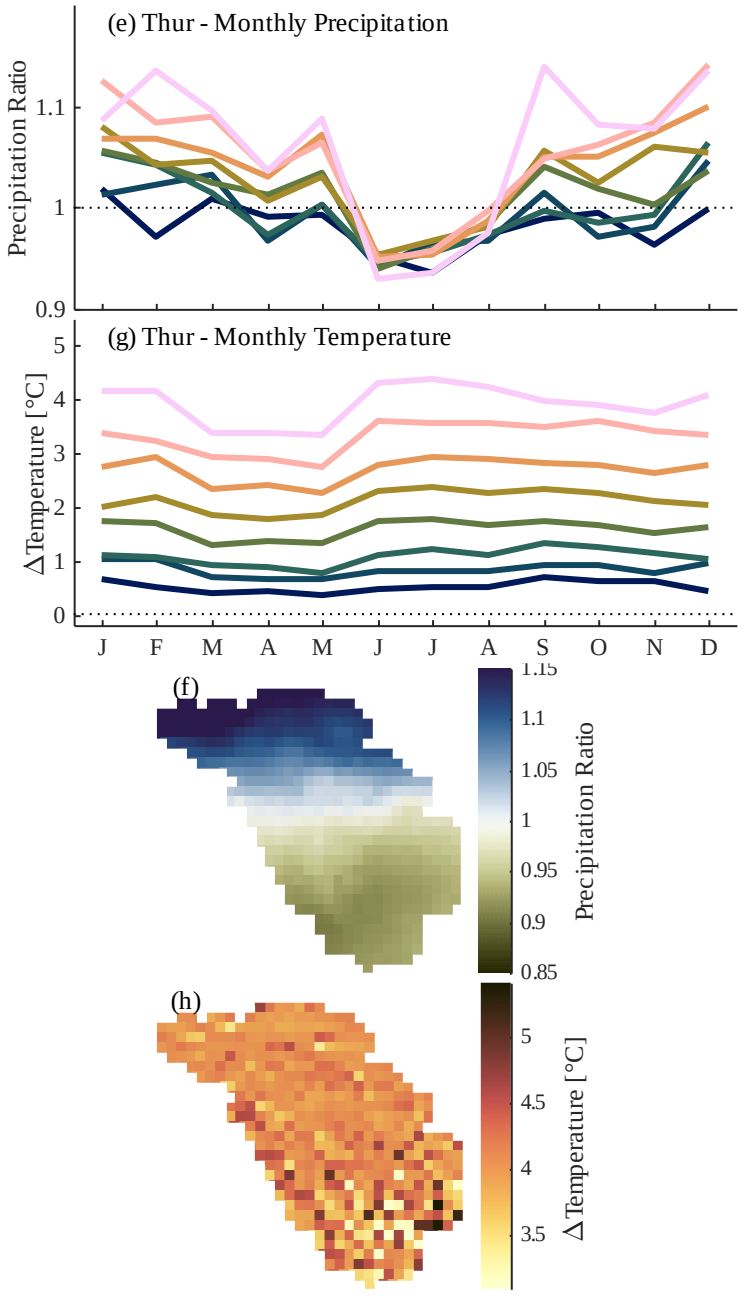

Figure 2-2: Changes in precipitation (ratio of future and present climate) and temperature (difference of future and present climate) in Kleine Emme (a–d) and Thur (e–h). Panels (a, e) and (c, g) show the monthly precipitation and temperature anomalies for each future period, respectively, whereas panels (b, f) and (d, h) show the spatial distribution of the mean annual changes of the climatic variables when comparing simulations of the present climate (1976–2005) with those of the end of the century (2080–2089).

The changes in temperature and precipitation influence changes in streamflow. Comparing the end of the century (2080-2089) and the present period, both catchments experience an increase in winter flows at the outlets by up to 40%, while summer flows at the outlets are predicted to decrease by about 20% in the Kleine Emme and by 40% in the Thur (Figure 2-3c, d). The changes in streamflow at the outlet are largely following the changes in precipitation and snowmelt (Figure 2-3c, d). The mean annual snow water equivalent (SWE) in the Thur decreases from 23.9 mm to 5.5 mm leading to a 48% decrease in snowmelt contribution to streamflow at the outlet on an annual average. In the Kleine Emme, the SWE change is similar,

with a decrease in the mean from 29.9 mm to 5.1 mm and a 57% decrease in snowmelt contribution to streamflow (Figure A-12). The increase in streamflow at the outlet during winter (DJF, Figure 2-3c, d) is a result of both increase in total precipitation and a shift in precipitation type from snowfall to rainfall. The latter allows precipitation to reach streamflow sooner than in the present climate (i.e., during DJF instead of MAM), as a larger portion of precipitation is not stored in the snowpack and subsequently released as snowmelt. During spring (MAM), the loss in snowmelt offsets the small increase in precipitation in both catchments. At least at the outlet, the streamflow is not affected by the changes in snowmelt during summer (JJA) and autumn (SON).

Likewise, the effect of climate change can be noticed on other hydrological components. For example, the average effective saturation of the top soil layer in the Thur remains nearly the same (25.5% to 25.7%, Figure 2-4d), while a small increase is detected in Kleine Emme from 55% to 59% (Figure 2-4a). The mean annual ET is projected to increase by 8% (Thur) and 10% (Kleine Emme) by the end of the century (Figure 2-4c, 4f). The changes to ET have minor effects on the streamflow at the outlet during spring and summer, and no effect during autumn and winter (Figure 2-3c, 3d).

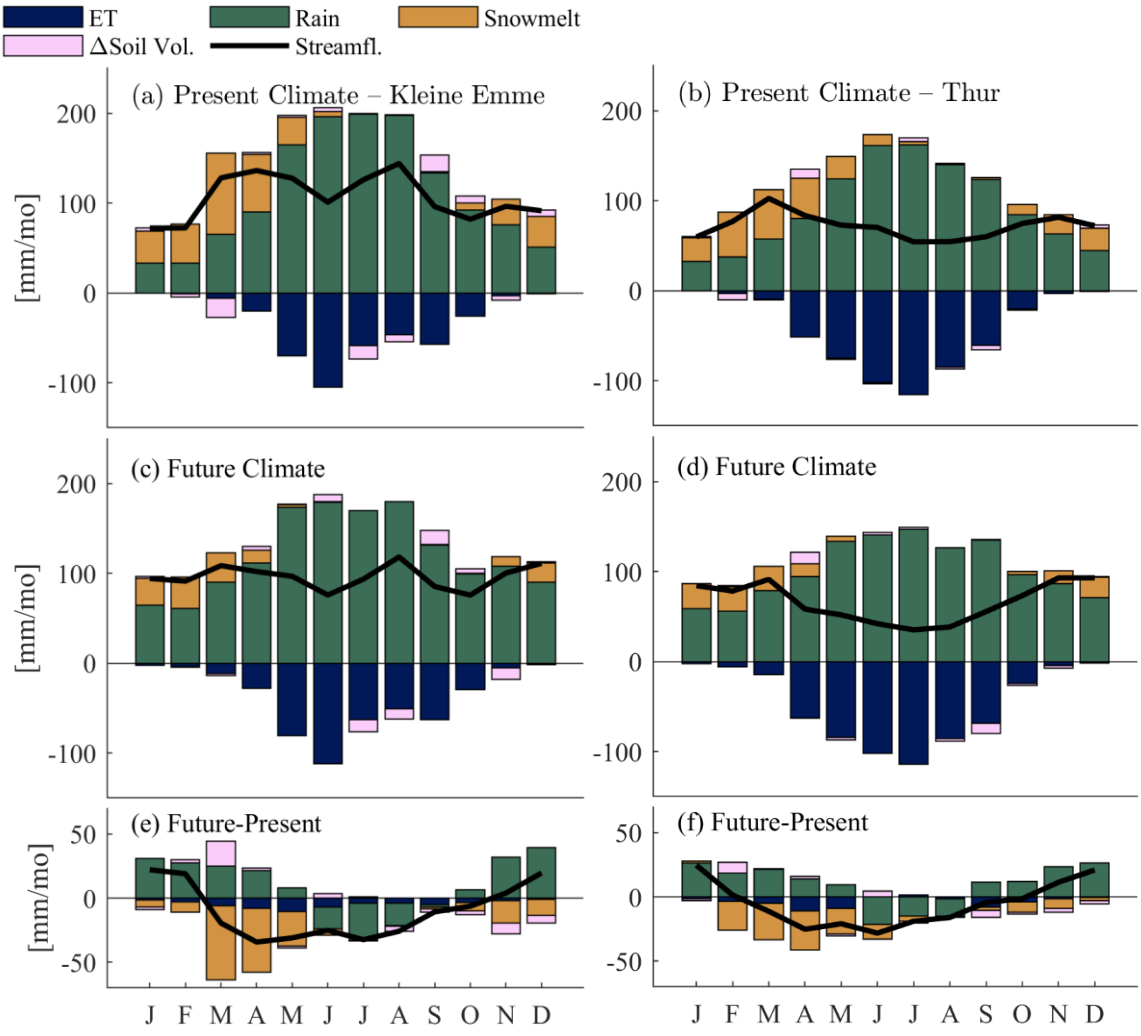

Figure 2-3: Monthly streamflow (thick black line) and its hydrological components at the outlet of the Kleine Emme (left) and Thur (right) river catchments for simulations of the present climate (1976–2005, a and b), of the end of the century (2080–2089, c and d), and their difference (e and f). The bars corresponding to evapotranspiration (blue) and an

increase in soil water volume (pink) are depicted as negative contributions to the water balance.

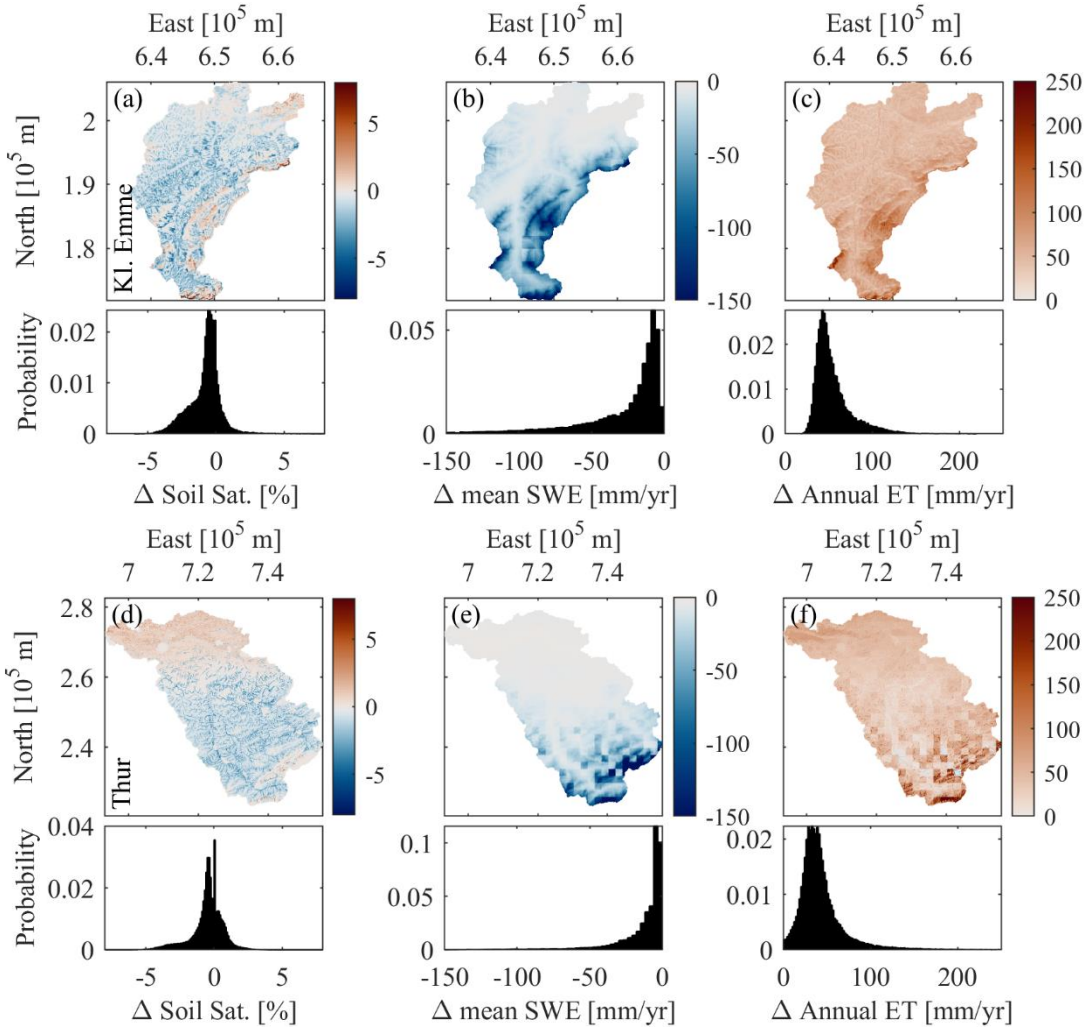

Figure 2-4: Spatial distribution and histograms of the change (end-of-the-century minus present) in mean annual effective saturation (left column), snow water equivalent (middle) and evapotranspiration (right) for the Kleine Emme (a–c) and Thur (d–f) catchments.

In addition to the changes in mean streamflow at the outlet, we also explored the changes to extreme flows and their main driving factor – the areal extreme precipitation intensity over the catchment. Extreme hourly and daily precipitation intensities (computed from annual maxima, fitted using Generalized Extreme Value (GEV) distribution) in both the Kleine Emme and the Thur catchments will not change considerably under climate change for the high-frequency extremes, but are projected to slightly intensify for less frequent events (up to 10% for T = 25y, Figure 2-5a–d). However, these changes are not statistically significant as the change in the median of the computed values is minor compared to the stochastic variability obtained from analyzing multiple realizations (Table A-3). In contrast, the magnitude of flood events (Figure 2-5e–h) shows, with one exception, a statistically significant decrease at the Kleine Emme (with a 5% significance level using a Mann-Whitney-Wilcoxon test, Table A-3), and particularly for the more frequent, low return-period events, whereas the decrease is not statistically significant in the Thur. This apparent contradiction, i.e. an intensification (although of minor magnitude) in extreme precipitation intensities but a decrease in extreme streamflow, can be explained by changes in the antecedent soil conditions (Figure 2-4, Figure A-13), and is discussed in Section 5. Additionally, a shift in the timing of the flood events is also projected;

while summer will still be the season with most flood events, the frequency of floods is projected to decline during summertime and increase in the other seasons in the future (Figure 2-6), following the foreseen changes in precipitation (Figure 2-2).

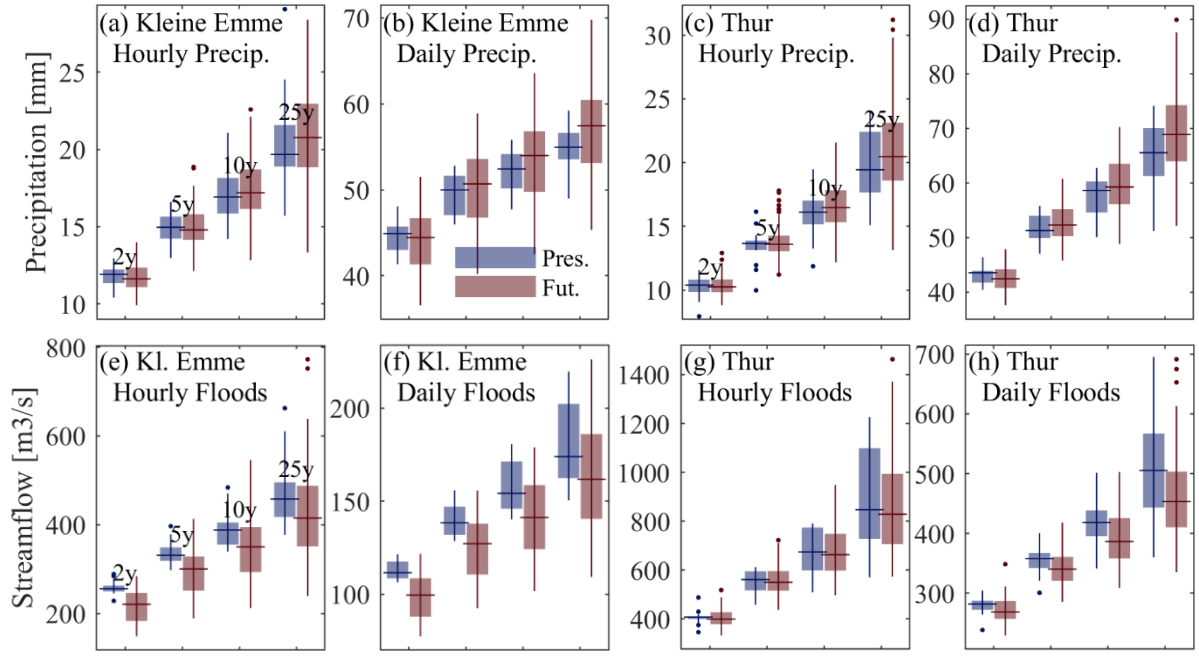

Figure 2-5: Hourly and daily areal precipitation extremes (a–d) and streamflow extremes (e–h) for given return periods under present (blue) and end-of-the-century (red) climate in the Kleine Emme and Thur catchment outlets. The central lines in the box plots represent the median value computed from the simulated ensembles fitted to a GEV distribution, while the boxes represent the 25–75th percentile range emerging from the climate ensemble.

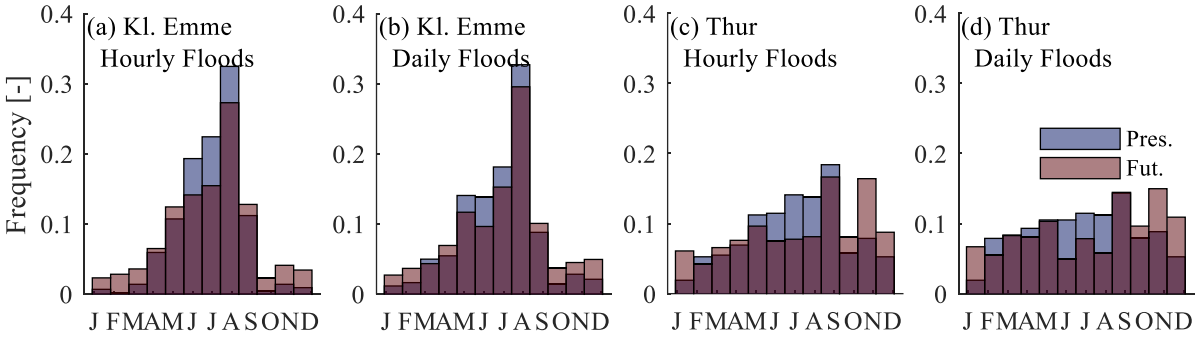

Figure 2-6: Monthly frequency of the time of occurrence of hourly (a, c) and daily (b, d) annual maximum streamflow at the outlet in the Kleine Emme (a–b) and Thur (c–d) catchments simulated for present (1976–2005, blue) and for end-of-the-century (2080–2089, red) climate conditions.

2.4.2 Climate change impacts at the sub-catchment scale

At the sub-catchment scale, the impacts of climate change on streamflow vary considerably in space. To show that, we explore the relationship between the elevation of the sub-catchments and the change rate of the annual maximum hourly flow (simply termed 'maximum' from hereafter), mean annual flow ('mean'), and the 7 days with the lowest flow every year ('minimum'), computed as the difference between the future and the present streamflow divided by the present streamflow.

The changes in maximum (Figure 2-7a, b) and mean flows (Figure 2-7c, d) show a clear negative correlation with sub-catchment elevation: higher elevation sub-catchments show a decrease in mean and maximum streamflow, while the lower elevation sub-catchments show an increase, particularly for maximum flows, with increments up to +30% in the Thur and +10% in the Kleine Emme. Changes to the minimum flows, on the other hand, have no clear relation with elevation (Figure 2-7e, f). We did not find any significant correlation between the flow change rate and the size of the catchments or stream order (not shown).

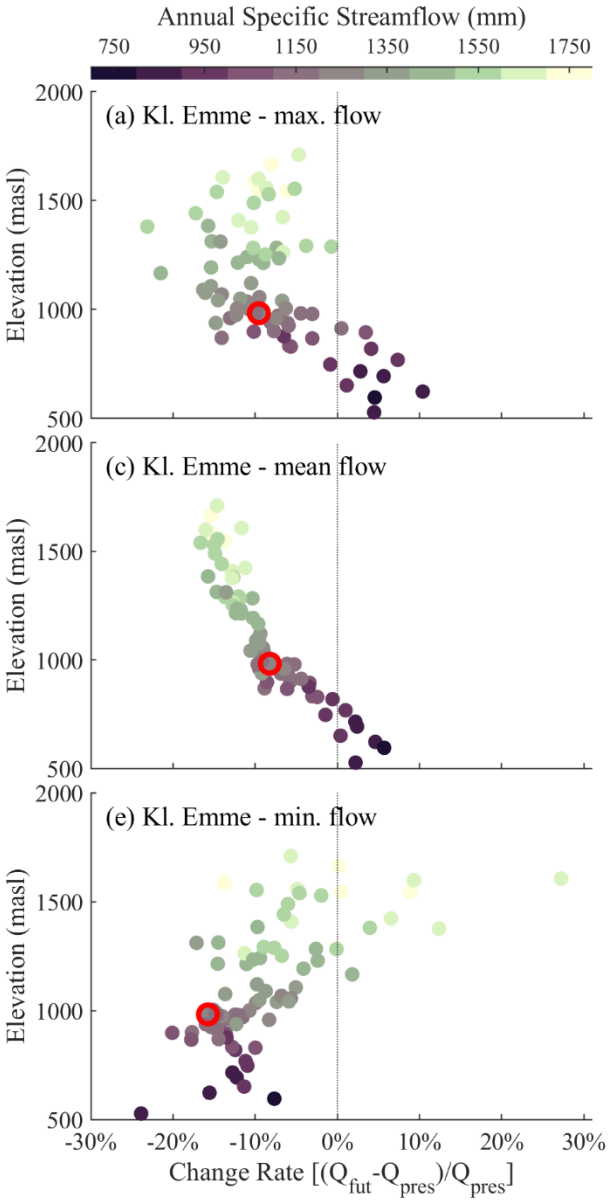
Annual Specific Streamflow (mm)
750
950
1150
1350
1550
1750
(a) Kl. Emme - max. flow
(c) Kl. Emme - mean flow
(e) Kl. Emme - min. flow
Elevation (masl)
2000
1500
1000
500
-30%
-20%
-10%
0%
10%
20%
30%
Change Rate [(Q_fut -Q_pres)/Q_pres]

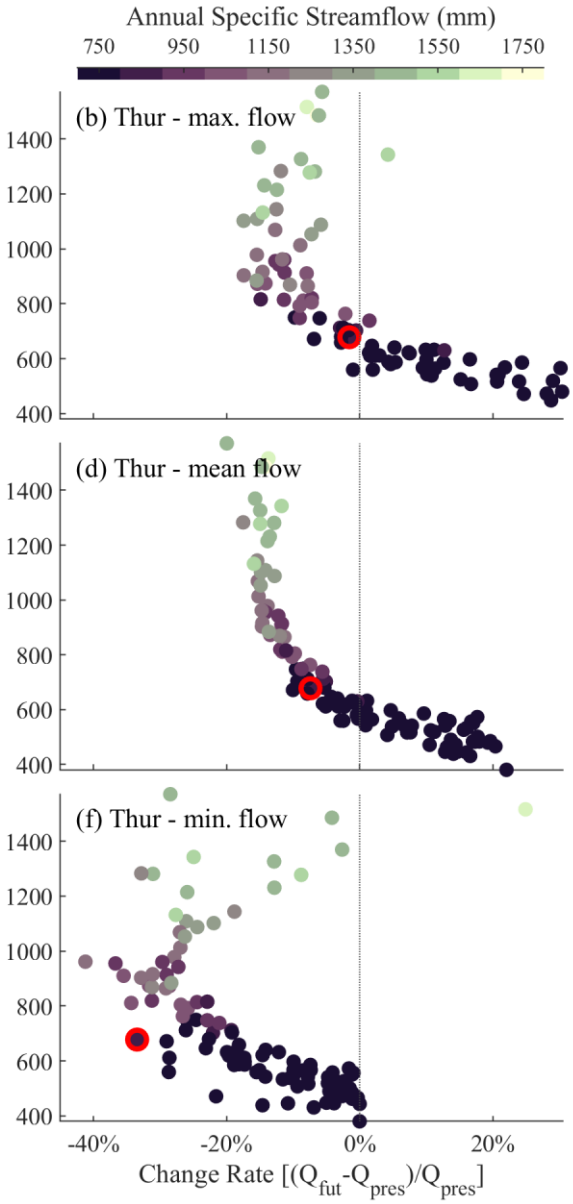

Figure 2-7: Impacts on streamflow in 97 Kleine Emme river sub-catchments (a, c, e) and 140 Thur river sub-catchments (b, d, f). The change rates between the present climate and the end-of-the-century are computed for the maximum hourly flow (a, b), mean flow (c, d) and 7-day minimum flow (e, f). The markers in all plots are colored according to the mean specific streamflow (the ratio of streamflow to sub-catchment area) in the present climate, and the point corresponding to the outlet of the catchment is marked with a red border.

Six sub-catchments within the Kleine Emme catchment (as defined in Figure A-14) that cover a range of elevations (low, mid, and high) and sizes (small and large) were selected for a further examination of the causality of the changes to the hydrological budget (Figure 2-8). We found that snowmelt is a significant contributor to streamflow in sub-catchments located in high elevations during spring for the present climate, and its decrease is the main cause of decreasing flows in spring months. Sub-catchments located at lower elevation are less sensitive to changes in snowmelt. The reduction in precipitation and streamflow during summer is more noticeable higher up in the river network. The ET contribution to changes in streamflow is relatively small in all sub-catchments; however, this contribution increases in the lower elevations where ET is higher. Overall, the expected impacts of climate changes on the streamflow of lower sub-catchments in Kleine Emme are almost negligible, not only at the

annual scale (Figure 2-7c) but at the seasonal scale as well (Figure 9b, 9d). For Thur (Figure A-15), however, changes are considerably larger at these lower elevations and mostly dictated by higher precipitation.

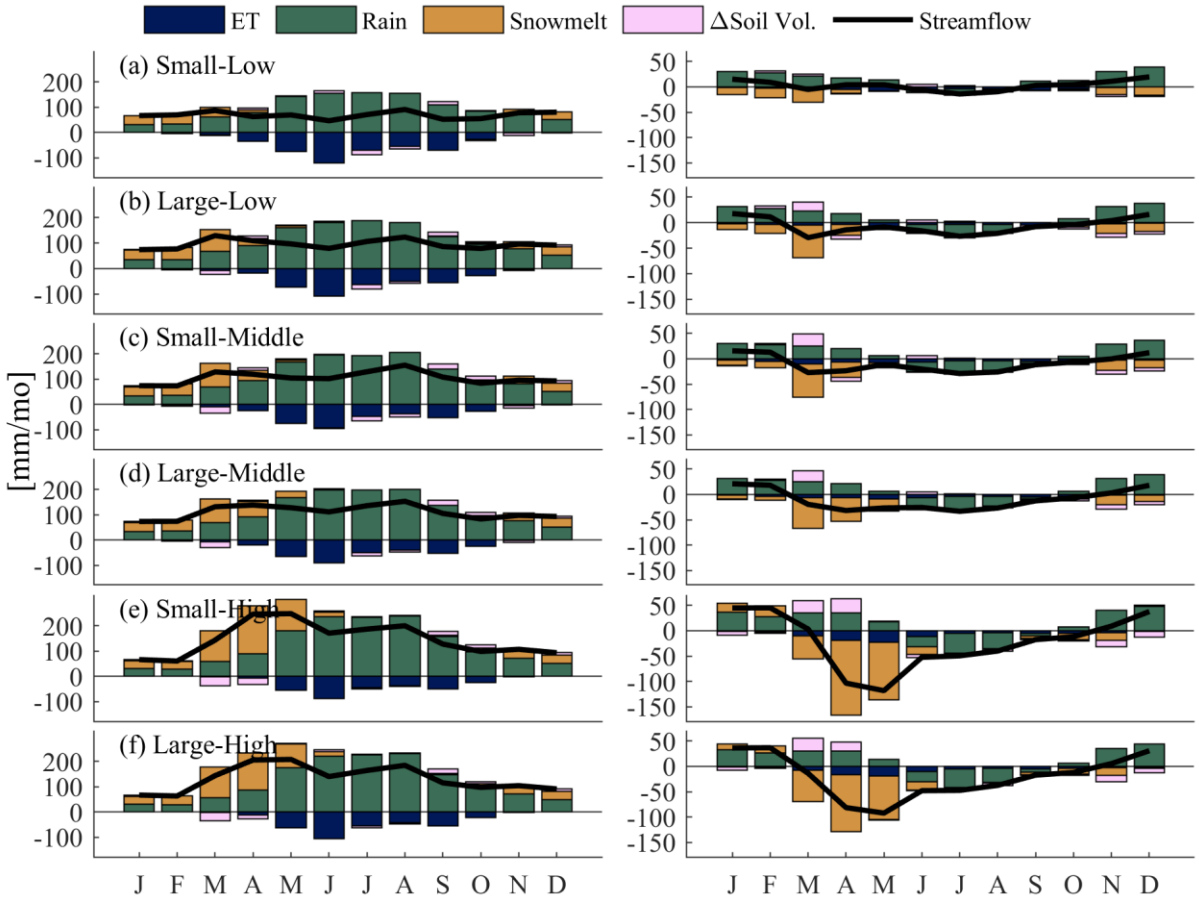

Figure 2-8: Monthly streamflow (black line) and the hydrological components (bars) for six selected sub-catchments of the Kleine Emme river simulated under present climate conditions (left column), and their change towards the end of the century (right column). The bars corresponding to ET (blue) and increase in soil water volume (pink) are depicted as negative contributions to the water balance.

Moreover, we computed the first and second most important hydrological component in terms of the total volume contributed to the sub-catchment streamflow in the Kleine Emme catchment in each season, for the present and end-of-the-century climates (Figure 2-9). In the present climate, rainfall is the most dominant component across all seasons, excluding low sub-catchments in DJF and high sub-catchments in MAM where snowmelt is the most important contributor to streamflow. With the decreasing snowmelt by the end of the century, however, even the streamflow in these sub-catchments will be dominated by liquid precipitation. Furthermore, for many of the sub-catchments where snowmelt is currently the second most important component, ET will replace it as a relatively larger contributor by the end of the century.In summer (JJA) and autumn (SON), rainfall will remain the most important contributor throughout the catchment as the ET increase in JJA drives a decrease in overall streamflow. In SON we note that very little variation in streamflow is expected. Similar results are found for the Thur catchment (Figure A-15).

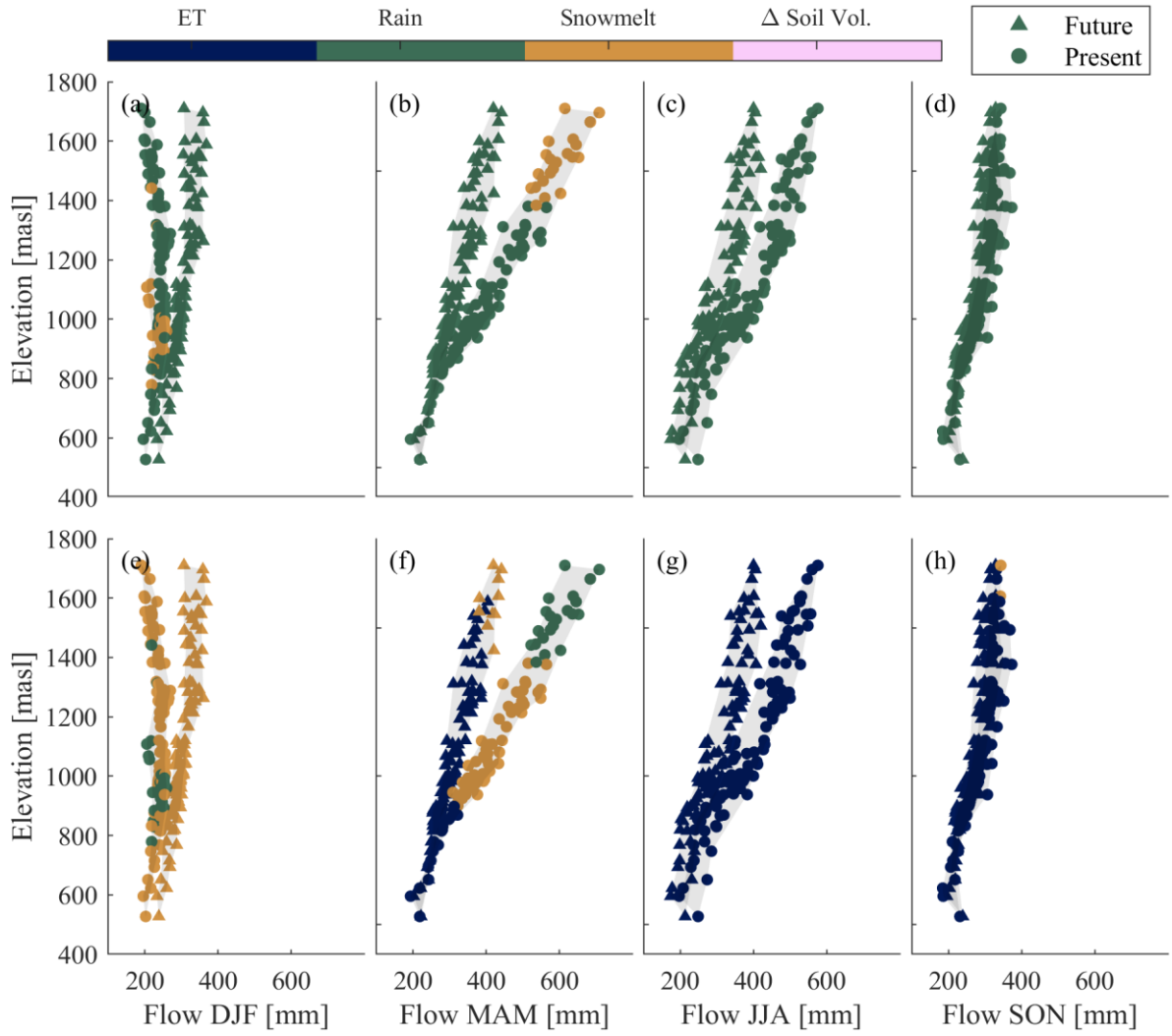

Figure 2-9: First (a–d) and second (e–h) most important components contributing to the seasonal flow in the Kleine Emme river network under present (circles) and future (triangles) climate conditions. Mean seasonal specific flow is plotted as a function of sub-catchment elevation and colored by the components ET (evapotranspiration), Rain, Snowmelt, ΔSoil Volume (change in soil water volume).

2.5 Discussion

2.5.1 Impacts of climate change on Swiss mountainous catchments

Considering streamflow changes at the outlet for both catchments, the mean annual streamflow is projected to decrease by around 7–8% toward the end of the century (Figure 2-3). For the Thur catchment, similar estimates of change were found by Jasper et al. (2004), Köplin et al. (2012), Addor et al. (2014) and Muelchi et al. (2020). These studies used different hydrological models (WaSiM-ETH; PREVAH; 3 hydrological models: HBV, PREVAH, and WaSiM; and PREVAH, respectively) and climate scenarios as inputs (GCMDAT; CH2011; CH2011; and CH2018, respectively). This points to a convergence in the estimate of the average magnitude of the change. Likewise, the above studies agree with the projected changes to streamflow at the seasonal scale, i.e. a decrease in summer streamflow and an increase in winter streamflow by the end 21st century (Figure 2-3). Similar degrees of change in mean annual and seasonal streamflow were reported in other European alpine catchments

(Bavay et al., 2013; Etter et al., 2017; Fatichi et al., 2015; Meißl et al., 2017; Ragettli et al., 2019).

In this study, we add a new perspective on elevation-dependent changes in the sign and magnitude of streamflow at sub-catchment scales (Figure 2-7). While at almost all elevations and in all seasons precipitation is found to be the key driver of the change (Figure 2-9), we show that snowmelt (for sub-catchments located at high elevation) and ET (at low elevations) can also become important contributors to the changes in streamflow in a warmer climate (Figure 2-8). As the changes in precipitation are a key driver, their uncertainties and impacts on the streamflow in mountainous catchments need to be better understood, and this should be investigated in more detail. For example, in our simulation of future precipitation, only the intensities were modified using FC, while the spatial and temporal structure of the precipitation process remained unchanged, i.e. we assumed the wet periods, the temporal intermittency, and the wet area ratio to follow the same statistics as of today. Modelling these parameters in a future climate requires precipitation data outputs from climate models at a sub-daily resolution that are not commonly available in current experiments.

The projection of a decrease in snow water equivalent and its temporal shift in a future climate is in agreement with other studies in the region (Bavay et al., 2013; Etter et al., 2017; Frei et al., 2018; Jenicek et al., 2018), particularly at higher elevations (Figure 2-8). Bavay et al (2013) forecast a loss of between 1/3 and 2/3 of SWE by the end of the century depending on the driving climate model, which is in line with our results. Although results agree that winter flows will increase, they foresee increases in spring as well, albeit for a domain with overall higher elevations than the study sites analysed here. Frei et al. (2018) show that snowfall will decrease dramatically by the end of the century, except during the winter months for higher elevations (above 2000 m.a.s.l.). Likewise, our results show snowfall rates at around 70% of the present climate for the same months and elevations (Figure A-16). Jenicek et al. (2018) conclude that changing SWE availability will translate into a stark decrease of low flows in the lowest catchments, but not at higher elevations, whereas our results are more ambiguous (Figure 2-7). Lastly, it has to be mentioned that the presence of glaciers will certainly affect flow seasonality and especially low flow statistics in a future climate (Bavay et al., 2013), which is obviously not reflected in the results presented here for these two glacier-free catchments.

The rising temperature will cause evapotranspiration to increase all over the study catchments (Figure 2-4). Mastrotheodoros et al. (2020) noted a clear correlation between ET increase and elevation simulated over the European Alps, which we observe for the Kleine Emme, but not for the Thur (Figure A-17).

2.5.2 Changes to high and low flow extremes

The changes in extreme precipitation are not significant as extreme rainfall remains the same for the high-frequency return periods and increases only slightly at low-frequencies (Figure 2-5, top row), yet hourly and daily streamflow extremes in our analysis are projected to slightly decrease (Figure 2-5, bottom row). This apparent contradiction can largely be explained by drier antecedent soil wetness conditions prior to heavy rainfall events. Paschalis et al. (2014) used the same hydrological model (Topkapi-ETH) and catchment (Kleine Emme) in an event-based analysis to show that drier pre-event soil moisture conditions lead to lower flood peaks on average. Indeed, in both catchments, we detect a deficit in the soil wetness before high-flow events, when comparing the present and end-of-century periods (Figure A-13). This is caused by more intense drying of the soils by ET and soil water drainage during inter-storm periods in the warm season in a future climate.

We found that the magnitudes of the annual maximum flows are projected to decrease slightly for almost all return periods at the outlets of the Thur and Kleine Emme catchments at the end

of the century (Figure 2-5). Our findings seem to contradict results from other studies in Switzerland, also using the CH2018 data but with other hydrological models and different parameterization, that report a projected increase in annual maximum daily streamflow toward the end-of-the-century (Brunner et al., 2019; Molnar et al., 2020; Ruiz-Villanueva and Molnar, 2020), although it is worth noting that all the studies agree on the high uncertainty that accompanies such predictions. The discrepancy in the changes of the annual maximum flow magnitudes in these studies can be explained by the climatic input data used to run the hydrological models. Although the same data source was used (i.e. climate variables processed in the CH2018 project), here we further downscaled the precipitation and temperature data to obtain higher space-time resolution by the WG. While the space-time structure of precipitation is statistically similar to the native CH2018 data (the WG is calibrated to reproduce these statistics, see Peleg et al., 2017), it is not identical. In terms of timing, flood occurrence is foreseen to partly shift toward the cold season; nonetheless, warm-season extreme flow events, driven mostly by high-intensity rainfall events (Barton et al., 2020; Panziera et al., 2018, 2015), are projected to continue to be the most frequent extreme events also in the future (Figure 2-6). Another possible contributor to floods are rain-on-snow events (RoS), which may play an important role in alpine settings (Beniston & Stoffel, 2016). Although Topkapi-ETH does consider events of rainfall over snow-covered grid cells, it does so in a simplified way that does not fully account for interactions with the snowpack. A more sophisticated approach, including the distributed modelling of snowpack characteristics, could provide interesting insight into the occurrence of RoS-triggered events.

2.5.3 Elevation dependence of the hydrological response to climate change

The results of this study clearly show that the hydrological response to climate change in mountainous catchments at the sub-catchment scale is strongly dependent on elevation (Figure 2-7). For example, we show that annual mean streamflow is foreseen to decrease by -10% (-15%) in the upper sub-catchments of the Thur (Kleine Emme), while an increase of +15% (+5%) is projected in some of the lower-elevation reaches, and the estimated change at the outlet is -7% (-8%). Similarly, floods at the hourly scale are projected to decrease by up to -15% (-20%) in the upper sub-catchments, but increase up to +30% (+10%) in the lowest parts of the catchment, and change only -2% (-10%) at the outlet. Fatichi et al. (2015) also examined the changes to the streamflow response with elevation, using the same hydrological model but with different climate scenarios as inputs, for a much larger Alpine catchment – the upper Rhone in Switzerland. They reported a much higher variability in the hydrological response than found here, mostly related to a much larger variability in the projected rainfall patterns. Based on the two catchments explored here and the work of Fatichi et al. (2015), we conclude that the variability of the response with elevation is strongly related to the projected rainfall patterns and the catchment size and river network connectivity.

Overall, the results highlight the need to analyze the hydrological response to climate change not only at the outlet of mountainous catchments but also within catchments. Settlements in these catchments are often located at the lower elevation, in valleys closer to the river outlet. The villages are located not only along the main river channel but also in the sub-catchments at lower elevations connected to it. Analyzing only the response at the outlet, the risk emerging from floods in future climate can be significantly underestimated (or even the direction of change may be misrepresented). For example, in the Thur River, no change is projected to the maximum streamflow at the outlet of the catchment, while the maximum streamflow in some of the sub-catchments near the outlet is projected to increase by more than 20% (Figure 2-7). This type of information is critical for urban planners, civil and environmental engineers, and policymakers that aim at planning a flood-resilient environment. This shows how the methodological framework presented in this work leads to results that emphasize the

relevance of using high-resolution, distributed climatic and hydrological models for revealing important details of the hydrological response in such mountainous environments.

2.6 CONCLUSIONS

The impacts of climate change on mountainous catchments were studied using a high-resolution weather generator and a fully-distributed hydrological model to analyze the spatially-explicit hydrological response within two mountainous catchments in the Swiss Alps. Changes in precipitation patterns and a strong reduction in snowfall and snowmelt drive noticeable changes in streamflow at the outlet of the catchments throughout the 21st century, with decreasing summer and increasing winter flows. In terms of streamflow extremes, we show that, despite no significant change in extreme precipitation magnitudes, maximum floods at the outlets of the catchments will decline slightly and shift in time towards the cold season. Most importantly, exploring the changes at the sub-catchment scale, we show that the mean and extreme streamflow at high-elevation sub-catchments is projected to decrease, whereas for the lower sub-catchments an increase in both mean and extreme streamflow is foreseen, in contrast with less significant changes at the catchment outlets. While rainfall was found to be the most critical component in driving the changes in streamflow, we show that snow-related processes dominate the changes at the sub-catchments located at higher elevations, while changes in ET are relevant for the changes in streamflow only for lower elevation sub-catchments. Overall, this study highlights the value of using high-resolution climatic and hydrological modelling to reveal the spatial heterogeneity of hydrological responses to a changing climate in mountainous catchments.

2.7 REFERENCES

Abegg, B., Agrawala, S., Crick, F., & de Montfalcon, A., 2007. Climate change impacts and adaptation in winter tourism. Climate change in the European Alps: Adapting winter tourism and natural hazards management, 25-58.

Addor, N., Rössler, O., Köplin, N., Huss, M., Weingartner, R., Seibert, J., 2014. Robust changes and sources of uncertainty in the projected hydrological regimes of Swiss catchments. Water Resour. Res. 50, 7541–7562. https://doi.org/10.1002/2014WR015549

Ban, N., Schmidli, J., Schär, C., 2015. Heavy precipitation in a changing climate: Does short-term summer precipitation increase faster? Geophys. Res. Lett. 42, 1165–1172. https://doi.org/10.1002/2014GL062588

Bao, J., Sherwood, S.C., Alexander, L. V., Evans, J.P., 2017. Future increases in extreme precipitation exceed observed scaling rates. Nat. Clim. Chang. 7, 128–132. https://doi.org/10.1038/nclimate3201

Barton, Y., Sideris, I. V., Raupach, T.H., Gabella, M., Germann, U., Martius, O., 2020. A multi-year assessment of sub-hourly gridded precipitation for Switzerland based on a blended radar—rain-gauge dataset. Int. J. Climatol. joc.6514. https://doi.org/10.1002/joc.6514

Battista, G., Molnar, P., Burlando, P., 2020a. Modelling impacts of spatially variable erosion drivers on suspended sediment dynamics. Earth Surf. Dyn. 8, 619–635. https://doi.org/10.5194/esurf-8-619-2020

Battista, G., Schlunegger, F., Burlando, P., Molnar, P., 2020b. Modelling localized sources of sediment in mountain catchments for provenance studies. Earth Surf. Process. Landforms 45, 3475–3487. https://doi.org/10.1002/esp.4979

Bavay, M., Grünewald, T., Lehning, M., 2013. Response of snow cover and runoff to climate change in high Alpine catchments of Eastern Switzerland. Adv. Water Resour. 55, 4–16. https://doi.org/10.1016/j.advwatres.2012.12.009

Beniston, M., Farinotti, D., Stoffel, M., Andreassen, L.M., Coppola, E., Eckert, N., Fantini, A., Giacona, F., Hauck, C., Huss, M., Huwald, H., Lehning, M., López-Moreno, J.I., Magnusson, J., Marty, C., Morán-Tejéda, E., Morin, S., Naaim, M., Provenzale, A., Rabatel, A., Six, D., Stötter, J., Strasser, U., Terzago, S., Vincent, C., 2018. The European mountain cryosphere: A review of its current state, trends, and future challenges. Cryosphere. https://doi.org/10.5194/tc-12-759-2018

Beniston, M., & Stoffel, M. (2016). Rain-on-snow events, floods and climate change in the Alps: Events may increase with warming up to 4 °C and decrease thereafter. Science of the Total Environment, 571, 228–236. https://doi.org/10.1016/j.scitotenv.2016.07.146

Blanc, P., and B. Schaedler, 2014: Water in Switzerland—an overview. Swiss Hydrological Commission Rep., 28 pp.

Bodeneignungskarte: 77.2 Digitale Bodeneignungskarte der Schweiz, https://www.blw.admin.ch/blw/de/home/politik/datenmanagement/ geografisches-informationssystem-gis/download-geodaten.html, 2012.

Bordoy, R., Burlando, P., 2014. Stochastic downscaling of climate model precipitation outputs in orographically complex regions: 2. Downscaling methodology. Water Resour. Res. 50, 562–579. https://doi.org/10.1002/wrcr.20443

Brunner, M.I., Farinotti, D., Zekollari, H., Huss, M., Zappa, M., 2019. Future shifts in extreme flow regimes in Alpine regions. Hydrol. Earth Syst. Sci. 23, 4471–4489. https://doi.org/10.5194/hess-23-4471-2019

Brunner, M.I., Sikorska, A.E., Seibert, J., 2018. Bivariate analysis of floods in climate impact assessments. Sci. Total Environ. 616–617, 1392–1403. https://doi.org/10.1016/j.scitotenv.2017.10.176

Bultot, F., Gellens, D., Schädler, B., Spreafico, M., 1994. Effects of climate change on snow accumulation and melting in the Broye catchment (Switzerland). Clim. Change 28, 339–363. https://doi.org/10.1007/BF01104078

Camici, S., Brocca, L., Moramarco, T., 2017. Accuracy versus variability of climate projections for flood assessment in central Italy. Clim. Change 141, 273–286. https://doi.org/10.1007/s10584-016-1876-x

CH2018, 2018. CH2018—Climate Scenarios for Switzerland: Technical Report. Zurich: National Centre for Climate Services.

CLC, 2014. Corine Land Cover (CLC) map 2012, https://land.copernicus.eu/pan-european/corine-land-cover/clc-2012.

Entekhabi, D., Rodriguez-Iturbe, I., Eagleson, P.S., 1989. Probabilistic representation of the temporal rainfall process by a modified Neyman-Scott Rectangular Pulses Model: Parameter estimation and validation. Water Resour. Res. 25, 295–302. https://doi.org/10.1029/WR025i002p00295

Etter, S., Addor, N., Huss, M., Finger, D., 2017. Climate change impacts on future snow, ice and rain runoff in a Swiss mountain catchment using multi-dataset calibration. J. Hydrol. Reg. Stud. 13, 222–239. https://doi.org/10.1016/j.ejrh.2017.08.005

Fatichi, S., Ivanov, V.Y., Caporali, E., 2011. Simulation of future climate scenarios with a weather generator. Adv. Water Resour. 34, 448–467. https://doi.org/10.1016/j.advwatres.2010.12.013

Fatichi, S., Ivanov, V.Y., Caporali, E., 2013. Assessment of a stochastic downscaling methodology in generating an ensemble of hourly future climate time series. Clim. Dyn. 40, 1841–1861. https://doi.org/10.1007/s00382-012-1627-2

Fatichi, S., Ivanov, V.Y., Paschalis, A., Peleg, N., Molnar, P., Rimkus, S., Kim, J., Burlando, P., Caporali, E., 2016a. Uncertainty partition challenges the predictability of vital details of climate change. Earth's Futur. 4, 240–251. https://doi.org/10.1002/2015EF000336

Fatichi, S., Rimkus, S., Burlando, P., Bordoy, R., Molnar, P., 2015. High-resolution distributed analysis of climate and anthropogenic changes on the hydrology of an Alpine catchment. J. Hydrol. 525, 362–382. https://doi.org/10.1016/j.jhydrol.2015.03.036

Fatichi, S., Rimkus, S., Burlando, P, Bordoy, R., 2014. Does internal climate variability overwhelm climate change signals in streamflow? The upper Po and Rhone basin case studies. Sci. Total Environ., 493 1171–1182 http://dx.doi.org/10.1016/j.scitotenv.2013.12.014

Fatichi, S., Vivoni, E.R., Ogden, F.L., Ivanov, V.Y., Mirus, B., Gochis, D., Downer, C.W., Camporese, M., Davison, J.H., Ebel, B., Jones, N., Kim, J., Mascaro, G., Niswonger, R., Restrepo, P., Rigon, R., Shen, C., Sulis, M., Tarboton, D., 2016b. An overview of current applications, challenges, and future trends in distributed process-based models in hydrology. J. Hydrol. https://doi.org/10.1016/j.jhydrol.2016.03.026

Fischer, A.M., Keller, D.E., Liniger, M.A., Rajczak, J., Schär, C., Appenzeller, C., 2015. Projected changes in precipitation intensity and frequency in Switzerland: a multi-model perspective. Int. J. Climatol. 35, 3204–3219. https://doi.org/10.1002/joc.4162

Floriancic, M.G., Berghuijs, W.R., Jonas, T., Kirchner, J.W., Molnar, P., 2020. Effects of climate anomalies on warm-season low flows in Switzerland. Hydrol. Earth Syst. Sci. 24, 5423–5438. https://doi.org/10.5194/hess-24-5423-2020

Fowler, H.J., Blenkinsop, S., Tebaldi, C., 2007. Linking climate change modelling to impacts studies: recent advances in downscaling techniques for hydrological modelling. Int. J. Climatol. 27, 1547–1578. https://doi.org/10.1002/joc.1556

Frei, P., Kotlarski, S., Liniger, M.A., Schär, C., 2018. Future snowfall in the Alps: projections based on the EURO-CORDEX regional climate models. Cryosph. 12, 1–24. https://doi.org/10.5194/tc-12-1-2018

Gariano, S.L., Guzzetti, F., 2016. Landslides in a changing climate. Earth-Science Rev. https://doi.org/10.1016/j.earscirev.2016.08.011

Germann, U., Galli, G., Boscacci, M., Bolliger, M., 2006. Radar precipitation measurement in a mountainous region. Q. J. R. Meteorol. Soc. 132, 1669–1692. https://doi.org/10.1256/qj.05.190

Hakala, K., Addor, N., Teutschbein, C., Vis, M., Dakhlaoui, H., Seibert, J., 2019. Hydrological Modeling of Climate Change Impacts Intelligent parameter sampling (IntelSamp) View project Hydrological droughts in Sweden now and in the future: Hotspots of hazard, vulnerability, and risk View project Hydrological Modeling of Climate Change Impacts. https://doi.org/10.1002/9781119300762.wsts0062

Hirschberg, J., Fatichi, S., Bennett, G.L., McArdell, B.W., Peleg, N., Lane, S.N., Schlunegger, F., Molnar, P., 2020. Climate Change Impacts on Sediment Yield and Debris-Flow Activity in an Alpine Catchment. J. Geophys. Res. Earth Surf. https://doi.org/10.1029/2020jf005739

Jacob, D., Petersen, J., Eggert, B., Alias, A., Christensen, O.B., Bouwer, L.M., Braun, A., Colette, A., Déqué, M., Georgievski, G., Georgopoulou, E., Gobiet, A., Menut, L., Nikulin, G., Haensler, A., Hempelmann, N., Jones, C., Keuler, K., Kovats, S., Kröner, N., Kotlarski, S., Kriegsmann, A., Martin, E., van Meijgaard, E., Moseley, C., Pfeifer, S., Preuschmann, S., Radermacher, C., Radtke, K., Rechid, D., Rounsevell, M., Samuelsson, P., Somot, S., Soussana, J.-F., Teichmann, C., Valentini, R., Vautard, R., Weber, B., Yiou, P., 2014. EURO-CORDEX: new high-resolution climate change projections for European impact research. Reg. Environ. Chang. 14, 563–578. https://doi.org/10.1007/s10113-013-0499-2

Jasper, K., Calanca, P., Gyalistras, D., Fuhrer, J., 2004. Differential impacts of climate change on the hydrology of two Alpine river basins. Clim. Res. https://doi.org/10.3354/cr026113

Jenicek, M., Seibert, J., Staudinger, M., 2018. Modeling of Future Changes in Seasonal Snowpack and Impacts on Summer Low Flows in Alpine Catchments. Water Resour. Res. 54, 538–556. https://doi.org/10.1002/2017WR021648

Jörg-Hess, S., Griessinger, N., Zappa, M., 2015. Probabilistic Forecasts of Snow Water Equivalent and Runoff in Mountainous Areas. J. Hydrometeorol. 16, 2169–2186. https://doi.org/10.1175/JHM-D-14-0193.1

Keller, D.E., Fischer, A.M., Frei, C., Liniger, M. A., Appenzeller, C., Knutti, R., 2015. Implementation and validation of a Wilks-type multi-site daily precipitation generator over a typical Alpine river catchment. Hydrol. Earth Syst. Sci. 19, 2163–2177. https://doi.org/10.5194/hess-19-2163-2015

Keller, D.E., Fischer, A.M., Liniger, M.A., Appenzeller, C., Knutti, R., 2017. Testing a weather generator for downscaling climate change projections over Switzerland. Int. J. Climatol. 37, 928–942. https://doi.org/10.1002/joc.4750

Keller, L., Rössler, O., Martius, O., Weingartner, R., 2019. Comparison of scenario-neutral approaches for estimation of climate change impacts on flood characteristics. Hydrol. Process. 33, 535–550. https://doi.org/10.1002/hyp.13341

Köplin, N., Schädler, B., Viviroli, D., Weingartner, R., 2012. Relating climate change signals and physiographic catchment properties to clustered hydrological response types. Hydrol. Earth Syst. Sci. 16, 2267–2283. https://doi.org/10.5194/hess-16-2267-2012

Kos, A., Amann, F., Strozzi, T., Delaloye, R., von Ruette, J., Springman, S., 2016. Contemporary glacier retreat triggers a rapid landslide response, Great Aletsch Glacier, Switzerland. Geophys. Res. Lett. 43, 12,466-12,474. https://doi.org/10.1002/2016GL071708

Kotlarski, S., Keuler, K., Christensen, O.B., Colette, A., Déqué, M., Gobiet, A., Goergen, K., Jacob, D., Lüthi, D., Van Meijgaard, E., Nikulin, G., Schär, C., Teichmann, C., Vautard, R., Warrach-Sagi, K., Wulfmeyer, V., 2014. Regional climate modeling on European scales: a joint standard evaluation of the EURO-CORDEX RCM ensemble. Geosci. Model Dev 7, 1297–1333. https://doi.org/10.5194/gmd-7-1297-2014

Lenderink, G., Barbero, R., Loriaux, J.M., Fowler, H.J., 2017. Super-Clausius–Clapeyron Scaling of Extreme Hourly Convective Precipitation and Its Relation to Large-Scale Atmospheric Conditions. J. Clim. 30, 6037–6052. https://doi.org/10.1175/JCLI-D-16-0808.1

Maraun, D., Wetterhall, F., Ireson, A.M., Chandler, R.E., Kendon, E.J., Widmann, M., Brienen, S., Rust, H.W., Sauter, T., Themel, M., Venema, V.K.C., Chun, K.P., Goodess, C.M., Jones, R.G., Onof, C., Vrac, M., Thiele-Eich, I., 2010. Precipitation downscaling under climate change: Recent developments to bridge the gap between dynamical models and the end user. Rev. Geophys. 48. https://doi.org/10.1029/2009RG000314

Mascaro, G., Vivoni, E.R., Méndez-Barroso, L.A., 2015. Hyperresolution hydrologic modeling in a regional watershed and its interpretation using empirical orthogonal functions. Adv. Water Resour. 83, 190–206. https://doi.org/10.1016/j.advwatres.2015.05.023

Mastrotheodoros, T., Pappas, C., Molnar, P., Burlando, P., Manoli, G., Parajka, J., Rigon, R., Szeles, B., Bottazzi, M., Hadjidoukas, P., Fatichi, S., 2020. More green and less blue water in the Alps during warmer summers. Nat. Clim. Chang. 10, 155–161. https://doi.org/10.1038/s41558-019-0676-5

Mateo, C.M.R., Yamazaki, D., Kim, H., Champathong, A., Vaze, J., Oki, T., 2017. Impacts of spatial resolution and representation of flow connectivity on large-scale simulation of floods. Hydrol. Earth Syst. Sci. 21, 5143–5163. https://doi.org/10.5194/hess-21-5143-2017

Meißl, G., Formayer, H., Klebinder, K., Kerl, F., Schöberl, F., Geitner, C., Markart, G., Leidinger, D., Bronstert, A., 2017. Climate change effects on hydrological system conditions influencing generation of storm runoff in small Alpine catchments. Hydrol. Process. 31, 1314–1330. https://doi.org/10.1002/hyp.11104

MeteoSwiss, 2016. Daily Precipitation (Final Analysis): RhiresD, Switzerland. [Available at http://www.meteoswiss.admin.ch/home/search.subpage.html/en/data/products/2014/raeumliche-daten-niederschlag.html.]

Middelkoop, H., Daamen, K., Gellens, D., Grabs, W., Kwadijk, J.C.J., Lang, H., Parmet, B.W.A.H., Schädler, B., Schulla, J., Wilke, K., 2001. Impact Of Climate Change On Hydrological Regimes And Water Resources Management In The Rhine Basin, Climatic Change.

Milly, P.C.D., Betancourt, J., Falkenmark, M., Hirsch, R.M., Kundzewicz, Z.W., Lettenmaier, D.P., Stouffer, R.J., 2008. Climate change: Stationarity is dead: Whither water management? Science (80-.). https://doi.org/10.1126/science.1151915

Molnar, P., Chang, Y., Yuan, Peleg, N., Moraga, S., Zappa, M., Brunner, M.I., Seibert, J., Freudiger, D., Martius, O., Mülchi, R., 2020. Future changes in floods, in: Ruiz-Villanueva, V., Molnar, P.; (Eds.), Past, Current, and Future Changes in Floods in Switzerland. Hydro-CH2018 project. Commissioned by the Federal Office for the Environment (FOEN), Bern, Switzerland, pp. 51–58. https://doi.org/10.3929/ethz-b-000462778

Muelchi, R., Rössler, O., Schwanbeck, J., Weingartner, R., Martius, O., 2020. Future runoff regime changes and their time of emergence for 93 catchments in Switzerland. Hydrol. Earth Syst. Sci. https://doi.org/10.5194/hess-2020-516

Nyman, P., Yeates, P., Langhans, C., Noske, P.J., Peleg, N., Schärer, C., Lane, P.N.J., Haydon, S., Sheridan, G.J., 2021. Probability and Consequence of Postfire Erosion for Treatability of Water in an Unfiltered Supply System. Water Resour. Res. 57, 2019WR026185. https://doi.org/10.1029/2019WR026185

Panziera, L., Gabella, M., Germann, U., Martius, O., 2018. A 12-year radar-based climatology of daily and sub-daily extreme precipitation over the Swiss Alps. Int. J. Climatol. 38, 3749–3769. https://doi.org/10.1002/joc.5528

Panziera, L., James, C.N., Germann, U., 2015. Mesoscale organization and structure of orographic precipitation producing flash floods in the Lago Maggiore region. Q. J. R. Meteorol. Soc. 141, 224–248. https://doi.org/10.1002/qj.2351

Pappas, C., Fatichi, S., Rimkus, S., Burlando, P., Huber, M.O., 2015. The role of local-scale heterogeneities in terrestrial ecosystem modeling. J. Geophys. Res. Biogeosciences 120, 341–360. https://doi.org/10.1002/2014JG002735

Park, J., Onof, C., Kim, D., 2018. A Hybrid Stochastic Rainfall Model That Reproduces Rainfall Characteristics at Hourly through Yearly Time Scale. Hydrol. Earth Syst. Sci. Discuss. 1–31. https://doi.org/10.5194/hess-2018-267

Paschalis, A., Fatichi, S., Molnar, P., Rimkus, S., Burlando, P., 2014. On the effects of small scale space-time variability of rainfall on basin flood response. J. Hydrol. 514, 313–327. https://doi.org/10.1016/j.jhydrol.2014.04.014

Peleg, N., Fatichi, S., Paschalis, A., Molnar, P., Burlando, P., 2017. An advanced stochastic weather generator for simulating 2-D high-resolution climate variables. J. Adv. Model. Earth Syst. 9, 1595–1627. https://doi.org/10.1002/2016MS000854

Peleg, N., Marra, F., Fatichi, S., Molnar, P., Morin, E., Sharma, A., Burlando, P., 2018. Intensification of convective rain cells at warmer temperatures observed from high-resolution weather radar data. J. Hydrometeorol. JHM-D-17-0158.1. https://doi.org/10.1175/JHM-D-17-0158.1

Peleg, N., Molnar, P., Burlando, P., Fatichi, S., 2019. Exploring stochastic climate uncertainty in space and time using a gridded hourly weather generator. J. Hydrol. 571, 627–641. https://doi.org/10.1016/j.jhydrol.2019.02.010

Peleg, N., Morin, E., 2014. Stochastic convective rain-field simulation using a high-resolution synoptically conditioned weather generator (HiReS-WG). Water Resour. Res. 50, 2124–2139. https://doi.org/10.1002/2013WR014836

Peleg, N., Sinclair, S., Fatichi, S., Burlando, P., 2020. Downscaling climate projections over large and data sparse regions: Methodological application in the Zambezi River Basin. Int. J. Climatol. https://doi.org/10.1002/joc.6578

Ragettli, S., Tong, X., Zhang, G., Wang, H., Zhang, P., Stähli, M., 2019. Climate change impacts on summer flood frequencies in two mountainous catchments in China and Switzerland. Hydrol. Res. https://doi.org/10.2166/nh.2019.118

Rienecker, M.M., Suarez, M.J., Gelaro, R., Todling, R., Bacmeister, J., Liu, E., Bosilovich, M.G., Schubert, S.D., Takacs, L., Kim, G.-K., Bloom, S., Chen, J., Collins, D., Conaty, A., da Silva, A., Gu, W., Joiner, J., Koster, R.D., Lucchesi, R., Molod, A., Owens, T., Pawson, S., Pegion, P., Redder, C.R., Reichle, R., Robertson, F.R., Ruddick, A.G., Sienkiewicz, M., Woollen, J., 2011. MERRA: NASA's Modern-Era Retrospective Analysis for Research and Applications. J. Clim. 24, 3624–3648. https://doi.org/10.1175/JCLI-D-11-00015.1

Rössler, O., Kotlarski, S., Fischer, A.M., Keller, D., Liniger, M., Weingartner, R., 2019. Evaluating the added value of the new Swiss climate scenarios for hydrology: An example from the Thur catchment. Clim. Serv. 13, 1–13. https://doi.org/10.1016/j.cliser.2019.01.001

Ruiz-Villanueva, V., Molnar, P., 2020. Past, current, and future changes in floods in Switzerland. Hydro-CH2018 project. Commissioned by the Federal Office for the Environment (FOEN), Bern, Switzerland. https://doi.org/10.3929/ethz-b-000458556

Savelsberg, J., Schillinger, M., Schlecht, I., Weigt, H., 2018. The Impact of Climate Change on Swiss Hydropower. Sustainability 10, 2541. https://doi.org/10.3390/su10072541

Scheidl, C., Heiser, M., Kamper, S., Thaler, T., Klebinder, K., Nagl, F., Lechner, V., Markart, G., Rammer, W., Seidl, R., 2020. The influence of climate change and canopy disturbances on landslide susceptibility in headwater catchments. Sci. Total Environ. 742, 140588. https://doi.org/10.1016/j.scitotenv.2020.140588

Semenov, M.A., Barrow, E.M., 1997. Use of a stochastic weather generator in the development of climate change scenarios. Clim. Change. https://doi.org/10.1023/A:1005342632279

Singer, M.B., Michaelides, K., 2017. Deciphering the expression of climate change within the Lower Colorado River basin by stochastic simulation of convective rainfall. Environ. Res. Lett. 12. https://doi.org/10.1088/1748-9326/aa8e50

Singer, M.B., Michaelides, K., Hobley, D.E.J., 2018. STORM 1.0: A simple, flexible, and parsimonious stochastic rainfall generator for simulating climate and climate change. Geosci. Model Dev. 11, 3713–3726. https://doi.org/10.5194/gmd-11-3713-2018

Skinner, C.J., Peleg, N., Quinn, N., Coulthard, T.J., Molnar, P., Freer, J., 2020. The impact of different rainfall products on landscape modelling simulations. Earth Surf. Process. Landforms 45, 2512–2523. https://doi.org/10.1002/esp.4894

Smiatek, G., Kunstmann, H., 2019. Simulating future runoff in a complex terrain alpine catchment with EURO-CORDEX data. J. Hydrometeorol. 20, 1925–1940. https://doi.org/10.1175/JHM-D-18-0214.1

Strahler, A.N., 1957. Quantitative analysis of watershed geomorphology. Trans. Am. Geophys. Union 38, 913. https://doi.org/10.1029/TR038i006p00913

Swisstopo, 2002. DHM25: Das digitale Hoehenmodell der Schweiz, Level 2, Bundesamt für Landestopographie, Wabern, Switzerland.

Trzaska, S., Schnarr, E., 2014. Methods for climate change impact assessment.

Weingartner, R., Schädler, B., Hänggi, P., 2013. Auswirkungen der Klimaänderung auf die schweizerische Wasserkraftnutzung. Geogr. Helv. 68, 239–248. https://doi.org/10.5194/gh-68-239-2013

Westra, S., Fowler, H.J., Evans, J.P., Alexander, L. V., Berg, P., Johnson, F., Kendon, E.J., Lenderink, G., Roberts, N.M., 2014. Future changes to the intensity and frequency of short-duration extreme rainfall. Rev. Geophys. 52, 522–555. https://doi.org/10.1002/2014RG000464

Wheater, H.S., Chandler, R.E., Onof, C.J., Isham, V.S., Bellone, E., Yang, C., Lekkas, D., Lourmas, G., Segond, M.L., 2005. Spatial-temporal rainfall modelling for flood risk estimation. Stoch. Environ. Res. Risk Assess. 19, 403–416. https://doi.org/10.1007/s00477-005-0011-8

Wilks, D.S., Wilby, R.L., 1999. The weather generation game: a review of stochastic weather models. Prog. Phys. Geogr. 23, 329–357. https://doi.org/10.1177/030913339902300302

Wüest, M., Frei, C., Altenhoff, A., Hagen, M., Litschi, M., Schär, C., 2009. A gridded hourly precipitation dataset for Switzerland using rain-gauge analysis and radar-based disaggregation. Int. J. Climatol. 30, n/a-n/a. https://doi.org/10.1002/joc.2025

Zubler, E. M., Fischer, A. M., Liniger, M. A., & Schlegel, T., 2015. Auftausalzverbrauch im Klimawandel. Fachbericht MeteoSchweiz, 253, 36.

3 UNCERTAINTY IN HIGH-RESOLUTION HYDROLOGICAL PROJECTIONS: PARTITIONING THE INFLUENCE OF CLIMATE MODELS AND NATURAL CLIMATE VARIABILITY

Chapter based on the published article Moraga, J. S., Peleg, N., Molnar, P., Fatichi, S., & Burlando, P. (2022). Uncertainty in high-resolution hydrological projections: Partitioning the influence of climate models and natural climate variability. **Hydrological Processes**, 36(10), e14695. https://doi.org/10.1002/hyp.14695

ABSTRACT

A major challenge in assessing the impacts of climate change on hydrological processes lies in dealing with large degrees of uncertainty in the future climate projections. Part of the uncertainty is owed to the intrinsic randomness of climate phaenomena, which is considered irreducible. Additionally, modelling the response of hydrological processes to the changing climate requires the use of a chain of numerical models, each of which contributes some degree of uncertainty to the final outputs. As a result, hydrological projections, despite the progressive increase in the accuracy of the models along the chain, still display high levels of uncertainty, especially at small temporal and spatial scales. In this work, we present a framework to quantify and partition the uncertainty of hydrological processes emerging from climate models and internal variability, across a broad range of scales. Using the example of two mountainous catchments in Switzerland, we produced high-resolution ensembles of climate and hydrological data using a two-dimensional weather generator (AWE-GEN- 2d) and a distributed hydrological model (Topkapi-ETH). We quantified the uncertainty in hydrological projections towards the end of the century through the estimation of the values of signal-to-noise ratios (STNR). We found small STNR absolute values (<1) in the projection of annual streamflow for most sub-catchments in both study sites that are dominated by the large natural variability of precipitation (explains ~70% of total uncertainty). Furthermore, we investigated in detail specific hydrological components that are critical in the model chain. For example, snowmelt and liquid precipitation exhibit robust change signals, which translates into high STNR values for streamflow during warm seasons and at higher elevations, together with a larger contribution of climate model uncertainty. In contrast, projections of extreme high flows show low STNR values due to large internal climate variability across all elevations, which limits the potential for narrowing their estimation uncertainty.

3.1 INTRODUCTION

One of the main challenges in climate change impact studies is to quantify the large uncertainties associated with climate projections (IPCC, 2018) arising from three main sources (Deser, 2020; Deser, Knutti, et al., 2012; Deser, Phillips, et al., 2012; Fatichi et al., 2016; A. M. Fischer et al., 2012; E. M. Fischer et al., 2013): (i) anthropogenic greenhouse gases emission forcing (scenario uncertainty from here on), which reflects the unknowns regarding the policy and technological developments in the future; (ii) numerical climate models (model uncertainty), which are the result of imperfect understanding of climate dynamics, that leads to assumptions, simplification and parameterizations in the physics built into climate models; and (iii) natural internal climate variability (stochastic uncertainty), which is a measure of the inherent randomness of climate occurrences and is intrinsic to climate processes (Deser, 2020). Unlike scenario and model uncertainty, stochastic uncertainty is considered irreducible (e.g., Fatichi et al, 2016), i.e., it will persist despite advances in scientific knowledge and prediction tools. In the case of hydrological projections, there are additional sources of

uncertainties beyond the influence of climate variables. These include, for example, the difference among hydrological models (e.g., Addor et al., 2014), their parameterization (e.g., (Feng & Beighley, 2020)), or the hydrological effects induced by changes to land use and landscape (Chawla & Mujumdar, 2018) and other anthropogenic interventions (Magilligan and Nislow 2005).

The relative contribution of each factor depends on spatial and temporal scales, the time horizon of the analysis, and the examined variable. For example, at local scale while stochasticity dominates the uncertainty in precipitation, temperature uncertainty is mostly driven by climate model and scenario uncertainties (Fatichi et al., 2015, 2016). In general, stochastic uncertainty is relatively larger when looking at the near future (a few decades), thus suggesting a limited potential for uncertainty reduction for shorter lead times (Hawkins & Sutton, 2011). Whereas its contribution increases with finer temporal and spatial resolution (Addor et al., 2014; Fatichi et al., 2014, 2016; Hawkins & Sutton, 2011; Peleg et al., 2019). In contrast, scenario uncertainty plays a dominant role in the projection of temperature changes for long-term horizons because of the large influence of greenhouse gases emissions on global temperatures (IPCC, 2018).

These climate uncertainties propagate further down the model chain and affect response of catchments in future climate scenarios, as shown by numerous works that have studied the magnitude and partitioning of hydrological uncertainties, including the uncertainty introduced by the use of hydrological models (e.g., Chawla & Mujumdar, 2018; Chen et al., 2017; Clark et al., 2016; Feng & Beighley, 2020; Vetter et al., 2017). An important study of hydrological uncertainty estimation in mountain areas was presented by (Addor et al., 2014), who used a simulation ensembles approach to quantify and partition uncertainties of annual streamflow in six alpine catchments while comparing the outputs of three different hydrological models. They show that, as seen in larger-scale studies, most of the uncertainty in future streamflow prediction arises from climate models and natural climate variability, with only a small influence of scenario uncertainty or the choice of hydrological model for long-term horizons (end of the century).

Quantifying the contribution of each of these uncertainty sources, known as uncertainty partitioning, is therefore fundamental for understanding the potential for making more accurate hydrological projections. A major challenge, however, is that large ensembles of simulations are required to explore the range of natural climate variability. Climatic modelling is based on General Circulation Models (GCMs), or Regional Climate Models (RCM), which solve physically-based equations that simulate the climate of the past and future. An important limitation is that, due to their large computational requirements, the product of GCMs or RCMs usually consists of a single or at most few realizations of future climate variables, which means that an assessment of natural (stochastic) climate variability is generally not straightforward (Hawkins & Sutton, 2009, 2011). The few existing exceptions (e.g., Deser, 2020; Deser, Knutti, et al., 2012; Lehner et al., 2020; Thompson et al., 2015) have produced results of coarse resolution, which are not suitable for hydrological modelling at a broad range of catchment scales (Fatichi et al., 2015).

This deficiency can be overcome by simulating many possible realizations of a future climate at the right scale for hydrological modelling with stochastic weather generators (WG). By forcing a WG to follow the climate conditions estimated by GCMs or RCMs, it is possible not only to reproduce small-scale future climate variables but also to obtain an ensemble of simulations for uncertainty quantification. Using deterministic hydrological models forced by WG simulations allows to estimate future hydrological statistics, assess their variability, partition the different sources of uncertainties, and quantify the potential for narrowing the

uncertainty down. Some examples in using WGs to quantify sources of uncertainty include, among others, (Minville et al., 2008), who combined a WG with a hydrological model to partition the uncertainty of climate change impacts on a catchment in northern Canada and found that the choice of climate models has a larger effect on the assessed impacts than the selected emission scenario. (Fatichi et al., 2015) used multisite rainfall and temperature generators to study the hydrological response of the Upper Rhone basin, showing how the impact of uncertainty is reduced for heavily-regulated catchments and is highest for catchments fed predominantly by liquid precipitation. Likewise, (Camici et al., 2017) used a rainfall generator and hydrological model chain to examine hourly discharge extremes in the upper Tiber basin, in Italy, and highlighted the influence of catchment permeability on the response to climate change; also showing that natural variability is a much larger driver of uncertainty than climate models. In general, these and other studies agree that stochastic and climate model uncertainties are the two most relevant uncertainty sources for streamflow projections (Chawla & Mujumdar, 2018; Gao & Booij, 2020; Giuntoli et al., 2018; Shen et al., 2018). Accordingly, this work focuses on analyzing those two uncertainty sources, omitting the effects of emission scenario and hydrological-model uncertainties.

While the scale dependency and spatial and elevation variability of climate change impacts on hydrology have been previously studied, the uncertainty of those projections has not received the same level of attention. This study aims to address this knowledge gap and to do so at the seldom explored sub-catchment and hourly scales. Consequently, we address here three specific research goals: (i) to quantify the uncertainty of changes on distributed climatic and hydrological variables at sub-catchment scales, and determine their relation with elevation; (ii) to estimate the fraction of stochastic and climate model uncertainty in the future projections, and thus show the importance of natural variability when assessing climate impacts; and (iii) to assess the potential for narrowing down the uncertainty of streamflow extremes projections by estimating their signal-to-noise ratio and quantifying the magnitude of the irreducible stochastic uncertainty.

To this effect, we present in the following sections an experimental framework based on the work presented in (Moraga et al., 2021), which consists of combining the use of a two-dimensional stochastic weather generator, AWE-GEN-2d (Peleg et al., 2017, 2019), with a distributed hydrological model, Topkapi-ETH (Fatichi et al., 2015) to generate ensembles of climate and hydrological variables characterizing the present climate and, based on the outputs of nine GCM-RCM modelling chains, their response to climate change throughout the 21st century. This framework allows us to go beyond previous studies as we quantify the contribution of stochastic uncertainty on an array of climate and hydrological variables – including extreme events–, at considerably high resolution in space. Thus, we provide a reference for quantifying and partitioning uncertainty related to the effects of climate change on catchment hydrology.

3.2 METHODS AND DATA

3.2.1 Study area

The numerical experiments are based on data from two Swiss mountainous catchments: Kleine Emme and Thur. The Kleine Emme is located in the northern Alpine region in central Switzerland and extends over an area of 478 km^2. Its mean elevation is 1047 m, and highest elevation is 2330 m, and its outlet is at 438 m near the city of Lucerne. It receives mean annual precipitation of 1650 mm yr^{-1}, has an average temperature of 7 °C and its outlet discharges on average 12.6 m^3 s^{-1} (833 mm yr^{-1}). The Thur river catchment, while part of the greater Alpine area, is mostly located in the Swiss plateau physiographic division in northeast Switzerland. It

has an area of 1,730 km^2, a highest point of 2434 m, a mean elevation of 773 m, and a lowest point at 361 m in the town of Andelfingen. The mean annual precipitation over the Thur catchment is 1350 mm yr^{-1}, an average temperature of 8.4 °C and the average streamflow at the outlet is 46.7 $m^3 s^{-1}$ (851 mm yr^{-1}). A particular feature of these catchments is that they do not have major stream regulations, water extractions, or large urbanized surfaces, as the prevalent land cover is cropland and natural pasture. A summary of their location, elevation map, and elevation distribution is presented in Figure B-1.

The topography of the catchments was characterized using a regular grid with a cell size of 100 m x 100 m, based on topographic information obtained from a digital elevation model (SwissTopo, 2002). Soil properties, used to assign hydraulic soil parameters as well as soil depth, were determined from the soil map of Switzerland (Bodeneignungskarte, 2012). Likewise, the Corine dataset (CLC, 2012) was used to derive land cover classifications to determine surface roughness and evapotranspiration parameters.

3.2.2 Models and data

The two-dimensional weather generator AWE-GEN-2d (Peleg et al., 2017, 2019) was used to simulate gridded climate variable time series at a high spatial (2-km for precipitation, 100-m for the other variables) and temporal (5-minute for precipitation, hourly for the other variables) resolutions. Among its features, AWE-GEN-2d is capable of realistically modelling the arrival process of storms as well as their spatiotemporal evolution based on ground stations and weather radar observations. Satellite images are used to calibrate the cloud cover module (cross-correlated with the precipitation fields), which in turn controls the distributed incoming shortwave radiation. Furthermore, the advection of cloud and precipitation fields was estimated based on statistics of geostrophic wind velocities obtained from reanalysis data, with the cartesian components of convection modelled as a bivariate autoregressive process at a 5 min resolution. Near-surface air temperature is characterized as a stochastic process using modelled incoming long-wave radiation and the previous hour air temperature as inputs, and is distributed in space via a stochastic lapse rate, with the capability to reproduce thermal inversion events. AWE-GEN-2d was calibrated using a large dataset of climate observations and validated by analyzing statistics not used in the calibration process, as described in (Peleg et al., 2017), where a comprehensive description of the model structure is provided.

The hydrological simulations were performed using Topkapi-ETH (Fatichi et al., 2015), a distributed hydrological model, suitable for characterizing surface and sub-surface processes at high resolutions (sub-kilometer grids) and efficient enough to use for long simulations in relatively large domains. As such, it has been employed successfully to model the hydrological response of a number of mountainous catchments (Battista, Molnar, et al., 2020; Battista, Schlunegger, et al., 2020; Fatichi et al., 2014; Pappas et al., 2015; Paschalis et al., 2014). With precipitation, temperature and cloud transmissivity as input, the model simulates a broad range of hydrological variables including streamflow, snowmelt, soil moisture, groundwater flows, and evapotranspiration. It models surface and subsurface flows through two soil layers plus a groundwater compartment by approximating lateral water transfer with the kinematic-wave equation following topographic gradients (Liu & Todini, 2005). Infiltration capacity is explicitly computed at each grid cell and surface runoff may occur due to either infiltration excess or saturation of the upper soil layer. Additionally, potential evapotranspiration is calculated with the Priestley-Taylor equation (Priestley & Taylor, 1972) as a function of incoming shortwave radiation, albedo, and temperature.

Climate observations from an array of sources were used as a model forcing and for calibration. As required by AWE-GEN-2d, point temperature, precipitation and radiation observations at hourly resolution were obtained from ground stations operated by

MeteoSwiss, who also provided the gridded daily datasets for temperature and precipitation at 2-km resolution, (Wüest et al., 2009), as well as C-band weather radar information used to characterize the spatial structure of rainfall (Germann et al., 2006). Geostrophic wind velocity, used to model the advection of storm cells, as well as cloud cover, were extracted from the MERRA-2 reanalysis dataset (Rienecker et al., 2011). The temperature and precipitation statistics from nine different GCM-RCM model chains, developed in the context of the EURO-CORDEX initiative (Jacob et al., 2014; Kotlarski et al., 2014), and later post-processed by MeteoSwiss (CH2018, 2018), were used to re-calibrate AWE-GEN-2d parameters for future climate following the procedure described in Peleg *et al.* (2019).

The calibration of Topkapi-ETH was based on hourly observations of streamflow at the outlet of the catchments, which were provided by the Swiss Federal Office for the Environment (FOEN). The model was manually calibrated by optimizing the Nash-Sutcliffe Efficiency statistic (NSE) at the catchments' outlet at the hourly (NSE of 0.64 at the Kleine Emme and 0.60 at the Thur) and monthly (0.76 and 0.78) scales for the 2000–2009 period, as detailed in (Moraga et al., 2021).

3.2.3 Design of the Experiment

The experiment aimed to generate a large enough dataset of simulated variables, representing different climate trajectories, to allow for the quantification of uncertainty in the resulting climate and hydrological variables. The numerical experiment consisted of three parts, schematized in Figure 3-1 and detailed in the following sub-sections: the generation of present and future climate ensembles following multiple climate trajectories, the simulation of high-resolution hydrological variables, and the quantification of changes and associated uncertainties. The procedure to obtain the statistics for extreme events is also explained in Section 3.2.3.4.

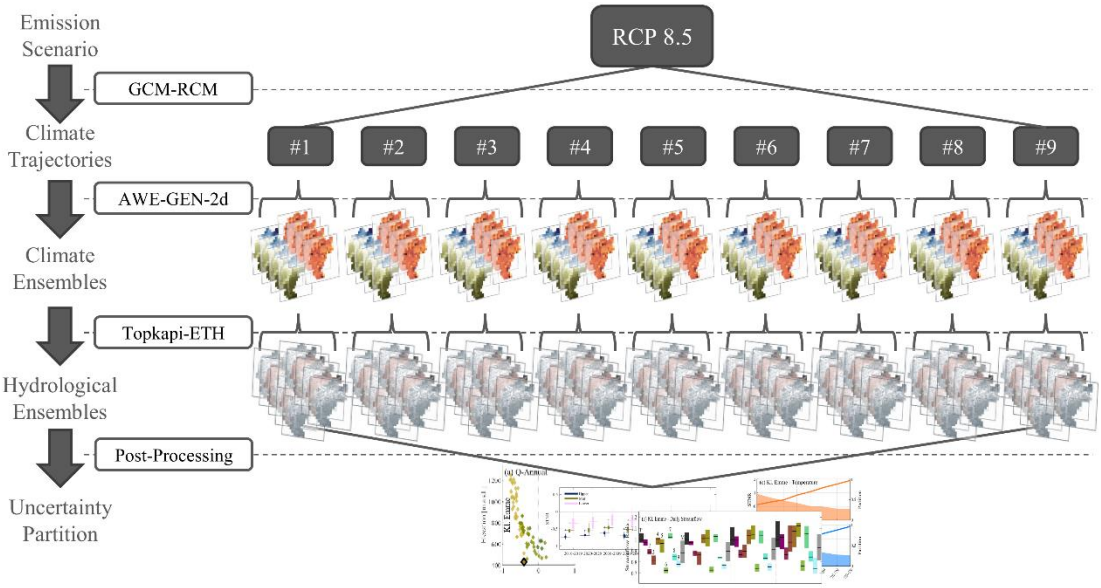

Figure 3-1: Schematic representation of the numerical experiment used to quantify and partition uncertainty. Nine climate model outputs, which follow an RCP 8.5 emission scenario, are stochastically downscaled to produce ensembles of climate variables, which in turn feed a deterministic hydrological model. The large array of climate and hydrological results are post-processed to quantify the uncertainty in the climate and hydrological projections and to compute the uncertainty partition.

3.2.3.1 Ensembles of climate variables

AWE-GEN-2d was first used to simulate 15 realizations of 30-year-long time series (equivalent to 450 years) of variables that characterize the period 1976–2005 (present climate). To simulate the future climate variables, the climate change signals were obtained from the results of RCM transient simulations: nine different climate trajectories (Model chains) were used (Table B-1), all of which follow the RCP 8.5 emission scenario.

The Factors of Change approach (Bordoy & Burlando, 2014; Fatichi et al., 2011; Peleg et al., 2019) was used to re-parameterize the temperature and precipitation parameters until the end of the 21st century. Unlike direct forcing methods, the factors of change (also called delta-change) approach does not deal with the issue of biases in the RCM outputs, as it implicitly assumes that any bias affects similarly both the control and future scenarios (Lenderink et al., 2007; Rasmussen et al., 2012; Teutschbein & Seibert, 2012; van Roosmalen et al., 2011). The procedure consists, in the case of temperature, in obtaining the difference in monthly means between the control period and future climate RCM outputs and subsequently applying the additive factor to the temperature simulated by the WG. In the case of precipitation, the objective is to obtain the ratio between future and present daily precipitation mean and other statistics so as to follow not only the change in average precipitation, but also in higher order statistics (as in Fatichi et al., 2016; Peleg et al., 2019). To do this, the control and future RCM outputs are compared at the monthly level to extract the changes in mean, standard deviation, and kurtosis of daily precipitation using a moving average with a 30-year window and a 10-year shift. These changes are then forced onto the present-climate statistics so as to ensure that they are reflected in the estimation of the new WG parameters and consequently on the future climate simulations. In total, ensembles consisting of ten realizations of 80 years (2010–2089) for each of the nine climate trajectories were simulated, for a total of 7200 years of time series representing the future.

3.2.3.2 Hydrological simulations

The hydrological processes in the present and future for the Thur and Kleine Emme catchments were modelled using Topkapi-ETH. The climate inputs for the simulations were obtained from the previously described outputs of the weather generator. Specifically, ensembles of gridded time series of 2-km and hourly resolutions for precipitation, air temperature, and cloud transmissivity were fed to the model to perform multiple realizations of continuous hydrological simulations for the present and future climates.

The hydrological outputs consisted of gridded datasets at 100-meter and hourly resolutions for variables that represent the main components of the hydrological budget: streamflow, rainfall, snowmelt, evapotranspiration, and change in soil water storage. We saved outputs not only at the entire catchment scale at the outlet of the river but also at the scale of small sub-catchments along the river networks: 97 virtual stations were selected in the Kleine Emme and 112 in the Thur catchments for this purpose. The selected variables, the number of sub-catchments, and the size of the simulation ensembles represent a compromise between obtaining large and comprehensive enough datasets for the proposed uncertainty partition analysis and manageable size of data storage.

3.2.3.3 Quantifying uncertainty

The third part of the experiment refers to the processing of simulation results to quantify the uncertainty source in the simulated variables. Based on the concept of signal-to-noise ratio (STNR; (Fatichi et al., 2014; Hawkins & Sutton, 2009, 2011)), we summarize the magnitude of the uncertainty by means of a proposed STNR statistic, which we define as the ratio between the change in the median values of a given statistic for a given variable q (e.g., extreme streamflow, mean rainfall) between future and present climate (the signal) and the

spread measured by the average interquartile range IQR (the noise) around the median of the future and present simulation ensembles, computed considering only the stochastic variability, i.e.:

$$STNR = \frac{Signal}{Noise} = \frac{2*(q_{50}^{fut} - q_{50}^{pres})}{IQR_{fut} + IQR_{pres}} \quad \text{(Eq. 1)}$$

Absolute values of STNR larger than 1 indicate that the magnitude of the signal lies outside of the average natural variability of 50% of the sample (IQR is computed between the 25th and 75th percentiles) and is assumed to represent a robust change in that statistic. Conversely, absolute STNR values smaller than 1 imply that the change is comparable or smaller than the natural variability represented by 50% of the sample. The sign of STNR is given by the direction of the signal, thus positive values indicate an increase of the analyzed variable in the future.

The resulting variable uncertainty can be partitioned into two contributing factors (Hawkins & Sutton, 2011) namely, the internal climate variability and the climate model uncertainty. Internal climate variability represents stochastic uncertainty and is calculated as the mean of the interquartile ranges (IQR) from all climate trajectories (models) in the ensemble:

$$U_{ICV} = \frac{\sum_1^N IQR_n}{N} = \frac{\sum_1^N \left(q_{75_n} - q_{25_n}\right)}{N} \quad \text{(Eq. 2)}$$

where *N* is the total number of climate trajectories (equal to the number of climate model chains) in the ensemble. The climate model uncertainty was computed as the interquartile range of the means obtained for each climate trajectory, averaging the stochastic replicates:

$$U_{CM} = IQR(\{\mu_1, \mu_2, \ldots, \mu_n, \ldots \mu_N\}) \quad \text{(Eq. 3)}$$

where $_n$ is the mean of the selected variable for trajectory *n*. As such, the relative importance *P* of uncertainty attributed to each contributing factor is obtained as:

$$P_{ICV} = U_{ICV} \Big/ (U_{CM} + U_{ICV}) \; ; \; P_{CM} = U_{CM} \Big/ (U_{CM} + U_{ICV}) \quad \text{(Eq. 4)}$$

3.2.3.4 Estimation of hydrological extremes

The analysis of extreme event statistics presented in Section 3.3.3 was performed by selecting the annual maximum streamflow (hourly or daily) for each of the 30 years of continuous simulations representing the present (1976–2005) and end-of-the-century (2060–2089) climate, and then fitting the annual maxima with a Generalized Extreme Values distribution (GEV, (Jenkinson, 1955).

Return periods ranging from 2 to 25 years were computed for each of the 15 realizations simulated for the present climate and the 10 realizations simulated for each of the 9 future trajectories (see Section 2.3.1). These 15 and 9 x 10 estimated return periods compose the data sample from which the STNR and uncertainty partition were quantified as described in Section 3.2.3.3.

3.3 RESULTS

The proposed framework allows for the quantification of uncertainty and its partition not only for several variables of interest in hydrological practice, but also across spatial and temporal scales. First, the STNR and partition of stochastic and climate model uncertainties for distributed climate variables are presented in section 3.3.1. Then, section 3.3.2 is dedicated to the hydrological variables, including streamflow and the main components of the

hydrological budget in the various sub-catchments. Finally, section 3.3.3 shows the computed STNR and fraction of stochastic uncertainty for the changes in extreme high flows.

3.3.1 Uncertainty in climate projections

For both catchments, the expected values for each grid cell (ordered by elevation) in total precipitation (including liquid and solid phases) and near-surface air temperature are shown in Figure 3-2. Annual precipitation shows a non-trivial change pattern, as the higher parts of the catchments are expected to experience a decrease in precipitation in the Kleine Emme (Thur) of up to 11% (9%) whereas the drier, lower parts of the catchments will see an increase in projected precipitation by 10% (17%), for an overall change of -3.2% (+1.4%). Conversely, the projected changes in temperature are more homogeneous, with progressive catchment-average increases that reach 4.2 °C at the Kleine Emme and 4.0 °C at the Thur catchments by the end of the century.

In turn, the STNR and uncertainty partition of precipitation and temperature, computed using the end-of-century decade (2080–2089) and present climate simulations (1976–2005), show that, for both the Kleine Emme (Figure 3-3a) and Thur (Figure 3-3e), the signal of change in precipitation is weaker than the noise, as shown by the magnitude of STNR values with ranges between -0.56 and 0.57 in Kleine Emme, and between -0.51 and 0.89 in Thur. It is possible to observe clear spatial patterns that follow those of the overall change in precipitation predicted by the climate models (see Moraga et al., 2021), with negative values of STNR at higher elevations, in the southern part of the catchments, and positive values at lower elevations. Most of the uncertainty is explained by the stochastic uncertainty, with its share of the total uncertainty ranging between 53% and 79% for Kleine Emme (Figure 3-3b) and between 57% and 91% for Thur (Figure 3-3f). Moreover, there is a strong negative correlation between elevation and the share of uncertainty associated with stochastic variability in precipitation in the Kleine Emme (linear regression with $R^2 = 0.65$), but not in the Thur catchment ($R^2 = 0.02$).

The large increase in average temperatures is reflected in the STNR, with values ranging between 3.98 and 4.85 in the Kleine Emme (Figure 3-3c) and between 2.81 and 6.05 in the Thur (Figure 3-3g), which confirm a robust change signal. Unlike for precipitation, the uncertainty is spatially uniform, with ranges narrower than 1% for both catchments, and is mostly explained by climate model uncertainty: 73% of the total in the Kleine Emme (Figure 3-3d) and 65% in the Thur (Figure 3-3h). This becomes clearer in Figure B-2, as the stochastic uncertainty for each future climate trajectory is indeed very narrow, and the overall uncertainty observed in the multi-model mean is small compared to the expected temperature change in the order of 4 °C.

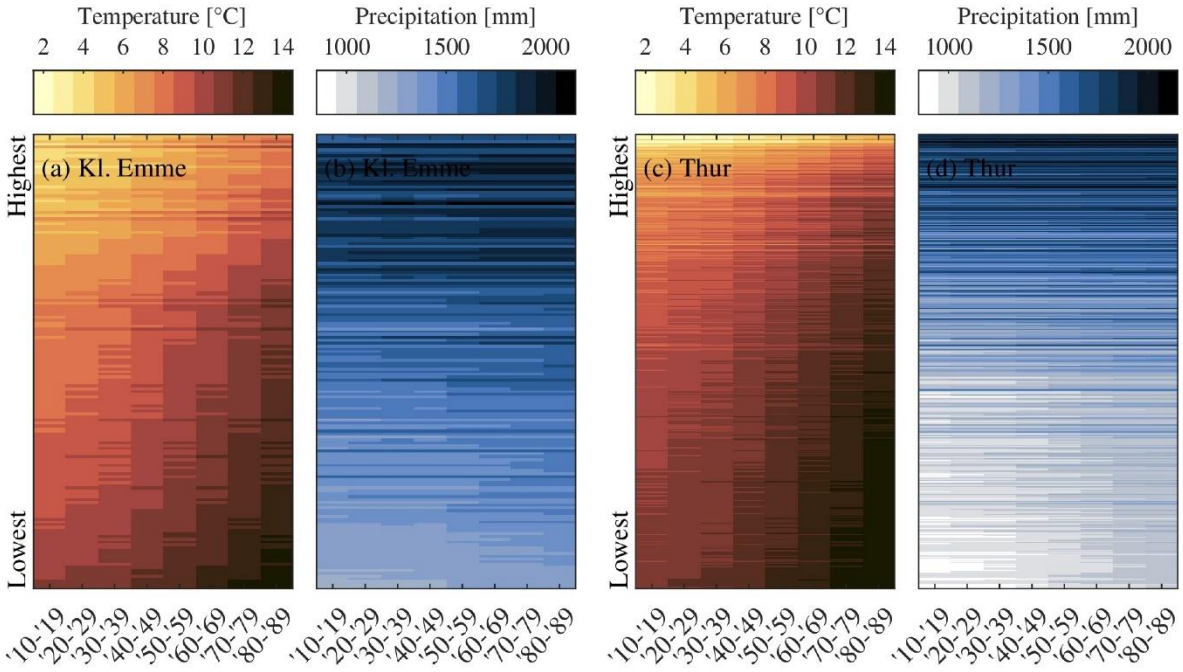

Figure 3-2: Temperature and precipitation values throughout the future climate simulations for each of the 160 grid cells in the Kleine Emme (a, b) and 497 in the Thur (c, d) river catchments. Each row represents a grid cell ordered from highest to the lowest elevation and the colors represent the decadal means.

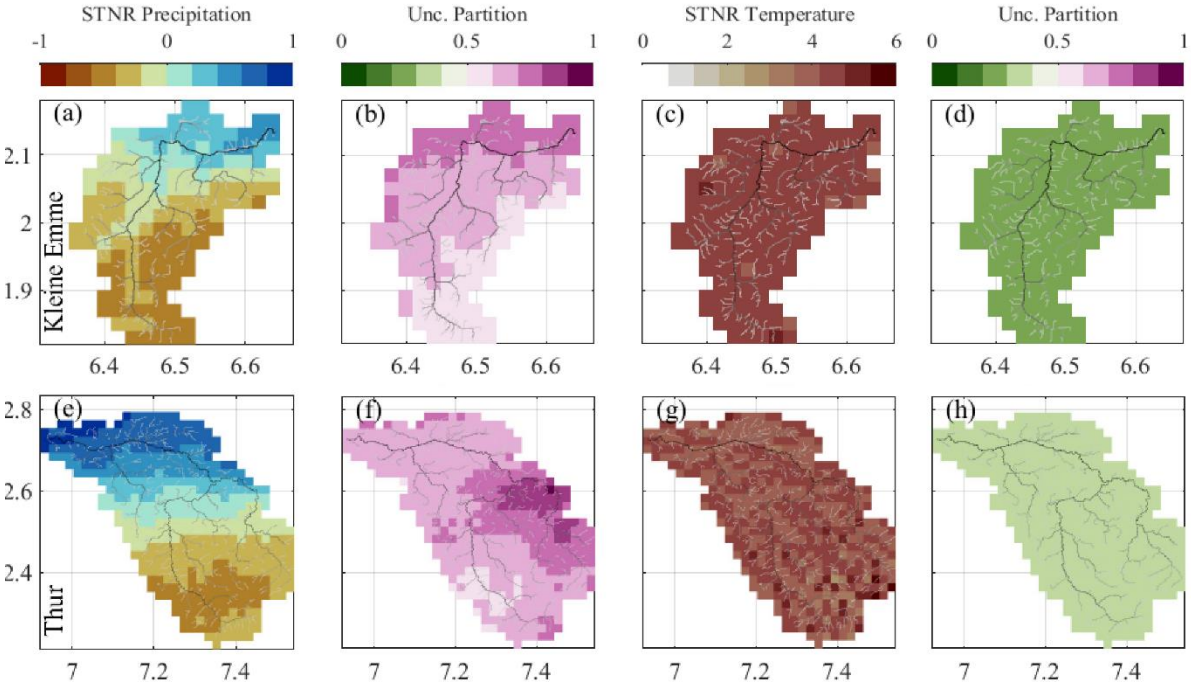

Figure 3-3: Signal-to-noise ratio (STNR) and uncertainty partition (share of stochastic uncertainty) of precipitation and temperature by the end of the century (2080–2089) in the Kleine Emme (a–d) and Thur (e–h) catchments. The coordinates are shown in 10^5 meters using the UTM 32N projection.

3.3.2 Uncertainty in hydrological projections

The total uncertainty attributed to natural climate variability (stochasticity) and climate models was computed for the hydrological components at the seasonal scale, following the procedure

detailed in section 3.2.3.3. Most of the uncertainty in streamflow projections (Figure 3-4a, 4c) is explained by stochastic uncertainty, although it can vary considerably across seasons from 58 to 83% in the Kleine Emme and from 68 to 74% in the Thur, with the largest difference between the two catchments being spring flows, as 81% of the uncertainty is explained by stochasticity in the Thur and only 64% in the Kleine Emme. At the annual scale (not shown), stochasticity explains 56% of future streamflow uncertainty in Kleine Emme and 73% in Thur, mostly due to the high uncertainty in liquid precipitation.

The uncertainty partition of specific components of the hydrological cycle are shown in Figure 3-4b and 4d. Spring snowmelt, which is a process largely driven by temperature, is the most sensitive component to climate model uncertainty, which accounts for 50% of uncertainty in the Kleine Emme and 40% in the Thur. However, its contribution to the hydrological response is expected to decrease drastically by the end of the century, to the point that its uncertainty range becomes too small to influence streamflow considerably (on average, spring snowmelt will represent only 15% and 22% of total spring streamflow, respectively). In contrast, evapotranspiration plays an important role in the hydrological response, especially during summer (JJA) at the Thur catchment, with trimestral contributions of around 250 mm, but its uncertainty range is relatively narrow compared to that of liquid rainfall. Furthermore, its uncertainty partition indicates that it is also mostly driven by stochasticity, which suggests a large influence of summer precipitation rather than temperature on the total evapotranspiration fluxes.

The evolution of the STNR and the fraction of stochastic uncertainty throughout the 21st century are shown in Figure 3-5. While the absolute values in the STNR of streamflow for both catchments remains relatively constant and low, the partition of the uncertainty shows different progressions. In the Kleine Emme, the fraction assigned to internal climate variability decreases from around 90% in the early 21st century to under 60% by the end of it, whereas in the Thur it remains constant at around 75%. The combination of low STNR values for the end-of-century streamflow projections, combined with a high contribution of stochastic uncertainty, clearly suggest that high uncertainties in streamflow projections will persist even if perfect climate models were available.

The driving climate variables, temperature and precipitation, show similar behaviors in both catchments, with a clear decrease in the uncertainty related to internal climate variability, which shows the increasing importance of climate models with longer simulation times.

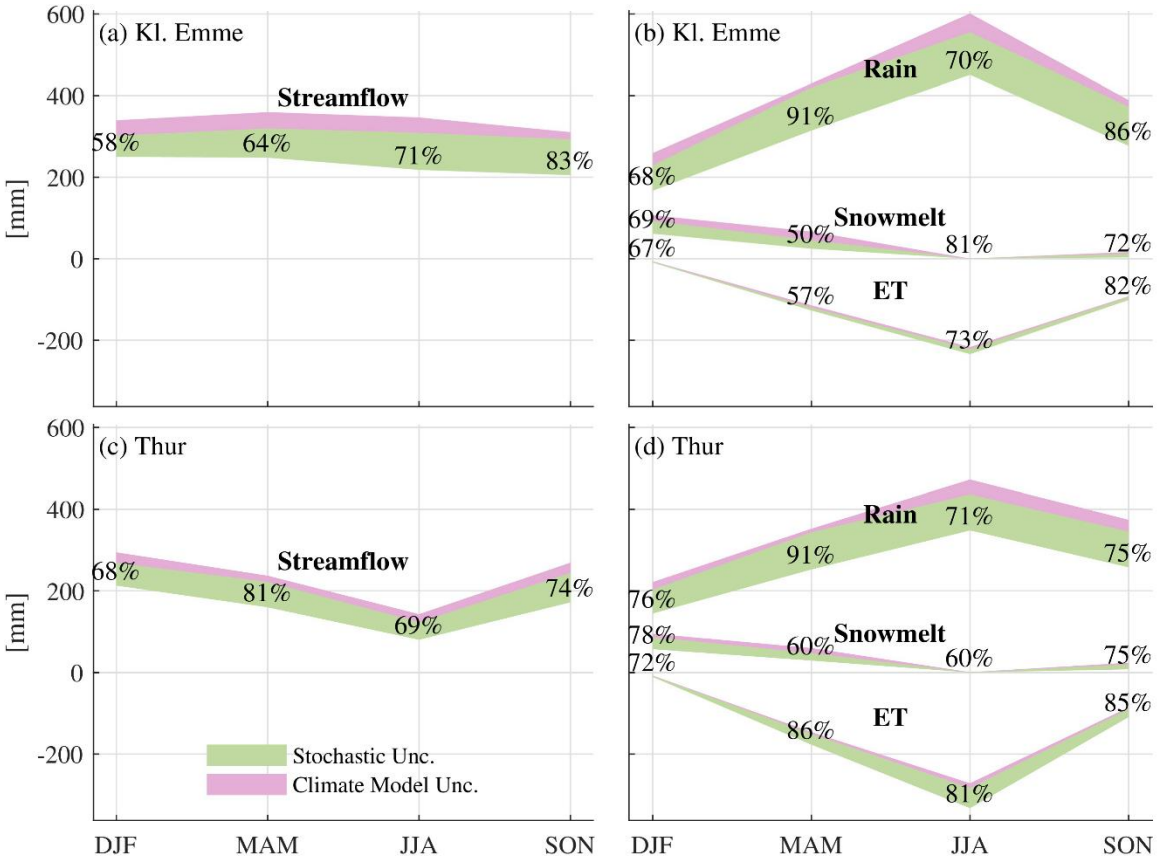

Figure 3-4: Future stochastic and climate model uncertainty for streamflow (a, c) and the main hydrological components (b, d): evapotranspiration (ET, presented as a negative value), rainfall, and snowmelt at the seasonal scales in the Kleine Emme (a, b) and Thur (c, d) river catchments. The vertical axis represents the amount of water volume in mm over the season attributed to each hydrological component with corresponding uncertainty source and the percentages indicate the fraction of uncertainty attributed to internal climate variability (stochastic uncertainty).

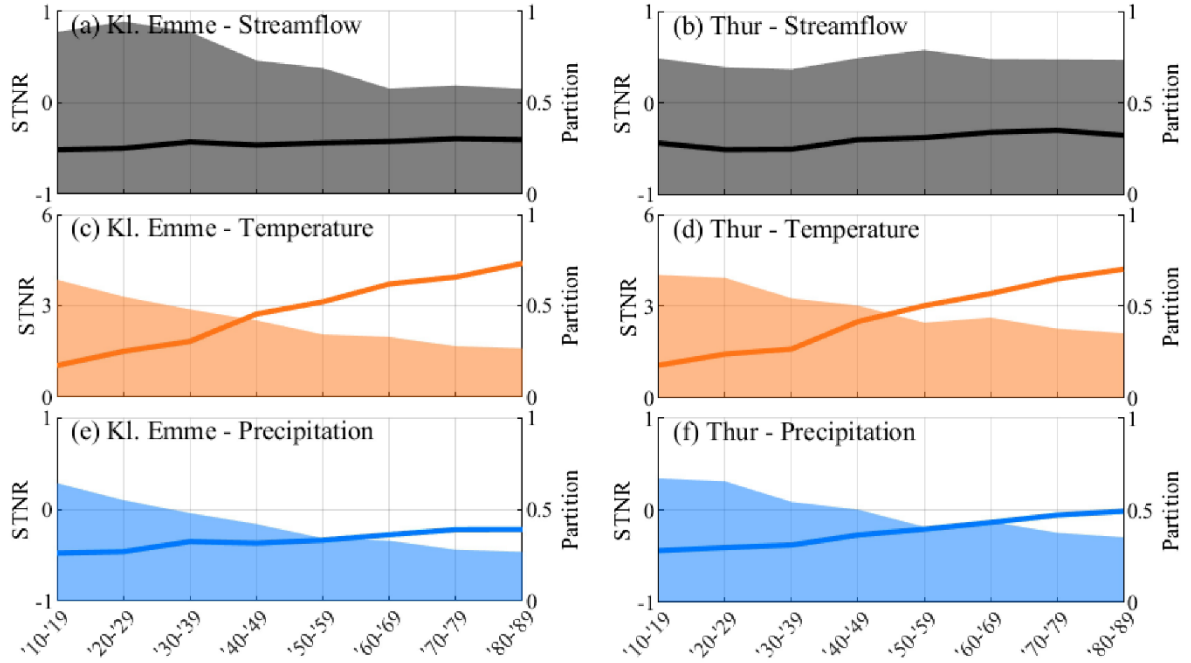

Figure 3-5: Temporal evolution of the signal-to-noise ratio (solid lines) and partition of uncertainty attributed to stochasticity (shaded areas) for streamflow at the outlet of the catchments (a, b), mean temperature (c, d), and mean precipitation (e, f) throughout the simulation period for the Kleine Emme and the Thur river catchments.

The distributed hydrological simulations allow extending the uncertainty analysis to the sub-catchment scale by computing the STNR at multiple points throughout the catchments for key hydrological variables. Figure 3-6 shows the relation between sub-catchment elevation, the STNR of seasonal and annual hydrological statistics at the end-of-the-century, as well as the uncertainty partition. As reported by Moraga *et al.* (2021), the change in mean annual streamflow in a future climate exhibits an inverse correlation with elevation. However, the results here show that this change is not statistically strong, as the STNR is lower than one for virtually all sub-catchments, indicating a signal of change smaller than the noise (Figure 3-6a and 6i), mostly due to stochastic uncertainty. Furthermore, both study sites exhibit a clear and similar negative correlation between sub-catchment elevation and the STNR value.

The change signals for individual hydrological components are clearer than for the overall streamflow. The signal of rainfall, for example, is larger than the noise (and positive in sign) for all the sub-catchments in the Kleine Emme and for the highest ones in the Thur (Figure 3-6b and 6j, respectively), also showing a clear positive correlation with elevation. The partition of stochastic uncertainty for rainfall is higher at the Thur (between 67% and 95%) than at the Kleine Emme (45%–79%), and the model uncertainty becomes more relevant at higher elevations. Likewise, the STNR for snowmelt reduction shows high absolute values (Figure 3-6c and 6k). In Kleine Emme, values range between -2.2 and -1.6, and the fraction of stochastic uncertainty goes from 48% to 64%. In the Thur, STNR is negatively correlated with elevation and ranges between -2.9 and -1.1, and the stochastic uncertainty is between 49% to 80%, with the lowest values corresponding to the highest sub-catchments. For evapotranspiration, the partition of stochastic uncertainty fluctuates around 70% for all elevations (between 63% and 78% in Kleine Emme, and between 60% and 87% in Thur) with an overall weak positive STNR (< 1) for all the sub-catchments in Kleine Emme and for 85% of sub-catchments in Thur.

Because of their different importance in the total response, the influence of these hydrological components on the overall uncertainty of streamflow needs to be weighted by their respective contribution to the hydrological budget. As seen in Figure 3-4, rainfall plays the largest role in the hydrological budget, thus suggesting that its large stochastic uncertainty is responsible for most of the uncertainty in streamflow, which explains the predominance of stochastic uncertainty over climate model uncertainty for streamflow projections. Snowmelt is, conversely, the hydrological component that is most sensitive to temperature and, therefore, to climate model uncertainty. Nonetheless, internal climate variability takes an equal or slightly larger share of its uncertainty partition (Figure 3-4i, 4j). This means that the amount of precipitation, driven mostly by stochastic uncertainty, is as relevant to the uncertainty of snowmelt as temperature, which is driven mostly by climate model uncertainty, likely due to the role played by precipitation on snow accumulation.

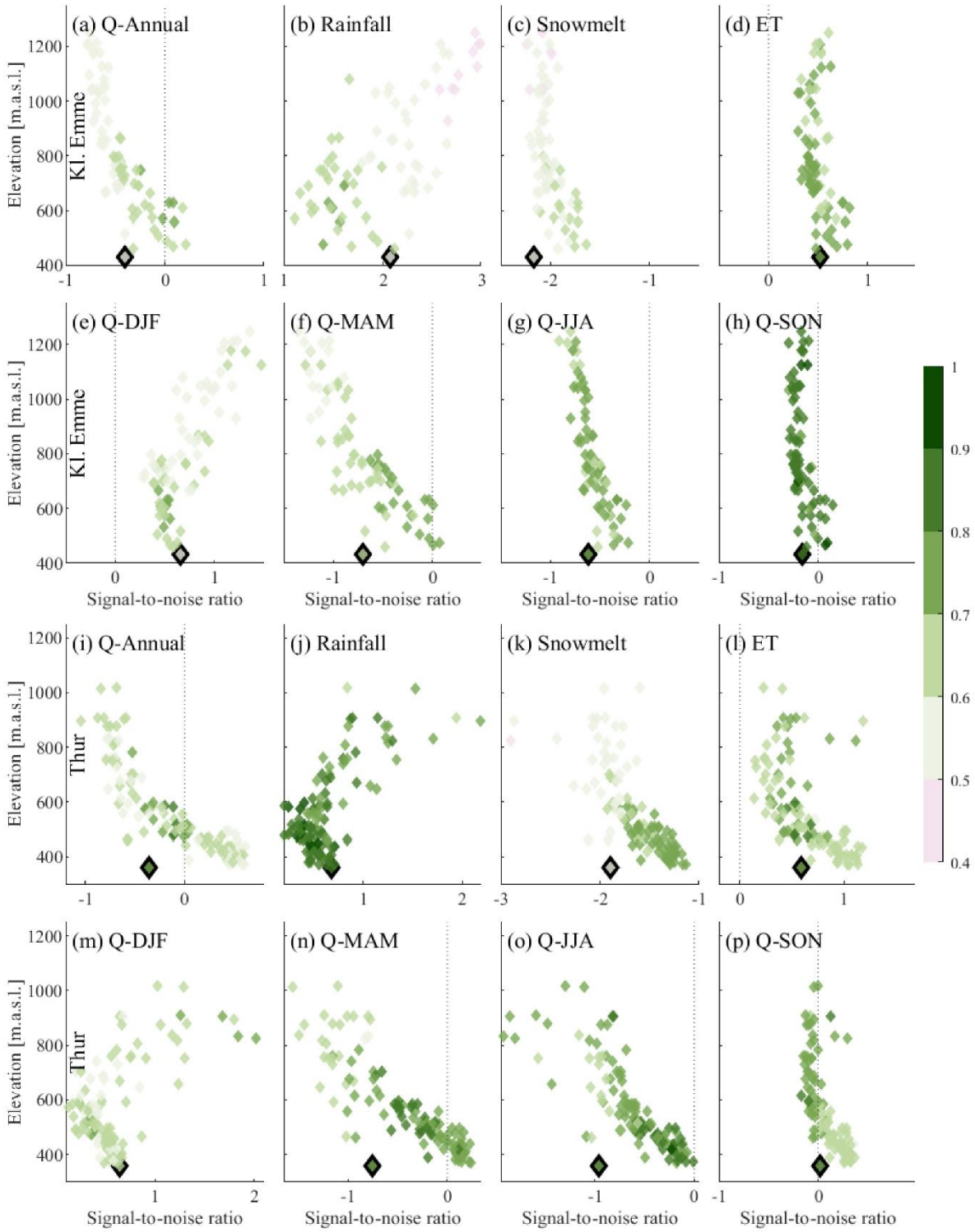

Figure 3-6: Signal-to-noise ratio (STNR) of key hydrological variables in the Kleine Emme (a–h) and Thur (i–p) catchment. The subplots show the scatter plot between STNR (comparing end-of-the-century multi-model mean and present climate simulations) of the mean three-month season flows and the elevation of the sub-catchment's outlet. The outlined symbol is the outlet of the entire catchment. The colors in the markers show the fraction of uncertainty attributed to the natural climate variability.

In contrast with the weak STNR magnitudes of annual streamflow, the projections of seasonal flows show stronger signals, particularly in the highest sub-catchments. Winter flows (Figure

6e and 6m) show a positive STNR, which is positively correlated with elevation, as winter rainfall will increase at higher altitudes. Spring (MAM) and Summer (JJA) flows, which are influenced by snowmelt, show the opposite behavior, with negative STNR values which are negatively correlated with elevation. The highest partition for stochastic uncertainty is found in the lower reaches of the river networks.

3.3.3 Uncertainty in future hydrological extremes

The large simulation ensembles allow investigating changes in the frequency of occurrence of extreme hydrological events and analyzing the relative importance of climate model and stochastic uncertainties. Figure 3-7 shows the uncertainty of the annual maximum discharge for return periods between 2 and 25 years and for both hourly and daily resolutions. From the plots, dissimilar trends for both catchments can be observed at different return periods and resolutions. In general, the magnitude of uncertainty is high, especially for hourly extreme streamflow, and as expected, increases it with higher return periods: for the hourly extremes, the uncertainty range changes from -16% to -6% for the 2-year return period to -13% to 4% for the 25-year return period in the Kleine Emme and from -8% to +4% for T = 2y to -14% to +19% for T = 25y in the Thur. Although it is apparent that climate model uncertainty is relevant, as evident from the difference among the medians of the different climate trajectories (shown with gray bars), most of the uncertainty is again explained by the stochastic uncertainty. According to the multi-model mean, both hourly and daily maxima in the Kleine Emme will become slightly smaller, even though with a large uncertainty range. The results for the Thur show, conversely, no clear change signal for hourly extremes, and a small decrease in daily extremes.

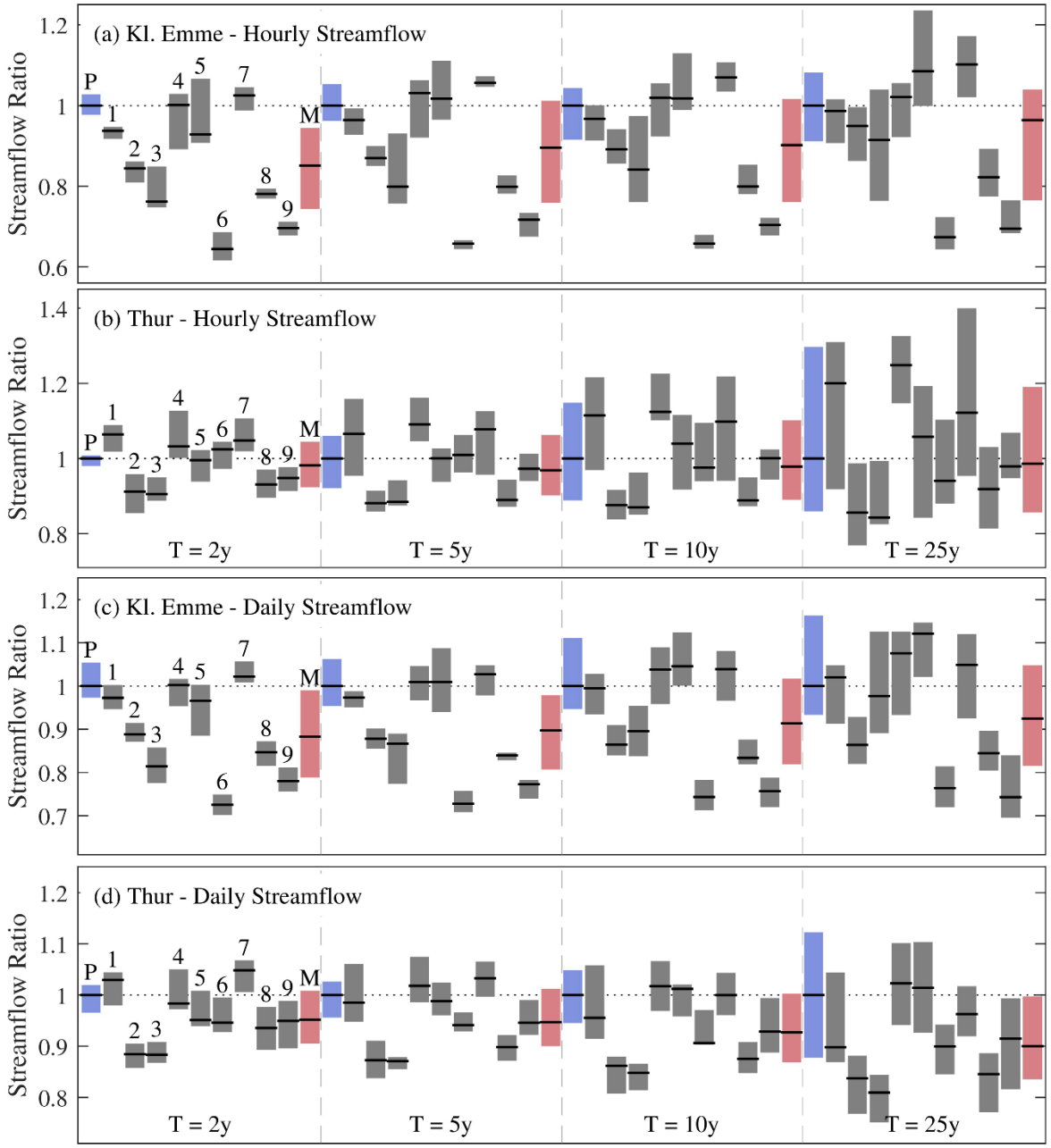

Figure 3-7: Annual maximum streamflow for a given return period for present and future climate (2060–2089) at the hourly (a, b) and daily (c, d) scales at the Kleine Emme (a, c) and Thur (b, d) catchment outlets. The values are normalized by the median of the present climate. P refers to the present climate ensemble, numbers 1 to 9 refer to the nine different model projections for future climate, and M refers to the multi-model mean of future climate. Central lines in the box plots represent the median of the values obtained from fitting the simulated ensembles of annual maxima to a GEV distribution, while the boxes represent the interquartile range.

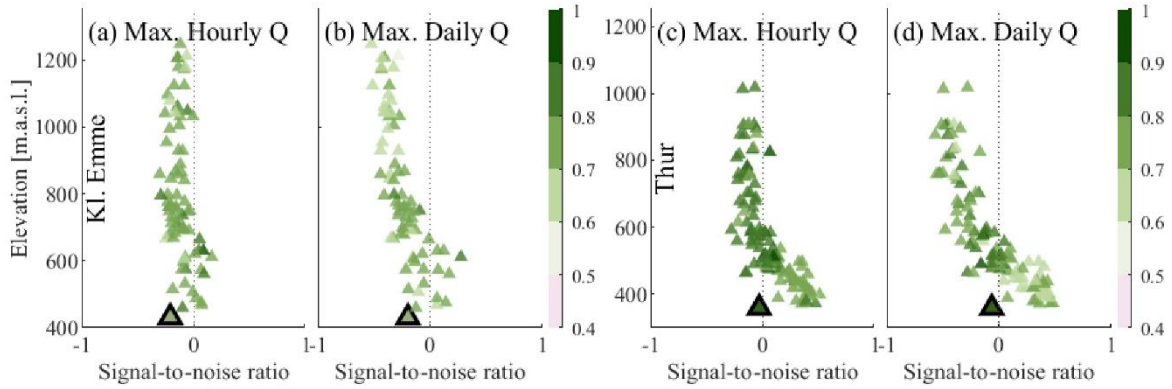

Figure 3-8: Signal-to-noise ratio (STNR) in the Kleine Emme (a–b) and Thur (c–d) catchment. The plots show the STNR (comparing end-of-the-century multi-model mean and present climate simulations) of hourly (a, c) and daily (b, d) maximum flows compared to the elevation of the sub-catchment's outlet. The outlined symbol is the outlet of the entire catchment. The colors in the markers show the fraction of uncertainty attributed to the internal climate variability.

Extreme streamflow statistics were also computed for every sub-catchment of both river basins. Figure 3-8 shows that the STNR for maximum hourly and daily flows has absolute values well below one for all sub-catchments, thus highlighting the large uncertainty in the projection of hydrological extremes into the future with a slight decrease of daily extreme streamflow at high elevations. As before, stochasticity is the dominant source of uncertainty, with average values in the Kleine Emme of 76% (81% in the Thur) for hourly maximum, and 72% (76% in the Thur) for daily maximum. The large relative importance of stochasticity, combined with weak change signals, points to a very limited potential for providing more accurate projections of hydrological extremes.

3.4 DISCUSSION

We have presented a framework that, by combining the use of a weather generator and a distributed hydrological model, allowed us to project future climate and hydrological variables at high resolution, estimate their signal-to-noise ratio and the contribution of two major uncertainty sources: stochastic (internal climate variability) and climate model uncertainty. While we explored those two uncertainty sources due to their higher relevance to hydrological projections, this framework can easily be extended to quantify the partition of uncertainty due to emission scenarios—to which the temperature-driven processes are very sensitive—or to other uncertainty sources, such as hydrological model uncertainty, which does not appear to contribute considerably to the total uncertainty in the Alpine region (Addor *et al*., 2014) but can be a major factor in catchments located in other climates (e.g., Giuntoli *et al.*, 2018).

The projections for mean streamflow are characterized by low STNR values and a large contribution of stochastic uncertainty (Fig. 4–6). This contrasts with studies on larger domains (as well as regional scales), that conclude that GCMs have a larger influence on future uncertainty than internal climate variability (e.g., Chawla and Mujumdara, 2018.; Gao and Booij, 2020; Giuntoli *et al*., 2018), but is consistent with the expectation of an increment of the importance of stochasticity for smaller spatial scales (Addor et al., 2014; Fatichi et al., 2014, 2016; Hawkins & Sutton, 2011; Peleg et al., 2019). Furthermore, the large magnitude of stochastic uncertainty suggests that high uncertainties in streamflow projections at our study sites will persist even if perfect climate models were available.

In contrast, the analysis at the level of hydrological components reveals high absolute values of STNR for liquid precipitation (rainfall), particularly in the Kleine Emme, as well as for snowmelt, indicating robust change signals in the projections because of the influence of rising temperature on precipitation form and on snowmelt. The signals for a positive change in ET are also generally weaker than the noise, although at low elevations in the Thur catchment the temperature rise will drive a significant ET increase. Just as the relative contribution of specific hydrological components can be large at the seasonal scale, so is their influence on the magnitude and partition of uncertainty in the resulting streamflow. For example, due to the high influence of (temperature-dominated) snowmelt, summer, and spring flows (Figure 3-6) present a larger share of climate model uncertainties than the annual average flow, especially for sub-catchments at high elevations, where the share of climate model uncertainty approaches 60%. Consequently, an improvement in climate model predictions with reduced spread among models implies a potential for narrowing the uncertainty of snowmelt predictions and, thus, of total streamflow during warm seasons and at high elevations. Furthermore, this is a clear indication that other catchments in the alpine region should present a similar behavior, i.e., the climate model uncertainty is much more important where the influence of snowmelt in the total hydrological budget is significant.

The projections for extreme high flows, summarized in Fig. 7 and 8, reveal an uncertainty magnitude much larger than median climate change signal projected towards the end of the century. The vast majority of this uncertainty is again attributed to stochasticity rather than to climate model signals, in line with the findings of previous studies at different locations (Fatichi et al., 2014, 2016; Gao and Booij, 2020), thus suggesting that the improvement of climate models may have a rather limited potential (in the range of 10% to 20%) for narrowing the uncertainty of the future predictions of flood extremes. Although these results do not allow us to make confident claims about the trends in future extremes on these specific catchments, our findings point at the need for awareness of the large uncertainty that affects prediction of future extremes, highlighting the need for quantifying the uncertainty of hydrological projections, and, at the very least, acknowledge the large uncertainty surrounding the projections of extremes when only deterministic results are presented. At the same time, as pointed out by Fatichi et al. (2014), the lack of significant trends in our projections implies that infrastructure correctly designed with present-day variability in mind is likely to perform as expected in the future.

It is worth noting that the temperature-dependent patterns of high-intensity precipitation events may also change under warmer conditions. This is not explicitly considered in the models used in this study as rainfall and temperature generators are both dependent on cloud cover generation, but no physical dependence mimicking the Clausius-Clapeyron (C-C) relationship between precipitation intensity and temperature increase is built into the current structure of the AWE-GEN-2d model. This represents a limitation of the stochastically downscaled climate scenarios, because theory (i.e., the C-C relation) and confirmatory observations indicate that a warming climate is expected to often cause a temperature-induced increase in extreme rainfall (Berg et al., 2009; Trenberth et al., 2003); among others), as well as modifying other spatial characteristics of storms (H. J. Fowler et al., 2021b; Lochbihler et al., 2017, 2019; Peleg, Marra, Fatichi, Molnar, et al., 2018; Peleg, Skinner, et al., 2020; Wasko et al., 2016), which may have effects on the hydrological response of catchments (Peleg et al., 2021; Peleg, Sinclair, et al., 2020).

Given that our study sites are largely representative of the alpine region; it is likely that the results apply to most catchments in the European Alps. Catchments with high regulation of flow (for example, with hydropower dams) or with a large variation in land cover (e.g., large expanses covered with glaciers) may have different uncertainty compositions (Fatichi et al.,

2014, 2015; Schirmer et al., 2022). Moreover, the proposed novel framework to partition hydrological uncertainties at high space-time resolution is not tailored to a specific case study and, thus, it is easily applicable to other regions, particularly when the interest is in characterizing either small catchment areas or complex topography in other climates beyond the European Alps. As a result, this work contributes to expanding the applicability of climate change uncertainty quantification studies.

3.5 CONCLUSIONS

This article presents a novel framework for quantifying and partitioning the uncertainty of small-scale hydrological processes, based on combining regional climate model outputs, a high-resolution weather generator, and a distributed hydrological model. Using two mountainous catchments in Switzerland as study sites, ensembles of gridded climate and hydrological variables were generated to represent the present and future climate under an RCP 8.5 emission scenario and multiple climate model chains, and quantify the stochastic uncertainty of the projections. Using a newly introduced signal-to-noise ratio (STNR) metric, it is shown that, for the entire simulation period, the change signal for annual streamflow is weak, mostly due to high values of stochastic uncertainty. The STNR of specific hydrological components such as liquid precipitation or snowmelt were, in contrast, higher and more dependent on climate model uncertainty, which suggests that improvements in climate models have the potential to narrow down the uncertainty on these variables. As a consequence, the largest potential for narrowing the uncertainty of mean streamflow was found during warm seasons and at higher elevations, where hydrological processes are more sensitive to temperature changes. As for extreme high flows, the results show low absolute values of STNR for all elevations explained by the dominant role of stochastic uncertainty, thus suggesting a limited potential for projecting flood extremes in the future with precision.

3.6 REFERENCES

Addor N, Rössler O, Köplin N, Huss M, Weingartner R, Seibert J. 2014. Robust changes and sources of uncertainty in the projected hydrological regimes of Swiss catchments. Water Resources Research 50 (10): 7541–7562 DOI: 10.1002/2014WR015549

Anandhi A, Frei A, Pierson DC, Schneiderman EM, Zion MS, Lounsbury D, Matonse AH. 2011. Examination of change factor methodologies for climate change impact assessment, Water Resources Research 47, W03501, DOI:10.1029/2010WR009104

Battista G, Molnar P, Burlando P. 2020a. Modelling impacts of spatially variable erosion drivers on suspended sediment dynamics. Earth Surface Dynamics 8 (3): 619–635 DOI: 10.5194/esurf-8-619-2020

Battista G, Schlunegger F, Burlando P, Molnar P. 2020b. Modelling localized sources of sediment in mountain catchments for provenance studies. Earth Surface Processes and Landforms 45 (14): 3475–3487 DOI: 10.1002/esp.4979

Berg P, Haerter JO, Thejll P, Piani C, Hagemann S, Christensen JH. 2009. Seasonal characteristics of the relationship between daily precipitation intensity and surface temperature. Journal of Geophysical Research 114 (D18): D18102 DOI: 10.1029/2009JD012008

Bodeneignungskarte: 77.2 Digitale Bodeneignungskarte der Schweiz, https://www.blw.admin.ch/blw/de/home/politik/datenmanagement/ geografisches-informationssystem-gis/download-geodaten.html, 2012.

Bordoy R, Burlando P. 2014. Stochastic downscaling of climate model precipitation outputs in orographically complex regions: 2. Downscaling methodology. Water Resources Research 50 (1): 562–579 DOI: 10.1002/wrcr.20443

Camici S, Brocca L, Moramarco T. 2017. Accuracy versus variability of climate projections for flood assessment in central Italy. Climatic Change 141 (2): 273–286 DOI: 10.1007/s10584-016-1876-x

CH2018, 2018. CH2018—Climate Scenarios for Switzerland: Technical Report. Zurich: National Centre for Climate Services.

Chawla I, Mujumdar PP. 2018. Partitioning uncertainty in streamflow projections under nonstationary model conditions. Advances in Water Resources 112: 266–282 DOI: 10.1016/j.advwatres.2017.10.013

Chen J, Brissette FP, Liu P, Xia J. 2017. Using raw regional climate model outputs for quantifying climate change impacts on hydrology. Hydrological Processes 31 (24): 4398–4413 DOI: 10.1002/hyp.11368

Clark MP, Wilby RL, Gutmann ED, Vano JA, Gangopadhyay S, Wood AW, Fowler HJ, Prudhomme C, Arnold JR, Brekke LD. 2016. Characterizing Uncertainty of the Hydrologic Impacts of Climate Change. Current Climate Change Reports 2 (2): 55–64 DOI: 10.1007/s40641-016-0034-x

CLC, 2014. Corine Land Cover (CLC) map 2012, https://land.copernicus.eu/pan-european/corine-land-cover/clc-2012.

Deser C, Knutti R, Solomon S, Phillips AS. 2012a. Communication of the role of natural variability in future North American climate. Nature Climate Change 2 (11): 775–779 DOI: 10.1038/nclimate1562

Deser C, Phillips A, Bourdette V, Teng H. 2012b. Uncertainty in climate change projections: The role of internal variability. Climate Dynamics 38 (3–4): 527–546 DOI: 10.1007/s00382-010-0977-x

Deser C. 2020. “Certain uncertainty: The role of internal climate variability in projections of regional climate change and risk management”. Earth’s Future 8 (12) DOI: 10.1029/2020ef001854

Fatichi S, Ivanov VY, Caporali E. 2011. Simulation of future climate scenarios with a weather generator. Advances in Water Resources 34 (4): 448–467 DOI: 10.1016/j.advwatres.2010.12.013

Fatichi S, Ivanov VY, Paschalis A, Peleg N, Molnar P, Rimkus S, Kim J, Burlando P, Caporali E. 2016. Uncertainty partition challenges the predictability of vital details of climate change. Earth’s Future 4 (5): 240–251 DOI: 10.1002/2015EF000336

Fatichi S, Rimkus S, Burlando P, Bordoy R, Molnar P. 2015. High-resolution distributed analysis of climate and anthropogenic changes on the hydrology of an Alpine catchment. Journal of Hydrology 525: 362–382 DOI: 10.1016/j.jhydrol.2015.03.036

Fatichi S, Rimkus S, Burlando P, Bordoy R. 2014. Does internal climate variability overwhelm climate change signals in streamflow? The upper Po and Rhone basin case studies. Science of the Total Environment 493: 1171–1182 DOI: 10.1016/j.scitotenv.2013.12.014

Feng D, Beighley E. 2020. Identifying uncertainties in hydrologic fluxes and seasonality from hydrologic model components for climate change impact assessments. Hydrology and Earth System Sciences 24 (5): 2253–2267 DOI: 10.5194/hess-24-2253-2020

Fischer AM, Weigel AP, Buser CM, Knutti R, Künsch HR, Liniger MA, Schär C, Appenzeller C. 2012. Climate change projections for Switzerland based on a Bayesian multi-model approach. International Journal of Climatology 32 (15): 2348–2371 DOI: 10.1002/joc.3396

Fischer EM, Beyerle U, Knutti R. 2013. Robust spatially aggregated projections of climate extremes. Nature Climate Change 3 (12): 1033–1038 DOI: 10.1038/nclimate2051

Fowler HJ, Lenderink G, Prein AF, Westra S, Allan RP, Ban N, Barbero R, Berg P, Blenkinsop S, Do HX, et al. 2021. Anthropogenic intensification of short-duration rainfall extremes. Nature Reviews Earth & Environment 2021 2:2 2 (2): 107–122 DOI: 10.1038/s43017-020-00128-6

Gao C, Booij MJ. 2020. Assessment of extreme flows and uncertainty under climate change: Disentangling the uncertainty contribution of representative concentration pathways, global climate models and internal climate variability. Hydrology and Earth System Sciences 24 (6): 3251–3269 DOI: 10.5194/hess-24-3251-2020

Germann U, Galli G, Boscacci M, Bolliger M. 2006. Radar precipitation measurement in a mountainous region. Quarterly Journal of the Royal Meteorological Society 132 (618 A): 1669–1692 DOI: 10.1256/qj.05.190

Giuntoli I, Villarini G, Prudhomme C, Hannah DM. 2018. Uncertainties in projected runoff over the conterminous United States. Climatic Change 150 (3–4): 149–162 DOI: 10.1007/s10584-018-2280-5

Hawkins E, Sutton R. 2009. The potential to narrow uncertainty in regional climate predictions. Bulletin of the American Meteorological Society 90 (8): 1095–1107 DOI: 10.1175/2009BAMS2607.1

Hawkins E, Sutton R. 2011. The potential to narrow uncertainty in projections of regional precipitation change. Climate Dynamics 37 (1–2): 407–418 DOI: 10.1007/s00382-010-0810-6

IPCC, 2018. Summary for Policymakers. In: Masson-Delmotte, V., Zhai, P., Pörtner, H.-O., Roberts, D., Skea, J., Shukla, P.R., Pirani, A., Moufouma-Okia, Péan, C., Pidcock, R., Connors, S., Matthews, J.B.R., Chen, Y., Zhou, X., Gomis, M.I., Lonnoy, E., Maycock, Tignor, M., Waterfield, T., (Eds.), Global Warming of 1.5°C. An IPCC Special Report on the impacts of global warming of 1.5°C above pre-industrial levels and related global greenhouse gas emission pathways, in the context of strengthening the global response to the threat of climate change, sustainable development, and efforts to eradicate poverty. World Meteorological Organization, Geneva, Switzerland, pp. 32.

Jacob D, Petersen J, Eggert B, Alias A, Christensen OB, Bouwer LM, Braun A, Colette A, Déqué M, Georgievski G, et al. 2014. EURO-CORDEX: new high-resolution climate change projections for European impact research. Regional Environmental Change 14 (2): 563–578 DOI: 10.1007/s10113-013-0499-2

Jenkinson AF. 1955. The frequency distribution of the annual maximum (or minimum) values of meteorological elements. Quarterly Journal of the Royal Meteorological Society 81 (348): 158–171 DOI: 10.1002/QJ.49708134804

Kotlarski S, Keuler K, Christensen OB, Colette A, Déqué M, Gobiet A, Goergen K, Jacob D, Lüthi D, Van Meijgaard E, et al. 2014. Regional climate modeling on European scales: a joint

standard evaluation of the EURO-CORDEX RCM ensemble. Geosci. Model Dev 7: 1297–1333 DOI: 10.5194/gmd-7-1297-2014

Lehner F, Deser C, Maher N, Marotzke J, Fischer E, Brunner L, Knutti R, Hawkins E. 2020. Partitioning climate projection uncertainty with multiple Large Ensembles and CMIP5/6. Earth System Dynamics Discussions 11 (2): 1–28 DOI: 10.5194/esd-2019-93

Lenderink G, Buishand A, Van Deursen W. 2007. Estimates of future discharges of the river Rhine using two scenario methodologies: Direct versus delta approach. *Hydrology and Earth System Sciences* **11** (3): 1145–1159 DOI: 10.5194/HESS-11-1145-2007

Liu Z, Todini E. 2005. Assessing the TOPKAPI non-linear reservoir cascade approximation by means of a characteristic lines solution. Hydrological Processes 19 (10): 1983–2006 DOI: 10.1002/hyp.5662

Lochbihler K, Lenderink G, Siebesma AP. 2017. The spatial extent of rainfall events and its relation to precipitation scaling. Geophysical Research Letters 44 (16): 8629–8636 DOI: 10.1002/2017GL074857

Lochbihler K, Lenderink G, Siebesma AP. 2019. Response of Extreme Precipitating Cell Structures to Atmospheric Warming. Journal of Geophysical Research: Atmospheres 124 (13): 2018JD029954 DOI: 10.1029/2018JD029954

Magilligan FJ, Nislow KH. 2005. Changes in hydrologic regime by dams. Geomorphology 71 (1–2): 61–78 DOI: 10.1016/J.GEOMORPH.2004.08.017

MeteoSwiss, 2016. Daily Precipitation (Final Analysis): RhiresD, Switzerland. [Available at http://www.meteoswiss.admin.ch/home/search.subpage.html/en/data/products/2014/raeumliche-daten-niederschlag.html.]

Minville M, Brissette F, Leconte R. 2008. Uncertainty of the impact of climate change on the hydrology of a nordic watershed. Journal of Hydrology 358 (1–2): 70–83 DOI: 10.1016/j.jhydrol.2008.05.033

Moraga JS, Peleg N, Fatichi S, Molnar P, Burlando P. 2021. Revealing the impacts of climate change on mountainous catchments through high-resolution modelling. Journal of Hydrology 603: 126806 DOI: 10.1016/j.jhydrol.2021.126806

Pappas C, Fatichi S, Rimkus S, Burlando P, Huber MO. 2015. The role of local-scale heterogeneities in terrestrial ecosystem modeling. Journal of Geophysical Research: Biogeosciences 120 (2): 341–360 DOI: 10.1002/2014JG002735

Paschalis A, Fatichi S, Molnar P, Rimkus S, Burlando P. 2014. On the effects of small scale space-time variability of rainfall on basin flood response. Journal of Hydrology 514: 313–327 DOI: 10.1016/j.jhydrol.2014.04.014

Peleg N, Fatichi S, Paschalis A, Molnar P, Burlando P. 2017. An advanced stochastic weather generator for simulating 2-D high-resolution climate variables. Journal of Advances in Modeling Earth Systems 9 (3): 1595–1627 DOI: 10.1002/2016MS000854

Peleg N, Marra F, Fatichi S, Molnar P, Morin E, Sharma A, Burlando P. 2018. Intensification of convective rain cells at warmer temperatures observed from high-resolution weather radar data. Journal of Hydrometeorology: JHM-D-17-0158.1 DOI: 10.1175/JHM-D-17-0158.1

Peleg N, Molnar P, Burlando P, Fatichi S. 2019. Exploring stochastic climate uncertainty in space and time using a gridded hourly weather generator. Journal of Hydrology 571 (3): 627–641 DOI: 10.1016/j.jhydrol.2019.02.010

Peleg N, Sinclair S, Fatichi S, Burlando P. 2020a. Downscaling climate projections over large and data sparse regions: Methodological application in the Zambezi River Basin. International Journal of Climatology DOI: 10.1002/joc.6578

Peleg N, Skinner C, Fatichi S, Molnar P. 2020b. Temperature effects on the spatial structure of heavy rainfall modify catchment hydro-morphological response. Earth Surf. Dynam 8: 17–36 DOI: 10.5194/esurf-8-17-2020

Peleg N, Skinner C, Ramirez JA, Molnar P. 2021. Rainfall spatial-heterogeneity accelerates landscape evolution processes. Geomorphology 390: 107863 DOI: 10.1016/J.GEOMORPH.2021.107863

Priestley CHB, Taylor RJ. 1972. On the Assessment of Surface Heat Flux and Evaporation Using Large-Scale Parameters. Monthly Weather Review 100 (2): 81–92 DOI: 10.1175/1520-0493(1972)100<0081:otaosh>2.3.co;2

Rasmussen J, Sonnenborg TO, Stisen S, Seaby LP, Christensen BSB, Hinsby K. 2012. Climate change effects on irrigation demands and minimum stream discharge: Impact of bias-correction method. *Hydrology and Earth System Sciences* **16** (12): 4675–4691 DOI: 10.5194/HESS-16-4675-2012

van Roosmalen L, Sonnenborg TO, Jensen KH, Christensen JH. 2011. Comparison of Hydrological Simulations of Climate Change Using Perturbation of Observations and Distribution-Based Scaling. *Vadose Zone Journal* **10** (1): 136–150 DOI: 10.2136/VZJ2010.0112

Shen M, Chen J, Zhuan M, Chen H, Xu CY, Xiong L. 2018. Estimating uncertainty and its temporal variation related to global climate models in quantifying climate change impacts on hydrology. Journal of Hydrology 556: 10–24 DOI: 10.1016/j.jhydrol.2017.11.004

Schirmer, M., Winstral, A., Jonas, T., Burlando, P., Peleg, N., 2021. Natural climate variability is an important aspect of future projections of snow water resources and rain-on-snow events. The Cryosphere Discussions, 1-27 [in review], DOI: 10.5194/tc-2021-276.

Swisstopo, 2002. DHM25: Das digitale Hoehenmodell der Schweiz, Level 2, Bundesamt für Landestopographie, Wabern, Switzerland.

Teutschbein C, Seibert J. 2012. Bias correction of regional climate model simulations for hydrological climate-change impact studies: Review and evaluation of different methods. *Journal of Hydrology* 456–457: 12–29 DOI: 10.1016/J.JHYDROL.2012.05.052

Thompson DWJ, Barnes EA, Deser C, Foust WE, Phillips AS, Thompson DWJ, Barnes EA, Deser C, Foust WE, Phillips AS. 2015. Quantifying the Role of Internal Climate Variability in Future Climate Trends. Journal of Climate 28 (16): 6443–6456 DOI: 10.1175/JCLI-D-14-00830.1

Trenberth KE, Dai A, Rasmussen RM, Parsons DB. 2003. The changing character of precipitation. Bulletin of the American Meteorological Society 84 (9): 1205-1217+1161 DOI: 10.1175/BAMS-84-9-1205

Vetter T, Reinhardt J, Flörke M, van Griensven A, Hattermann F, Huang S, Koch H, Pechlivanidis IG, Plötner S, Seidou O, et al. 2017. Evaluation of sources of uncertainty in projected hydrological changes under climate change in 12 large-scale river basins. Climatic Change 141 (3): 419–433 DOI: 10.1007/s10584-016-1794-y

Wasko C, Sharma A, Westra S. 2016. Reduced spatial extent of extreme storms at higher temperatures. Geophysical Research Letters 43 (8): 4026–4032 DOI: 10.1002/2016GL068509

Wüest M, Frei C, Altenhoff A, Hagen M, Litschi M, Schär C. 2009. A gridded hourly precipitation dataset for Switzerland using rain-gauge analysis and radar-based disaggregation. International Journal of Climatology 30 (12): n/a-n/a DOI: 10.1002/joc.2025

4 MODELING TEMPERATURE-DEPENDENT SUB-DAILY EXTREME RAINFALL WITH A GRIDDED WEATHER GENERATOR

Chapter based on the unpublished article Moraga, J. S., Peleg, N., & Burlando, P. (In review). Modeling temperature-dependent sub-daily extreme rainfall with a gridded weather generator.

ABSTRACT

Temperature increases are associated with an intensification of heavy sub-daily extreme rainfall by approximately 7% per °C, in accordance with the Clausius-Clapeyron (CC) relation. As a result of this intensification, there are concerns regarding the increased frequency and magnitude of floods in small to medium-sized catchments. The high-resolution two-dimensional weather generator (WG), AWE-GEN-2d, offers an ideal tool to simulate the climate variables required to assess the catchment-scale hydrological response at high resolution. However, it lacked an explicit representation of the relationship between temperature and precipitation that can mimic the CC relationship. Therefore, we introduce a newly revised version of the model, named AWE-GEN-2d-CC, designed to mirror the observed CC scaling by conditioning the simulation of precipitation properties (intensity and area) on temperature. We demonstrate the model's efficacy in representing future extreme rainfall by simulating their potential impact on the hydrological response of a mountainous catchment in the Swiss Alps. Based on observations and future climate model projections, AWE-GEN-2d-CC was used to generate large ensembles of present and end-of-century climate data at hourly and 2-km resolutions, used subsequently as input to Topkapi-ETH, a physically-based, distributed hydrological model. The new version of the WG successfully mimics the CC scaling of heavy rainfall, leading to an intensification of short-duration heavy rainfall in future climates, in contrast with the results obtained using the original model. This allows for a more realistic assessment of future rainfall impact on hydrological response, which, in the demonstration application, shows a modulated effect even for short durations.

4.1 INTRODUCTION

Short, intense rainfall events have the potential to trigger pluvial floods, especially in small to medium-sized rural catchments (Wasko et al., 2021), as well as in mountainous (Moraga et al., 2021) and urban areas (O'Donnell & Thorne, 2020). The Clausius-Clapeyron (CC) relation, a well-established theory, postulates that the water-holding capacity of the atmosphere increases by ~7% for each °C increase in temperature (O'Gorman & Schneider, 2009; Trenberth et al., 2003). Consistent with this theory, numerous studies have shown that short-duration (daily to sub-daily) heavy rainfall intensities are indeed scaled with the temperature (Berg et al., 2013; Fischer and Knutti, 2016; Fowler et al., 2021; Molnar et al., 2015; Westra et al., 2014) While there have been reports of discrepancies, such as cases with no or negative scaling (Drobinski et al., 2016), it is now generally accepted that the scaling of short-duration rainfall intensity with temperature is indeed close to or above the theoretical CC-scale (Ali, Fowler, et al., 2021; Ali, Peleg, et al., 2021). Moreover, temperature appears to influence not only the rainfall intensity but also the area and temporal structure of the rainfall (Lochbihler et al., 2017, 2019; Peleg et al., 2018, 2022; Wasko et al., 2016).

General circulation models (GCMs) and regional climate models (RCMs) are frequently employed to project atmospheric changes, which result from varying greenhouse gas

emission scenarios. However, the spatial resolution of these models, even that of the finer RCMs (with over 10 km x 10 km grid cells and daily time steps), is often too coarse to effectively resolve convective processes. Consequently, they depend on simplified parameterizations, leading to less reliable estimations of sub-daily extremes, and frequently missing the observed temperature-scaling evident in real-world observations (Ban et al., 2014; Fischer et al., 2015).

Alternatively, convection-permitting models (CPMs) are designed to explicitly resolve the convection at finer spatial resolutions (1–10 km^2), which allows for realistic simulations of short-duration rainfall (Ban et al., 2021; Lucas-Picher et al., 2021; Pichelli et al., 2021; Prein et al., 2015, 2020; Vergara-Temprado et al., 2021). In fact, simulations by CPMs have shown that heavy short-duration rainfall, typically associated with events with intensities exceeding the 99th percentile (Fowler et al., 2021), often results from convection and that RCMs usually underestimate the rate of CC-scaling (Ban et al., 2018, 2021; Pichelli et al., 2021).

Furthermore, CPM simulations indicate that the rates of temperature-scaling are expected to persist under future global warming scenarios (Ban et al., 2018; Kendon et al., 2017; Pichelli et al., 2021; Vergara-Temprado et al., 2021). This underlines the importance of CPM projections for modeling the effects of climate change on short-duration heavy rainfall. The limitation of CPMs, however, lies in their high computational cost, which typically restricts their outputs to a single realization of a relatively short future climate simulation (Gutowski et al., 2020; Schär et al., 2020), limiting the possibility of conducting robust extreme value analysis or assessing projection uncertainties, such as those stemming from different emission scenarios or climate models (Addor et al., 2014; Fatichi et al., 2016; Moraga et al., 2022).

One potential solution to this challenge involves downscaling climate projections using stochastic weather generators (WG, Bordoy & Burlando, 2014; Fatichi et al., 2011; Fowler et al., 2007; Maraun et al., 2010; Peleg et al., 2019; Trzaska & Schnarr, 2014; Wilby, 1999). Being relatively inexpensive in computational terms, WG are suitable to generate large ensembles of climate variables that are statistically similar to the observations used for calibration (Maraun et al., 2010; Wilks & Wilby, 1999). WGs can be re-parameterized using information from GCM/RCM to generate an ensemble of the future climate (e.g., Peleg et al., 2019). Moreover, by incorporating data from several climate models and multiple emission scenarios, WG can generate an ensemble that accounts not only for natural climate variability but also for the uncertainties emerging from climate models and emission scenarios (Fatichi et al., 2016; Moraga et al., 2022).

Numerous types of WGs exist, ranging from single-site (Fatichi et al., 2011) to multi-site (Sparks et al., 2018; Steinschneider et al., 2019; Verdin et al., 2018) to fully two-dimensional (Peleg et al., 2017; Singer et al., 2018; Verdin et al. 2019), with the latter being the most suitable for characterizing highly heterogeneous climates. The AWE-GEN-2d model (Peleg et al., 2017) is a two-dimensional WG that can simulate the climate variables necessary for distributed hydrological modeling for both present and future climates at a high space-time resolution, as it is capable of simulations at sub-kilometer and sub-hourly scales (Peleg et al., 2019). Consequently, it has been employed for hydrological climate impact studies in many rural, urban, and mountainous catchments (Fatichi et al., 2021; Fischer et al., 2022; Moraga et al., 2021; Nyman et al., 2021; Peleg et al., 2020; Ramirez et al., 2022; Schirmer et al., 2022). However, one limitation of AWE-GEN-2d is its lack of explicit representation of the influence of temperature on rainfall fields, especially on heavy (convective) rainfall. This omission can lead to unrealistic scaling of storm properties with temperature, with disproportionate effects on short-duration rainfall. This limitation is particularly pronounced for

future climate simulations, where the model relies on coarse-scale projections, which typically underestimate the intensity of convective storms.

Consequently, we introduce a new CC-scaling-capable version of the AWE-GEN-2d model, named AWE-GEN-2d-CC, which improves on the original model by Peleg et al., (2017) by explicitly conditioning rainfall properties to the near-surface air temperature at the onset of the event. We applied the new model version to a well-studied mountainous catchment in the Swiss Alps to demonstrate the effect that the new model has on the estimation of climate change impacts on streamflow by comparing the outputs obtained using the new and original models. Furthermore, we used the outputs of the WG to feed a physically-based, distributed hydrological model, Topkapi-ETH (Fatichi et al., 2015), to assess the response of a mountainous catchment to extreme hydrometeorological events within the context of a warming climate.

4.2 THE ORIGINAL AWE-GEN-2D MODEL

The original AWE-GEN-2d model (Peleg et al., 2017) was designed to downscale coarse or sparse observational data into fine two-dimensional arrays of climate variables. It accomplishes this by combining physically-based equations with data-driven stochastic models which require observations from multiple sources, thus leveraging the capabilities of both stochastic and deterministic approaches. A thorough description of the model's structure is provided by Peleg et al. (2017), along with a Technical Reference detailing the equations that compose the different components of the model. In this section, we focus on a concise, qualitative overview of AWE-GEN-2d's modules (Figure 4-1a), aiming to facilitate the comparisons with our newly proposed model formulation (Figure 4-1b).

As illustrated in Figure 4-1a, AWE-GEN-2d operates in a sequence of interconnected modules. The simulation begins with the so-called storm arrival process, which determines the duration of alternating 'wet' (indicating a precipitation event) and 'dry' spells. For each precipitation event, the model simulates the joint temporal evolution of its mean areal statistics, i.e., the wet area ratio (WAR), the mean precipitation over the domain (IMF), and the cloud cover area (CAR) at each time step. Notably, AWE-GEN-2d is built to preserve the auto- and cross-correlations among the three variables (Paschalis et al., 2013). For each dry spell, in turn, the model computes the evolution of CAR, which is influenced by the simulation of the preceding wet spell.

In parallel to the mean areal statistics module, the wind advection module simulates the velocity and direction of geostrophic winds as a stochastic process calibrated independently for wet and dry spells. Subsequently, advection drives the movement of storm cells in the precipitation fields module. In this module, AWE-GEN-2d generates gridded precipitation that follows the temporal evolution of the mean areal statistics, as well as the spatial correlation and variability derived from remote sensing observations. Afterward, the model uses the precipitation fields to simulate the cloud cover evolution over every cell in the domain.

The temperature module in AWE-GEN-2d can be divided into two parts: first, the near-surface air temperature for a given reference elevation is computed as the sum of a deterministic and a stochastic component. The deterministic component depends on the previously simulated cloud cover, the incoming solar long-wave radiation at a given time, and the domain location and topology, whereas the stochastic component is modeled as an autoregressive process, calibrated based on ground observations. The second part of the module consists of computing near-surface air-temperature as the sum of the temperature at a reference elevation and a stochastic lapse-rate for each grid-cell, which allows the model to generate semi-continuous temperature fields over the domain.

Furthermore, the model generates the mean areal atmospheric pressure through an autoregressive model and then extends the calculations to the entire domain based on the simulated air temperature. The temperature is also used to calculate the vapor pressure, incoming shortwave radiation, relative humidity, and dew-point temperature; all of which are, in turn, dependent on each other and are therefore calculated iteratively. Lastly, the near-surface wind velocity is simulated based on cloud cover and storm advection.

Even from this brief description, it is apparent that AWE-GEN-2d is structured to preserve the observed cross-correlations between various climate variables. A conspicuous absence, however, is the influence of climate variables on the magnitude of precipitation intensities, which is our main motivation to develop the new AWE-GEN-2d-CC that is described next.

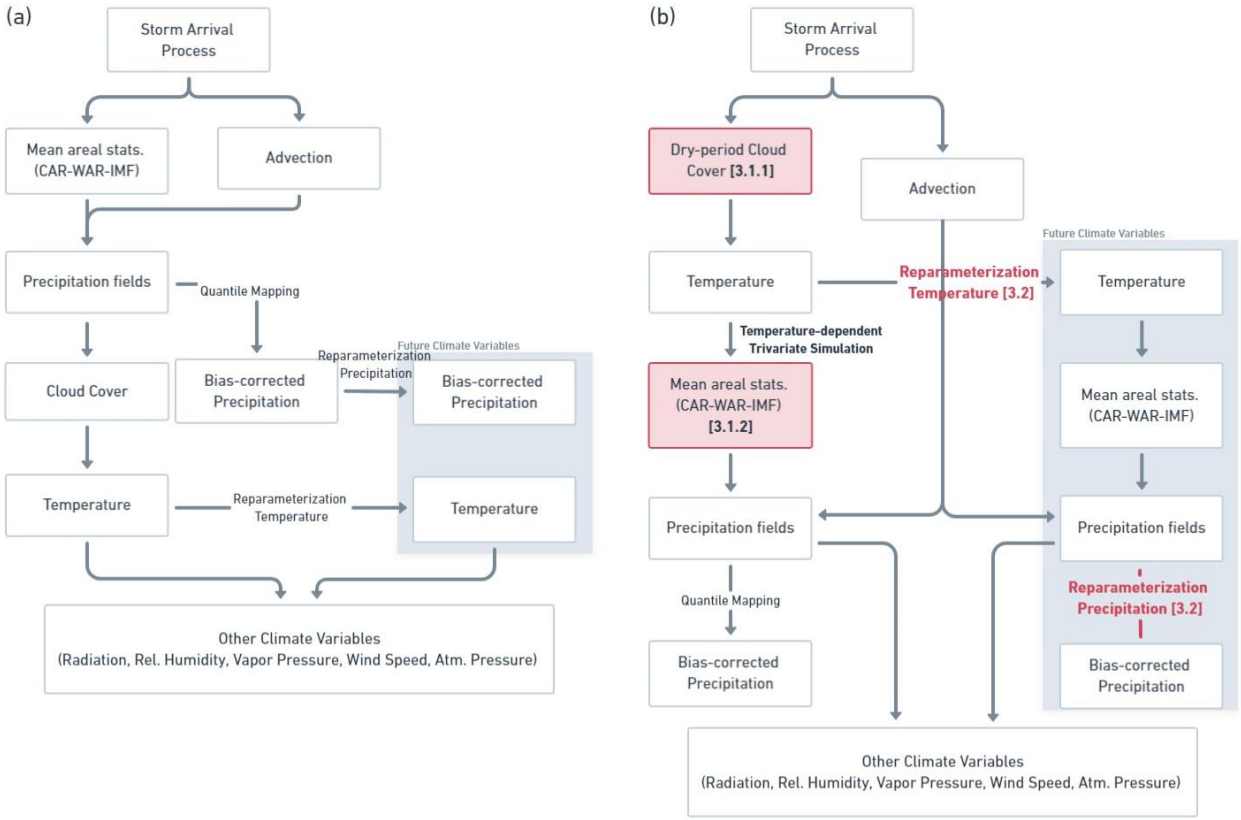

Figure 4-1. Flowchart describing the components of the two weather generators compared in this work. Panel (a) shows the structure of the original AWE-GEN-2d model (Peleg et al., 2017). Panel (b) shows the structure of the new version of the model here presented, AWE-GEN-2d-CC. The numbers in brackets indicate the section of this paper describing the corresponding procedure.

4.3 The AWE-GEN-2d-CC Model

Compared to its predecessor, the new formulation of the model presents a revised structure to include the dependency of heavy rainfall intensity and area on temperature. Consequently, the near-surface air temperature is now simulated before simulating the precipitation (Figure 4-1b). This generation sequence requires first simulating the cloud cover (i.e., CAR), as the temperature depends also on the shortwave radiation, which reaches the Earth is modulated by the effect of cloud cover. The CAR is simulated in two steps: first, the dry-spell cloud cover

is simulated together with provisional values for the wet-spell cloud cover to simulate the temperature values; second, the final wet-spell CAR is simulated as part of a tri-variate process jointly with the area affected by precipitation WAR and the areal mean precipitation intensity IMF.

A flowchart illustrating the new model structure of AWE-GEN-2d-CC is shown in Figure 4-1b, whereas the description of the different modules is presented in the following sub-sections. Only the revised modules are presented and discussed as the rest of the model structure (i.e., the simulation of all other climate variables, besides precipitation, cloud cover, and temperature) is unchanged with respect to the original AWE-GEN-2d model. As in Peleg et al. (2017), the Supplementary Material of this manuscript contains the Technical Reference that provides the details about the formulations and equations of the new model.

4.3.1 Cloud Cover

The new model structure requires the computation of cloud cover before the simulation of storm mean areal statistics, given that these are now dependent on the near-surface air temperature simulation and this, in turn, relies on the cloud cover. To reconcile this apparent paradox, the cloud cover for dry periods between storms (CAR_d) and the cloud cover during storms (CAR_w) are simulated by separate modules.

As in AWE-GEN-2d, CAR_d is modeled as a stochastic process where its mean value is a function of the distance to a storm occurrence and the stochastic component simulated as an autoregressive moving average model calibrated from observations. The novelty in the new structure is in the inclusion of an initial placeholder value for the cloud during wet events (CAR_w^*), which can take the form of a trivial climatological estimation such as the mean during the observed record. The final CAR_w value replacing the placeholder value is subsequently simulated in the module that computes the mean areal statistics as one component of a tri-variate stochastic process along with the IMF and WAR variables.

4.3.2 Mean Areal Statistics

The temporal evolution of a storm is first described by three domain-averaged variables: (i) the fraction of the domain covered by clouds or wet-spell cloud area ratio (CAR_w); (ii) the fraction of the domain cells experiencing precipitation denoted as wet area ratio (WAR); and (iii) the mean areal intensity (IMF), which is the average of the precipitation (encompassing solid and liquid precipitation) over the entire domain at any given time. In AWE-GEN-2d-CC, as in its predecessor, the three variables are modeled jointly as part of a tri-variate stochastic process to preserve the observed auto- and cross-correlations of each field. The variables are simulated in the probability domain as a Gaussian stochastic process with a Whittle-Matérn class covariate function (Gneiting et al., 2010), which allows for taking advantage of the highly efficient Fast Fourier Transform (FFT) method (Chambers, 1995; Frigo & Johnson, 1998) to obtain the correlated probabilities for the three variables. Finally, the probabilities are used to compute the real values of each areal statistic as the inverse of their corresponding marginal distribution.

In contrast with the previous model version, where seasonal parameter sets were used, the parameters that describe the Matérn covariate function (10 parameters), as well as the tri-variate Gaussian copula (7 parameters), are calibrated according to the average domain temperature at the onset of the precipitation event. Accordingly, as described in detail in Section 5.1 of the Technical Reference, the time series of the three variables are transformed from the frequency to the real space using temperature-bin-dependent marginal distributions. By adapting the calibration and modeling to specific temperature ranges, this approach seeks to preserve the correlation of mean areal statistics with temperature as observed in real-world

data, without assuming predefined temperature scaling rates of the marginal variables. This formulation ensures that the model captures the variable correlation between temperature and storm characteristics as empirically observed across different domains, rather than imposing a universal CC scaling rate.

4.3.3 Reparameterization Under Climate Change

To simulate future climate variables, Moraga et al. (2021, 2022) reparametrized AWE-GEN-2d following the blueprint laid out by Peleg et al. (2019). The procedure consists of using the so-called Factors of Change (FC) approach (see e.g., Bordoy & Burlando, 2014; Burlando & Rosso, 1991; Fatichi et al., 2011), which computes FCs from the outputs of present and future climate model simulations to alter the model parameters. For instance, the distributions for precipitation intensities are adjusted by combining a quantile mapping bias-correction method with the FC, thus ensuring that future precipitation simulations reflect the climate change signals.

To take advantage of the features introduced in AWE-GEN-2d-CC, it is key that the reparameterization preserves the observed scaling of storm properties with temperature, particularly regarding high precipitation extremes. For this reason, we adapted the approach presented by Peleg et al. (2019) to find an objective distribution function of the precipitation that fulfills two objectives: (i) aligning the location statistics (e.g., mean or median) with the FC, and (ii) ensuring that the distribution's right-tail (as represented, e.g., by the variance or by a specific high quantile) corresponds to the changes simulated by the mean areal statistics module that results from the enforced temperature changes. The reparameterization algorithm can be accordingly summarized as follows:

a. From GCMs/RCMs simulations, compute the FC of the location statistics of precipitation and temperature on a monthly or seasonal basis. For example, the FC for the mean of precipitation (FC_μ_{Pr}) is calculated as the ratio of the future ($\mu_{Pr}^{RCM,fut}$) and present ($\mu_{Pr}^{RCM,pres}$) means (Eq.), whereas the FC of mean temperature (FC_μ_{T}) is calculated as the difference (Eq. 2):

$$FC\_\mu_{Pr} = \mu_{Pr}^{RCM,fut} / \mu_{Pr}^{RCM,pres} \quad (1)$$

$$FC\_\mu_{T} = \mu_{T}^{RCM,fut} - \mu_{T}^{RCM,pres} \quad (2)$$

b. Use the FC to modify the future temperature simulations in AWE-GEN-2d-CC, which in turn influences the simulation of future mean areal statistics.

c. After executing the mean areal statistics module of AWE-GEN-2d-CC, compare the outputs of present and future IMF and use them to compute the FC for the precipitation right-tail statistics. For instance, the Factor of Change for the 99th quantile, $FC\_q^{99}{}_{Pr}$, is calculated in Eq. 3:

$$FC\_q^{99}{}_{Pr} = q^{99}{}_{Pr}^{fut,\ sim} / q^{99}{}_{Pr}^{pres,sim} \quad (3)$$

d. At each domain grid cell find the parameters (location, shape, and scale) of the future precipitation distribution function F_x so that it most closely follows the observed statistics multiplied by the FCs computed in (a) and (c), such that:

$$\bar{F_x} \approx \mu_{Pr}^{RCM,pres} * FC\_\mu_{Pr}, \text{ and} \quad (4)$$

$F_x(q=.99) \approx q^{99}{}_{Pr}{}^{pres,obs} * FC\_q^{99}{}_{Pr}$ (5)

e. Use quantile mapping, as shown by Peleg et al. (2019), to adjust the precipitation intensities simulated in the "Precipitation fields" module so that they follow the distribution found in (d).

Through this revised reparameterization approach, the model maintains the observed auto- and cross-correlations inferred under current climate conditions while, at the same time, it accommodates adjustments to climate-model-derived coarse-scale seasonal statistics.

4.4 Model Demonstration on a Case Study

4.4.1 Experiment Structure

The three objectives of the proposed demonstration experiment are: (i) to compare precipitation simulations between the original and new versions of the model and demonstrate that the new model structure reliably reproduces the observed climate while improving the simulation of extremes; (ii) to evaluate the performance of AWE-GEN-2d-CC in reproducing the temperature dependence of storm properties in present and future climate simulations; and (iii) to assess the effect of more realistic characterization of future precipitation extremes on the hydrological response of an exemplary mountainous catchment.

To accomplish the first two objectives, the numerical experiment was structured to generate a large number of simulations that allow for a robust analysis of extreme values. Concretely, a present-climate ensemble consisting of 900 years of simulations was generated based on the observed climate statistics representative of the 1976–2005 period. Likewise, we used the model to generate an ensemble of 900 years of future climate simulations following climate model projections for the end of the 21st century (period 2080–2089).

To address the third objective and measure the hydrological response under present and future climates, the 900 years of stochastic simulations generated for each climate scenario (present and future) were divided into 36 subsets of 25 years each. Each subset was used as input to the physically based, distributed hydrological Topkapi-ETH model (Fatichi et al., 2015), which is designed to reproduce a comprehensive set of hydrological processes, including the partition of liquid and solid precipitation, snow accumulation, redistribution, and melting, superficial runoff and channelized flow, evapotranspiration, infiltration and percolation of flow through lower soil layers, as well as soil and groundwater fluxes, among others. The resulting simulations, which characterize the present and end-of-century response of the catchment, enabled the analysis of the effects of climate change on hydrological statistics and their comparison with the results of a similar experiment carried out by Moraga et al. (2021, 2022), who used ensembles generated with the original AWE-GEN-2d model as inputs to Topkapi-ETH.

4.4.2 Study Area

The Kleine Emme is a mesoscale (478 km^2) mountainous catchment located on the northern side of the central Swiss Alps. It has a complex topography, characterized by a relatively wide elevation range (from 438 to 2330 m.a.s.l.) The mean annual precipitation over the catchment is around 1650 mm and features heavy (convective) rainfall events during the warm season from May to September (Molnar et al., 2015). It has an average temperature of 7.6°C with January being the coldest month with an average of -1.1°C and July being the warmest month with an average of 16.2°C. The mean discharge at its outlet is 15.5 m^3 s^{-1} (1024 mm y^{-1}) with a maximum instantaneous observed peak of 650 m^3 s^{-1} recorded in August 2005. In general,

there are no major stream regulations, diversion, or abstractions, and most of the land cover is either natural pasture or crops, with little presence of urbanized areas. The location, elevation map, and elevation distribution are shown in Figure C-1.

4.4.3 Data

The data used in this experiment was retrieved from multiple publicly available data sources including geographical information, weather stations, remote sensing, and reanalysis datasets. To set up the two versions of the WG model (the same data was used for both versions), the domain's topography was described by a high-resolution digital elevation model (DEM, Swisstopo, 2002). Weather radar observations were used to extract information regarding the storm-arrival process as well as the spatiotemporal structure of storms. This was complemented by ground temperature measurements used to determine the temperature at the onset of events and model the temperature lapse rate over the domain. Cloud cover data and advection velocities were modeled to follow the MERRA-2 reanalysis dataset (Rienecker et al., 2011). Finally, the gridded, hourly precipitation reanalysis dataset CombiPrecip (Sideris et al., 2014), produced by the Swiss meteorological office MeteoSwiss, is used as a reference to correct the bias in simulated AWE-GEN-2d-CC outputs.

The domain for the Topkapi-ETH simulations was characterized using the aforementioned DEM, as well as soil types and land cover maps (see Table 4-1) to assign hydraulic soil properties, soil depth, evapotranspiration parameters, and surface roughness values to each grid cell. The streamflow data to perform the calibration of the model, described in Moraga et al. (2021), was obtained from hourly records at the outlet of the catchment located in the locality of Emmen, Lucerne, provided by the Swiss Federal Office for the Environment. A summary of the data used in this study is provided in Table 4-1.

Table 4-1. Data sources used to characterize the Kleine Emme catchment

Data	Source	Resolution
Digital elevation model	Swiss Federal Office of Topography (SwissTopo, 2002)	100 m x 100 m grid
Ground weather stations	SwissMetNet by MeteoSwiss (Table C-1)	10-minutes
Weather radar	C-Band weather radar by MeteoSwiss (Germann et al., 2006)	2 km x 2 km grid, 5-minute
Cloud cover	MERRA-2 reanalysis dataset (Rienecker et al., 2011)	Hourly
Gridded precipitation	CombiPrecip by MeteoSwiss (Sideris et al, 2014)	2 km x 2 km grid, daily
Geostrophic wind velocity (500 hPa)	MERRA-2 reanalysis dataset (Rienecker et al., 2011)	Hourly
Soil properties	Swiss Federal Office for Agriculture FOAG (Bundesamt für Statistik (BFS), 2020)	100 m x 100 m grid
Land cover types	Corine dataset (*Corine Land Cover (CLC) Map 2012*, 2014)	100 m x 100 m grid

Data	Source	Resolution
Streamflow (Kleine Emme at Emmen)	Swiss Federal Office for the Environment (FOEN)	Hourly

4.4.4 Extreme Value Analysis

The frequency and magnitude of extreme hydrometeorological events were quantified using the Generalized Extreme Values distribution (GEV, Jenkinson, 1955). First, the simulations of climate and hydrological data were divided into 36 realizations of 25-year durations. For each realization, the yearly block maxima were fitted to the GEV distribution, from which the return periods of each considered variable were extracted. Lastly, the interquartile ranges (IQR) of the return periods of the (36) realizations were calculated to quantify the variability of the outputs.

4.4.5 Calibration

The calibration procedure of AWE-GEN-2d for the Kleine Emme catchment is presented in detail by Moraga et al. (2021) and will not be addressed in this text. Instead, this section will focus on the calibration aspects relevant to the changes introduced with the new model structure of AWE-GEN-2d-CC, i.e. the cloud cover and storm properties simulations (see Sections 4.3.1 and 4.3.2). A detailed account of the calibration methodology, encompassing the equations underpinning all the modules of AWE-GEN-2d-CC, can be found in the Technical Reference included in the Supporting Information.

The hourly time series of CAR reanalysis data was divided into months and into wet and dry spells based on weather radar observations of precipitation used to determine the occurrence of wet or dry spells. The calibration of the dry-spell cloud cover, CAR_d was split into a deterministic and a stochastic component: First, the mean of its deterministic component was assumed to follow a two-term exponential function of the distance from the closest wet period, whereas the standard deviation is modeled simply as the average of all observations (Table C-3). Subsequently, the stochastic component was modeled as an autoregressive moving-average process of the CAR_d time series (Table C-4), previously normalized by fitting them to a Johnson-SB distribution as shown in **Error! Reference source not found.**. In turn, the placeholder wet-spell cloud cover CAR_w^* values were obtained as a constant monthly value equal to the average cloud cover during wet events (Table C-5).

Unlike the monthly-calibrated dry-spell cloud cover, the statistics of cloud and precipitation during storms are calibrated based on the temperature during a wet spell. To this effect, we split the record of event-averaged CAR_w, WAR, and IMF into temperature bins based on the domain-averaged temperature at the onset of a wet period (similar concept as presented by Ali et al., 2021). We defined a total of 8 temperature bins with a width of 3°C for the six intermediate ones and an infinite width for the extremes (Figure C-3). This configuration allowed us to balance a sufficient number of samples in each bin with a smooth transition of the temperatures in the 5–25 °C range where, as shown in Figure C-4, we observe a strong correlation between extreme precipitation and temperature.

For each temperature bin, we normalized the subset of event-averaged CAR_w, WAR, and IMF and computed their auto- and cross-correlation coefficients (Table C-6**Error! Reference source not found.**), which are used as parameters to the Whittle-Matérn function used to model the covariate of the tri-variate probabilities. Subsequently, we used the mean and

standard deviations of the normalized CAR_w, WAR, and IMF sequence to fit the seven-dimensional copula of the Gaussian process that describes their joint temporal evolution.

To simulate future climate statistics as outlined in Section 4.3.3, we obtained FC_μ_{Pr} and FC_μ_T (Table C-7**Error! Reference source not found.**) from the outputs of nine GCM-RCM model chains (Table C-2***Error! Reference source not found.***) developed under the EURO-CORDEX initiative (Jacob et al., 2014; Kotlarski et al., 2014) and later post-processed by MeteoSwiss (CH2018, 2019). The model's simulated temperature was adjusted by adding the monthly FC_μ_T to the simulated time series. Subsequently, after simulating the future precipitation (conditioned by future temperatures) we computed the 99th quantiles of hourly precipitation for the present and future simulations to obtain $FC\_q^{99}{}_{Pr}$ (***Error! Reference source not found.***). We parameterized the distributions of present-climate precipitation by fitting the hourly time series of each grid cell to either a Generalized Pareto (GP) or Gamma distributions based on a typical goodness of fit criterion. Then, the GP or Gamma distributions of future precipitation were obtained by optimizing the fit to the objective monthly means (Eq. 4) and 99th quantiles (Eq. 5) and were used to correct the future precipitation intensities using quantile mapping.

As for the hydrological model employed in this experiment, we made no changes to the configuration of Topkapi-ETH used to model the response of the Kleine Emme in the previous work of Moraga et al. (2021), where the authors describe the calibration and validation procedures.

4.4.6 Validation

We tested AWE-GEN-2d-CC's capacity to reproduce plausible climate variables by comparing the statistics of the simulated ensembles with those of observed datasets that were not directly used in the calibration, as well as with the outputs of AWE-GEN-2d simulations. Here, we focus on the validation of the novel aspects of AWE-GEN-2d-CC relative to its predecessor, namely, the change in the modeling of cloud cover, the effect that it has on temperature, especially during wet periods, and the new temperature-dependent simulation of areal storm properties. As for the remaining modules, their calibration and validation have been presented in a previous work (Moraga et al., 2021, 2022) and remain unaffected by the new model formulation. Conversely, although the calibration of the Topkapi-ETH hydrological model for Kleine Emme has also been addressed in the cited experiments, the newly generated climate data prompts us to revisit how the catchment responds to present-climate inputs, which we do in Section 4.4.6.4.

4.4.6.1 Cloud Cover

Although the simulation of cloud cover is executed by the same procedure as that used in AWE-GEN-2d, the new structure of AWE-GEN-2d-CC simulating the dry-period CAR_d before the wet-period CAR_w, implies that it is not possible to ensure smooth transitions between wet and dry periods in the CAR time series, as illustrated, for instance, in Figure C-5. However, this effect is relatively minor and does not impact the overall CAR distribution. Figure C-6 compares the observed and simulated CAR monthly distributions for the dry periods using both model versions. We find that AWE-GEN-2d-CC simulations underestimate the frequency of very low (<0.1) and very high (> 0.9) cloud cover values at similar rates to AWE-GEN-2d (e.g., the proportion of very high values is 1.8% less than in the observations). Nonetheless, this new way of calculating the CAR allows for a satisfactory computation of the near-surface air temperature, as is shown in Section 4.4.6.2.

4.4.6.2 Temperature

The calibration and simulation of temperature in AWE-GEN-2d-CC are performed as in its predecessor and therefore exhibit a good performance in resembling the observed seasonality, daily cycle, and spatial distribution, as shown in Figure 4-2. For instance, the root mean squared error of the monthly areal averages is 0.7°C (0.77°C when using AWE-GEN-2d) and 0.29°C (0.40°C) for the average hourly daily cycle. A remaining concern has to do with the effect of using a placeholder value of cloud cover, CAR_w^*, in the modeling of temperature. As shown in Figure C-7: , which depicts the monthly distributions of temperature during wet events, the new model formulation behaves similarly to the previous model, hence we conclude that the use of the placeholder CAR_w^* does not have a noticeable impact on the temperature simulations.

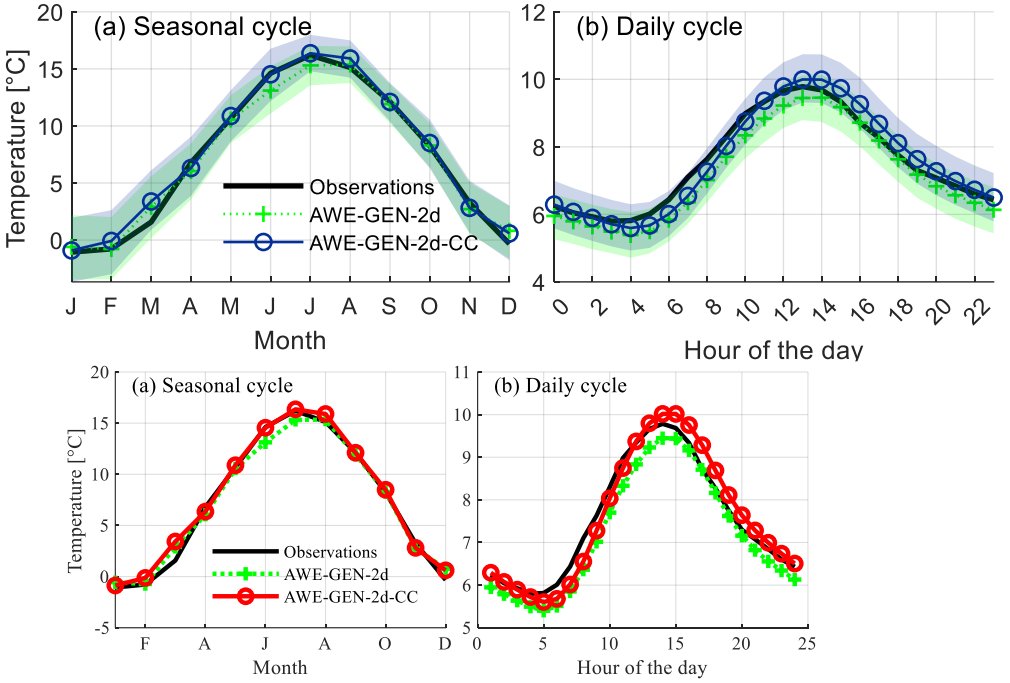

Figure 4-2. The two panels show the seasonal (a) and daily (b) cycles of near-surface air temperature as computed from the observations (solid black line), the AWE-GEN-2d simulations (dotted green line) and the new AWE-GEN-2d-CC simulations (solid blue line). The shaded areas depict the 5th–95th quantile range of the simulation ensembles.

4.4.6.3 Precipitation

The main novelty of AWE-GEN-2d-CC is the temperature-dependent parameterization of storm properties, which aims to preserve the observed temperature scaling of intense precipitation. Consequently, we verify that change in the model structure does not affect the model performance in reproducing the storm properties under present climate conditions, and that these are as well characterized as by the previous model version. Indeed, as the boxplots plots of the event-averaged IMF and WAR in Figure 4-3 show, the statistics coming from the new AWE-GEN-2d-CC (e.g. WAR median of 0.34, IMF median of 0.43 mm h^{-1}) match those coming from the CombiPrecip (0.30 and 0.40 mm h^{-1}, respectively) reanalysis even better than the previous model version (0.57 and 0.32 mm h^{-1}). Furthermore, the monthly distribution of the simulated hourly IMF time series, shown in Figure C-8: , matches the results using the previous model version. A closer look at the extreme IMF values is shown in the q-q plots of Figure C-9: , where it is evident that the weather generator underestimates the highest IMF

quantiles, especially during the colder months (e.g., 24% in February, 21% in November). Moreover, the model successfully reproduces the seasonality of precipitation, as shown in Figure 4-4, with minor underestimations of up to 9% (January), well within the IQR of simulated outcomes. When compared against the three long-standing weather stations in the domain (Figure C-10), the model matches satisfactorily the monthly precipitation for the Luzern station located in the valley but struggles to match the statistics of the stations Napf and Pilatus, which are located in mountain tops. This is likely due to discrepancies between the CombiPrecip interpolated dataset, which has been used for the WG calibration and validation, and the ground observations. In turn, the spatial distribution of precipitation shows an excellent agreement with errors below 3% of annual precipitation, as shown in Figure 4-5.

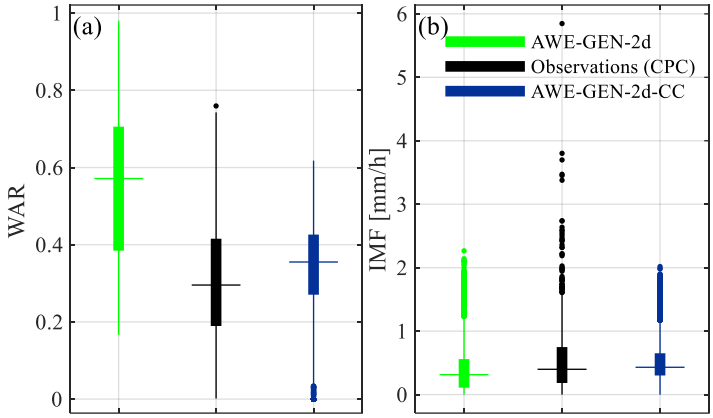

Figure 4-3. Boxplots of event-averaged wet-area ratio (WAR,a) and intensity mean field (IMF, b) as obtained from hourly records of CombiPrecip (black, middle) and simulations using AWE-GEN-2d (green, left), and the new AWE-GEN-2d-CC (blue, right). Note that we only considered events with WAR over 0.1.

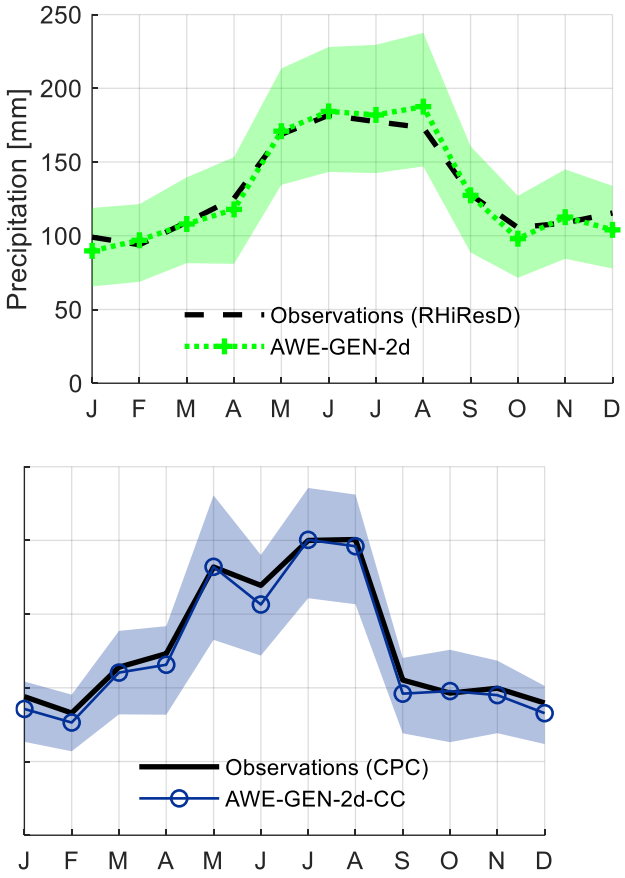

Figure 4-4. Comparison of the simulated and observed mean monthly precipitation using the AWE-GEN-2d model (left panel) and the new AWE-GEN-2d-CC model (right panel), with the interquartile range of the simulated outputs shown as shaded area. Each model is compared against respective precipitation dataset used for correcting the bias of the simulated outputs: CombiPrecip (CPC, Sideris et al. 2014) for AWE-GEN-2D-CC and RHiResD (MeteoSwiss, 2016) for AWE-GEN-2d in the study by Moraga et al. (2021; 2022).

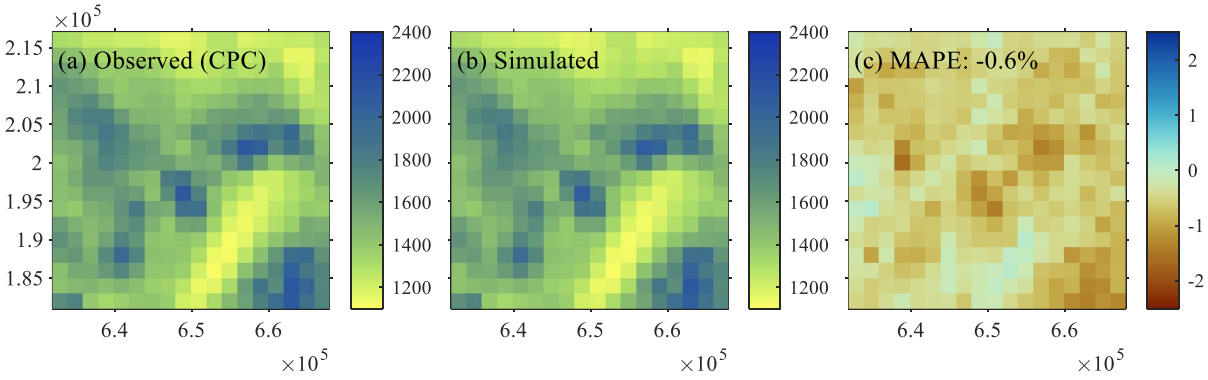

Figure 4-5. Mean annual precipitation (in mm) over the Kleine Emme domain according to CombiPrecip reanalysis data (a), present-climate AWE-GEN-2d-CC simulations (b), and mean absolute percentual error (MAPE) of the simulations (c). The coordinates are shown in meters using the UTM 32N projection.

4.4.6.4 Hydrological Response

To assess the influence of accounting for CC-scaling in future climate as simulated by the new model on the catchment response, the generated data was used as input to Topkapi-ETH, for which we used the same parameterization adopted by Moraga et al. (2021). As shown in Figure 4-6, the flow duration curve corresponding to this experiment matches the shape of that corresponding to the use of AWE-GEN-2d but has a lower magnitude across the entire domain of exceedance probabilities. The average underestimation is on average 12% and is more pronounced for lower exceedance probabilities. While this variation falls within the uncertainty range of model simulations (depicted as dashed lines in the figure), it is primarily attributable to the overall lower rainfall amounts simulated by the new weather generator compared to its predecessor. Regardless of the differences between the two experiments, the statistics of low exceedance streamflow (representing higher flows) align in both cases closely with the observations, while lower flows tend to be overestimated.

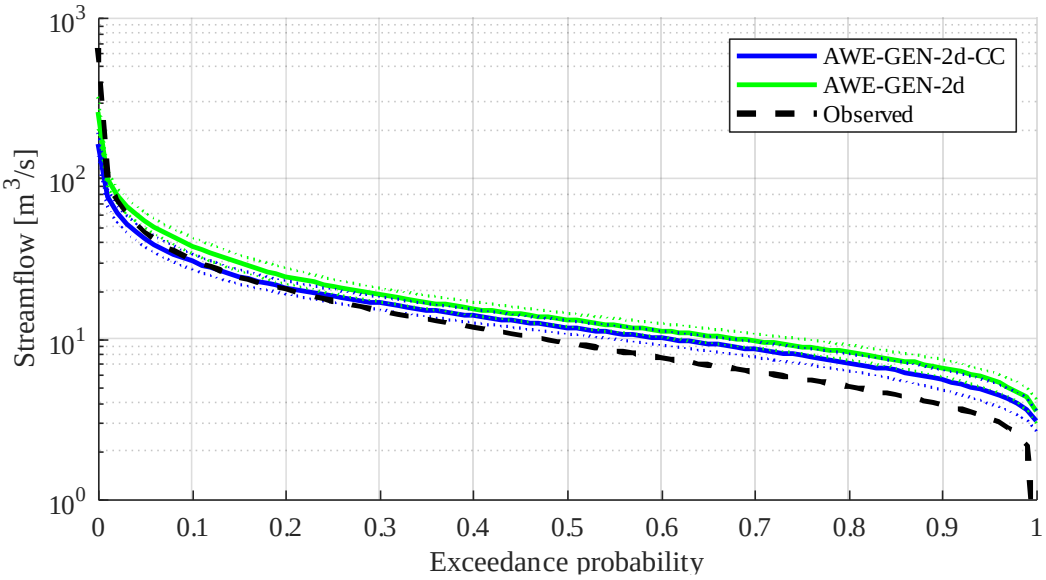

Figure 4-6. Duration curves for the observed streamflow record (black dashed line) and the ensembles of present-climate simulations using Topkapi-ETH. Input data was generated with AWE-GEN-2d (green) and AWE-GEN-2d-CC (blue). The solid lines represent the median across realizations and the dashed lines indicate the interquartile range for each exceedance probability.

4.4.7 Results

4.4.7.1 Impacts on Precipitation

As shown in Figure 4-7a, the monthly mean areal precipitation follows the overall signal of the GCM-RCM climate trajectories projecting a slight average decrease in precipitation (-3.9%), which is concentrated in the summer months. The changes are spatially heterogeneous, with projected increases in the northeast part of the catchment of up to 14% and decreases in other areas of up to -11% (Figure 4-7b).

The newly formulated AWE-GEN-2d-CC model successfully emulates the scaling relationship between high precipitation intensities (above the 99th percentile) and temperature for the historical climate. Consequently, this capability is effective also in future climate simulations, as can be noted by the quantile regressions shown in Figure 4-8. Although the scaling slope is less pronounced compared to that computed from the observed data (e.g., slopes of 5.4%

and 5.5% for the .99 quantile regression compared to an observed 6.0%, as shown in Figure C-4Figure C-4:), the impact of accounting for temperature-precipitation dependence is discernible when calculating return periods for extreme precipitation events (Figure 4-9) following the methodology detailed in Section 4.4.4.

Consequently, we project a significant increase in hourly precipitation extremes by the end of the century, with the mean change lying within a range of 5–11% for a broad range of return periods. Conversely, daily precipitation extremes are projected to decrease for lower return periods, with a median value of 9% lower than in the present climate for the 2-year extremes. However, the intensity of less frequent events (e.g., the 200-year return period) is not expected to exhibit any change at the daily scale (a median decrease of 4.1% with IQRs in the order of 16%). These findings contrast glaringly with those derived from the simulations obtained using the previous model. As shown in Moraga et al. (2021), the AWE-GEN-2d simulations projected only minor, statistically insignificant changes to precipitation extremes in the Kleine Emme region for all return periods. This highlights the importance of accounting for the temperature-precipitation dependence and, thus, the influence that the new AWE-GEN-2d-CC formulation has on producing a plausible quantification of climate change impacts on precipitation extremes.

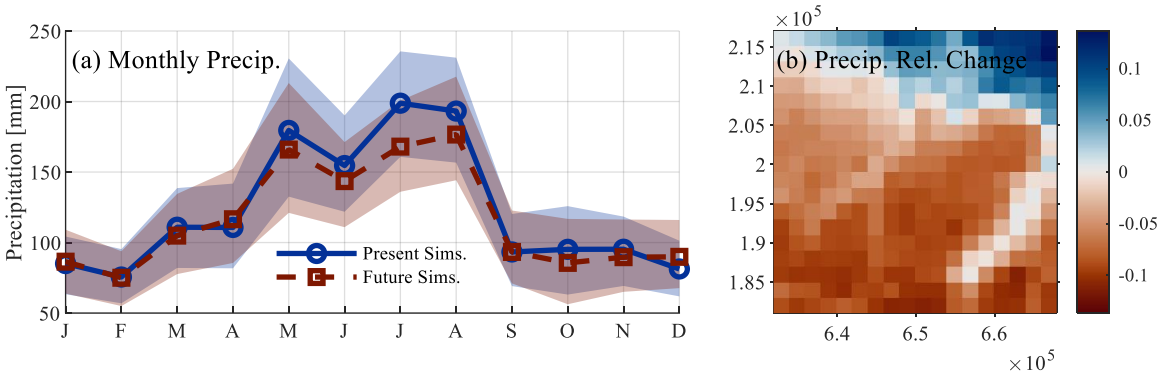

Figure 4-7. Panel (a) shows the mean monthly areal precipitation over the Kleine Emme domain according to the present (blue) and future (red) climate simulations. The shaded areas represent the interquartile range of the means across 900 realizations. The change in total precipitation by the end of the century for each grid cell in the domain is shown in panel (b).

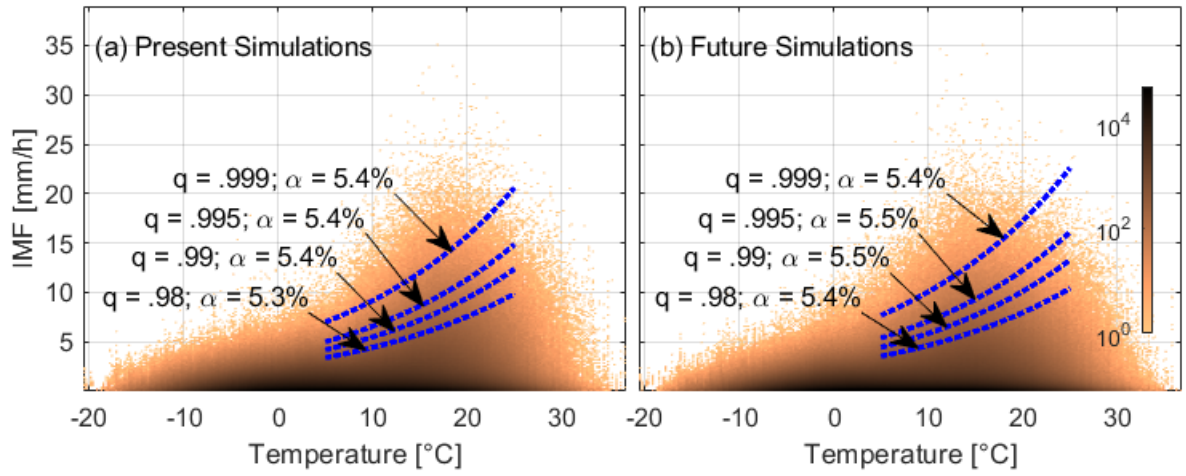

Figure 4-8. Heat maps for the present (left) and future (right) simulated 5-minute intensity mean field (IMF) vs. temperature. The colors represent the number of points within each pixel. The quantile regressions for the 98th, 99th, 99.5th, and 99.9th percentiles are superposed as dotted lines. The coefficient α, included in the labels, denotes the slope of the logarithmic regression for each quantile.

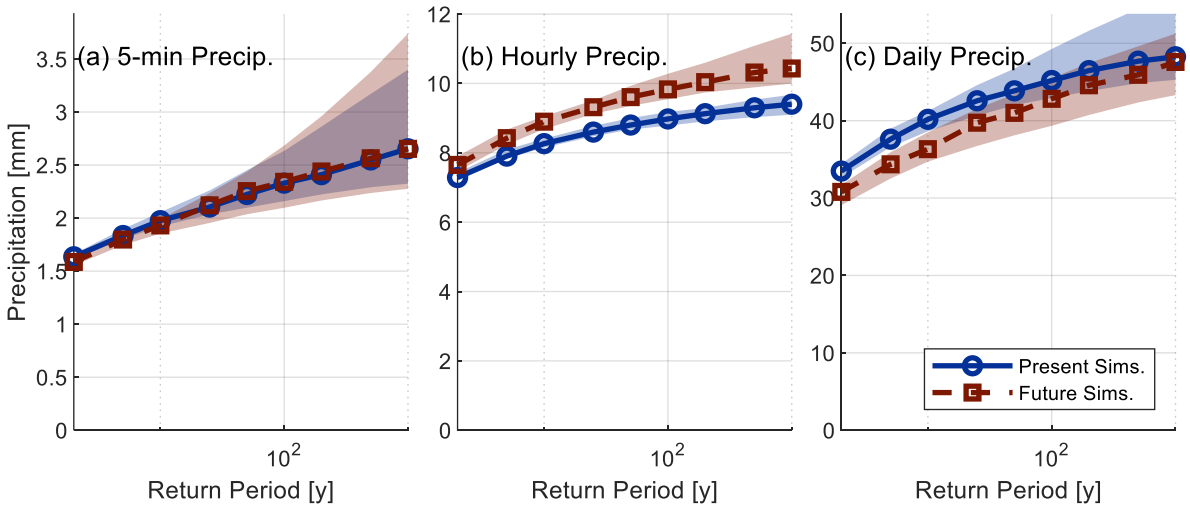

Figure 4-9. Return periods of the 5-minute (a), hourly (b), and daily (c) precipitation in present (blue) and future (red) climate conditions. The shaded areas represent the interquartile range.

4.4.7.2 Catchment Response

The increase of hourly precipitation extremes due to accounting for the CC dependence exerts a mild but noticeable influence on streamflow extremes, particularly for rare events. Figure 10a shows this by depicting no change for relatively common hourly peak flows, such as those corresponding to 2 or 5-year return periods, and a manifest increase for rarer events, exemplified, for instance, by a 15% rise in the median 50-year return period hourly peak.

Given the distributed nature of the basin response simulation, we can also show how the temperature-precipitation dependence, more pronounced for small-scale convective storm events, is reflected by the magnitude of the peak-flow increase, which looks more pronounced for small-scale basins. This is evident from Figure 10c, where the maximum hourly streamflow exhibits the most dramatic increases for higher elevation and smaller catchments. The improvements due to using the new AWE-GEN-2d-CC model become evident when contrasting the results of these numerical experiments with those obtained using the previous model version. In some instances, the new model chain predicts an over 50% increase for peak flows that exhibited a small decrease in Moraga et al. (2021). Concerning daily extremes, the experiment predicts a decrease ranging from 12 to 15% across return periods, as shown in Figure 10b. This mirrors the projections made using the original AWE-GEN-2d and is explained by the decrease in the intensities of future longer-duration precipitations (Figure 4-9c) and the increased air temperature that drives drier antecedent conditions for floods (Moraga et al., 2021). In this, our results coincide with other studies showing weak or negative trends in floods over central Europe despite increases in rainfall peaks (Wasko, Nathan, et al., 2021; Wasko, Westra, et al., 2021). Moreover, we explored the impact of climate change on the timing of floods, as illustrated in Figure C-11: , The analysis reveals only a minor shift

towards earlier occurrence of events, aligning with the weak trends observed for this region by Blöschl et al. (2017).

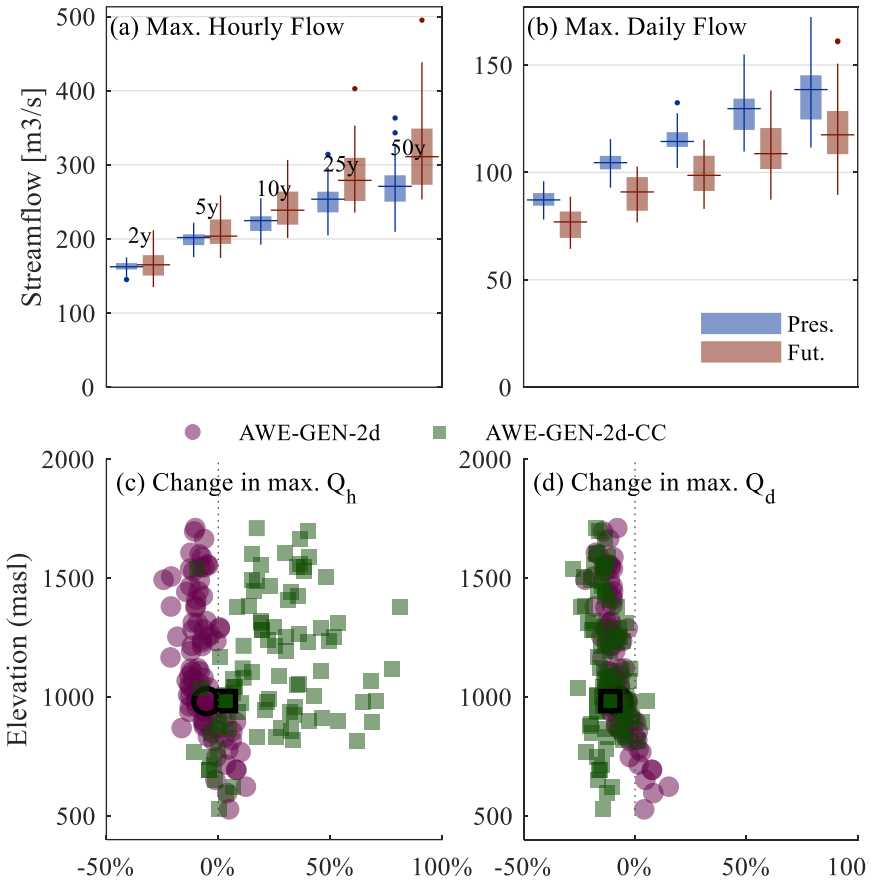

Figure 4-10. The present (blue) and future (red) return periods of maximum hourly and daily streamflow at the outlet of the catchment are shown as boxplots in panels (a) and (b), respectively. Panels (c) and (d) show a comparison of the projected change in the median annual maximum hourly and daily streamflow over the Kleine Emme sub-catchments using the current AWE-GEN-2d-CC model (green squares) and the previous version AWE-GEN-2d (magenta circles).

4.5 Discussion

AWE-GEN-2d-CC marks a step forward in modeling small-scale climate features, particularly over complex terrains. It improves upon AWE-GEN-2d by modeling the characteristics of storms as a temperature-dependent process, therefore implicitly allowing it to reproduce the statistics of high-intensity events that are associated with convective storms. AWE-GEN-2d-CC performs as well or better than its predecessor in reproducing the seasonality, spatial distribution, and marginal distribution of precipitation and temperature, as shown in Section 4.4.6. Furthermore, AWE-GEN-2d-CC maintains the same level of model parsimony as it requires the same type of data for calibration and does not increase the number of fitted parameters, and AWE-GEN-2d-CC requires the same—rather modest—amount of computational resources as AWE-GEN-2d. For example, a year of simulation for the Kleine Emme domain takes in the order of 15 min using a typical commercial processor.

In our model setup, we consider the temperature-precipitation relationship to be the same for all precipitation events (as shown by Molnar et al (2015) for this region) instead of an explicit representation of different storm types (e.g., stratiform and convective), mainly because the latter requires identifying storm types from observational records (Gaál et al., 2014; Jergensen et al., 2020), which, depending on the local climate characteristics, is not straightforward and would add further complexity to the calibration of the weather generator. As shown in Figure 4-8, AWE-GEN-2d-CC successfully mimics the observed temperature-precipitation scaling of extreme hourly precipitations. This demonstrates the robustness of the approach to parameterization of the T-P dependence, which, through temperature-bin-dependent calibration, captures the behavior of precipitation extremes in response to temperature variations. It is important to emphasize that the success of the model in emulating the CC scaling relationship arises not from directly imposing of this relationship in the calibration process but from the ability of the model to reproduce observed data patterns. This ensures that the climate projections are grounded in empirically observed relationships, offering a plausible, site-specific and flexible framework for anticipating future climate scenarios.

As demonstrated trough the Kleine Emme case study, the temperature scaling feature of the model translates into a predicted intensification in future hourly extremes due to rising temperature (Figure 4-9). This contrasts with the negligible changes to intensities projected with the previous model formulation (Moraga et al., 2021), and thus demonstrates the value of the new model version. Moreover, studies relying on CPM simulations for central Europe (e.g., Ban et al., 2018; Lenderink et al., 2021) are consistent with the AWE-GEN-2d-CC projections for extreme precipitation. While CPM simulations remain the gold-standard approach to assess small-scale climate change impacts, we argue that comparatively low-cost weather generators that can simulate ensembles of credible future climate statistics play a significant role in understanding and adapting to climate change. As such, AWE-GEN-2d-CC offers a versatile alternative suitable for a myriad of applications in water resource management, agricultural planning, and preparing for natural catastrophes.

It is worth noting that we have limited the scope of this research to the simulation of cloud cover, temperature, and precipitation. However, the satisfactory performance of AWE-GEN-2d-CC in simulating those variables ensures that it can perform as well as AWE-GEN-2d in simulating the remaining climate variables such as relative humidity, atmospheric pressure, incoming short-wave radiation, dew-point temperature, vapor pressure, and near-surface wind speed (Peleg et al., 2017).

Our results also cast light on the future hydrology of the Kleine Emme catchment and how it responds to intensifying extreme precipitations. By the end of the century, rare extreme hourly flows, particularly at higher-elevation sub-catchments, will experience a significant increase (Figure 4-10). Notably, this is in stark contrast with the results obtained using the previous model, which did not account for temperature scaling in the input precipitation data. For daily extreme flows, however, we project a significant decrease in magnitude explained by the decrease in longer-duration precipitation extremes (Figure 4-9), and drier antecedent soil conditions (Moraga et al., 2021). In this, our results contradict similar studies carried out for nearby catchments (Brunner, Farinotti, et al., 2019; Molnar et al., 2020; Ruiz-Villanueva & Molnar, 2020). We speculate the main sources of discrepancy are related to the treatment of snow-related processes of the respective hydrological models, and the diversity in size and geomorphological properties of the study catchments. In this regard, only replicating this study for a significant number of cases may provide further insight.

4.6 CONCLUSIONS

We introduced the AWE-GEN-2d-CC model, a new version of a two-dimensional stochastic weather generator AWE-GEN-2d-CC (Peleg et al., 2017), which improves upon its predecessor by incorporating the relationship between storm properties and temperature. The improved model was shown to maintain the ability to generate high-resolution gridded climate variables that accurately preserve the auto- and cross-correlations found in the observed records for the Kleine Emme, an exemplary catchment in the Swiss Alps. In particular, the model's performance was evaluated by examining projected climate change impacts on the hydrometeorology of the catchment. AWE-GEN-2d-CC was calibrated using multiple observational and reanalysis datasets, generating a large ensemble (900 years) of present-climate time series. Subsequently, it was re-parameterized to generate downscaled scenarios from nine different GCM-RCM model chains and obtain an equally large ensemble of end-of-the-century climate data.

The ensembles simulated using AWE-GEN-2d-CC successfully replicated the observed temperature scaling of the largest intensities within the 5–25°C temperature range, albeit displaying slightly lower scaling rates. In turn, the simulations yielded an increase in hourly precipitation extremes in the order of 5–11% by the end of the century, but a decrease in daily precipitation extremes of around 9%. The hydrological response of the Kleine Emme to the changes in precipitation extreme was then examined. It was found that while the high frequency (<5 y return period) hourly high flows remain at the same level, an increase in the magnitude of hourly high flow rare events (>50 y return period) was found. Moreover, we found a significant reduction in future daily streamflow extremes.

Our results underscore how the temperature-scaling of storm properties will affect short-duration extreme rainfall events under climate change projections and how it impacts hydrological responses. Consequently, this research highlights the need for a fine-resolution gridded model that accurately simulates the precipitation-temperature relationship, as the AWE-GEN-2d-CC model presented here does. We note that it is essential to model future hydrological extremes utilizing an accurate representation of temperature-induced rainfall intensification, which may extend beyond Alpine catchments, as the one presented here, but may also apply to any fast-responding catchment prone to high-intensity convective storms in general.

Data and Software Availability

The AWE-GEN-2d-CC model code, as well as an example of the case study presented, is available as a Zenodo repository (Moraga and Peleg, 2023) under a CC BY-NC 4.0 license.

4.7 REFERENCES

Addor, N., Rössler, O., Köplin, N., Huss, M., Weingartner, R., Seibert, J., 2014. Robust changes and sources of uncertainty in the projected hydrological regimes of Swiss catchments. Water Resources Research, 50(10), 7541–7562. https://doi.org/10.1002/2014WR015549

Ali, H., Fowler, H.J., Lenderink, G., Lewis, E., Pritchard, D., 2021a. Consistent Large-Scale Response of Hourly Extreme Precipitation to Temperature Variation Over Land. Geophysical Research Letters 48, e2020GL090317. https://doi.org/10.1029/2020GL090317

Ali, H., Peleg, N., Fowler, H.J., 2021b. Global Scaling of Rainfall With Dewpoint Temperature Reveals Considerable Ocean-Land Difference. Geophysical Research Letters 48, e2021GL093798. https://doi.org/10.1029/2021GL093798

Ban, N., Schmidli, J., Schär, C., 2014. Evaluation of the convection-resolving regional climate modeling approach in decade-long simulations. Journal of Geophysical Research: Atmospheres 119, 7889–7907. https://doi.org/10.1002/2014JD021478

Ban, N., Rajczak, J., Schmidli, J., Schär, C., 2018. Analysis of Alpine precipitation extremes using generalized extreme value theory in convection-resolving climate simulations. Climate Dynamics 1–15. https://doi.org/10.1007/s00382-018-4339-4

Ban, N., Caillaud, C., Coppola, E., Pichelli, E., Sobolowski, S., Adinolfi, M., et al., 2021. The first multi-model ensemble of regional climate simulations at kilometer-scale resolution, part I: evaluation of precipitation. Climate Dynamics 2021, 1–28. https://doi.org/10.1007/S00382-021-05708-W

Berg, P., Moseley, C., Haerter, J.O., 2013. Strong increase in convective precipitation in response to higher temperatures. Nature Geoscience 6, 181–185. https://doi.org/10.1038/ngeo1731

Blöschl, G., Hall, J., Parajka, J., Perdigão, R.A.P., Merz, B., Arheimer, B., Aronica, G.T., Bilibashi, A., Bonacci, O., Borga, M., Čanjevac, I., Castellarin, A., Chirico, G.B., Claps, P., Fiala, K., Frolova, N., Gorbachova, L., Gül, A., Hannaford, J., Harrigan, S., Kireeva, M., Kiss, A., Kjeldsen, T.R., Kohnová, S., Koskela, J.J., Ledvinka, O., Macdonald, N., Mavrova-Guirguinova, M., Mediero, L., Merz, R., Molnar, P., Montanari, A., Murphy, C., Osuch, M., Ovcharuk, V., Radevski, I., Rogger, M., Salinas, J.L., Sauquet, E., Šraj, M., Szolgay, J., Viglione, A., Volpi, E., Wilson, D., Zaimi, K., Živković, N., 2017. Changing climate shifts timing of European floods. Science 357, 588–590. https://doi.org/10.1126/science.aan2506

Bordoy, R., Burlando, P., 2014. Stochastic downscaling of climate model precipitation outputs in orographically complex regions: 2. Downscaling methodology. Water Resources Research, 50(1), 562–579. https://doi.org/10.1002/wrcr.20443

Brunner, M. I., Farinotti, D., Zekollari, H., Huss, M., Zappa, M., 2019. Future shifts in extreme flow regimes in Alpine regions. Hydrology and Earth System Sciences, 23(11), 4471–4489. https://doi.org/10.5194/hess-23-4471-2019

Bundesamt für Statistik (BFS) (Ed.)., 2020. Bodeneignungskarte der Schweiz. Retrieved from https://dam-api.bfs.admin.ch/hub/api/dam/assets/13147140/master

Burlando, P., Rosso, R., 1991. Extreme storm rainfall and climatic change. Atmospheric Research, 27(1), 169–189. https://doi.org/10.1016/0169-8095(91)90017-Q

CH2018., 2019. CH2018 – Climate Scenarios for Switzerland, Technical Report. National Centre for Climate Services, Zurich, Switzerland.

Chambers, M. J., 1995. The simulation of random vector time series with given spectrum. Mathematical and Computer Modelling, 22(2), 1–6. https://doi.org/10.1016/0895-7177(95)00106-C

Corine Land Cover (CLC) map 2012., 2014. Retrieved from https://land.copernicus.eu/paneuropean/corine-land-cover/clc-2012

Drobinski, P., Silva, N. D., Panthou, G., Bastin, S., Muller, C., Ahrens, B., et al., 2016. Scaling precipitation extremes with temperature in the Mediterranean: past climate assessment and projection in anthropogenic scenarios. Climate Dynamics, 1–21. https://doi.org/10.1007/s00382-016-3083-x

Fatichi, S., Ivanov, V. Y., Caporali, E., 2011. Simulation of future climate scenarios with a weather generator. Advances in Water Resources, 34(4), 448–467. https://doi.org/10.1016/j.advwatres.2010.12.013

Fatichi, S., Rimkus, S., Burlando, P., Bordoy, R., Molnar, P., 2015. High-resolution distributed analysis of climate and anthropogenic changes on the hydrology of an Alpine catchment. Journal of Hydrology, 525, 362–382. https://doi.org/10.1016/j.jhydrol.2015.03.036

Fatichi, S., Ivanov, V.Y., Paschalis, A., Peleg, N., Molnar, P., Rimkus, S., Kim, J., Burlando, P., Caporali, E., 2016. Uncertainty partition challenges the predictability of vital details of climate change. Earth's Future 4, 240–251. https://doi.org/10.1002/2015EF000336

Fatichi, S., Peleg, N., Mastrotheodoros, T., Pappas, C., Manoli, G., 2021. An ecohydrological journey of 4500 years reveals a stable but threatened precipitation–groundwater recharge relation around Jerusalem. Science Advances, 7(37), eabe6303. https://doi.org/10.1126/sciadv.abe6303

Fischer, A.M., Keller, D.E., Liniger, M.A., Rajczak, J., Schär, C., Appenzeller, C., 2015. Projected changes in precipitation intensity and frequency in Switzerland: a multi-model perspective. International Journal of Climatology 35, 3204–3219. https://doi.org/10.1002/joc.4162

Fischer, A. M., Strassmann, K. M., Croci-Maspoli, M., Hama, A. M., Knutti, R., Kotlarski, S., et al., 2022. Climate Scenarios for Switzerland CH2018 – Approach and Implications. Climate Services, 26, 100288. https://doi.org/10.1016/j.cliser.2022.100288

Fischer, E.M., Knutti, R., 2016. Observed heavy precipitation increase confirms theory and early models. Nature Climate Change 6, 986–991. https://doi.org/10.1038/nclimate3110

Fowler, H.J., Blenkinsop, S., Tebaldi, C., 2007. Linking climate change modelling to impacts studies: recent advances in downscaling techniques for hydrological modelling. International Journal of Climatology 27, 1547–1578. https://doi.org/10.1002/joc.1556

Fowler, H.J., Lenderink, G., Prein, A.F., Westra, S., Allan, R.P., Ban, N., Barbero, R., Berg, P., Blenkinsop, S., Do, H.X., Guerreiro, S., Haerter, J.O., Kendon, E.J., Lewis, E., Schaer, C., Sharma, A., Villarini, G., Wasko, C., Zhang, X., 2021. Anthropogenic intensification of short-duration rainfall extremes 2, 107–122. https://doi.org/10.1038/s43017-020-00128-6

Frigo, M., Johnson, S. G., 1998. FFTW: an adaptive software architecture for the FFT. In Proceedings of the 1998 IEEE International Conference on Acoustics, Speech and Signal Processing, ICASSP '98 (Cat. No.98CH36181) (Vol. 3, pp. 1381–1384 vol.3). https://doi.org/10.1109/ICASSP.1998.681704

Gaál, L., Molnar, P., Szolgay, J., 2014. Selection of intense rainfall events based on intensity thresholds and lightning data in Switzerland. Hydrology and Earth System Sciences, 18(5), 1561–1573. https://doi.org/10.5194/hess-18-1561-2014

Germann, U., Galli, G., Boscacci, M., Bolliger, M., 2006. Radar precipitation measurement in a mountainous region. Quarterly Journal of the Royal Meteorological Society, 132(618 A), 1669–1692. https://doi.org/10.1256/qj.05.190

Gneiting, T., Kleiber, W., Schlather, M., 2010. Matérn Cross-Covariance Functions for Multivariate Random Fields. Journal of the American Statistical Association, 105(491), 1167–1177. https://doi.org/10.1198/jasa.2010.tm09420

Gutowski, W.J., Ullrich, P.A., Hall, A., Leung, L.R., O'Brien, T.A., Patricola, C.M., Arritt, R.W., Bukovsky, M.S., Calvin, K.V., Feng, Z., Jones, A.D., Kooperman, G.J., Monier, E., Pritchard, M.S., Pryor, S.C., Qian, Y., Rhoades, A.M., Roberts, A.F., Sakaguchi, K., Urban, N., Zarzycki, C., 2020. The Ongoing Need for High-Resolution Regional Climate Models: Process Understanding and Stakeholder Information. Bulletin of the American Meteorological Society 101, E664–E683. https://doi.org/10.1175/BAMS-D-19-0113.1

Jacob, D., Petersen, J., Eggert, B., Alias, A., Christensen, O. B., Bouwer, L. M., et al., 2014. EURO-CORDEX: new high-resolution climate change projections for European impact research. Regional Environmental Change, 14(2), 563–578. https://doi.org/10.1007/s10113-013-0499-2

Jenkinson, A. F., 1955. The frequency distribution of the annual maximum (or minimum) values of meteorological elements. Quarterly Journal of the Royal Meteorological Society, 81(348), 158–171. https://doi.org/10.1002/QJ.49708134804

Jergensen, G. E., McGovern, A., Lagerquist, R., Smith, T., 2020. Classifying Convective Storms Using Machine Learning. Weather and Forecasting, 35(2), 537–559. https://doi.org/10.1175/WAF-D-19-0170.1

Kendon, E.J., Ban, N., Roberts, N.M., Fowler, H.J., Roberts, M.J., Chan, S.C., Evans, J.P., Fosser, G., Wilkinson, J.M., 2017. Do Convection-Permitting Regional Climate Models Improve Projections of Future Precipitation Change? Bulletin of the American Meteorological Society 98, 79–93. https://doi.org/10.1175/BAMS-D-15-0004.1

Kotlarski, S., Keuler, K., Christensen, O. B., Colette, A., Déqué, M., Gobiet, A., et al., 2014. Regional climate modeling on European scales: a joint standard evaluation of the EURO-CORDEX RCM ensemble. Geosci. Model Dev, 7, 1297–1333. https://doi.org/10.5194/gmd-7-1297-2014

Lenderink, G., de Vries, H., Fowler, H. J., Barbero, R., van Ulft, B., van Meijgaard, E., 2021. Scaling and responses of extreme hourly precipitation in three climate experiments with a convection-permitting model. Philosophical Transactions. Series A, Mathematical, Physical, and Engineering Sciences, 379(2195), 20190544. https://doi.org/10.1098/rsta.2019.0544

Lochbihler, K., Lenderink, G., Siebesma, A. P., 2017. The spatial extent of rainfall events and its relation to precipitation scaling. Geophysical Research Letters, 44(16), 8629–8636. https://doi.org/10.1002/2017GL074857

Lochbihler, K., Lenderink, G., Siebesma, A. P., 2019. Response of Extreme Precipitating Cell Structures to Atmospheric Warming. Journal of Geophysical Research: Atmospheres, 124(13), 2018JD029954. https://doi.org/10.1029/2018JD029954

Lucas-Picher, P., Argüeso, D., Brisson, E., Tramblay, Y., Berg, P., Lemonsu, A., et al., 2021. Convection-permitting modeling with regional climate models: Latest developments and next steps. WIREs Climate Change, 12(6), e731. https://doi.org/10.1002/wcc.731

Maraun, D., Wetterhall, F., Ireson, A.M., Chandler, R.E., Kendon, E.J., Widmann, M., Brienen, S., Rust, H.W., Sauter, T., Themel, M., Venema, V.K.C., Chun, K.P., Goodess, C.M., Jones, R.G., Onof, C., Vrac, M., Thiele-Eich, I., 2010. Precipitation downscaling under climate change: Recent developments to bridge the gap between dynamical models and the end user. Reviews of Geophysics 48. https://doi.org/10.1029/2009RG000314

Marra, F., Koukoula, M., Canale, A., Peleg, N., 2024. Predicting extreme sub-hourly precipitation intensification based on temperature shifts, Hydrology Earth System Science, 28, 375–389, https://doi.org/10.5194/hess-28-375-2024, 2024

MeteoSwiss, 2016. Daily Precipitation (Final Analysis): RhiresD, Switzerland. [Available at http://www.meteoswiss.admin.ch/home/search.subpage.html/en/data/products/2014/raeumliche-daten-niederschlag.html.]

Molnar, P., Fatichi, S., Gaál, L., Szolgay, J., Burlando, P., 2015. Storm type effects on super Clausius-Clapeyron scaling of intense rainstorm properties with air temperature. Hydrology and Earth System Sciences, 19(4), 1753–1766. https://doi.org/10.5194/hess-19-1753-2015

Moraga, J. S., Peleg, N., Fatichi, S., Molnar, P., & Burlando, P., 2021. Revealing the impacts of climate change on mountainous catchments through high-resolution modelling. Journal of Hydrology, 603, 126806. https://doi.org/10.1016/j.jhydrol.2021.126806

Moraga, J.S., Peleg, N., Molnar, P., Fatichi, S., Burlando, P., 2022. Uncertainty in high-resolution hydrological projections: Partitioning the influence of climate models and natural climate variability. Hydrological Processes 36, e14695. https://doi.org/10.1002/hyp.14695

Moraga, J. S., & Peleg, N., 2023. AWE-GEN-2d-CC [Software]. Zenodo. https://doi.org/10.5281/zenodo.10033795

Nyman, P., Yeates, P., Langhans, C., Noske, P. J., Peleg, N., Schärer, C., et al. , 2021. Probability and Consequence of Postfire Erosion for Treatability of Water in an Unfiltered Supply System. Water Resources Research, 57(1), 2019WR026185. https://doi.org/10.1029/2019WR026185

O'Donnell, E. C., Thorne, C. R., 2020. Drivers of future urban flood risk. Philosophical Transactions of the Royal Society A: Mathematical, Physical and Engineering Sciences, 378(2168), 20190216. https://doi.org/10.1098/rsta.2019.0216

O'Gorman, P.A., Schneider, T., 2009. The physical basis for increases in precipitation extremes in simulations of 21st-century climate change. Proceedings of the National Academy of Sciences 106, 14773–14777. https://doi.org/10.1073/pnas.0907610106

Paschalis, A., Molnar, P., Fatichi, S., & Burlando, P., 2013. A stochastic model for high-resolution space-time precipitation simulation. Water Resources Research, 49(12), 8400–8417. https://doi.org/10.1002/2013WR014437

Peleg, N., Fatichi, S., Paschalis, A., Molnar, P., Burlando, P., 2017. An advanced stochastic weather generator for simulating 2-D high-resolution climate variables. Journal of Advances in Modeling Earth Systems 9, 1595–1627. https://doi.org/10.1002/2016MS000854

Peleg, N., Marra, F., Fatichi, S., Molnar, P., Morin, E., Sharma, A., Burlando, P., 2018. Intensification of convective rain cells at warmer temperatures observed from high-resolution weather radar data. Journal of Hydrometeorology JHM-D-17-0158.1. https://doi.org/10.1175/JHM-D-17-0158.1

Peleg, N., Molnar, P., Burlando, P., Fatichi, S., 2019. Exploring stochastic climate uncertainty in space and time using a gridded hourly weather generator. Journal of Hydrology, 571(3), 627–641. https://doi.org/10.1016/j.jhydrol.2019.02.010

Peleg, N., Sinclair, S., Fatichi, S., Burlando, P., 2020. Downscaling climate projections over large and data sparse regions: Methodological application in the Zambezi River Basin. International Journal of Climatology. https://doi.org/10.1002/joc.6578

Peleg, N., Ban, N., Gibson, M. J., Chen, A. S., Paschalis, A., Burlando, P., Leitão, J. P., 2022. Mapping storm spatial profiles for flood impact assessments. Advances in Water Resources, 166, 104258. https://doi.org/10.1016/j.advwatres.2022.104258

Pichelli, E., Coppola, E., Sobolowski, S., Ban, N., Giorgi, F., Stocchi, P., Alias, A., Belušić, D., Berthou, S., Caillaud, C., Cardoso, R.M., Chan, S., Christensen, O.B., Dobler, A., de Vries, H., Goergen, K., Kendon, E.J., Keuler, K., Lenderink, G., Lorenz, T., Mishra, A.N., Panitz, H.-J., Schär, C., Soares, P.M.M., Truhetz, H., Vergara-Temprado, J., 2021. The first multi-model ensemble of regional climate simulations at kilometer-scale resolution part 2: historical and future simulations of precipitation. Clim Dyn 56, 3581–3602. https://doi.org/10.1007/s00382-021-05657-4

Prein, A. F., Langhans, W., Fosser, G., Ferrone, A., Ban, N., Goergen, K., et al., 2015. A review on regional convection-permitting climate modeling: Demonstrations, prospects, and challenges. Reviews of Geophysics, 53(2), 323–361. https://doi.org/10.1002/2014RG000475

Prein, A.F., Rasmussen, R., Castro, C.L., Dai, A., Minder, J., 2020. Special issue: Advances in convection-permitting climate modeling. Clim Dyn 55, 1–2. https://doi.org/10.1007/s00382-020-05240-3

Ramirez, J. A., Mertin, M., Peleg, N., Horton, P., Skinner, C., Zimmermann, M., Keiler, M., 2022. Modelling the long-term geomorphic response to check dam failures in an alpine channel with CAESAR-Lisflood. International Journal of Sediment Research, 37(5), 687–700. https://doi.org/10.1016/j.ijsrc.2022.04.005

Rienecker, M. M., Suarez, M. J., Gelaro, R., Todling, R., Bacmeister, J., Liu, E., et al., 2011. MERRA: NASA's Modern-Era Retrospective Analysis for Research and Applications. Journal of Climate, 24(14), 3624–3648. https://doi.org/10.1175/JCLI-D-11-00015.1

Ruiz-Villanueva, V., Molnar, P., 2020. Past, current, and future changes in floods in Switzerland. Hydro-CH2018 project. Commissioned by the Federal Office for the Environment (FOEN), Bern, Switzerland. https://doi.org/10.3929/ethz-b-000458556

Schär, C., Fuhrer, O., Arteaga, A., Ban, N., Charpilloz, C., Girolamo, S.D., Hentgen, L., Hoefler, T., Lapillonne, X., Leutwyler, D., Osterried, K., Panosetti, D., Rüdisühli, S., Schlemmer, L., Schulthess, T.C., Sprenger, M., Ubbiali, S., Wernli, H., 2020. Kilometer-Scale Climate Models: Prospects and Challenges. Bulletin of the American Meteorological Society 101, E567–E587. https://doi.org/10.1175/BAMS-D-18-0167.1

Schirmer, M., Winstral, A., Jonas, T., Burlando, P., Peleg, N., 2022. Natural climate variability is an important aspect of future projections of snow water resources and rain-on-snow events. The Cryosphere, 16(9), 3469–3488. https://doi.org/10.5194/tc-16-3469-2022

Sideris, I. V., Gabella, M., Erdin, R., Germann, U., 2014. Real-time radar–rain-gauge merging using spatio-temporal co-kriging with external drift in the alpine terrain of Switzerland. Quarterly Journal of the Royal Meteorological Society, 140(680), 1097–1111. https://doi.org/10.1002/qj.2188

Singer, M.B., Michaelides, K., Hobley, D.E.J., 2018. STORM 1.0: a simple, flexible, and parsimonious stochastic rainfall generator for simulating climate and climate change. Geoscientific Model Development 11, 3713–3726. https://doi.org/10.5194/gmd-11-3713-2018

Sparks, N. J., Hardwick, S. R., Schmid, M., Toumi, R.2018. IMAGE: a multivariate multi-site stochastic weather generator for European weather and climate. Stochastic environmental research and risk assessment, 32, 771-784.

Steinschneider, S., Ray, P., Rahat, S.H. Kucharski, J., 2019. A weather-regime-based stochastic weather generator for climate vulnerability assessments of water systems in the western United States. Water Resources Research, 55(8), pp.6923-6945.

Swisstopo, 2002. DHM25: Das digitale Hoehenmodell der Schweiz. Bundesamt für Landestopographie, Wabern, Switzerland.

Trenberth, K.E., Dai, A., Rasmussen, R.M., Parsons, D.B., 2003. The changing character of precipitation. Bulletin of the American Meteorological Society 84, 1205-1217+1161. https://doi.org/10.1175/BAMS-84-9-1205

Trzaska, S., Schnarr, E., 2014. Methods for climate change impact assessment. United States Agency for International Development by Tetra Tech ARD.

Verdin, A., Rajagopalan, B., Kleiber, W., Podestá, G. Bert, F., 2018. A conditional stochastic weather generator for seasonal to multi-decadal simulations. Journal of Hydrology, 556, pp.835-846.

Verdin, A., Rajagopalan, B., Kleiber, W., Podestá, G. Bert, F., 2019. BayGEN: A Bayesian space-time stochastic weather generator. Water resources research, 55(4), pp.2900-2915.

Vergara-Temprado, J., Ban, N., Schär, C., 2021. Extreme Sub-Hourly Precipitation Intensities Scale Close to the Clausius-Clapeyron Rate Over Europe. Geophysical Research Letters 48, e2020GL089506. https://doi.org/10.1029/2020GL089506

Wasko, C., Sharma, A., Westra, S., 2016. Reduced spatial extent of extreme storms at higher temperatures. Geophysical Research Letters, 43(8), 4026–4032. https://doi.org/10.1002/2016GL068509

Wasko, C., Nathan, R., Stein, L., O'Shea, D., 2021. Evidence of shorter more extreme rainfalls and increased flood variability under climate change. Journal of Hydrology, 603, 126994. https://doi.org/10.1016/j.jhydrol.2021.126994

Wasko, C., Westra, S., Nathan, R., Orr, H. G., Villarini, G., Villalobos Herrera, R., Fowler, H. J., 2021. Incorporating climate change in flood estimation guidance. Philosophical Transactions. Series A, Mathematical, Physical, and Engineering Sciences, 379(2195), 20190548. https://doi.org/10.1098/rsta.2019.0548

Wasko, C., Sharma, A., Pui, A., 2021. Linking temperature to catastrophe damages from hydrologic and meteorological extremes. Journal of Hydrology, 602, 126731. https://doi.org/10.1016/j.jhydrol.2021.126731

Westra, S., Fowler, H.J., Evans, J.P., Alexander, L.V., Berg, P., Johnson, F., Kendon, E.J., Lenderink, G., Roberts, N.M., 2014. Future changes to the intensity and frequency of short-duration extreme rainfall. Reviews of Geophysics 52, 522–555. https://doi.org/10.1002/2014RG000464

Wilby, R.L., 1999. The weather generation game: A review of stochastic weather models. Progress in Physical Geography 23, 329–357. https://doi.org/10.1177/030913339902300302

Wilks, D.S., Wilby, R.L., 1999. The weather generation game: a review of stochastic weather models. Progress in Physical Geography: Earth and Environment 23, 329–357. https://doi.org/10.1177/030913339902300302

5 DISCUSSION AND CONCLUSIONS

5.1 SUMMARY

Throughout this thesis I show how newly developed methods and tools were used to quantify the impacts of climate change on hydrological systems, with a special focus on complex mountainous terrains. Using regional climate model outputs alongside advanced weather generators, initially AWE-GEN-2d and later the refined AWE-GEN-2d-CC, I introduce a methodology to simulate large ensembles of high-resolution climate data. These ensembles were used to explore the impacts of climate change on the climate statistics over two Alpine catchments, the Thur and the Kleine Emme. Furthermore, the impacts over the catchments' response were quantified by feeding detailed climate inputs to the Topkapi-ETH hydrological model. This modelling framework served as the basis for this research as it allowed for an unprecedented level of detail in hydrological projections.

Remarkably, the hydrological simulations shed light on the role of hydrological processes in determining the small-scale response of mountain catchments in a future climate, thus answering the Research Question 1 (RQ1) posed in Chapter 1. In Chapter 2 I show how these responses are elevation-dependent and reveal, for instance, how a substantial decline in snowmelt will significantly alter streamflow patterns, especially for higher-elevation catchments. Conversely, for lower river reaches, changes in streamflow are primarily dictated by shifts in precipitation patterns, which generally lead to reduced flows. Furthermore, extreme hydrological events are significantly influenced by these changing precipitation patterns and antecedent conditions, causing changes to flood patterns, i.e. their magnitude and timing, will vary significantly within the study catchments.

In Chapter 3 I detail how the large simulation ensembles made possible by stochastic downscaled climate scenarios are exploited to quantify uncertainties in climate projections. It introduces a methodology that allows to quantify and partition stochastic and model-related uncertainties. As an answer to RQ2, the results indicate that uncertainties related to annual streamflow are high throughout the catchments. These are mostly driven by stochastic uncertainty, which implies a limited potential for narrowing the overall uncertainty in hydrological projections. However, there is room for narrowing the uncertainty of specific hydrological components, such as snowmelt.

Finally, in Chapter 4 I introduce AWE-GEN-2d-CC, a novel weather generator designed specifically to better assess changes to sub-daily extreme rainfall by implementing physics-based dependencies on changes in air temperatures. The model successfully reproduces the observed Clausius-Clapeyron relation and can thus realistically simulate the effect of warming future temperatures on the intensification of extreme precipitation events. RQ3 is answered by applying the new WG to the Kleine Emme catchment. The results show that while rising global temperatures are poised to amplify rainfall extremes, this intensification will not lead to higher streamflow extremes over small sub-catchments due to the complex interplay between non-linear rainfall-runoff transformation and dryer antecedent conditions of catchments and streams.

5.2 DISCUSSION

In this section, I discuss the unique contributions of this thesis to the broader understanding of future hydrological scenarios in Switzerland, and how it fills the research gaps identified in section **Error! Reference source not found.** by enhancing the resolution of climate data,

quantifying uncertainties in climate projections, and elucidating the role of temperature in shaping future extreme hydrological events.

5.2.1 Updating Swiss hydrological scenarios

This thesis offers a detailed analysis of the effects of climate change on future Swiss hydrology at the seldom-studied sub-catchment and sub-daily scales. In Chapters 2 and 4, I focus particularly on the expected changes in the occurrence and magnitude of sub-daily to daily extreme events and delve into the implications of climate change on streamflow in Swiss mountainous catchments, using the Thur and Kleine Emme catchments as case studies.

The emphasis on small-scale, distributed impacts of climate change contrasts with other studies, which often provide coarser, simpler catchment characterizations, but in turn, consider a much larger number of study sites. Such is the case of other studies developed in the context of the Hydro-CH2018 initiative (Brunner, et al., 2019; Molnar et al., 2020; Muelchi et al., 2020, 2021; Ruiz-Villanueva & Molnar, 2020). In them, researchers from three academic groups in Switzerland have modelled the catchment response of hundredths of mesoscale catchments throughout the Swiss Alps using two different semi-distributed hydrological models: HBV-light (Seibert & Vis, 2012) and PREVAH (Viviroli et al., 2009). Like my research, they base their projections of future responses on the change signals revealed by the CH2018 RCM ensemble (CH2018, 2019).

Despite the considerable diversity of the study catchments and modelling approaches, the cited studies find several points of agreement. For instance, the mean annual streamflow over the Swiss catchments is projected to decrease by 7-8% by the end of this century, in line with the Topkapi-ETH simulations presented in Chapter 2.4. Similarly, our studies agree that the seasonality of catchments all over Switzerland will be affected, with diminished streamflow in summer and increases in winter accompanied driven by a decrease and temporal shift in snow water equivalent (SWE) particularly at higher elevations. Likewise, a rise in temperature is expected to boost evapotranspiration across the studied catchments, albeit with considerable variability depending on the specific catchment and elevation. Concerning future floods, although the HBV and PREVAH models differ on the magnitude of the changes, they generally agree that floods will become weaker at lower-elevation catchments while intensifying at higher-elevation ones—except for glaciered catchments, which I did not consider in this work.

Beyond these points of consensus, the novel modelling framework offers a more comprehensive perspective through which to study mountainous catchments. For instance, by examining elevation-dependent changes at sub-catchment scales, I find that the Swiss-wide projections of decreasing (mean and maximum) flows at higher elevations and decrease for lower elevations are also present over much smaller domains. This type of analysis can reveal information crucial to stakeholders that would be otherwise obscured. For instance, I show how high flows at the lower reaches of basins may increase because of climate change, even when the statistics at the outlet indicate no impact. Moreover, I delve into the components of streamflow production and show how they will be dissimilarly affected by climate change, with important consequences for water resources management. For example, the simulations project a change in the hydrological regime of the study catchments, with decreasing spring and summer flows due to a diminishing snowmelt volume and an increase in winter flows driven by higher liquid precipitation. Lastly, the quantification of uncertainty due to natural climate variability presented in Chapter 3 (and discussed in more detail in the following), adds another frequently missing piece to the puzzle of Swiss hydrological scenarios. As such, this thesis represents, at a minimum, an asset in the quest to improve the understanding of hydrology over the Alps as well as any highly heterogeneous basin. As part of the Hydro-CH2018 initiative to update future hydrological scenarios, it is my hope that this work aids

adaption and mitigation measures by public and private stakeholders in anticipation of a future of change and uncertainty.

While acknowledging the scope of this study focused on only two catchments, this approach has facilitated an in-depth understanding and precise model calibration. Although the Thur and Kleine Emme catchments do not encompass the full diversity of Swiss terrain, they offer valuable insights into sub-daily to daily hydrological extremes that are representative of similar mountainous catchments. his study provides a detailed snapshot that, while not exhaustive, contributes significantly to our understanding of hydrological responses influenced by variations in elevation and climate change.

To build on the strengths of this study and further enhance its robustness, it would be advisable to expand the spatial coverage of the model. By including a wider variety of catchment types—ranging from small, lowland basins to extensive, alpine systems—we can broaden the applicability of our findings and deepen the understanding of hydrological changes across Switzerland. Such expansion would also allow us to refine our projections for future hydrological scenarios and improve the precision of flood predictions, thus providing valuable information for both mitigation and adaptation strategies in diverse hydrological settings.

5.2.2 Generating high-resolution climate ensembles

A critical research gap is the need for high-resolution climate data to effectively study complex landscapes, including mountainous terrains, in the context of climate change. This thesis bridges this gap by employing sophisticated WGs capable of i) generating large ensembles efficiently, as illustrated by the simulation of a year of climate for the Kleine Emme catchment within just 10 to 15 minutes using a standard consumer-level computer; ii) achieving high-resolution data, with a granularity in precipitation simulations of 5-minute intervals and 2-km spatial resolution, as well as hourly ensembles of temperature and other climate variables at 100-m resolution; and iii) basing projections on physical relations instead of merely relying on observed statistical correlations; thus enabling realistic modelling of the behaviour of climate variables under future conditions.

To highlight the value of high-resolution datasets, one option is to directly contrast the results obtained using coarse and fine resolution inputs in a sensitivity analysis fashion. A good example of this is presented by Kay (2022), who compared high-resolution Convection Permitting Models (CPMs) with lower-resolution GCM/RCMs and demonstrated that the resolution of the input climate data affects not only the magnitude of present-day floods, but also influences the impact under future climate conditions. In this work, I instead sought to quantify the impacts of climate change over small sub-catchments, which cannot be characterized through coarse datasets. Using the Topkapi-ETH hydrological model, this study highlights how high-resolution data can reveal nuanced, elevation-dependent hydrological processes at the sub-catchment scale, a pattern, which has been noted by other studies operating at different scales and sometimes using (e.g., Daly et al., 2017; He et al., 2019; Xu & Di Vittorio, 2021; Zhu et al., 2023), also altering the characteristics of modelled flood responses (Constabile et al., 2023). Consequently, the outcomes of this study can serve as valuable inputs for managing water resources and disaster preparedness, particularly over complex terrains.

Beyond detailed simulation of temperature and precipitation dynamics, the tools developed in this thesis can simulate a broad spectrum of near-surface climate variables that significantly influence hydrological and ecological processes. Variables such as wind speed, solar radiation, humidity, and atmospheric pressure also play crucial roles in determining the microclimates of mountainous terrains and consequently affect water balance and ecosystem dynamics. The high-resolution simulation of these variables offered by advanced weather

generators presents an opportunity to explore their interdependencies and their combined effects on mountainous ecosystems and water cycles. The present work thus offers the potential to expand the small-scale analysis to impacts beyond hydrological extremes.

Moreover, the modelling framework presented in this thesis challenges the reliance on costly dynamical models to generate physically-sound, high-resolution climate projections, with the added benefit of inexpensively generating large ensembles that allow a robust estimation of extreme events—a feat that cannot (yet) be realistically matched by dynamical models at the granularity required by impact assessment studies (e.g., Coppola et al., 2018; Gebrechorkos et al., 2023; Pichelli et al., 2021; Ban et al., 2021). Furthermore, the framework not only enriches the toolkit of climate scientists seeking to generate detailed and comprehensive climate projections but contributes another dimension by allowing a rigorous assessment of the uncertainties introduced throughout the modelling chain.

5.2.3 Uncertainty in climate projections

Communicating the uncertainty inherent in climate projections presents significant challenges. Despite various efforts to refine these communications, such as the guidelines by the IPCC for communicating uncertainty and risk (Budescu et al., 2012), finding the right balance between clarity and comprehensiveness remains elusive (Kause et al., 2021). This balance is crucial because it impacts how stakeholders perceive and utilize the information. Often, the complexity of conveying uncertain results can lead to its underrepresentation in climate impact studies, perhaps by causing reluctance among scientists and practitioners as stakeholders may perceive the information as less credible or actionable. In other words, as Pappenberger and Beven (2006) warned, for some, ignorance is bliss, and this oversight that can negatively affect decision-making.

Addressing the full scope of communicating uncertainty is beyond the ambit of this thesis. However, I propose that one step in the right direction involves clearly distinguishing and partitioning the sources of uncertainty. In this thesis I sought to do just that and dedicate Chapter 3 to dissecting the different drivers of uncertainty—whether they stem from natural climate variability or from limitations inherent in modelling techniques—thus providing a clearer picture of what underlies the projections and forecasts presented in climate science.

But perhaps the main contribution of this thesis lies in tackling a technical barrier to studying uncertainty sources: the lack of robust methods to accurately quantify them, particularly concerning stochastic uncertainty. This work provides a practical framework for quantifying stochastic uncertainty, assessing its importance relative to other uncertainty sources (i.e. climate models), and, especially, understanding its influence throughout the modelling chain. Furthermore, it does so at the in a distributed fashion, thus offering a level of granularity that has not been reached by other studies.

By leveraging weather generators to produce large ensembles of climate data, I inspected both the climate model and stochastic components of uncertainty. For example, in the two catchments studied in Chapter 3, the stochastic uncertainty in precipitation—the natural climate variability—is high throughout the domain, whereas the climate model uncertainty exhibits a positive correlation with elevation, which is largely in agreement with other recent works researching how uncertainty propagates into the projections of hydrological variables using a variety of data, models and methods (e.g., Chawla & Mujumdar, 2018; Chen et al., 2017; Clark et al., 2016; Das et al., 2018; Feng & Beighley, 2020; Gao & Booij, 2020; Meresa et al., 2021; Vetter et al., 2017). Additionally, the uncertainty of climate projections further propagates into the hydrological response of the catchment, as demonstrated by the weak signal-to-noise ratios (STNR) observed for the statistics of high-streamflow which is credited mostly to the irreducible stochastic uncertainty. The results suggest, however, that there is

some potential to narrow down the uncertainty of specific hydrological components such as rainfall or snowmelt at higher elevations and during warm seasons, when the impacts are driven mostly by temperature changes.

This thesis has focused on understanding and quantifying two major sources of uncertainty in climate impact studies on hydrology: internal climate variability and climate model uncertainty. These two aspects are critical as they have shown to introduce the largest variability in the subsequent hydrological projections, particularly regarding hydrological extremes (Addor et al., 2014; Fatichi et al., 2014, 2016). The decision to focus on internal climate variability and climate model uncertainty stemmed primarily from the specific aims of this study to isolate and understand the effects of these uncertainty sources on Swiss hydrology at a highly granular level. This focus allowed for a more detailed exploration of how different climate models and inherent climatic changes impact hydrological extremes at the sub-catchment scale, providing valuable insights into the robustness of hydrological projections.

Nevertheless, it's crucial to recognize that other sources of uncertainty also influence these projections. The uncertainty stemming from greenhouse gas emissions scenario, for example, was not analysed in this work. Naturally, this framework can easily be expanded to assess the influence of emission scenarios by re-calculating the factors of change based on additional climate projections and subsequently re-parametrizing the weather generator to account for the climate change signal according to the selected climate projections. Considering the findings detailed in Chapter 3, it is to be expected that emission scenario uncertainty will drive the variability of temperature-dependent hydrological processes, as is the case of snow and ice melt, which should result in higher uncertainty over catchments with mixed precipitation regimes as is the case of most mid-elevation Alpine catchments.

Another uncertainty source worth consideration is the hydrological model used to quantify the catchment response to climate inputs. Partly, its omission from this thesis is justified by its low contribution to Swiss Alpine projections according to Addor et al. (2014). Notwithstanding, the incorporation of hydrological model uncertainty into this framework would enhance our understanding of the overall variability in catchment response, which may vary significantly across different catchment types as demonstrated, for example, by Giuntoli et al. (2018) in their study over a vast number of US catchments.

Beyond these specific results, this framework lends itself for application to diverse cases including different geographies, model chains, and uncertainty sources. It is my hope that the methodology used to create large simulation ensembles can be adopted to inform the decisions of water resource managers and disaster risk reduction practitioners. An example of this is the conclusion that a focus on adapting to uncertainty may be more effective than attempting to increase the accuracy in the estimation of extremes for Alpine domains. Furthermore, this research underscores the critical importance of considering multiple forms of uncertainty in hydrological projections to inform more effective adaptation and mitigation strategies, especially concerning rare but impactful hydrological events.

5.2.4 Temperature and extreme events

Convective events, responsible for extreme precipitation in large swathes of the globe, often result in costly natural catastrophes (Taszarek et al., 2021). Multiple studies demonstrate that these types of events—characterised by high temperatures and bursts of intense rainfall—will become more frequent and/or more intense under future climate conditions. Reproducing the temperature dependence of intense rainfall (the so-called Clausius-Clapeyron relation) is therefore essential to any attempt to understand future extreme events and their consequences.

This poses a significant challenge as most dynamical climate models (e.g., GCMs or RCMs), on which we base climate and hydrological projections, are not capable of characterizing this phenomenon (Prein et al., 2015, Ban et al., 2021; Lucas-Picher et al., 2021; Pichelli et al., 2021). The new AWE-GEN-2d-CC weather generator is developed precisely to tackle this issue. by conditioning the simulation of precipitation intensities on the air temperature at the onset of storm events, thus moving past the implicit assumption of no correlation between temperature and precipitation statistics. Instead, the new model utilizes an empirical relationship derived from observational records, enabling the model to reproduce the physical influence of temperature on storm characteristics which results in a satisfactory representation of observed temperature-dependent storm characteristics.

Moreover, the AWE-GEN-2d-CC model makes two further assumptions regarding the spatiotemporal characteristics of storms—such as duration, size, and spatial variability of the precipitation fields. The first is that these characteristics can be modelled as if they were part of one population, albeit conditioned on the temperature of the event. This is a simplification which avoids explicitly modelling different event types (e.g. convective and stratiform storms) as separate processes. The second assumption is the distribution of these storm characteristics will remain constant under changing climate conditions. Emerging evidence suggests that, beyond the expected intensification of storms, extreme events may also become longer, thereby dampening the intensification of peaks below what is explained by the Clausius-Clapeyron temperature scaling (Ban et al, 2021; Pichelli et al., 2021). This implies that simulations assuming stationarity of spatiotemporal characteristics of storms may slightly overestimate peak rainfall amounts, highlighting an area for future research and model adjustment.

Despite these caveats, re-parameterizing AWE-GEN-2d-CC to reflect changes in large-scale temperature and precipitation patterns, as projected by climate models, allows it to more realistically simulate future precipitation intensification at high temporal and spatial resolutions. As such, it represents not only an improvement upon its predecessor AWE-GEN-2d—up to now one of the most sophisticated WGs available in scientific literature—but also serves as a blueprint to advance the development of new models looking to characterize future climate conditions.

In addition to improving upon an already state-of-the-art WG, this thesis offers the methodological framework to project future hydrological extremes. As I demonstrate with the case study of the Kleine Emme presented in Chapter 4, AWE-GEN-2d-CC reproduces the significant influence that the temperature-scaling of storm properties has on the magnitude of short-duration (hourly) rainfall extremes. The hydrological simulations portray a surge in rare extreme events—those with return periods exceeding 50 years—in stark contrast with the results using AWE-GEN-2d. Daily rainfall events, in turn, are not projected to increase which, compounded by drier antecedent conditions over the catchment, results in an expected decrease of daily high flows, albeit with a large uncertainty range.

Overall, these results underscore the importance of considering the temperature dependence of rainfall in our models. With this relatively simple improvement to an already advanced weather generator, I expect AWE-GEN-2d-CC to become a valuable tool to model intense precipitation wherever convective storms play a substantial role. Given the vast presence of convective events in other geographies, and the preponderance they have in the records of highest precipitations, I expect the model will find appeal far beyond the Swiss mountains.

5.3 OUTLOOK

5.3.1 Further developments to advanced weather generators

The AWE-GEN-2d-CC model has effectively reproduced the observed temperature-precipitation relationship in present and future climate simulations. To enhance its predictive capabilities for future extreme event characteristics, an alternative development avenue could be to transcend the use of static spatiotemporal storm characteristics. This can be achieved without reformulating the model structure by recalibrating the parameters of storm duration, wet-area ratio, and mean intensity field based on change signals from dynamical climate models. An obvious source for the detailed data required for this recalibration could be the outputs of Convection Permitting Models (CPMs), which offer high-resolution insights into climate dynamics. These models provide a rich dataset that can be analysed to establish relationships between changing climate signals and storm parameters, thereby refining the weather generator's ability to simulate future conditions accurately. Future work could help quantify the added value of this approach by establishing whether the increase in data requirements and calibration efforts has any significant effect on future simulations.

Moving forward, an additional enhancement would involve explicitly modelling different storm types within the AWE-GEN-2d-CC framework. By distinguishing among storm types—such as convective and stratiform—this approach would allow to improve the accuracy of precipitation simulations significantly. Most intense weather events, depending on the local climate, stem from specific types of storms. Accurately modelling these events thus requires developing probabilistic models that predict the emergence of different storm types based on observed climatic conditions. This requires access to extensive, high-resolution observational datasets, enabling the weather generator to mimic the unique characteristics of each storm type more precisely. Such an enhancement would not only improve the model's realism but also its utility in predicting the hydrological impacts of climate change, particularly in regions prone to extreme weather events, as well as other types of hazards resulting from strong convective storms.

5.3.2 New applications of AWE-GEN-2d-CC

The versatility of AWE-GEN-2d-CC extends to its potential applications in climate studies beyond the effects of climate on river-network response. The model inherits the remarkable capabilities of AWE-GEN-2d in simulating realistic time series of relative humidity, incoming short-wave radiation, dew-point temperature, and wind fields, as demonstrated by Peleg et al. (2017). In the agricultural sector, AWE-GEN-2d-CC can be instrumental in simulating microclimatic conditions that affect crop growth and yield. By providing detailed weather data at a granular level, the model enables researchers and farmers to simulate potential future climate scenarios and their direct impact on crop productivity. This can guide more informed decisions about crop selection, irrigation needs, and harvesting times, optimizing agricultural practices to better withstand the unpredictability of climate change. For energy production, AWE-GEN-2d-CC's ability to model wind fields and radiation can be particularly beneficial to plan the production and storage operations of renewable energy projects. In terms of natural disaster risk assessment, the model's high-resolution simulations of extreme weather events make it an invaluable asset for disaster preparedness and mitigation strategies. By assessing the frequency and magnitude of potential extreme weather, such as heavy rainfall, heatwaves, or high winds, emergency management agencies can better plan evacuation routes, prepare response strategies, and design infrastructure to be more resilient against these natural threats. Moreover, the capability of AWE-GEN-2d-CC to simulate a large number of stochastic weather scenarios is particularly valuable for conducting robust economic analyses. Financial institutions, insurance companies, and governmental bodies can utilize these simulations to

develop loss curves and other risk assessment models. These tools help in quantifying potential economic impacts under different climate scenarios, enabling more informed decision-making regarding financial investments, insurance policies, and climate adaptation strategies.

Although this work offers a highly detailed analysis of the hydrological response of mountainous catchments, the resolution of hydrological simulations still falls short of capabilities of the WGs' employed. Exploiting the 5-minute precipitation simulations, for example, offers a readily accessible path to evaluate hydrological responses at sub-hourly scales. While this approach has not been pursued in the current work due to time and resource constraints, it represents a great opportunity to enhance our understanding of rapid hydrological changes, such as those observed during flash floods. Likewise, the advanced weather generators are perfectly capable of reproducing the statistics of temperature, radiation, and other non-precipitation variables at the sub-kilometre scale, as demonstrated by Peleg et al. (2017). While there is a trade-off between temporal and spatial granularity and the computational feasibility of long-term simulations, the bigger challenge lies in ensuring that the physical characteristics of the study catchment are accurately represented, as the reliability of physically based hydrological models hinges on the quality of the domain representation just as it does on the characterization of external inputs. If these challenges are addressed, leveraging tools like Topkapi-ETH alongside reliable streamflow observations for validation could substantially advance our capability to model and predict sub-hourly hydrological dynamics.

5.3.3 Expanding the domain of distributed WGs

Another intriguing direction for research involves using the distributed climate simulations generated by AWE-GEN-2d-CC as inputs to multiple (semi-)distributed hydrological models. A comprehensive comparison between these models could offer valuable insights into the propagation of uncertainty across different hydrological frameworks, revealing critical insights into their relative performance and reliability. This comparative analysis is particularly valuable for identifying the strengths and limitations of each model, especially in handling extreme and rapid weather events. The combination of AWE-GEN-2d-CC with physically based hydrological models offers modelers an ideal toolkit for comparing the efficacy of hydrological models and for unravelling the complex sub-hourly hydrological dynamics within fast-responding catchments. This approach not only enhances our understanding of hydrological processes but also improves our preparedness for managing water resources in the face of increasingly unpredictable climate patterns.

Climate studies in regions with complex topographical features are ideal settings to test the features of AWE-GEN-2d-CC. Mountainous regions, particularly in mid-latitudes, will benefit from a weather generator designed to handle the complexity of steep slopes and high-elevation gradients. With careful consideration for regional climate specificities, the model should prove robust across varying landscapes. Furthermore, the computational efficiency of AWE-GEN-2d-CC also suggests that applications over larger domains (e.g., Peleg, et al., 2020) or over multiple mesoscale domains are technically feasible without incurring in prohibitive computational costs. Extending the model's geographic coverage would serve as both a validation exercise and an opportunity to identify local nuances that may not be captured in the current study. As it stands, the main challenge to applying the model over a large number of catchments is the manual calibration for each individual domain. Developing an automatic calibration algorithm to readily take advantage of large remote-sensing observation and reanalysis data would allow the generation of high-resolution weather time series across multiple sites. Combined with distributed, physically based modelling of the catchments' responses, such an effort could shed light on the impacts of climate change over

complex catchments within large regions (e.g., different impacts among Alpine catchments) or in vastly different contexts.

In contrast with modelling many relatively small domains, expanding the application of AWE-GEN-2d and AWE-GEN-2d-CC to model large domains beyond the mesoscale is, in any case, not straightforward. One of the main limitations in this regard is that the simulation of storms requires an explicit definition of the event interarrival sequence, which simply loses its meaning as domains grow large enough to host simultaneous yet independent events. Similarly, another cornerstone of the model is the definition of mean areal statistics, which assume that spatiotemporal characteristics of storms can be characterized with domain-wide parameters. Overcoming these limitations would require moving past the paradigms of the powerful STREAP model (Paschalis et al., 2013) for the continuous simulation of precipitation fields, which is at the heart of AWE-GEN-2d and AWE-GEN-2d-CC. Instead, modelling high resolution climate data at regional or even global scales may be better achieved through alternative, top-down approaches that seek to refine large but coarse data, rather than aggregating high-resolution simulations from the bottom up.

5.3.4 High resolution ensembles over large scales

In the years since I began this thesis project, Single Model Initial-Condition Large Ensembles (SMILEs) have emerged as another powerful tool in the arsenal of climate and environmental scientists (Deser et al., 2020; Lehner et al., 2020; Maher et al., 2021; Milinski et al., 2020; Wyser et al., 2021). The operating principle behind SMILEs is deceptively simple: by making minuscule alterations to initial conditions, sometimes reaching back several hundredths of years, these dynamical models generate an array of distinct, but equally plausible climate time series despite identical external conditions. Thanks to advances in computational capacity and numerical modelling techniques climate modelers have simulated tens, and even hundreds, of climate realizations under a single emissions scenario. Although SMILEs promise to encapsulate internal climate variability, thus offering robust global uncertainty estimation, they are not without shortcomings and their broader utility is constrained by their typically coarse resolution. This limits their direct applicability for local-scale impact assessments and necessitates further downscaling and bias correction to align their outputs with observed climate data.

Parallel to this, Convection Permitting Models (CPMs) have grown in number and coverage (Lucas-Picher et al., 2021). CPMs are regarded as the most accurate tools available for simulating future climates at fine scales, as they can simulate convection and cloud formation processes which are essential to characterize small-scale extreme weather events. These models, however, are severely limited by their intensive computational requirements, which limits their use over regional domains to typically just one climate realization of relatively short simulations. While it is expected that computational costs will become relatively lower over time, it is not realistic to expect large ensembles of CPM simulations in the short or mid-term.

To quantify the small-scale impacts of climate change over large regions, we must find a way to generate large ensembles of physically sound, high-resolution climate simulations. Moving forward, I envision at least two promising paths to bridge the gap between SMILEs and CPMs and this ideal outcome through statistical models. The first is through statistical downscaling and bias correction of SMILEs: This involves applying statistical techniques to correct biases in SMILE outputs and to downscale them to higher resolutions suitable for impact assessments. By integrating advanced statistical methods, it’s possible to transform SMILEs into large ensembles of high-resolution, unbiased climate datasets that reflect the dynamic climate signals of the original ensemble members. A challenge to be addressed with this approach is, however, ensuring that the statistical relations built within the models are robust

enough to handle prediction data which, due to the changing nature of climate, are not within the scope of the training dataset. Should that be sorted, it will be possible to generate datasets that are not only fine-grained but also encompass the inherent variability and changing dynamics of future climates.

An intriguing second path forward involves the so-called emulation of CPMs. This approach entails developing statistical models which can link the fine outputs of CPMs with the coarse outputs of their driving global climate models. By doing so, the emulators replicate the results of the costly dynamical downscaling model using a mere fraction of the computational resources. The key advantage of this method is its ability to utilize the underlying physical relationships modelled by CPMs to extend downscaling across longer time periods and across various climate models and emission scenarios. Essentially, this makes it feasible to generate high-resolution climate data that retains the fidelity of CPM outputs but is produced much more efficiently. This approach holds the promise of expanding the accessibility and applicability of high-quality, fine-resolution climate projections, crucial for detailed local-scale climate impact assessments.

As we continue to explore these statistical methods, the recent strides in the field of machine learning (ML) present a compelling alternative to traditional statistical models. ML models, particularly those predicated on deep learning architectures, have shown great promise in fields requiring pattern recognition and predictive analytics, such as computer vision and image super-resolution. Over the last few years, these models have been repurposed for use in climate sciences, with some notable breakthroughs as in the case of weather forecasting (e.g., Lam et al., 2023). Although empirical evidence to support their efficacy in tasks downscaling tasks and emulation of climate models remains limited, some results appear promising (Addison et al., 2022; Hobeichi et al., 2023; Wang et al., 2021) and further developments could potentially combine computational efficiency with rich a characterization of spatiotemporal climate patterns. As observational data continues to improve, and dynamical models evolve further, I remain hopeful that ML models will eventually meet, if not exceed the expectations set for them.

In summary, the landscape of climate change simulation methodologies continues to evolve, and while no single approach is without its limitations, the potential for synergy between diverse models offers a multi-faceted lens through which to understand the complexities of our planet's changing climate.

5.4 REFERENCES

Addor, N., Rössler, O., Köplin, N., Huss, M., Weingartner, R., Seibert, J., 2014. Robust changes and sources of uncertainty in the projected hydrological regimes of Swiss catchments. Water Resources Research, 50(10), 7541–7562. https://doi.org/10.1002/2014WR015549

Addison, H., Kendon, E., Ravuri, S., Aitchison, L., Watson, P.A., 2022. Machine learning emulation of a local-scale UK climate model. https://doi.org/10.48550/arXiv.2211.16116

Ban, N., Caillaud, C., Coppola, E., Pichelli, E., Sobolowski, S., Adinolfi, M., Ahrens, B., Alias, A., Anders, I., Bastin, S., Belušić, D., Berthou, S., Brisson, E., Cardoso, R.M., Chan, S.C., Christensen, O.B., Fernández, J., Fita, L., Frisius, T., Gašparac, G., Giorgi, F., Goergen, K., Haugen, J.E., Hodnebrog, Ø., Kartsios, S., Katragkou, E., Kendon, E.J., Keuler, K., Lavin-Gullon, A., Lenderink, G., Leutwyler, D., Lorenz, T., Maraun, D., Mercogliano, P., Milovac, J., Panitz, H.-J., Raffa, M., Remedio, A.R., Schär, C., Soares, P.M.M., Srnec, L., Steensen, B.M., Stocchi, P., Tölle, M.H., Truhetz, H., Vergara-Temprado, J., Vries, H. de, Warrach-Sagi, K.,

Wulfmeyer, V., Zander, M.J., 2021. The first multi-model ensemble of regional climate simulations at kilometer-scale resolution, part I: evaluation of precipitation. Climate Dynamics 2021 1–28. https://doi.org/10.1007/S00382-021-05708-W

Budescu D.V., Por H.H., Broomell S.B., 2012. Effective communication of uncertainty in the IPCC reports. Clim. Change 113 181–200

Brunner, M.I., Hingray, B., Zappa, M., Favre, A.C., 2019. Future Trends in the Interdependence Between Flood Peaks and Volumes: Hydro-Climatological Drivers and Uncertainty. Water Resources Research 55, 4745–4759. https://doi.org/10.1029/2019WR024701

CH2018, 2019. CH2018 – Climate Scenarios for Switzerland, Technical Report. National Centre for Climate Services, Zurich, Switzerland.

Chawla, I., Mujumdar, P.P., 2018. Partitioning uncertainty in streamflow projections under nonstationary model conditions. Advances in Water Resources 112, 266–282. https://doi.org/10.1016/j.advwatres.2017.10.013

Chen, J., Brissette, F.P., Liu, P., Xia, J., 2017. Using raw regional climate model outputs for quantifying climate change impacts on hydrology. Hydrological Processes 31, 4398–4413. https://doi.org/10.1002/hyp.11368

Clark, M.P., Wilby, R.L., Gutmann, E.D., Vano, J.A., Gangopadhyay, S., Wood, A.W., Fowler, H.J., Prudhomme, C., Arnold, J.R., Brekke, L.D., 2016. Characterizing Uncertainty of the Hydrologic Impacts of Climate Change. Current Climate Change Reports 2, 55–64. https://doi.org/10.1007/s40641-016-0034-x

Costabile, P., Costanzo, C., Kalogiros, J., Bellos, V., 2023. Toward street-level nowcasting of flash floods impacts based on HPC hydrodynamic modeling at the watershed scale and high-resolution weather radar data. Water Resources Research, 59(10), p.e2023WR034599.

Coppola, E., Sobolowski, S., Pichelli, E., Raffaele, F., Ahrens, B., Anders, I., Ban, N., Bastin, S., Belda, M., Belusic, D., Caldas-Alvarez, A., Cardoso, R.M., Davolio, S., Dobler, A., Fernandez, J., Fita, L., Fumiere, Q., Giorgi, F., Goergen, K., Güttler, I., Halenka, T., Heinzeller, D., Hodnebrog, Jacob, D., Kartsios, S., Katragkou, E., Kendon, E., Khodayar, S., Kunstmann, H., Knist, S., Lavín-Gullón, A., Lind, P., Lorenz, T., Maraun, D., Marelle, L., van Meijgaard, E., Milovac, J., Myhre, G., Panitz, H.J., Piazza, M., Raffa, M., Raub, T., Rockel, B., Schär, C., Sieck, K., Soares, P.M.M., Somot, S., Srnec, L., Stocchi, P., Tölle, M.H., Truhetz, H., Vautard, R., de Vries, H., Warrach-Sagi, K., 2018. A first-of-its-kind multi-model convection permitting ensemble for investigating convective phenomena over Europe and the Mediterranean. Climate Dynamics 55, 3–34. https://doi.org/10.1007/s00382-018-4521-8

Das, J., Treesa, A., Umamahesh, N.V., 2018. Modelling Impacts of Climate Change on a River Basin: Analysis of Uncertainty Using REA & Possibilistic Approach. Water Resour Manage 32, 4833–4852. https://doi.org/10.1007/s11269-018-2046-x

Deser, C., Lehner, F., Rodgers, K.B., Ault, T.R., Delworth, T.L., DiNezio, P.N., Fiore, A.M., Frankignoul, C., Fyfe, J.C., Horton, D.E., Kay, J.E., Knutti, R., Lovenduski, N.S., Marotzke, J., McKinnon, K.A., Minobe, S., Randerson, J.T., Screen, J.A., Simpson, I.R., Ting, M., 2020. Insights from Earth system model initial-condition large ensembles and future prospects. Nature Climate Change. https://doi.org/10.1038/S41558-020-0731-2

Fatichi S, Ivanov VY, Paschalis A, Peleg N, Molnar P, Rimkus S, Kim J, Burlando P, Caporali E. 2016. Uncertainty partition challenges the predictability of vital details of climate change. Earth's Future 4 (5): 240–251 DOI: 10.1002/2015EF000336

Fatichi S, Rimkus S, Burlando P, Bordoy R. 2014. Does internal climate variability overwhelm climate change signals in streamflow? The upper Po and Rhone basin case studies. Science of the Total Environment 493: 1171–1182 DOI: 10.1016/j.scitotenv.2013.12.014

Feng, D., Beighley, E., 2020. Identifying uncertainties in hydrologic fluxes and seasonality from hydrologic model components for climate change impact assessments. Hydrology and Earth System Sciences 24, 2253–2267. https://doi.org/10.5194/hess-24-2253-2020

Gao, C., Booij, M.J., 2020. Assessment of extreme flows and uncertainty under climate change: Disentangling the uncertainty contribution of representative concentration pathways, global climate models and internal climate variability. Hydrology and Earth System Sciences 24, 3251–3269. https://doi.org/10.5194/hess-24-3251-2020

Gebrechorkos, S., Leyland, J., Slater, L., Wortmann, M., Ashworth, P.J., Bennett, G.L., Boothroyd, R., Cloke, H., Delorme, P., Griffith, H., Hardy, R., Hawker, L., McLelland, S., Neal, J., Nicholas, A., Tatem, A.J., Vahidi, E., Parsons, D.R., Darby, S.E., 2023. A high-resolution daily global dataset of statistically downscaled CMIP6 models for climate impact analyses. Sci Data 10, 611. https://doi.org/10.1038/s41597-023-02528-x

Hobeichi, S., Nishant, N., Shao, Y., Abramowitz, G., Pitman, A., Sherwood, S., Bishop, C., Green, S., 2023. Using Machine Learning to Cut the Cost of Dynamical Downscaling. Earth's Future 11, e2022EF003291. https://doi.org/10.1029/2022EF003291

Kause, A., Bruin, W.B. de, Domingos, S., Mittal, N., Lowe, J., Fung, F., 2021. Communications about uncertainty in scientific climate-related findings: a qualitative systematic review. Environ. Res. Lett. 16, 053005. https://doi.org/10.1088/1748-9326/abb265

Kay, A., 2022. Differences in hydrological impacts using regional climate model and nested convection-permitting model data. Climatic Change, 173(1-2), p.11.

Lam, R., Sanchez-Gonzalez, A., Willson, M., Wirnsberger, P., Fortunato, M., Alet, F., Ravuri, S., Ewalds, T., Eaton-Rosen, Z., Hu, W. and Merose, A., 2023. Learning skillful medium-range global weather forecasting. Science, 382(6677), pp.1416-1421. https://doi.org/10.1126/science.adi2336

Lehner, F., Deser, C., Maher, N., Marotzke, J., Fischer, E., Brunner, L., Knutti, R., Hawkins, E., 2020. Partitioning climate projection uncertainty with multiple Large Ensembles and CMIP5/6. Earth System Dynamics Discussions 11, 1–28. https://doi.org/10.5194/esd-2019-93

Lucas-Picher, P., Argüeso, D., Brisson, E., Tramblay, Y., Berg, P., Lemonsu, A., Kotlarski, S., Caillaud, C., 2021. Convection-permitting modeling with regional climate models: Latest developments and next steps. WIREs Climate Change 12, e731. https://doi.org/10.1002/wcc.731

Maher, N., Milinski, S., Ludwig, R., 2021. Large ensemble climate model simulations: introduction, overview, and future prospects for utilising multiple types of large ensemble. Earth System Dynamics 12, 401–418. https://doi.org/10.5194/esd-12-401-2021

Meresa, H., Murphy, C., Fealy, R., Golian, S., 2021. Uncertainties and their interaction in flood hazard assessment with climate change. Hydrology and Earth System Sciences 25, 5237–5257. https://doi.org/10.5194/hess-25-5237-2021

Milinski, S., Maher, N., Olonscheck, D., 2020. How large does a large ensemble need to be. Earth System Dynamics Discussions. https://doi.org/10.5194/ESD-11-885-2020

Molnar, P., Chang, Y., Yuan, Peleg, N., Moraga, S., Zappa, M., Brunner, M.I., Seibert, J., Freudiger, D., Martius, O., Mülchi, R., 2020. Future changes in floods, in: Ruiz-Villanueva, V.;, Molnar, P.; (Eds.), Past, Current, and Future Changes in Floods in Switzerland. Hydro-CH2018 project. Commissioned by the Federal Office for the Environment (FOEN), Bern, Switzerland, pp. 51–58. https://doi.org/10.3929/ethz-b-000462778

Muelchi, R., Rössler, O., Schwanbeck, J., Weingartner, R., Martius, O., 2021. River runoff in Switzerland in a changing climate – changes in moderate extremes and their seasonality. Hydrology and Earth System Sciences 25, 3577–3594. https://doi.org/10.5194/hess-25-3577-2021

Muelchi, R., Rössler, O., Schwanbeck, J., Weingartner, R., Martius, O., 2020. Future runoff regime changes and their time of emergence for 93 catchments in Switzerland. Hydrology and Earth System Science. https://doi.org/10.5194/hess-2020-516

Pappenberger, F. and Beven, K.J., 2006. Ignorance is bliss: Or seven reasons not to use uncertainty analysis. Water resources research, 42(5).

Paschalis, A., Molnar, P., Fatichi, S., Burlando, P., 2013. A stochastic model for high-resolution space-time precipitation simulation. Water Resources Research, 49(12), pp.8400-8417.

Peleg, N., Fatichi, S., Paschalis, A., Molnar, P., Burlando, P., 2017. An advanced stochastic weather generator for simulating 2-D high-resolution climate variables. Journal of Advances in Modeling Earth Systems 9, 1595–1627. https://doi.org/10.1002/2016MS000854

Peleg, N., Sinclair, S., Fatichi, S., Burlando, P., 2020. Downscaling climate projections over large and data sparse regions: Methodological application in the Zambezi River Basin. International Journal of Climatology. https://doi.org/10.1002/joc.6578

Pichelli, E., Coppola, E., Sobolowski, S., Ban, N., Giorgi, F., Stocchi, P., Alias, A., Belušić, D., Berthou, S., Caillaud, C., Cardoso, R.M., Chan, S., Christensen, O.B., Dobler, A., de Vries, H., Goergen, K., Kendon, E.J., Keuler, K., Lenderink, G., Lorenz, T., Mishra, A.N., Panitz, H.-J., Schär, C., Soares, P.M.M., Truhetz, H., Vergara-Temprado, J., 2021. The first multi-model ensemble of regional climate simulations at kilometer-scale resolution part 2: historical and future simulations of precipitation. Clim Dyn 56, 3581–3602. https://doi.org/10.1007/s00382-021-05657-4

Ruiz-Villanueva, V., Molnar, P., 2020. Past, current, and future changes in floods in Switzerland. Hydro-CH2018 project. Commissioned by the Federal Office for the Environment (FOEN), Bern, Switzerland. https://doi.org/10.3929/ethz-b-000458556

Seibert, J., Vis, M.J.P., 2012. Teaching hydrological modeling with a user-friendly catchment-runoff-model software package. Hydrology and Earth System Sciences 16, 3315–3325. https://doi.org/10.5194/hess-16-3315-2012

Taszarek, M., Allen, J.T., Marchio, M., Brooks, H.E., 2021. Global climatology and trends in convective environments from ERA5 and rawinsonde data. npj Clim Atmos Sci 4, 1–11. https://doi.org/10.1038/s41612-021-00190-x

Vetter, T., Reinhardt, J., Flörke, M., van Griensven, A., Hattermann, F., Huang, S., Koch, H., Pechlivanidis, I.G., Plötner, S., Seidou, O., Su, B., Vervoort, R.W., Krysanova, V., 2017. Evaluation of sources of uncertainty in projected hydrological changes under climate change

in 12 large-scale river basins. Climatic Change 141, 419–433. https://doi.org/10.1007/s10584-016-1794-y

Viviroli, D., Zappa, M., Gurtz, J., Weingartner, R., 2009. An introduction to the hydrological modelling system PREVAH and its pre- and post-processing-tools. Environmental Modelling & Software 24, 1209–1222. https://doi.org/10.1016/j.envsoft.2009.04.001

Wang, J., Liu, Z., Foster, I., Chang, W., Kettimuthu, R., Kotamarthi, V.R., 2021. Fast and accurate learned multiresolution dynamical downscaling for precipitation. Geoscientific Model Development 14, 6355–6372. https://doi.org/10.5194/gmd-14-6355-2021

Wyser, K., Koenigk, T., Fladrich, U., Fuentes-Franco, R., Karami, M., Kruschke, T., 2021. The SMHI Large Ensemble (SMHI-LENS) with EC-Earth3.3.1. Geoscientific Model Development. https://doi.org/10.5194/GMD-14-4781-2021

A SUPPORTING INFORMATION FOR CHAPTER 2

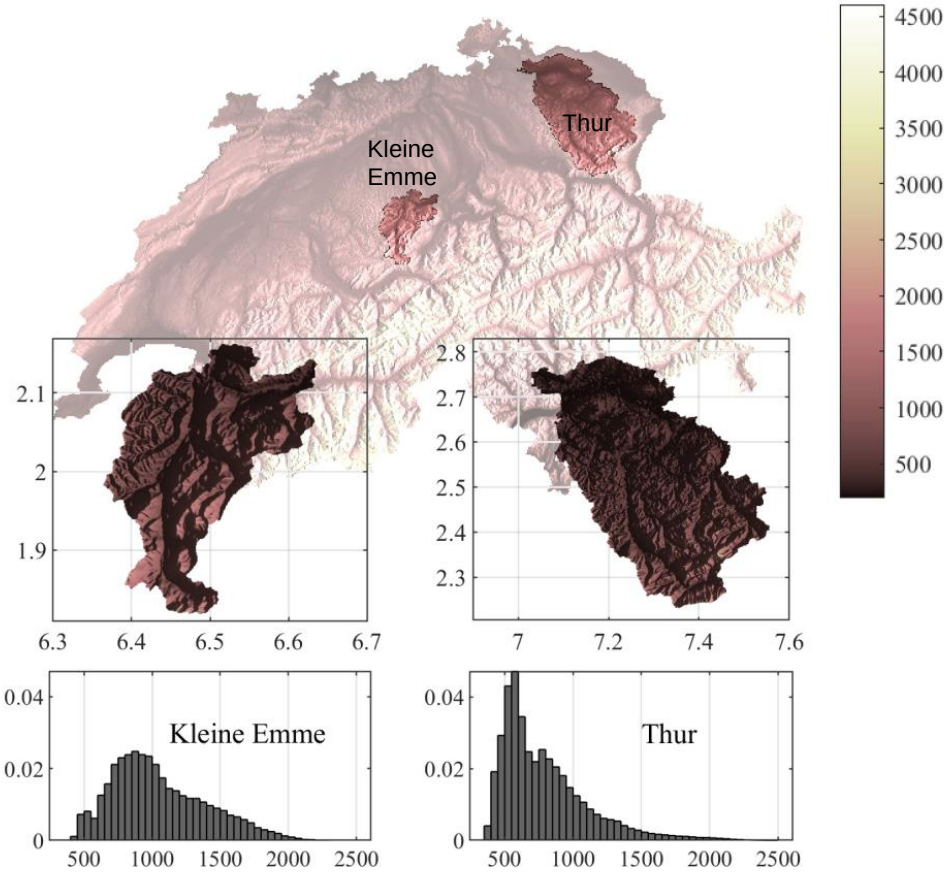

Figure A-1: Location, elevation distribution, and digital elevation models (DEM) of the Thur and Kleine Emme catchments. Coordinates are in Swiss projection (CH-1903) in m.

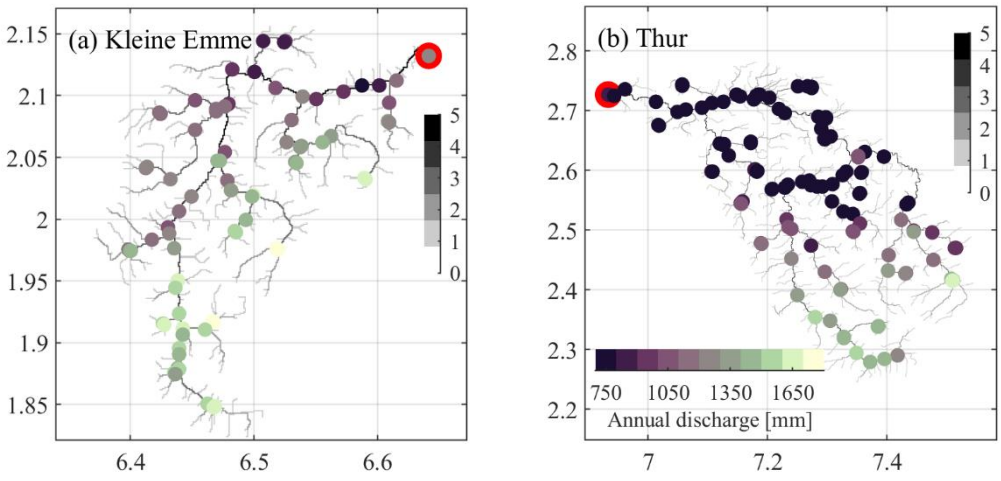

Figure A-2: Spatial distribution of 97 sub-catchments in the Kleine Emme river network (a) and 140 of the Thur river network (b). River reaches are drawn according to their Strahler

order and markers are coloured based on their average specific annual discharge in the present climate.

Catchment	Station name	Abbreviation	Elevation (m)	East (m)	North (m)
Thur	Ebnat-Kappel	EBK	623	726,346	237,176
	Säntis	SAE	2,502	744,200	234,920
	St. Gallen	STG	775	747,865	254,588
	Aadorf / Tänikon	TAE	539	710,514	259,821
Kleine Emme	Luzern	LUZ	454	665,540	209,848
	Napf	NAP	1,404	638,132	206,078
	Pilatus	PIL	2,106	661,910	203,410

Table S-1: List of ground weather stations managed by MeteoSwiss used as data sources. Coordinates based on Swiss projection (CH-1903).

ID	Driving GCM	RCM
1	ICHEC-EC-EARTH	CLMcom-CCLM4-8-17
2	ICHEC-EC-EARTH	DMI-HIRHAM5
3	ICHEC-EC-EARTH	SMHI-RCA4
4	MOHC-HadGEM2-ES	CLMcom-CCLM4-8-17
5	MOHC-HadGEM2-ES	SMHI-RCA4
6	IPSL-IPSL-CM5A-MR	SMHI-RCA4
7	MPI-M-MPI-ESM-LR	CLMcom-CCLM4-8-17
8	MPI-M-MPI-ESM-LR	MPI-CSC-REMO2009
9	MPI-M-MPI-ESM-LR	SMHI-RCA4

Table S-2: List of Euro-Cordex global circulation models (GCM) and regional climate models (RCM) chains used in the future climate simulations.

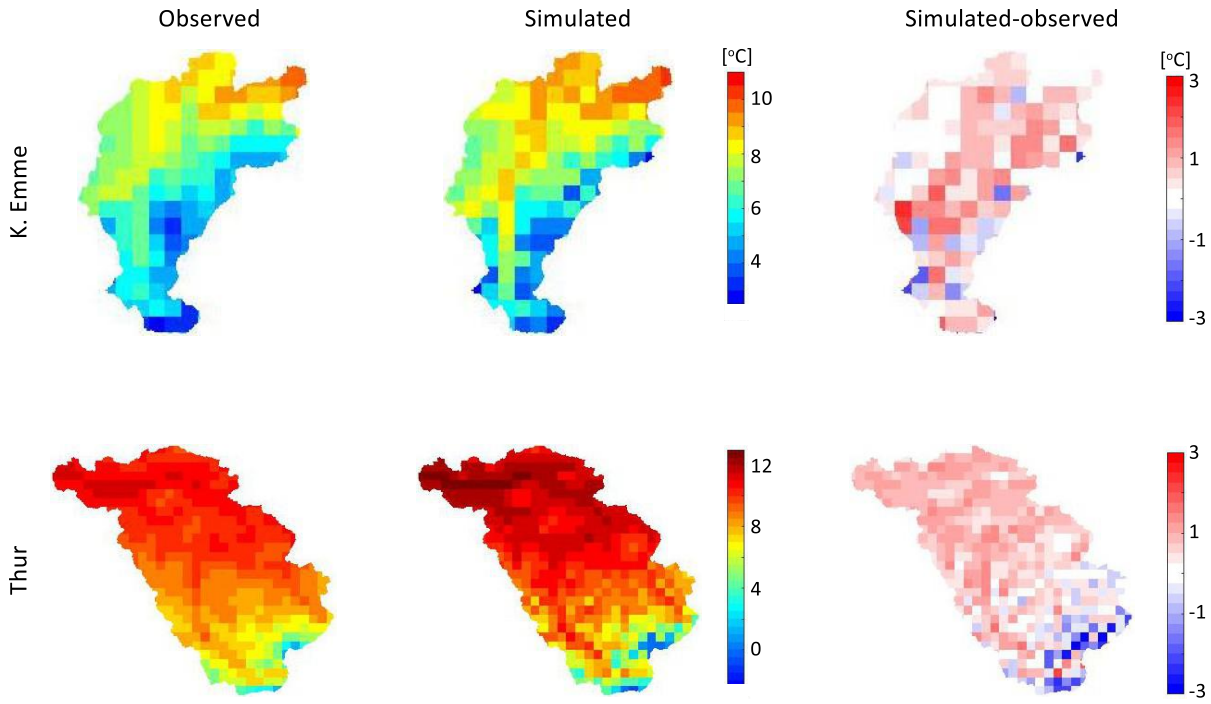

Figure A-3: Mean near-surface air temperature for the period 1982–2015 as obtained from the TabsY product (observed) in comparison with the mean ensemble generated by AWE-GEN-2d (simulated).

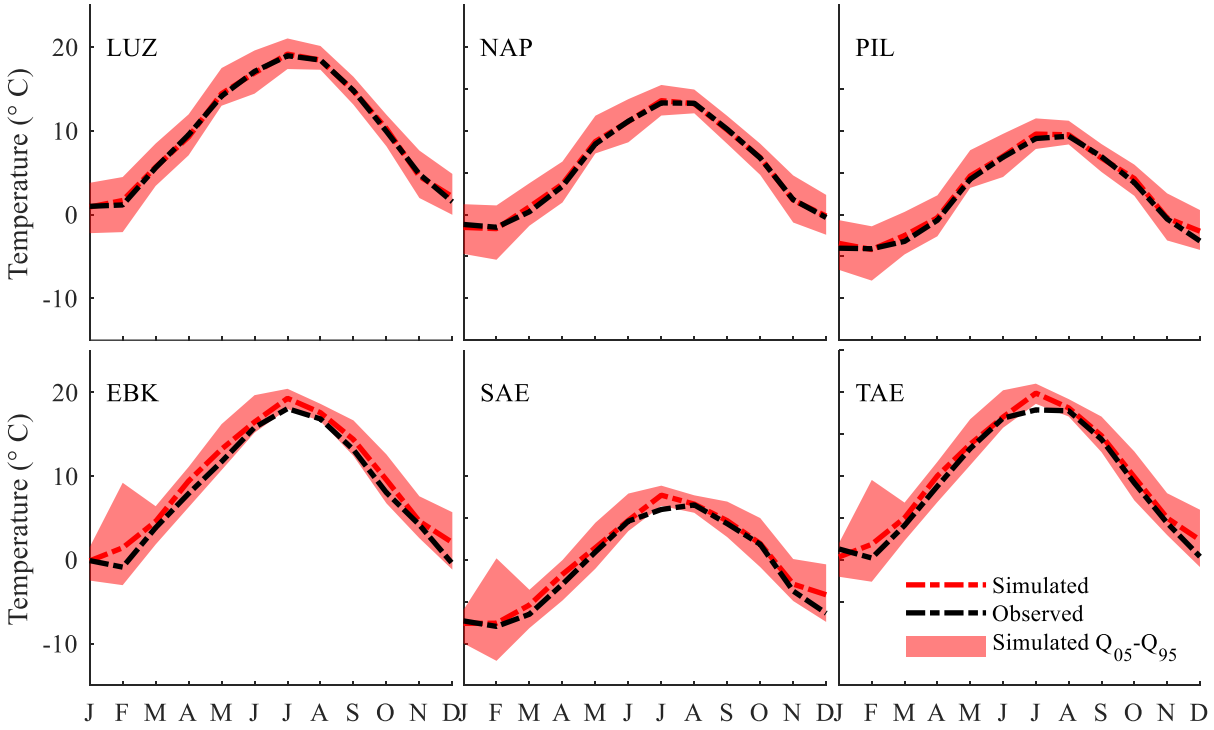

Figure A-4: Comparison between observed and simulated monthly temperatures at ground stations in Kleine Emme (top row) and Thur (bottom row). The black and red dashed lines represent the observed and simulated median values (respectively) and the bounded areas represent the observed and simulated 5–95th percentile ranges. The observed period covers 34 years of data (1982–2015), while simulations represent the mean of 30 realizations of 30 years each.

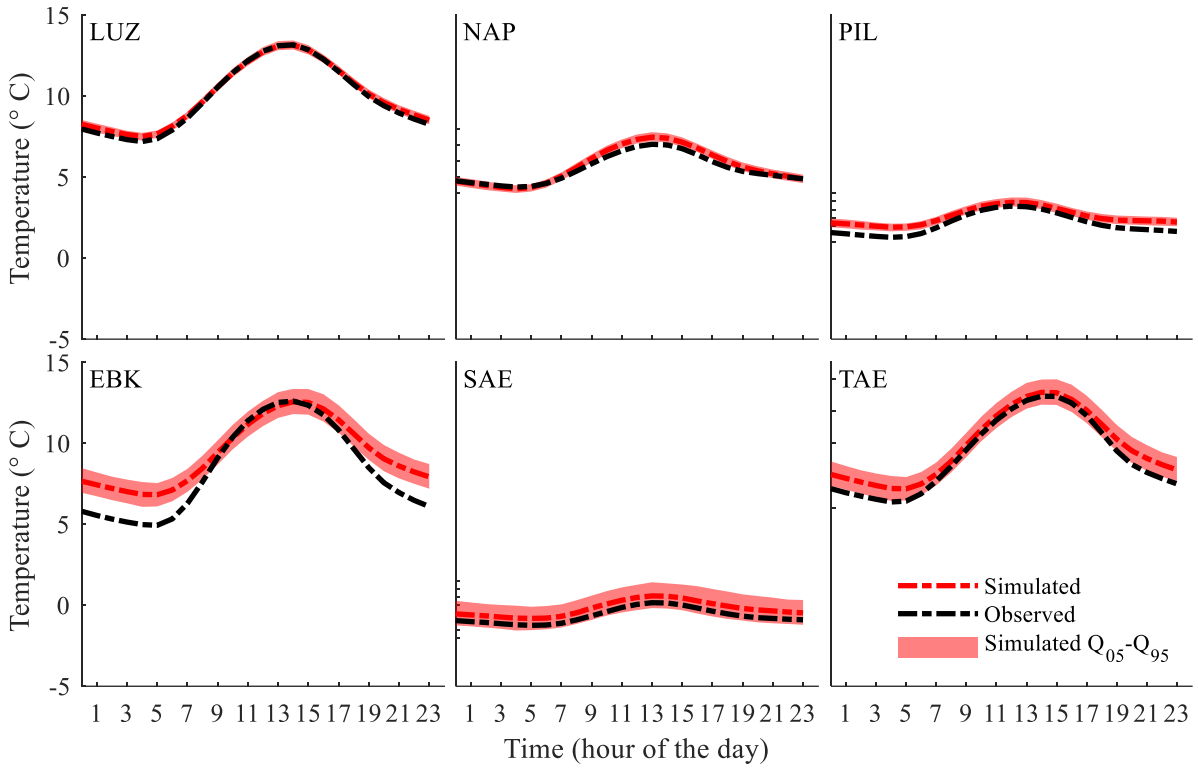

Figure A-5: Comparison between the observed and simulated daily cycle of temperatures at ground stations in Kleine Emme (top row) and Thur (bottom row). The black and red dashed lines represent the observed and simulated median values (respectively) and the bounded area represents the simulated 5–95th percentile ranges. The observed period covers 34 years of data (1982–2015), while simulations represent the mean of 30 realizations of 30 years each.

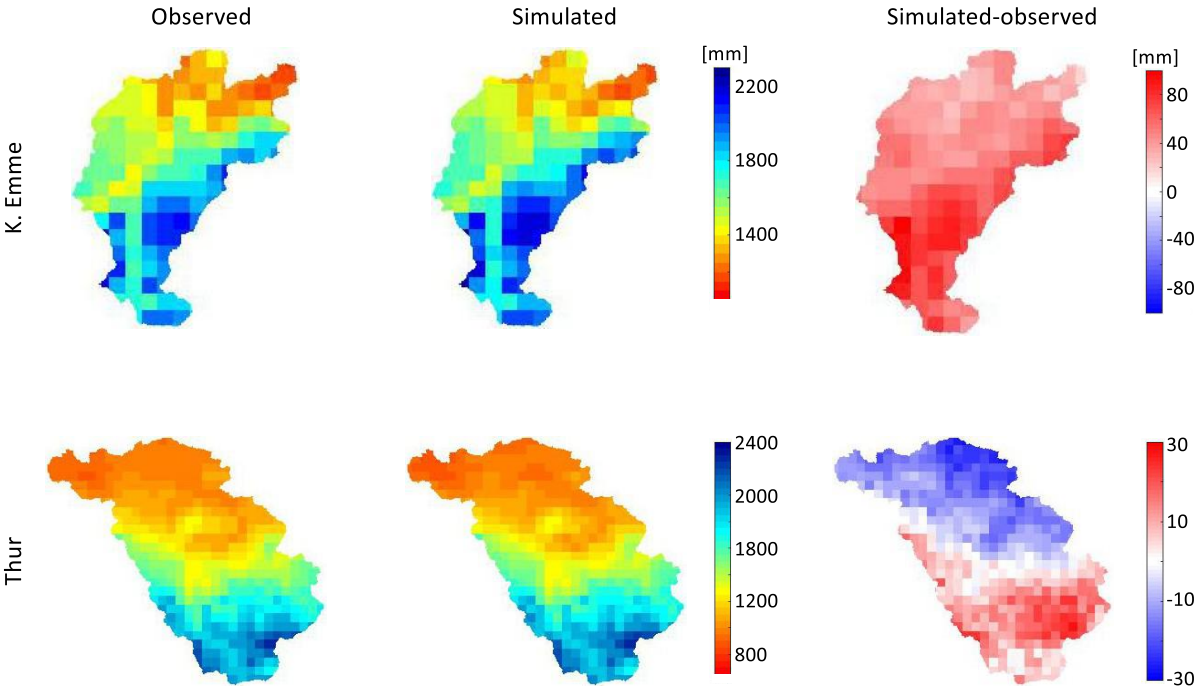

Figure A-6: Mean precipitation for the period 1982–2015 as obtained from the RhiresD product (observed) in comparison with the mean ensemble generated by AWE-GEN-2d (simulated).

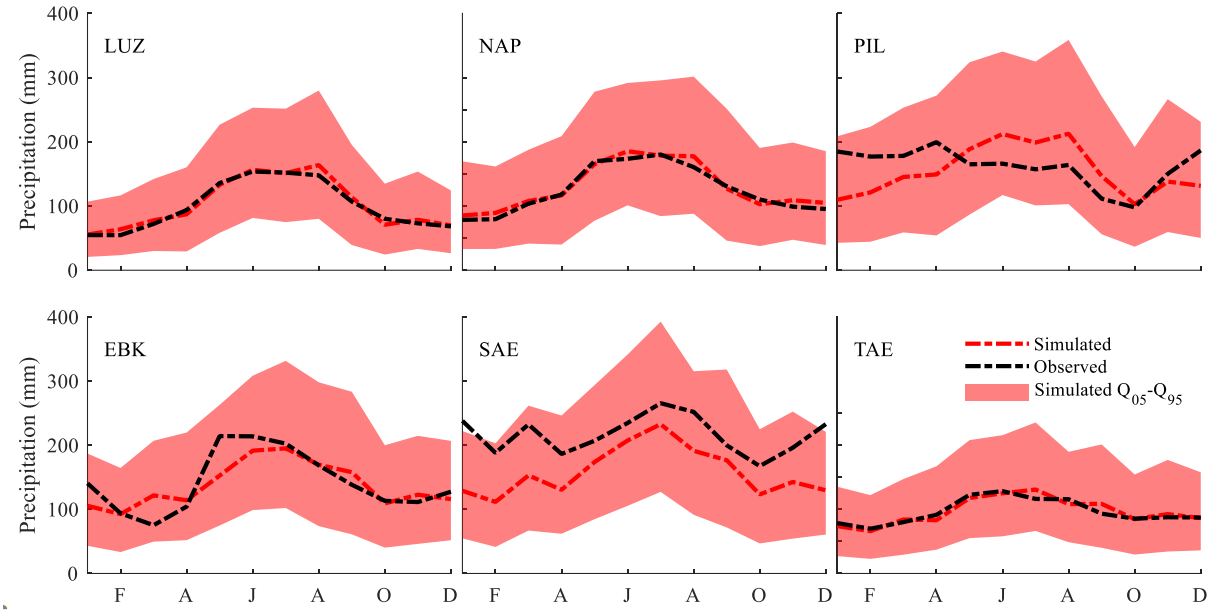

Figure A-7: A comparison between observed and simulated precipitation for each month. The black and red dashed lines represent the observed and simulated median values (respectively) and the bounded red area represents the 5–95th percentile range of simulations. The observed period covers 34 years of data (1982–2015), while simulations represent the mean of 30 realizations of 30 years each.

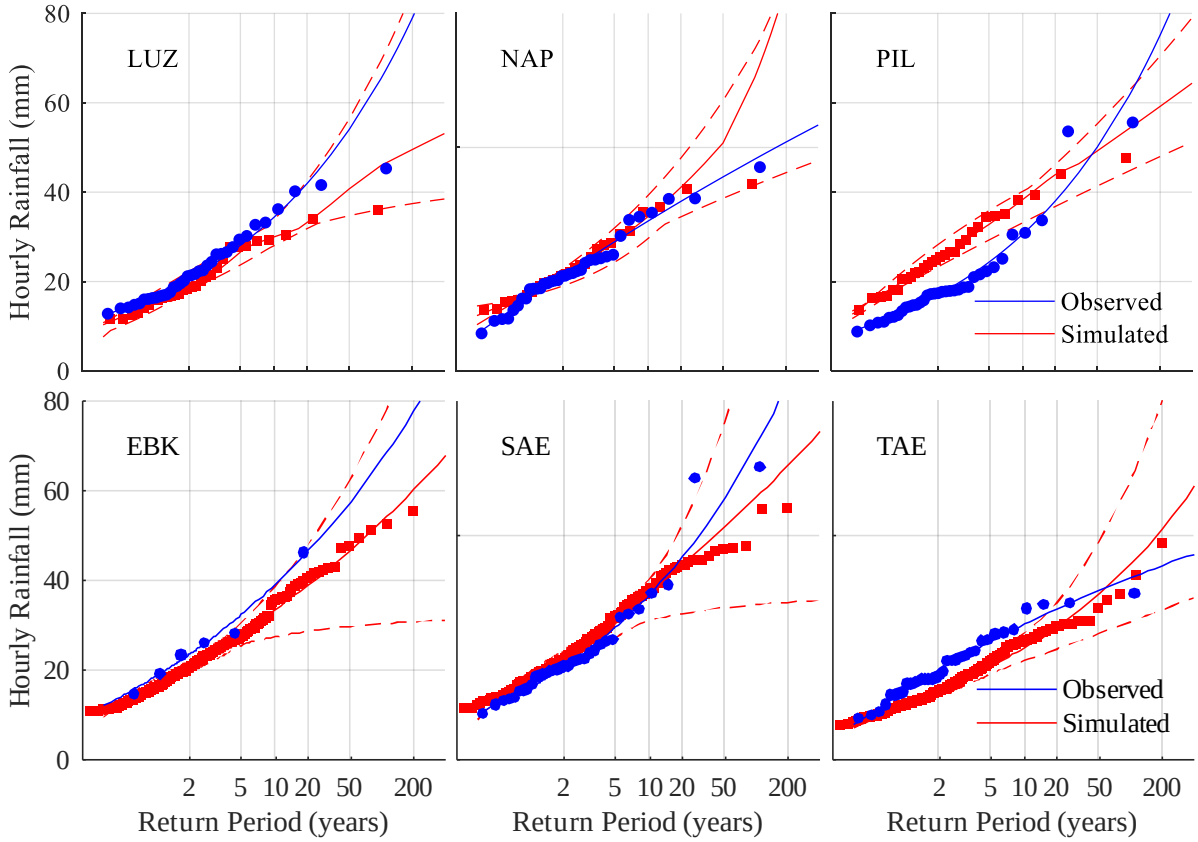

Figure A-8: Validation of annual maximum precipitation intensity at the hourly scale for different return periods in Kleine Emme (top row) and Thur (bottom row) weather stations. The continuous lines represent the observed (blue) and simulated (red) precipitation intensity computed by fitting GEV distribution to the recorded data, whereas the dashed red lines show the 5th–95th quantiles range of the simulations.

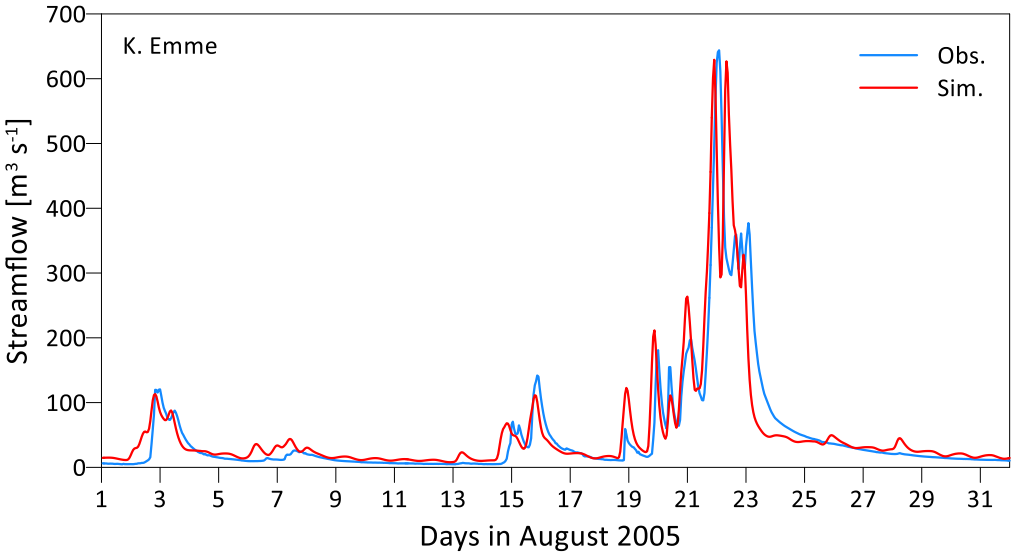

Figure A-9: Comparison between observed (blue) and Topkapi-ETH simulated (red) streamflow at the outlet of Kleine Emme catchment for the discharge peak of the validation period (2000–2009).

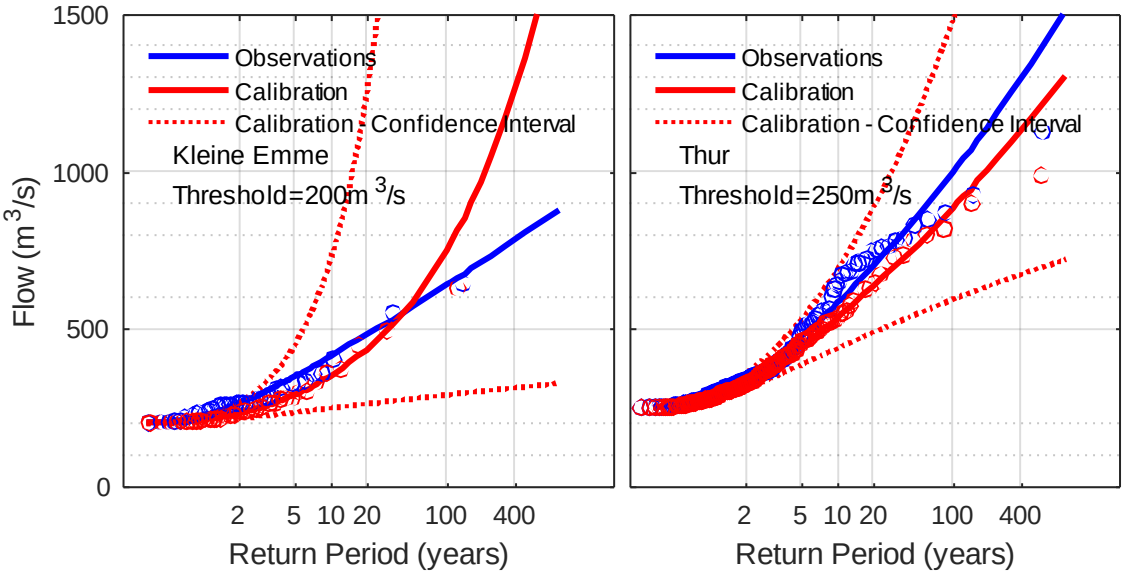

Figure A-10: Comparison between observed and simulated peaks over the threshold at the hourly scale for different return periods in Kleine Emme (left) Thur (right) catchments. The solid lines represent the observed (blue) and simulated (red) streamflow computed by fitting a Generalized Pareto distribution to the recorded data for the 2000–2009 period. The plotting positions were calculated using Gringorten's equation and the return periods are calculated via the reduced variate method.

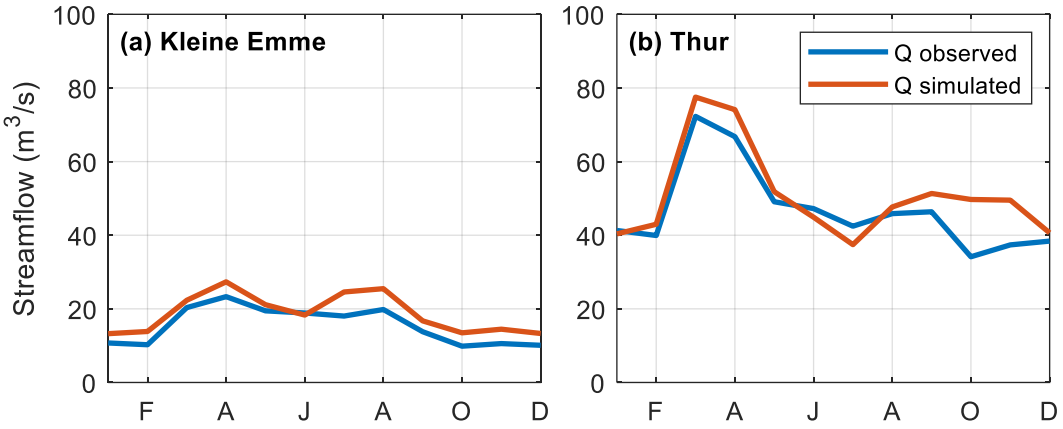

Figure A-11: Comparison between observed and simulated mean monthly streamflow for the 2000–2009 period in Kleine Emme (a) and Thur (b).

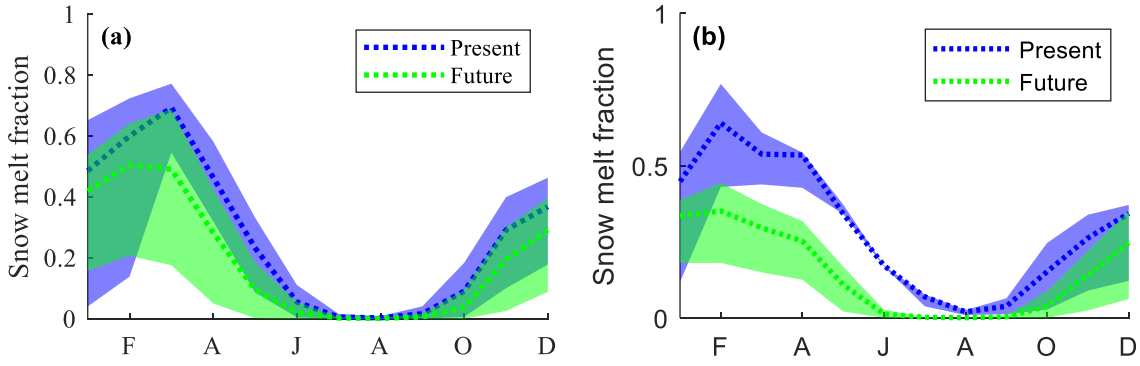

Figure A-12: Monthly snowmelt fraction of the total streamflow for the present (blue) and future multi-model mean at the end of the century (green) in Kleine Emme (a) and Thur (b). The dotted lines represent the mean and the bounded areas show the 5th–95th quantile range.

	Precipitation				*Streamflow*			
	Kleine Emme		*Thur*		*Kleine Emme*		*Thur*	
T (yr)	*hourly*	*daily*	*hourly*	*daily*	*hourly*	*daily*	*hourly*	*daily*
2	*0.650*	*0.794*	*0.815*	*0.377*	***0.000***	***0.000***	*0.745*	*0.139*
5	*0.894*	*0.513*	*0.724*	*0.413*	***0.001***	***0.001***	*0.953*	*0.054*
10	*0.519*	*0.192*	*0.299*	*0.106*	***0.012***	***0.004***	*0.787*	*0.080*
25	*0.372*	***0.047***	*0.303*	*0.054*	*0.072*	***0.025***	*0.873*	*0.068*

Table S-3: P-values according to the Mann-Whitney-Wilcoxon test for the null hypothesis that the present and future simulations have the same median value. Values below 5% are in bold and suggest there is a significant change in the median.

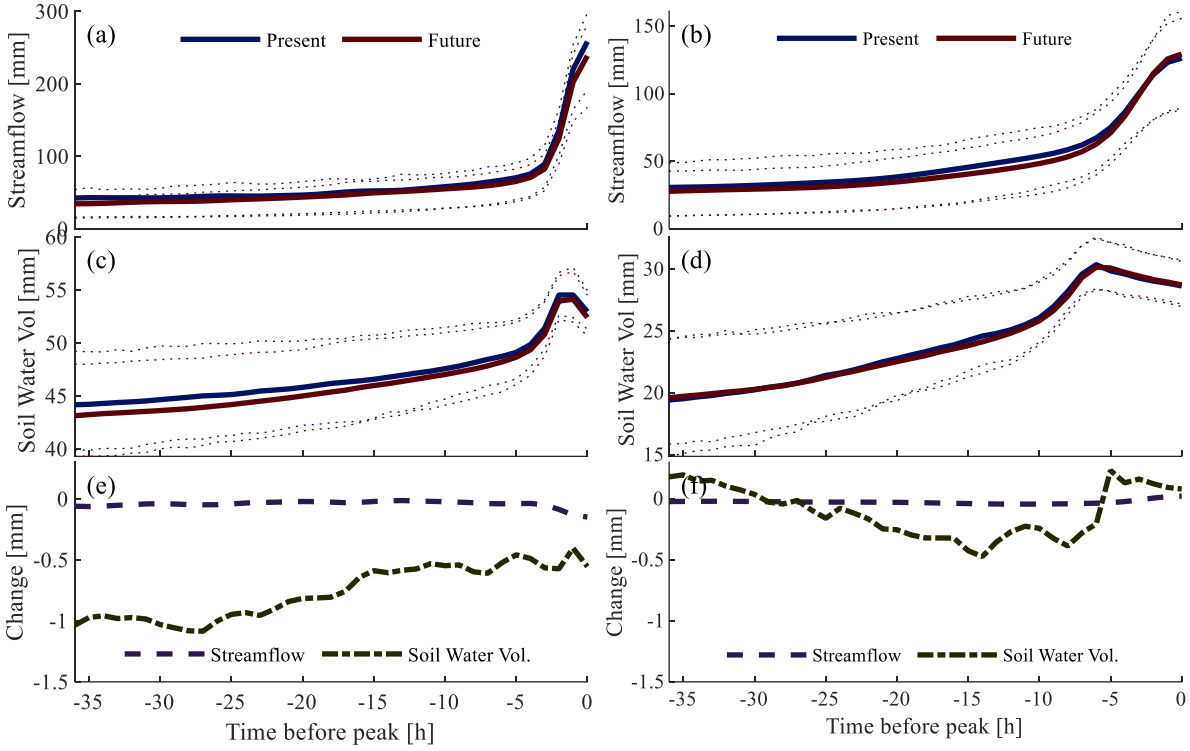

Figure A-13: Antecedent conditions to annual maximum hourly streamflow events at the outlet of the Kleine Emme (left column) and Thur (right) rivers. The panels show the average streamflow (a, b) and effective soil water volume (c, d) for present and end of the century conditions, as well as a comparison of their change (future-present; e, f).

	ELEVATION (MASL)	SIZE (KM^2)	CLASS
1	623	2.5	Low, Small
2	925	62.6	Low, Big
3	1036	2.8	Middle, Small
4	1001	64.0	Middle, Big
5	1565	8.1	High, Small
6	1466	76.0	High, Big

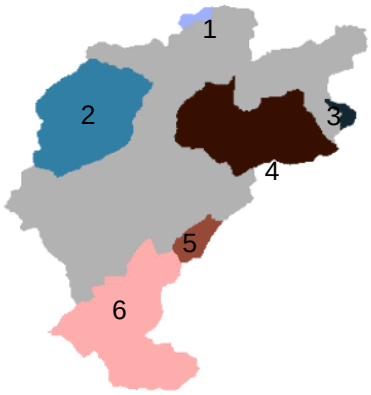

Figure A-14: Identification, location and main properties of six selected sub-catchments belonging to the Kleine Emme river network.

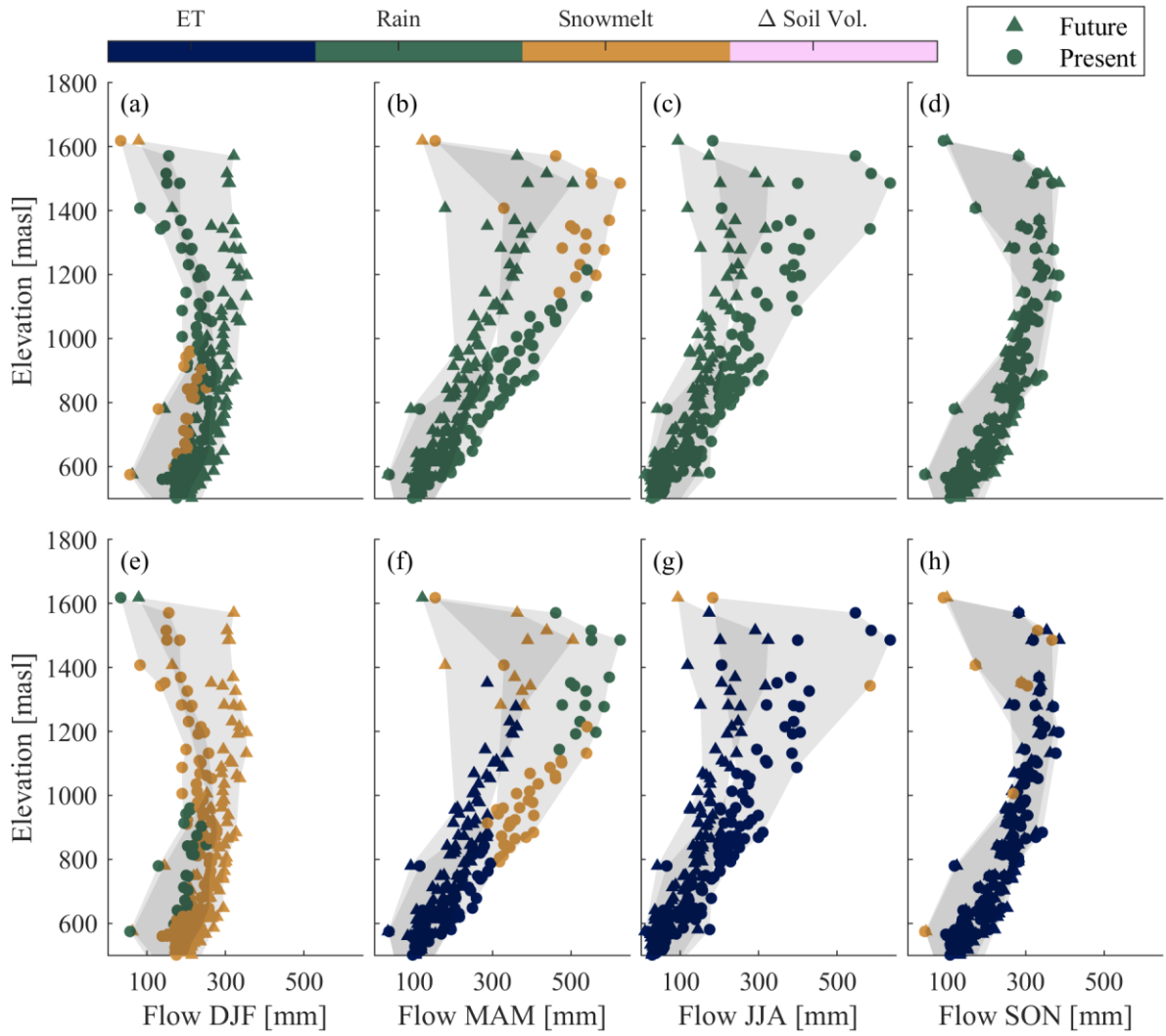

Figure A-15: First (a–d) and second (e–h) most important components contributing to the seasonal flow in the Thur river network under present (circles) and future (triangles) climate conditions. Mean seasonal specific flow is plotted as a function of sub-catchment elevation and coloured by the components ET (evapotranspiration), Rain, Snowmelt, ΔSoil Volume (change in soil water volume).

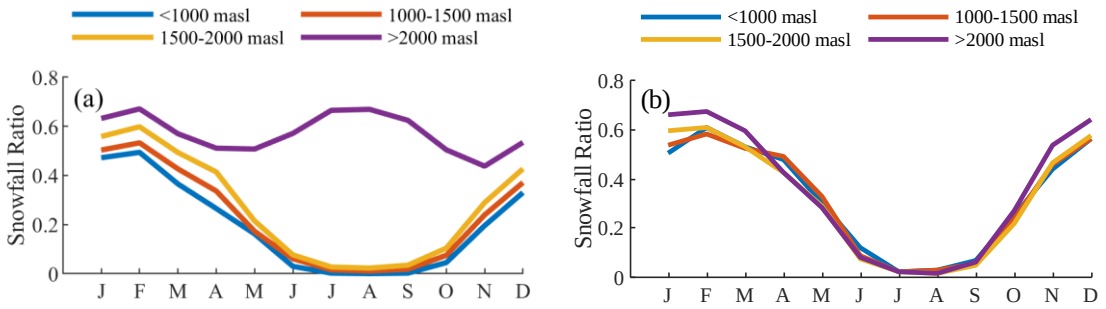

Figure A-16: Ratio of future (2080–2089) to present monthly snowfall at the Kleine Emme (a) and Thur (b) averaged over different elevation ranges

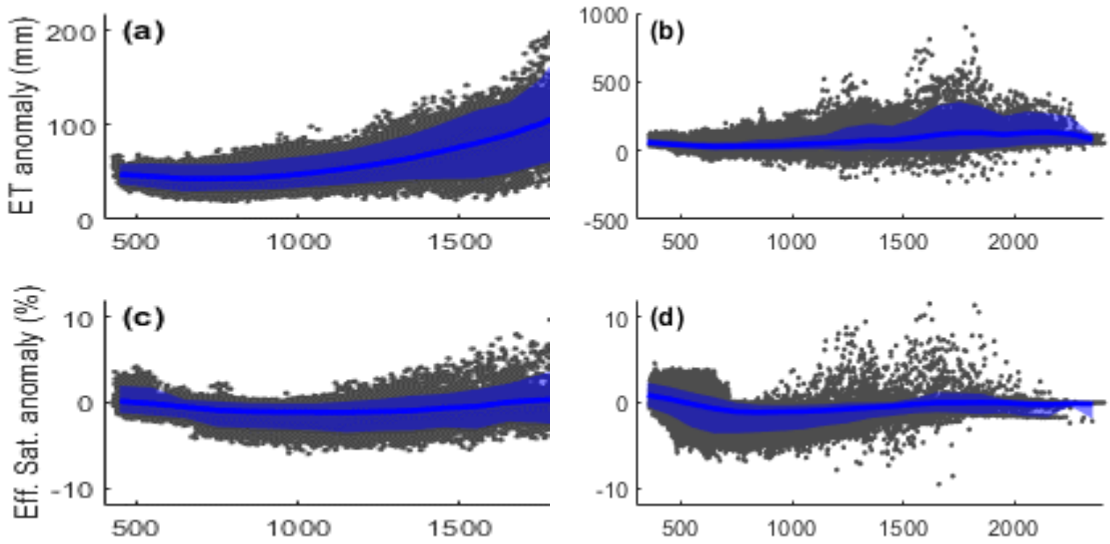

Figure A-17: Mean annual evapotranspiration (a, b) and effective saturation (c, d) anomalies comparing the end of the century multi-model mean with the present climate simulations in Kleine Emme (left) and Thur (right). The black points represent the value for each grid cell, while the solid lines and shaded areas show the mean and 5th–95th quantile range for every 100-meter elevation bin, respectively

B SUPPORTING INFORMATION FOR CHAPTER 3

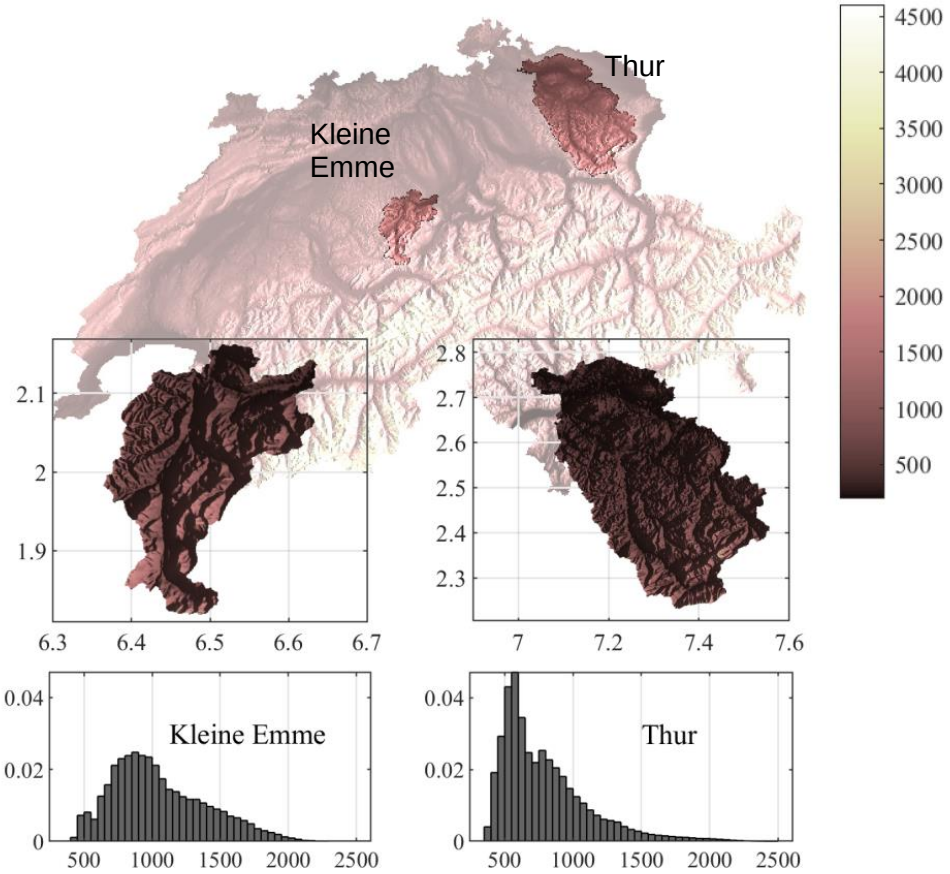

Figure B-1: Location, elevation distribution, and digital elevation models (DEM) of the Thur and Kleine Emme catchments. Coordinates are in Swiss projection (CH-1903) in m. The plot is based on Moraga *et al.* (2021).

Table B-1: List of Euro-Cordex global circulation models (GCM) and regional climate models (RCM) chains used in the future climate simulations.

ID	Driving GCM	RCM
1	ICHEC-EC-EARTH	CLMcom-CCLM4-8-17
2	ICHEC-EC-EARTH	DMI-HIRHAM5
3	ICHEC-EC-EARTH	SMHI-RCA4
4	MOHC-HadGEM2-ES	CLMcom-CCLM4-8-17
5	MOHC-HadGEM2-ES	SMHI-RCA4
6	IPSL-IPSL-CM5A-MR	SMHI-RCA4
7	MPI-M-MPI-ESM-LR	CLMcom-CCLM4-8-17
8	MPI-M-MPI-ESM-LR	MPI-CSC-REMO2009

ID	Driving GCM	RCM
9	MPI-M-MPI-ESM-LR	SMHI-RCA4

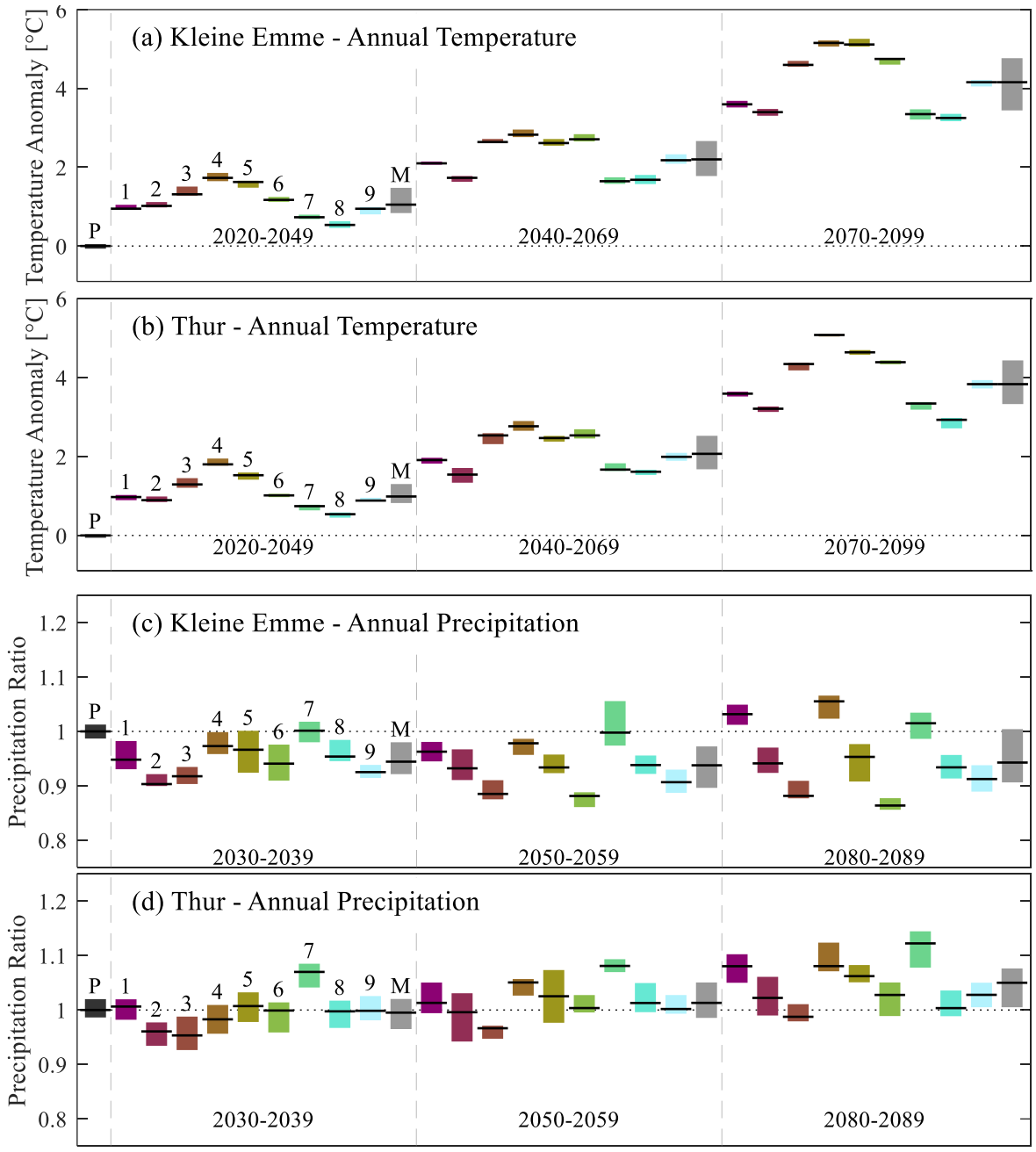

Figure B-2: Differences in annual temperature (a, b) and precipitation ratio (c, d) between the present period (1976–2005) and future periods averaged over the entire Kleine Emme and Thur catchments. Numbers 1 to 9 refer to the different climate models (seeTable B-1) and MMM refers to the multi-model mean. Central lines in the box plots show the median of the annual means, while the boxes represent the interquartile range of the data.

C SUPPORTING INFORMATION FOR CHAPTER 4

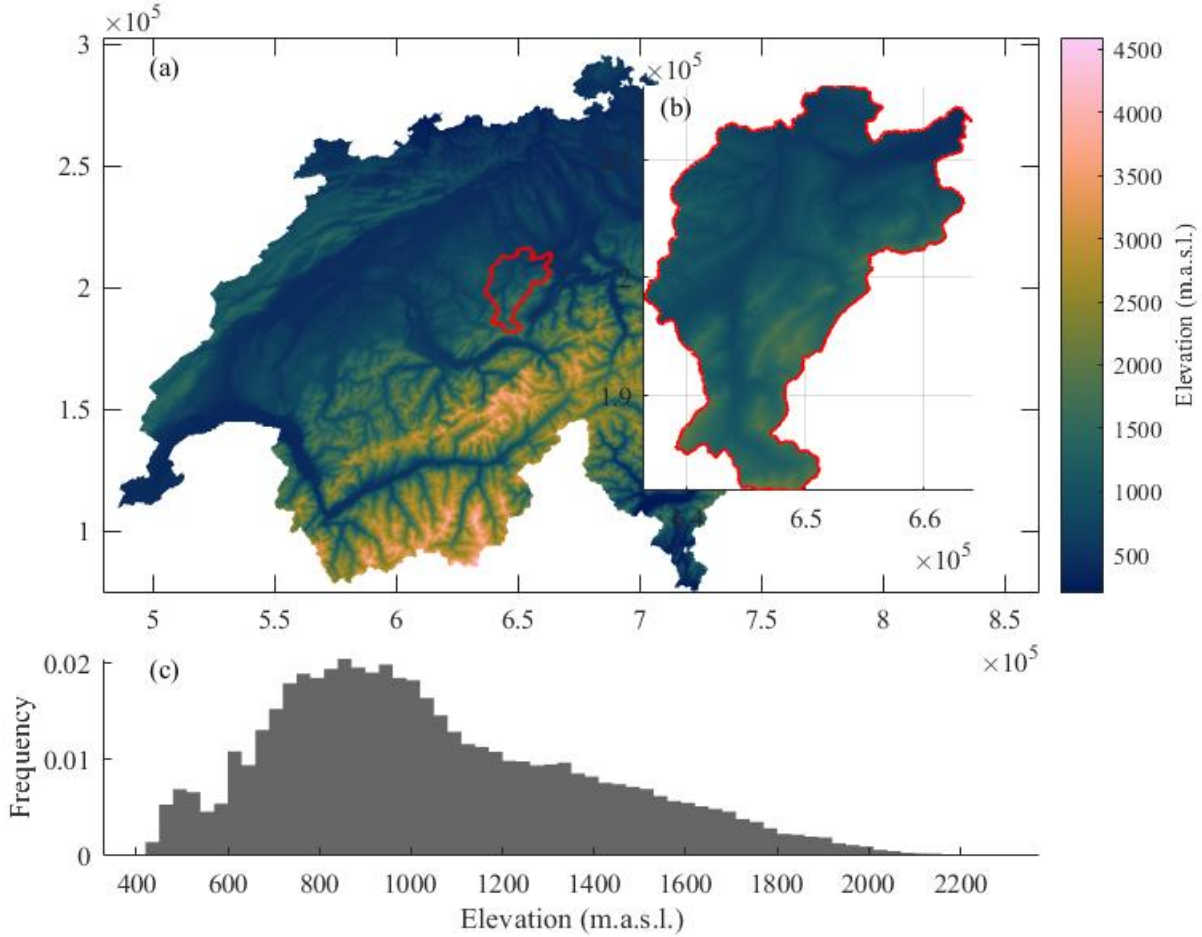

Figure C-1: Digital elevation model (DEM) of Switzerland (a), and the Kleine Emme catchment (b), along with its distribution of elevations (c). Coordinates are in Swiss projection (CH-1903) in m.

Table C-1: List of ground weather stations used in the calibration. Coordinates based on Swiss projection (CH-1903)

Location	Abbreviation	Elevation (masl)	East (m)	North (m)
Luzern	LUZ	454	665,540	209,848
Napf	NAP	1404	638,132	206,078
Pilatus	PIL	2106	661,910	203,410

Table C-2: Model chains of global circulation models (GCM) and regional climate models (RCM) used to compute the factors of change (FC) used in future climate simulations.

ID	Driving GCM	RCM
1	ICHEC-EC-EARTH	CLMcom-CCLM4-8-17
2	ICHEC-EC-EARTH	DMI-HIRHAM5

ID	Driving GCM	RCM
3	ICHEC-EC-EARTH	SMHI-RCA4
4	MOHC-HadGEM2-ES	CLMcom-CCLM4-8-17
5	MOHC-HadGEM2-ES	SMHI-RCA4
6	IPSL-IPSL-CM5A-MR	SMHI-RCA4
7	MPI-M-MPI-ESM-LR	CLMcom-CCLM4-8-17
8	MPI-M-MPI-ESM-LR	MPI-CSC-REMO2009
9	MPI-M-MPI-ESM-LR	SMHI-RCA4

Table C-3: Parameters for the two-term exponential function used to describe the values of the mean cloud area ratio (μ_{CAR}) as a function of the distance to a wet spell (t_{in}) as well as the standard deviation σ_{CAR} during the inter-storm periods.

	$\mu_{CAR}(t_{in}) = a*\exp(b*t_{in}) + c*\exp(d* t_{in})$				σ_{CAR}
Month	a	b	c	d	
Jan	1.76E-01	1.66E-04	6.13E-01	-1.48E-03	0.430
Feb	-6.40E-02	1.81E-04	6.80E-01	-3.49E-04	0.263
Mar	6.42E-01	-6.33E-04	-3.49E-07	3.07E-03	0.286
Apr	2.58E-01	-1.58E-05	3.40E-01	-8.57E-04	0.368
Mai	-9.92E-03	5.26E-04	6.87E-01	-7.18E-04	0.288
Jun	4.78E-01	-4.71E-04	1.31E-01	-9.83E-03	0.318
Jul	4.20E-02	5.57E-04	5.04E-01	-2.45E-03	0.278
Aug	6.36E-02	3.92E-04	4.68E-01	-1.91E-03	0.330
Sep	-4.16E-08	4.84E-03	3.11E-01	-3.88E-05	0.358
Oct	1.52E-03	1.44E-03	5.57E-01	-3.42E-04	0.392
Nov	1.23E-05	3.28E-03	6.83E-01	-4.78E-04	0.388
Dec	5.14E-01	-4.86E-04	2.30E-01	-4.36E-03	0.300

Table C-4: Parameters for the autoregressive moving-average model ARMA(4,2) used to describe the stochastic component of the dry-spell cloud cover.

Month	$y_t = c + \phi_1*y_{t-1} + \ldots \phi_p*y_{t-p} + \epsilon_t + \theta_1*\epsilon_{t-1} + \ldots \theta_q*\epsilon_{t-q}$					
	ϕ_1	ϕ_2	ϕ_3	ϕ_4	θ_1	θ_2
Jan	1.24	-0.05	0.03	-0.22	-0.03	-0.04
Feb	1.31	-0.07	-0.13	-0.12	-0.12	-0.15
Mar	1.32	-0.10	-0.10	-0.13	-0.14	-0.12

Month	$y_t = c + \phi_1 * y_{t-1} + \ldots \phi_p * y_{t-p} + \epsilon_t + \theta_1 * \epsilon_{t-1} + \ldots \theta_q * \epsilon_{t-q}$					
	ϕ_1	ϕ_2	ϕ_3	ϕ_4	θ_1	θ_2
Apr	1.18	0.06	-0.03	-0.22	0.03	-0.09
May	1.30	-0.05	-0.13	-0.13	-0.14	-0.14
Jun	1.32	-0.09	-0.10	-0.14	-0.16	-0.13
Jul	1.26	0.01	-0.17	-0.11	-0.10	-0.18
Aug	1.36	-0.15	-0.12	-0.10	-0.24	-0.13
Sep	1.27	-0.06	-0.01	-0.20	-0.09	-0.07
Oct	1.32	-0.15	-0.01	-0.18	-0.11	-0.03
Nov	1.26	-0.07	-0.02	-0.19	-0.06	-0.06
Dec	1.20	0.06	-0.06	-0.20	0.00	-0.11

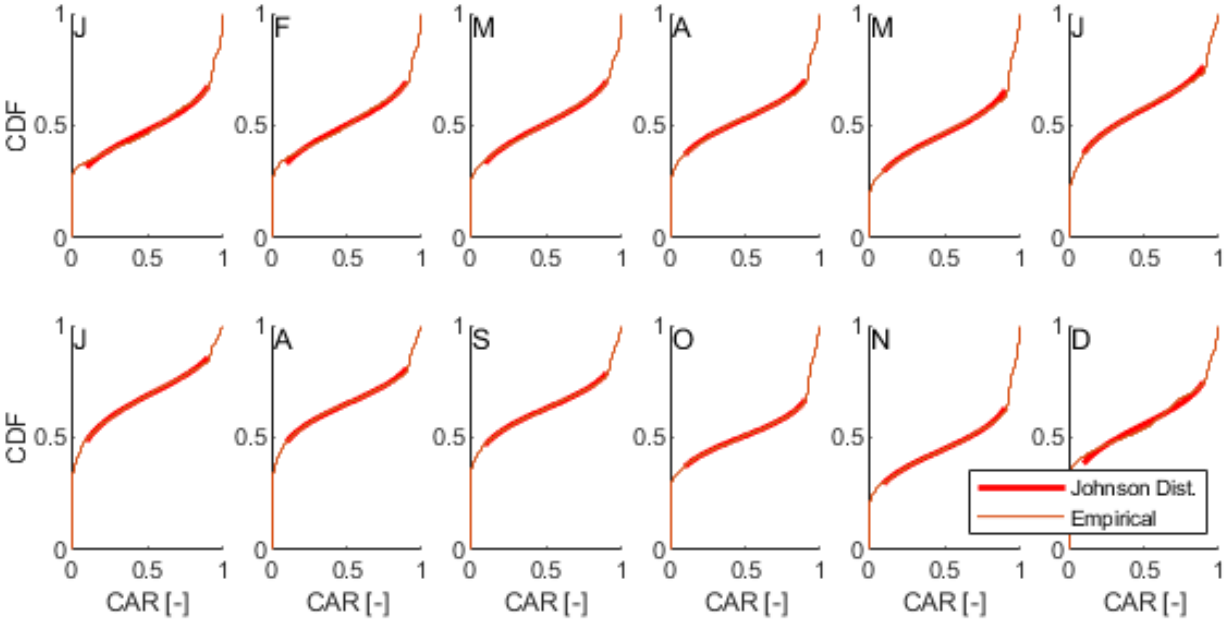

Figure C-2: Fit of the Johnson distribution to observations of dry-period cloud cover for each month.

Table C-5: Monthly mean of the observed wet-period cloud area ratio (CAR)

Month	*Mean* CAR_w
Jan	0.80
Feb	0.80
Mar	0.78
Apr	0.78
Mai	0.79
Jun	0.73

Jul	0.65
Aug	0.71
Sep	0.74
Oct	0.77
Nov	0.76
Dec	0.81

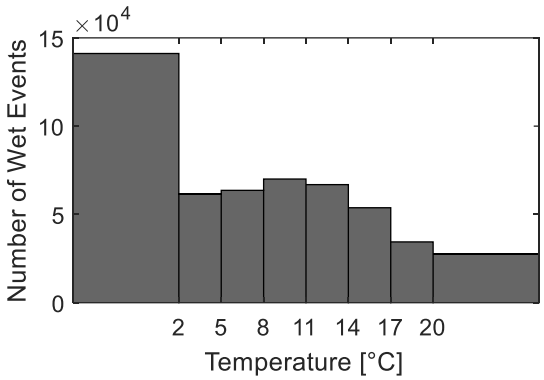

Figure C-3: Number of observed wet events for each bin of temperatures at the onset. Note that the bins in the extremes are semi-infinite ([-inf–2 °C] and [20°C–+inf], respectively)

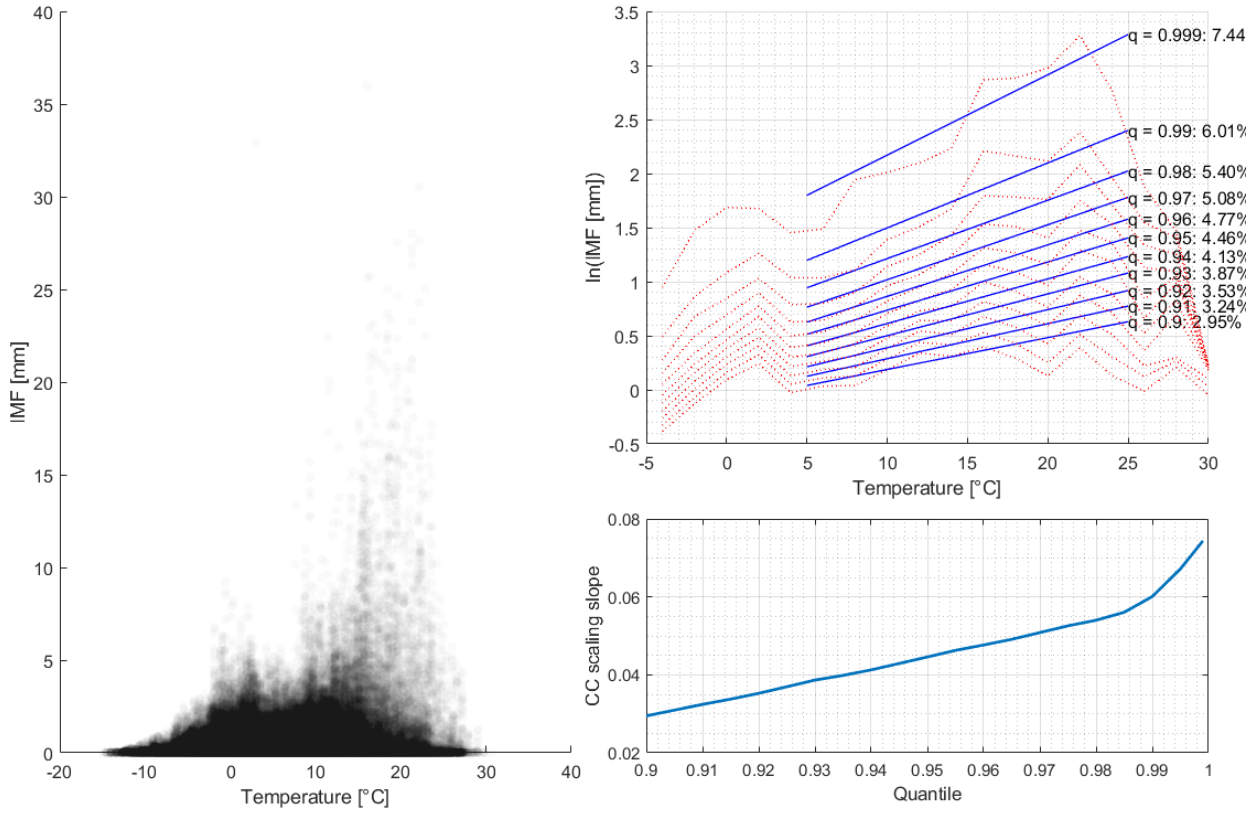

Figure C-4: Relation between temperature and mean areal intensity (IMF) in the observed record for the Kleine Emme catchment. Panel (a) on the left shows a scatterplot of IMF v/s temperature. Panel (b) on the top right shows the scaling of the highest intensities with

temperature using the temperature binning (dotted lines) and the quantile regression methods (solid lines) for quantiles from q = .90 to q = .999. Panel (c) on the bottom right shows the CC rate as obtained from the slope given by quantile regression method for each chosen quantile.

Table C-6: Parameters for the covariance matrix of the Whittle-Matérn function.

	α	v_W	v_I	v_C	v_{WI}	v_{WC}	v_{CI}	ρ_{WI}	ρ_{WC}	ρ_{CI}
Bin#1	0.96	0.89	1.11	0.08	102.10	101.08	97.30	0.21	0.18	0.11
Bin#2	1.04	0.62	1.05	0.09	94.63	104.50	96.97	0.13	0.07	0.03
Bin#3	1.08	1.28	0.96	0.22	93.79	117.71	95.96	0.14	0.04	0.07
Bin#4	0.62	0.39	0.85	0.07	94.77	100.73	88.20	0.11	0.06	0.01
Bin#5	0.85	0.30	0.85	0.07	78.93	93.85	100.90	0.13	0.05	0.02
Bin#6	0.66	0.47	2.00	0.18	1.09	4.41	1.03	0.51	0.18	0.12
Bin#7	1.30	0.92	2.00	0.35	3.78	37.58	79.34	0.43	0.15	0.07
Bin#8	0.14	0.17	0.33	0.04	0.14	0.20	0.31	0.81	0.27	0.10

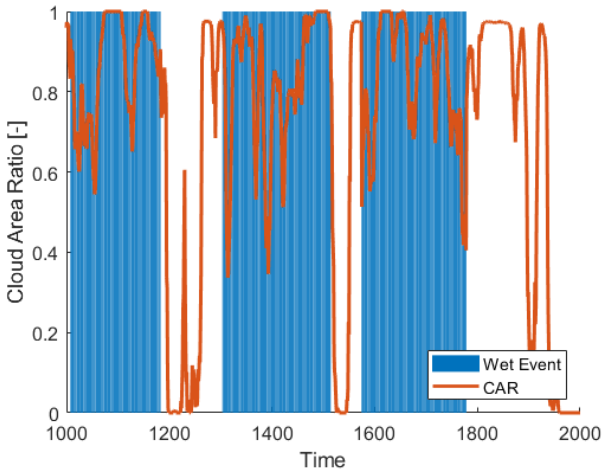

Figure C-5: Cloud area ratio (CAR) of a random simulation. The modification of the CAR module in AWE-GEN-2d-CC generates some discontinuity in the CAR time series at the beginning of the wet events.

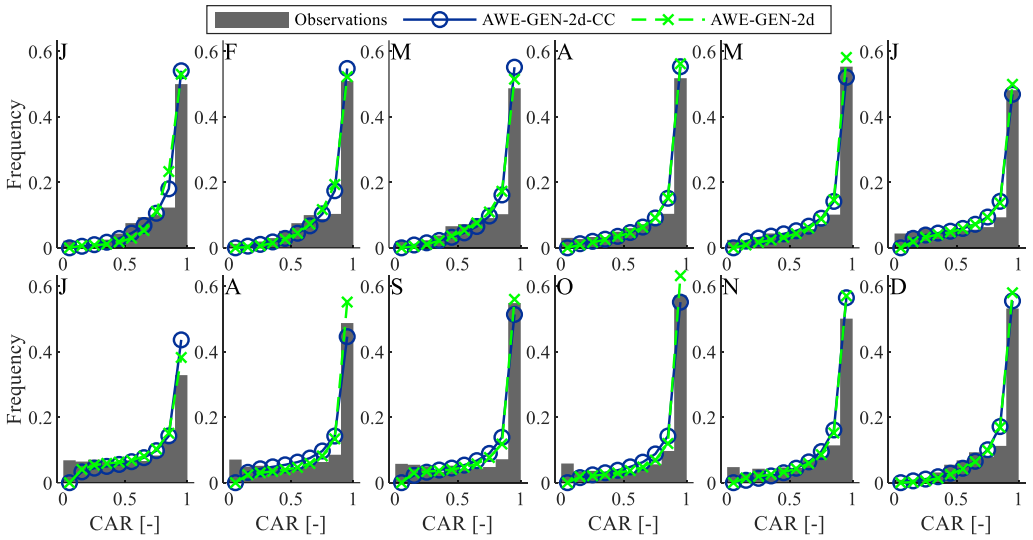

Figure C-6: Monthly distributions of the wet-period cloud area ratio (CAR_d) for the observations (gray bars) simulations using the new AWE-GEN-2d-CC (blue circles), and simulations using the previous AWE-GEN-2d model (green x's)

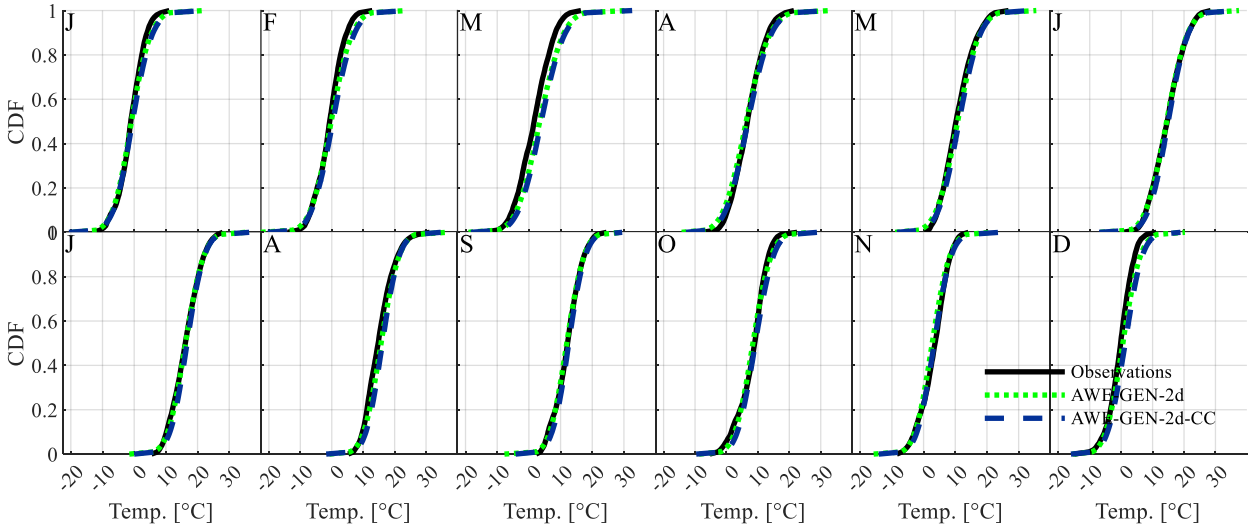

Figure C-7: Comparison of the cumulative distribution function (CDF) of the areal mean hourly temperature observed (black, solid line), simulated with AWE-GEN-2d-CC (blue, dashed line), and simulated with AWE-GEN-2d (green, dotted line) during wet events.

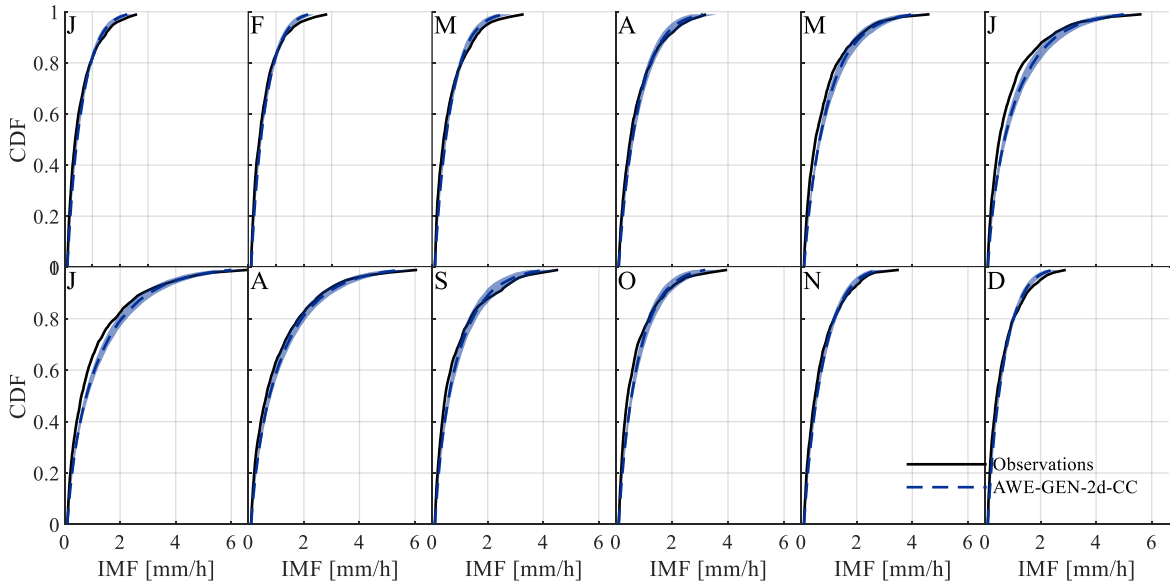

Figure C-8: Monthly cumulative distribution functions (CDF) of the observed (black line) and simulated (blue dashed line) hourly IMF. The shaded red area represents the IQR of the CDF across 900 simulations. Only non-zero values of IMF are considered.

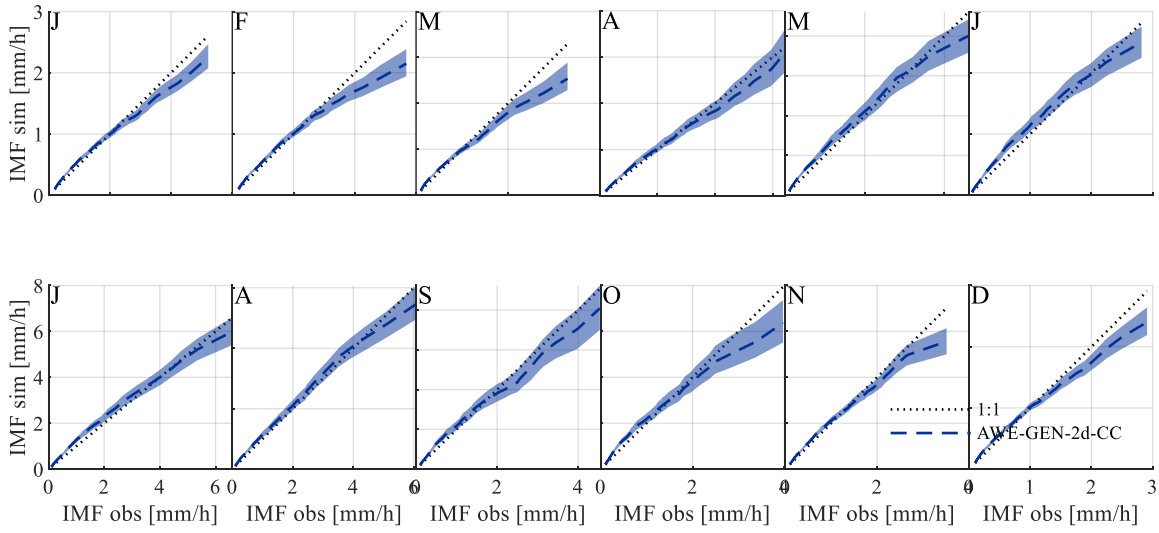

Figure C-9: Monthly q-q plots comparing the observed and simulated hourly IMF values up to the .99 quantile. The shaded blue area represents the IQR of the quantiles across 900 simulations. Only non-zero values of IMF are considered.

Table C-7:. Area and RCM-averaged monthly absolute change for mean temperature ΔT, relative change for mean precipitation ΔPr, and relative change for the hourly 99th quantile Δq^{99}

	Jan	Feb	Mar	Apr	May	Jun	Jul	Aug	Sep	Oct	Nov	Dec

ΔT [K]	3.93	3.88	3.85	3.88	3.90	4.67	4.73	4.65	4.14	4.17	4.17	3.93
ΔPr	1.023	1.003	1.003	0.997	0.993	0.898	0.897	0.917	0.982	0.999	1.009	1.053
Δq^{99}	1.104	1.157	1.244	1.157	1.264	1.061	1.089	1.079	1.198	1.211	1.244	1.031

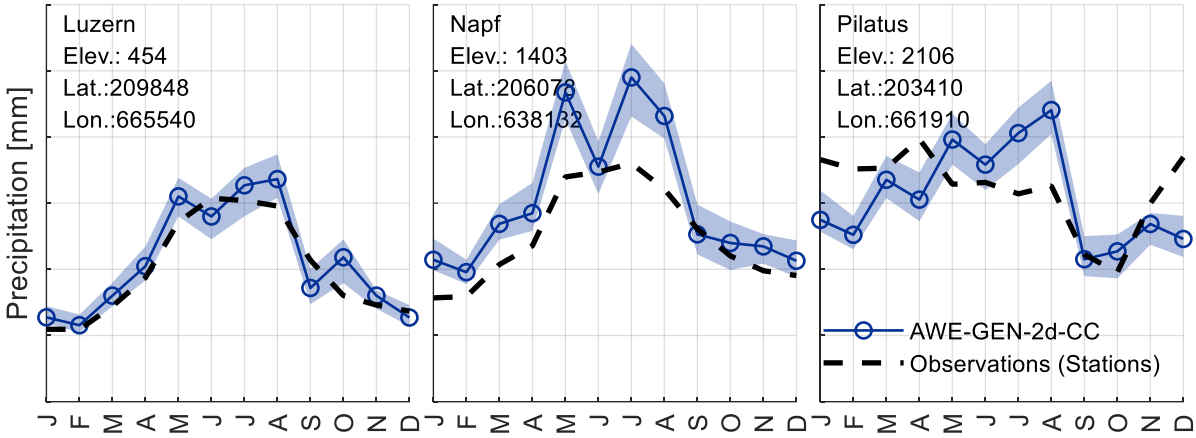

Figure C-10: Comparison of the simulated mean monthly precipitation using the AWE-GEN-2d-CC model (blue) and the corresponding observed statistics extracted from three ground weather stations of the MeteoSwiss network (Table S-1).

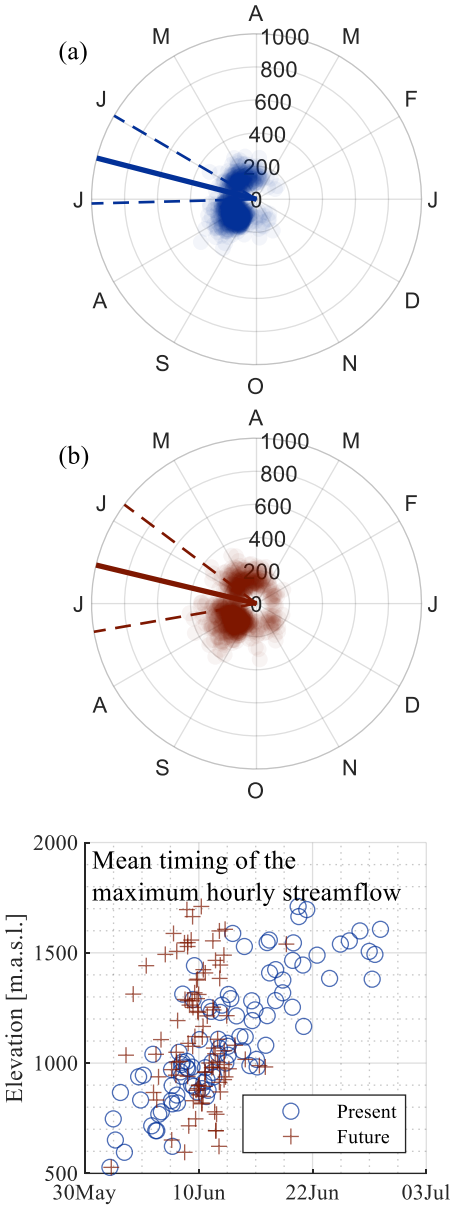

Figure C-11: Timing (angular axis) and magnitude (radial axis) of the maximum hourly streamflow at the outlet of the catchment for each of the 900 present (a, blue, top) and future (b, red, middle) hydrological simulations. The circular mean and standard deviation range of the timings are plotted as solid and dashed lines, respectively. Panel (c) shows the circular mean of the 900 timing values for each of the 97 sub-catchments of the Kleine Emme, plotted against their median elevation, the mean and the standard deviation range are shown by a solid line and dashed lines, respectively.